DOCTOR OF PHILOSOPHY

The post-glacial evolution and present-day sedimentary processes of the Mawddach Estuary

Larcombe, Piers

Award date:
1992

Awarding institution:
Bangor University

The Post-Glacial Evolution and Present-Day Sedimentary Processes of the Mawddach Estuary

by

Piers Larcombe B.Sc., M.Sc.

A thesis submitted to the University of Wales
for the degree of Doctor of Philosophy

March 1992

School of Ocean Sciences
University College of North Wales
Menai Bridge
Anglesey

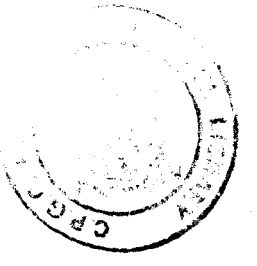

TEXT CUT OFF IN THE ORIGINAL

VOLUME 2

Abstract

The Post-glacial evolution and present-day

sedimentary processes of the Mawddach Estuary.

The Mawddach Estuary and Barmouth Bay now occupy what was a deeply incised glaciated valley at the last ice maximum. This valley is now filled by a complex suite of sediments, up to 75m thick at the present estuary mouth, which record increasing marine influence. A regressive coastline is also present today. In the Bay, Welsh glacial drifts were eroded to form deep depressions, infilled by complex cross- stratified Late- or Post-glacial sediments, overlain by a parallel-stratified sequence, perhaps formed behind a coast-parallel morainal barrier.

Net sediment transport of the fine sand in the Bay is shoreward, controlled by a strong mesotidal and wave regime. Calculated sediment transport rates infer long term sediment accumulation rates of 82mm per year for the estuary as a whole, but repeated surveys suggest much spatial variation within the estuary. Waves greatly enhance sediment transport in the bay, by approximately 30 times in storms, when coarse sand is mobilised. The estuarine sand fines landward, from medium- to very fine-grained. Grain size and petrological evidence suggest sediment is derived from erosion of glacial deposits in Cardigan Bay.

A highly skewed tidal wave creates strong flood currents and net flood sediment transport throughout the estuary and in the southwest portion of the bay. The estuary is generally well-mixed, and the tidal wave is a standing wave with a progressive component. The estuary comprises a two part hydrodynamic system, with decreased currents and sediment transport inland of a hard rock constriction.

Intertidal megaripples dominate large areas of the seaward portion of the estuary. They show very complex morphological and dynamic behaviour over a lunar cycle. Detailed velocity profile measurements over these megaripples, show complex relationships of bedform to flow. Flow parameters show considerable scatter, and have only weak correlations with bedform morphology or migration. Within each flood-ebb cycle, the relationship of shear velocity to roughness length appears related to the underlying bedforms. Natural variation of megaripple behaviour is a major factor in limiting palaeoflow estimates from deposits of intertidal megaripples.

A concluding chapter discusses the relationship between sea-level, sedimentation, and estuarine hydrodynamics, through the Holocene. Sea level rise brought drowning and erosion of coastal glacial complexes, leading to conditions allowing spit formation and growth, with, in the estuary, increased tidal asymmetry, salinity and low water elevation. Fine-grained estuarine sedimentation was initiated in the sheltered back-barrier region, intertidal flats and supratidal marshes prograded, and tidal channels were progressively restricted towards the northern side of the estuary mouth. Within the modern estuarine sand wedge, preserved estuarine sedimentary structures may exhibit an upwards-increasing expression of flood- directed sediment transport.

CONTENTS

VOLUME TWO

Chapter 6

Grain Size Investigations - Review and Results

Chapter 7

Sediment Transport Paths and Estuarine Morphological Change

Chapter 8

Concluding Remarks

List of Figures

Chapter 4

Chapter 5

Chapter 6

Chapter 7

Chapter 8

List of Enclosures

List of Tables

Chapter 4

Chapter 5

Chapter 6

Chapter 7

Chapter 3

Intertidal Bedform Behaviour

3.1 Introduction and Survey Objectives

This chapter describes a detailed study of the dynamics of intertidal megaripples, on a shoal in the Mawddach Estuary. There is a lack of studies of modern tidal bedforms, and a need for more work to understand the dynamics and controls of bedform behaviour. Little detail is known of the shape changes of megaripples over lunar cycles, and of the implications for the sedimentary structures preserved. Flow processes over tidal bedforms are important aspects of the flow-bed interaction, and these are considered in the following chapter.

A consequence of this lack of field studies, is that, presently, there are only rather simplified reconstructions of palaeoflow characteristics from preserved features of megaripples. Certainly, geologists have assumed that subtidal and intertidal bedforms exhibit very similar dynamic and structural characteristics, with little evidence one way or the other. This study directly addresses these questions.

Such process studies are justifiable in themselves, but this study is also relevant as an indication of the sedimentary structures likely to be dominant in the seaward half of the fine sand wedge at the surface of the estuary. Large areas of the estuary contain tidal megaripple fields (Fig. 3.0), which will be preserved as the tidal channels migrate. This study also provides data on sediment transport rates within the estuary, and an assessment of whether, when geologists measure preserved bedform migration rates, the measurements made are: firstly, representative of the bedform population; and, secondly, accurate measures of sediment transport rates.

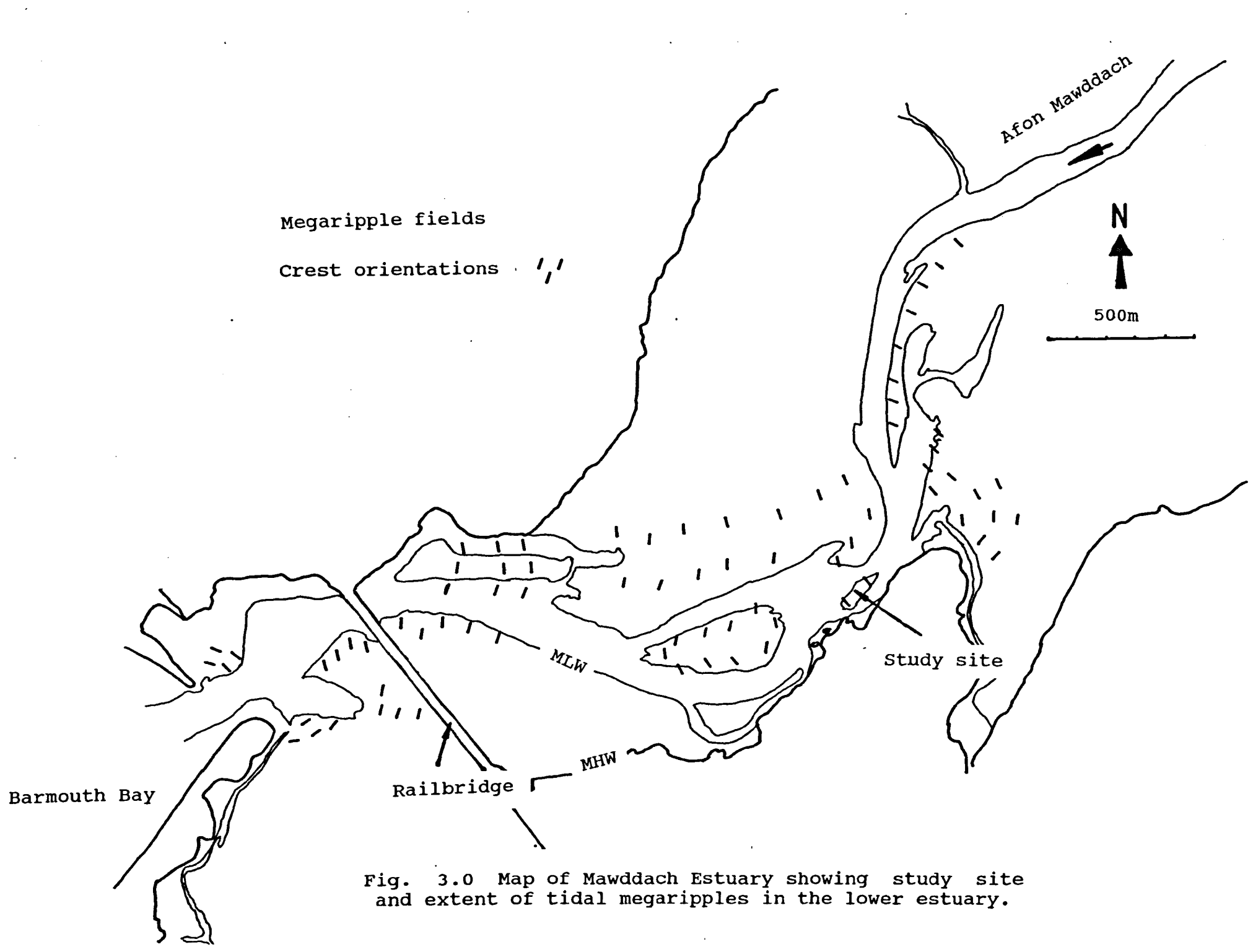

Fig. 3.0 Map of Mawddach Estuary showing study site and extent of tidal megaripples in the lower estuary.

Survey Objectives

Large areas of the Mawddach Estuary, particularly the lower estuary, contain intertidal or shallow subtidal megaripples. An intertidal site in the estuary which contained well developed bedforms was chosen for study. The objectives of this study of the intertidal megaripples were threefold :

1 - To provide a detailed study of intertidal megaripple morphology and dynamics. Such data have great use in both modern and ancient contexts, and there is a need to further explore megaripple behaviour in a variety of hydrodynamic settings;

2 - To examine the implications for reconstruction of palaeoflows from preserved megaripples. Terwindt & Brouwer (1986) stated; "(flow) reconstructions can only be based on a detailed analysis of the flow characteristics and bedform behaviour of recent analogues. Such studies are scarce for subtidal as well as intertidal settings." Allen & Homewood (1984) also make the case for further studies, because "despite the theoretical background which clearly indicates the very wide range of possibilities for sandwave geometry and structure, there is the danger that the few semi-quantitative documented examples will be regarded as the norm".

Aspects considered by this work will include how the geological measure of bedform migration, generally taken as representing net bed material transport, compares to other methods of measuring migration. Spatial and temporal variation in migration rates is also studied, to provide a measure of possible errors in sediment transport reconstructions.

Questions relevant to preservation potential of megaripples and associated features will also be considered; for example, how and under what circumstances are sedimentary structures preserved ? How much of a shoal is likely to be preserved, i.e. how much 'steady state' translative sediment transport occurs compared to net accumulation ?

The internal structures of megaripples have been sampled as part of this work, but will be published separately, when their analysis is complete;

3 - To develop the relationships of flow velocity and sediment flux via 'calibration' by megaripple migration; thus allowing estimates to be made of sediment flux within the Mawddach Estuary, using the measured current profiles presented in Chapter 2. These sediment fluxes will provide information on where and at what rate sediment accretion may be taking place.

In recent years, a great volume of literature on tidal bedforms and sediment transport has originated from workers in The Netherlands, who are concerned with the dynamics of the strongly tidal shallow estuaries (the 'Scheldes'); these constitute much of their North Sea coastline. There have also been significant contributions from workers studying the intertidal shoals of Bay of Fundy of the east coast of North America, an area of massive tidal ranges, up to 16.3m (McWhirter & McWhirter, 1975).

The study of such bedforms has been considered in many different contexts; these will be reviewed below after a brief definition of the terminology applied to these bedforms.

3.1.1 Bedform Terminology

In recent years, the nomenclature and classification of mesoscale sedimentary bedforms (i.e. those between 1m and 20-30m in wavelength) have been confused, as has their relationship to hydrodynamic setting (Boersma & Terwindt, 1981; Belderson et al, 1982; and Allen, 1984). Authors have used terms such as giant ripple, dune, sandwave, and megaripple; even this list is not exhaustive. The terms megaripple and sandwave are the ones used by most marine geologists; workers studying intertidal and shallow subtidal deposits especially use the term megaripple. Belderson et al (1982) discuss the use and merits of these terms.

Elliott & Gardiner (1981) described three tranverse intertidal bedform types from the Loughor Estuary :

1 - Ripples - Small scale bedforms produced either by tidal currents or local wind-generated waves;

2 - Megaripples - Mesoscale bedforms (wavelength 2.2 - 10.7m, height 0.08 - 0.36m) of two classes, distinguished by a range of morphological criteria;

3 - Sandwaves - Substantially larger two dimensional bedforms (wavelength <30m, height <1.25m) divisible into rippled and megarippled forms.

Here the term megaripple will be used, with the difference that their Type-1 and Type-2 distinction (from Dalrymple et al, 1978) is not used because it lacks immediate visualisation. Instead, the names 2D and 3D megaripple are used (meaning approximately two or three dimensional), so that:

2D megaripples have fairly straight, continuous, even elevation crests, lacking local scour pits in the trough;

and, 3D megaripples have sinuous, often discontinuous, uneven crests with well-developed scour pits.

In the field, there may be transitional forms between the categories described above.

Often a major feature of estuarine megaripples is the development of 'ebb caps' (Boersma & Terwindt, 1981), or 'ebb aprons' (Elliott & Gardiner, 1981), in the crestal area of flood-orientated forms. These reflect relatively limited reworking by the subordinate ebb tide; however, towards spring tides some megaripples may approach or attain complete reversal of asymmetry, i.e. ebb-orientation, and it is arguable whether the bedform possesses a large ebb cap or is a fully developed ebb bedform.

3.1.2 Previous Studies of Modern Bedforms

3.1.2.1 Recent Bed Sediment Transport

Megaripples indicate relatively high rates of bedload sediment transport and high tidal velocities, and as such can be indicators of the temporal and spatial variations in bedload sediment and water flux. Boothroyd & Hubbard (1975) used megaripple and sandwave orientation to infer direction and magnitude of sand movement; they directly related observed bedforms to the tidal current patterns over intertidal and shallow subtidal deltas in the Gulf of Maine. Klein (1970) found that bedform orientation showed excellent agreement with the dispersal pattern of sand stained with acrylic lacquer, and Wright et al (1975) used bedform orientation to study sediment transport patterns in the macrotidal Ord River, Western Australia. Harris (1988) provides excellent examples of the use of bedforms to indicate mutually evasive sediment transport paths in wide-mouthed estuaries.

Van den Berg (1982) describes the migration and deposits of megaripples in the Oosterschelde, The Netherlands, and shows how understanding of megaripple internal sedimentary structures can aid explanation of high sediment accretion rates in some tidal channels. Yang (1986b) investigated deducing sediment transport rates from current meter measurements over tidal megaripples, and Van den Berg (1987) tested bedload sediment transport equations by comparing results with megaripple migration data. Langhorne (1982) calibrated a sediment transport equation from the movement of subtidal bedforms.

Such studies have, therefore, demonstrable use in terms of navigation and engineering in coastal areas. For example, engineers may need to know by how much bed level may vary in an area before deciding whether and how to lay a structure on or beneath the sea bed, mariners may need to know how mobile a large sedimentary feature is.

3.1.2.2 Geological Significance

Recognition

Bedforms are also important in terms of their preserved sedimentary structures and, thus, the interpretation of the geological record. The recognition of structures, as products of a strongly tidal environment, is very important in terms of palaeogeographic reconstruction; this is of interest to mineral or hydrocarbon explorationists and academic researchers alike.

A benchmark in the description and process explanation of the suite of sedimentary structures formed by tidal megaripples was the paper by Boersma et al (1968). They described the internal structures in detail, including the role of the lee side eddy in producing the preserved structures. They were the first to discuss features of each 'tidal bundle'; that set of internal sedimentary structures produced by the action of one flood-ebb cycle over the bedform, which are separated from each other by erosional, non-depositional or mud-draped 'pause planes' (Kohsiek & Terwindt, 1981), the 'reactivation surfaces' of de Mowbray & Visser (1984) (see below). Visser (1980) noted an organised variation of structures, preserved in Holocene subtidal deposits. There was a sinusoidal variation of the thickness of preserved cross strata, which was related to spring - neap tidal cycles; furthermore, mud layers deposited in couplets were interpreted as related to high and low water slack water. They constituted, therefore, a unique criterion for distinguishing the subtidal environment.

The role of recognising flow unsteadiness in the identification of tidal deposits was emphasised by de Mowbray & Visser (1984), who discussed 'reactivation surfaces' (erosional or non-depositional surfaces within a cross stratified set) in deposits produced by migrating megaripples. They noted that such surfaces could be produced both by 'overtaking' of one megaripple by another, or by the action of a subordinate current. The morphology of the reactivation structures is most dependent on the relative strengths of the dominant and subordinate current - where the stronger the subordinate flow, the greater the reworking of the lee slope foresets. With strong subordinate

currents at spring tides, large low angle discordances are produced between the steep foresets of the previous dominant tide and the reactivation structures. At intermediate tides reactivation structures only developed in the upper parts of the foresets; at neap tides, no evidence of reworking was preserved.

Terwindt (1981) described, in great detail, the processes and products of tidal bedform migration, and he distinguished a number of lithofacies related to the intensity of tidal currents and wave action. His lithofacies 'STRO CUR' (strong currents) and 'MED CUR' (medium currents) both relate to sediment transported as migrating megaripples. Terwindt (1988) reviewed diagnostic criteria for distinguishing siliclastic tidal deposits.

Langhorne & Read (1986) described the occurrence, and discussed the preservation potential of various intertidal structures, related to megaripples; they noted that even in areas of net sediment accretion, 'master bedding' (Allen, 1980), (the largest cross- bedding type produced by migrating megaripples), may not be preserved. Larcombe (1986) noted that on a shoal with net flood-directed sediment transport, in places the dominant preserved structure was ebb- orientated megaripple foresets. This was explained in terms of systematic changes in the shape of an intertidal shoal over a spring-neap lunar cycle. Hubbard et al (1979) considered how tide-dominated inlet channels would be recorded in the geological record. They noted that the primary sedimentary structures of some intertidal and subtidal bedforms do not reflect their surface morphology.

Palaeoflow Reconstruction

A major part of bedform research has been directed towards attempts to reconstruct hydrodynamic parameters of palaeocurrents, from a study of preserved sedimentary structures. The reasoning has been that only when the relationship between the dynamics of modern-day tidal bedforms and their related flows are more fully understood, can the reconstruction of

palaeoflow conditions (such as flow velocity, water depth, tidal range and sediment transport rate) be seriously attempted.

One of the first detailed studies to combine description of megaripple internal structures with measurements of the flows which produced them was that of Boersma & Terwindt (1981). They noted that 2D and 3D megaripples had different structural responses to the neap-spring variation in tidal velocity. Terwindt (1981) provided limited threshold speeds for the formation of the lithofacies STRO CUR and MED CUR (see above). Kohsiek & Terwindt (1981) distinguished five different types of cross-bedding formed as topsets and foresets of intertidal megaripples; by using different colours of tracer sand, they were able to mark the 'pause planes' between tidal bundles and so date the deposits. Thus, they gave threshold depth mean velocities for the formation of the foreset and topset types, and pointed towards the use of studying topset types for palaeoflow reconstruction.

Yang & Nio (1985) considered a time-series of preserved tidal bundles from the Oosterschelde and the Roda Sandstone. By use of Fourier analysis of tidal bundle thickness, they were able to estimate the periods and phases of the most important periodic components. Use of filters resolved the sequence of tidal bundle thicknesses and they estimated the relative amplitude of diurnal, random, neap-spring and longer-period components. Through simple relationships between tidal range, shear velocity and a sediment transport function, they obtained very reasonable results for the spring and neap tidal ranges - and for the effect of storms on the tidal range. Their method contains some oversimplifications in its treatment of the tidal dynamics; likewise, bundle sequences long enough to allow frequency analysis are very rare. However, it is an elegant example of the use of time-series analysis for palaeoflow reconstruction.

Other studies have used empirical sediment transport equations to convert measured megaripple cross-bedding back to palaeotidal characteristics, (eg. Allen, 1981a,b; Siegenthaler, 1982; Nio et al, 1983; Teyssen, 1984). Allen & Homewood (1984) calculated palaeoflows using

grain size and preserved bedform type, combined with the von Karman logarithmic velocity profile. Their reliance on assumed flow roughness length has since gained criticism, due to the large potential errors it brings to the results. However, the work contributed greatly to the understanding of Miocene Alpine palaeogeography.

In an very important contribution to the study of bedform dynamics, Terwindt & Brouwer (1986) carried out a detailed survey of 2D and 3D megaripples in the Dutch Westerschlede estuary. Whilst not directly considering internal structures, they showed that palaeoflow depth determination was not possible from measures of megaripple size or migration. However, migration rate (i.e. tidal bundle horizontal width) was well correlated with the peak depth mean flow velocity of the dominant tide. Only this flow measure and the Velocity Symmetry Index (VAI, defined in Chapter 4) showed recognisable systematic variation with the neap- spring cycle.

Their work also increased information on velocity thresholds of megaripple migration, shape change and symmetry reversal. They also presented correlations of calculated total sediment transport with migration, inferring that migration rate may be useful as a measure of total sediment transport as well as the assumed good relation to (calculated) bedload transport. An important conclusion was that 3D megaripples undergo much more variability in current direction, during periods of appreciable sand transport, than do 2D forms.

Terwindt (1988) provides a review of work aimed at palaeoflow reconstruction in coastal siliclastic tidal environments.

Other Research

Some bedform research has not been directly aimed towards either the identification of tidal deposits or reconstruction of palaeohydraulics, although many have relevance in these fields. Broadly this research consists of one or more of field observations, flume work, theoretical analysis, and study of the

dynamics of individual megaripples and their populations.

Notable field descriptions include that of Dalrymple et al (1978) in the Bay of Fundy, who presented bedform phase diagrams constructed from a very large data base. They demonstrated that two types of megaripple occur on intertidal sand bodies, each with a discrete hydraulic stability field. Zarillo (1982) described tidal megaripples and sandwaves in an estuary in Georgia, and also discussed their stability fields.

A large volume of relevant work has been published by J.R.L. Allen and coworkers, including discussing bedform hierarchies (eg. Allen, 1968,74) and presenting data from repeated surveys of megaripples on an intertidal shoal (Allen & Friend, 1976a). From this Allen has developed concepts of dynamic bedform populations (Allen & Friend, 1976b; Allen, 1976a,b,d; Allen, 1978) applicable to bedforms in either unidirectional or tidal flows.

Various authors have used results of flume work and theoretical considerations to study megaripple shape, stability and change. Much of the work relates to prediction of bed roughness and resistance to flow in alluvial channels. Vanoni (1974) presented diagrams and derived relationships from which, using knowledge of Froude number, simple measures of grain size distribution, and grain Reynolds number, he could predict the type of bedform present. His method had varying degrees of agreement with field data. Yalin & Karahan (1979) discussed bedform steepness, showing that maximum megaripple steepness increases with relative flow depth. Costello & Southard (1981) found in flume experiments that 2D and 3D megaripples are hydrodynamically distinct forms, with the 3D forms occurring at higher flow velocities, agreeing with the field evidence of Dalrymple et al (1978) and Terwindt & Brouwer (1986). Wijbenga & Klaasen (1983) studied the changes in dimensions of flume-generated megaripples under unsteady flows, and developed the ideas of Allen (cited above) on the coefficient of change of bedform adaptation.

Methods of predicting megaripple dimensions and bed roughness were reviewed by van Rijn (1984), who proposed new predictive relationships

based on both flume and field data. His method was used also to predict the flow depth and the total bed material load. Contrary to Vanoni (1974), he found the Froude number was unimportant in the generation of ripples and megaripples.

3.2 The Fegla Fach Megaripple Shoal

This intertidal shoal is situated 2.2km landward of the estuary mouth, near the south bank of the lower estuary (Fig. 3.1). The shoal is approximately 150m long and 50m wide, at low water; much of the surrounding sandflats are also megarippled. The bed consists of well-sorted fine sand, of mean size 280um.

3.2.1 Surveying Megaripple Trains

The morphology and position of the megaripples of the shoal were studied using two parallel survey lines, 15m apart. Line A, nearest the shore, was 40m long; Line B, 48m. The survey lines were orientated 050 - 230 degrees, perpendicular to megaripple crestlines. Both lines were surveyed at each low tide at horizontal intervals of no more than 0.5m; often, considerably less in areas of highly variable relief such as crests, brink points, toes and troughs of the megaripples. The position of other features, such as late stage runoff microdeltas, eroded lee faces etc. were also noted.

During daylight hours, standard levelling techniques (i.e. a builders level and graduated staff) were employed to survey the two linear transects. The level was generally positioned near the centre of the survey line, offset from the line by a couple of metres. At night, it proved effective to illuminate the staff by a torch fixed to its top. Daytime accuracy was maintained by this method, even in heavy rain and at ranges of up to 50m. The transects were reduced to a common datum level, by reference to 3 independent points, sited one at each end of Line B and in the middle of Line A. Repeated sightings were taken to at least two of these points before and after each survey, and so survey accuracy could be gauged. Elevation readings were read to +/- 1mm, and horizontal accuracy was +/- 3cm, similar to that obtained by Larcombe (1986). The accuracy of measurement was therefore greater than the possible (or useful) precision of designating the position of a particular feature (such as the brink point, or toe, etc.) on the rippled megaripples.

Fig. 3.1
Location of Fegla Fach Shoal

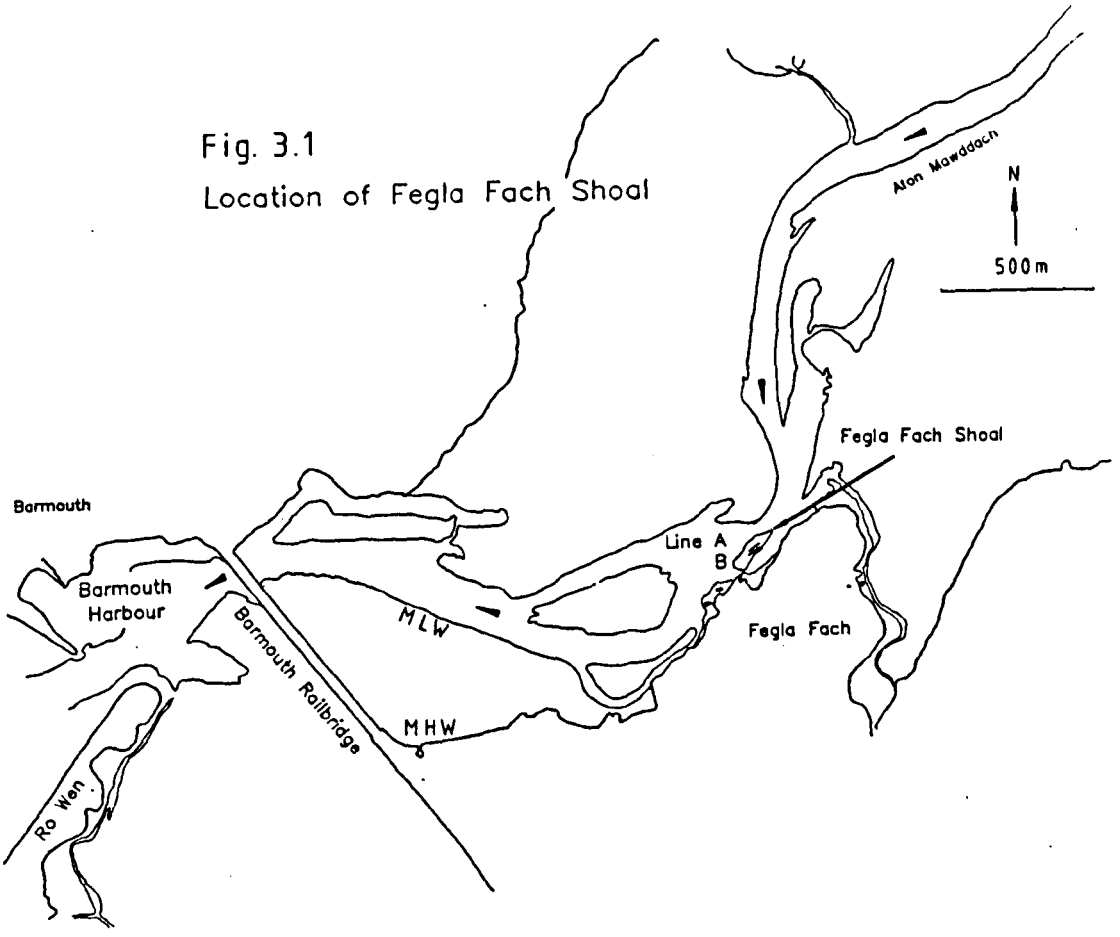

Fig. 3.2
Predicted Tidal Heights - July 1986

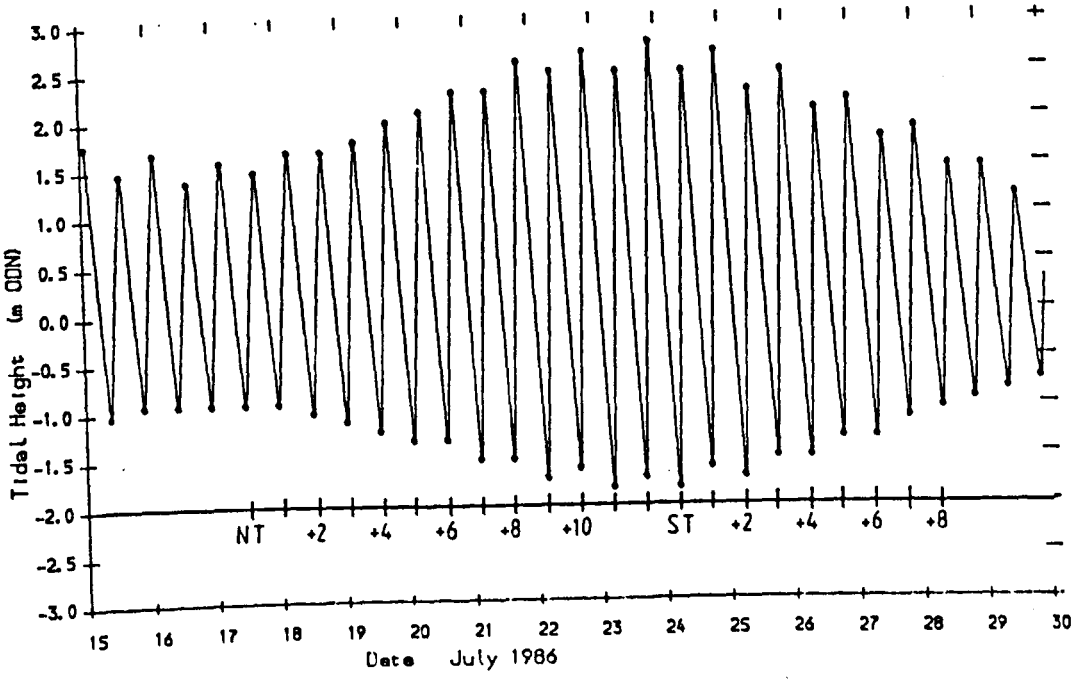

3.2.2 Survey Dates and Tides

The survey period covered 24 consecutive tides, i.e. day and night, from the 16th - 28th July 1986. Line A was surveyed throughout but was limited in length to 22m at NT-2 and 33m at NT-1. Line B was not surveyed at NT-2 and NT-1, and was limited in length to 35m at ST+4. Thus there are 20 full simultaneous data sets, NT - ST+3 and ST+5 - ST+8.

Neap tide (NT) occurred prior to LW3, with a predicted range of 2.45m. Spring tide (ST) was prior to LW16 with a range of 4.45m. The following neap tide occurred 6 tides after the end of the survey period, i.e. LW30 (Fig 3.2). As discussed in Chapter 2 the spatial variation of tidal height along the estuary is greatest for LW, not HW. However, as the shoal studied is exposed for a few hours around each LW it is the height of HW that is likely to be a greater factor in determining sediment transport, than the local LW elevation.

The diurnal variation in tidal heights, and in particular that of HW, is most pronounced at and following ST, corresponding to tides NT+9 - ST+6. Over this period, even-numbered tides experienced the greater tidal fall, i.e. greater relative ebb discharge, whereas odd-numbered profiles had greater relative flood flow. This pronounced diurnal variation in HW (which has an amplitude of up to 0.4m) may be a significant factor in controlling bedform morphometry, migration and sediment transport over the shoal.

The weather during the survey period was generally good, with light winds. However, the survey on tide NT+5 was conducted in heavy rain, and for tides ST+9 - ST+11, inclusive, continuous rain combined with a strong up-estuary wind caused the shoal to remain submerged at low water, so forcing the abandonment of the proposed levelling surveys.

Table 3.1 lists the dates of low waters, the profile number (i.e. the survey number) and the notation used in the text to refer to that time and survey. The notation serves to illustrate the stage of the lunar cycle.

Table 3.1

Notation used to refer to surveys

Date July'86	Survey No.	Notation	Date July'86	Survey No.	Notation
16.4	LW1	NT-2	22.6	LW13	NT+10
16.9	2	NT-1	23.1	14	NT+11
17.4	3	NT	23.7	15	NT+12
17.9	4	NT+1	24.2	16	ST
18.5	5	NT+2	24.7	17	ST+1
19.0	6	NT+3	25.2	18	ST+2
19.5	7	NT+4	25.7	19	ST+3
20.0	8	NT+5	26.2	20	ST+4
20.6	9	NT+6	26.7	21	ST+5
21.1	10	NT+7	27.3	22	ST+6
21.6	11	NT+8	27.8	23	ST+7
22.1	12	NT+9	28.3	24	ST+8

3.2.3 Megaripple Morphological Parameters

In order to describe the size and form of the megaripples, a number of terms are used; these are defined below and in Fig. 3.3.

Wavelength L = distance between successive troughs

Height h = crest - trough elevation difference

Flatness L/h = ratio of wavelength to height

Symmetry Index b/a = crest - trough distance divided by trough - crest distance. In this study a value of > 1 denotes an ebb-orientation and < 1 denotes a flood-orientation.

Mean bed level B = the mean level of sediment over the transect

Mean crest level C = the mean elevation of crests over the transect

Mean trough level T = the mean elevation of troughs over the transect.

Parameters B, C, and T are all relative to the same fixed datum level; so the variation in bed parameters can be related to the variation in sediment

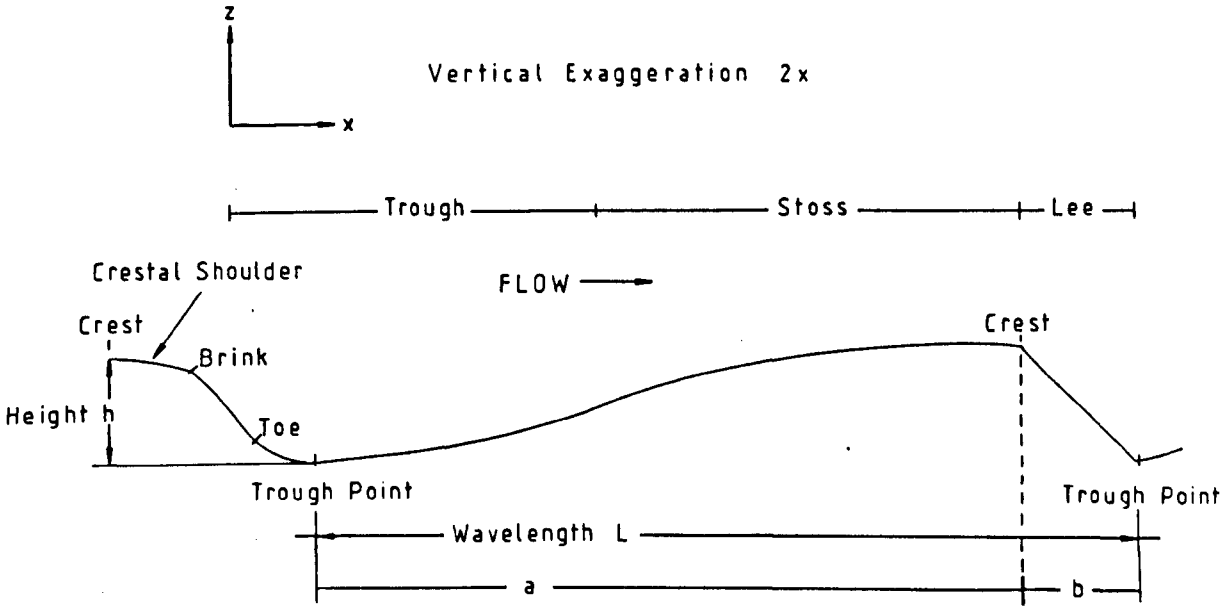

Fig. 3.3 Megaripple features and nomenclature

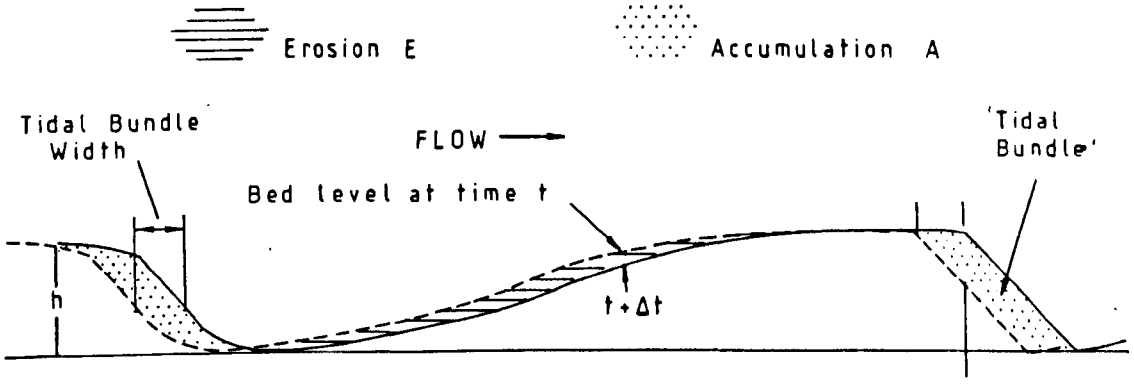

Fig. 3.4

Migration of megaripple showing form of tidal bundle (schematic)

levels over the transects. The equivalent parameters of Terwindt & Brouwer (1986) relate only to the mean bed level on the survey date, so the possible effects of net gain or loss of sediment on the bedforms were not ascertained.

The comparison of successive shoal transects enables the Volume of Erosion (E), and Volume of Accumulation (A) to be determined (Fig. 3.4). Bedform migration rate was calculated by three methods: one used a lag cross-correlation method (Numerical Algorithms Group Ltd., 1986), similar to that used by Langhorne & Read (1986), from which the Correlation Coefficient (CC) between successive profiles is also obtained; other methods used measured migration distances of particular bedform features (see Section 3.7.2, this chapter).

The number of bedforms on survey Line A varied between 6 and 10 (Figs. 3.5 & 3.7); on Line B, between 7 and 16 (Figs. 3.6 & 3.8).

The following section will detail the variation in bedform dimensions on Line A, which had the Velocity Gradient Unit (see Chapter 4) at its' centre. Detailed on how the data from Line B compares, and interpretation of the similarities and differences, is found in Section 3.6.

Fig. 3.5

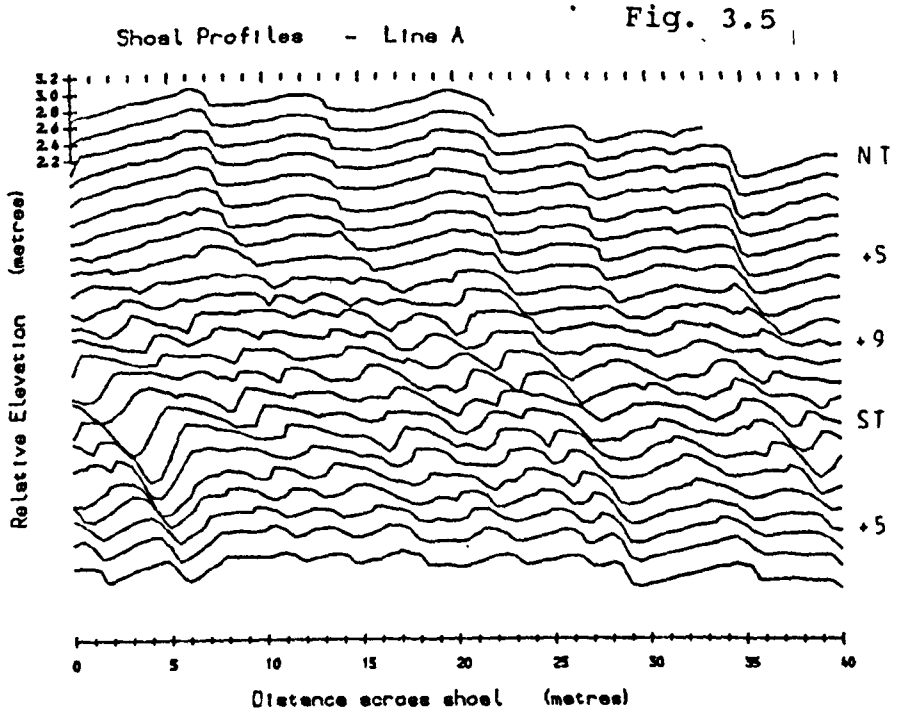
Shoal Profiles - Line A
Relative Elevation (metres)
3.2
3.0
2.8
2.6
2.4
2.2
NT
+5
+9
ST
+5
0
5
10
15
20
25
30
35
40
Distance across shoal (metres)

Fig. 3.6

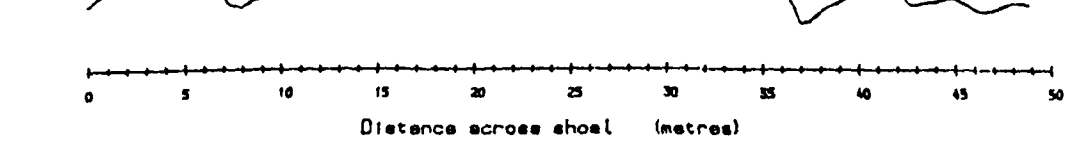
Shoal Profiles - Line B
Relative Elevation (metres)
3.2
3.0
2.8
2.6
2.4
2.2
NT
+5
+9
ST
+3
+5
0
5
10
15
20
25
30
35
40
45
50
Distance across shoal (metres)

Fig. 3.7

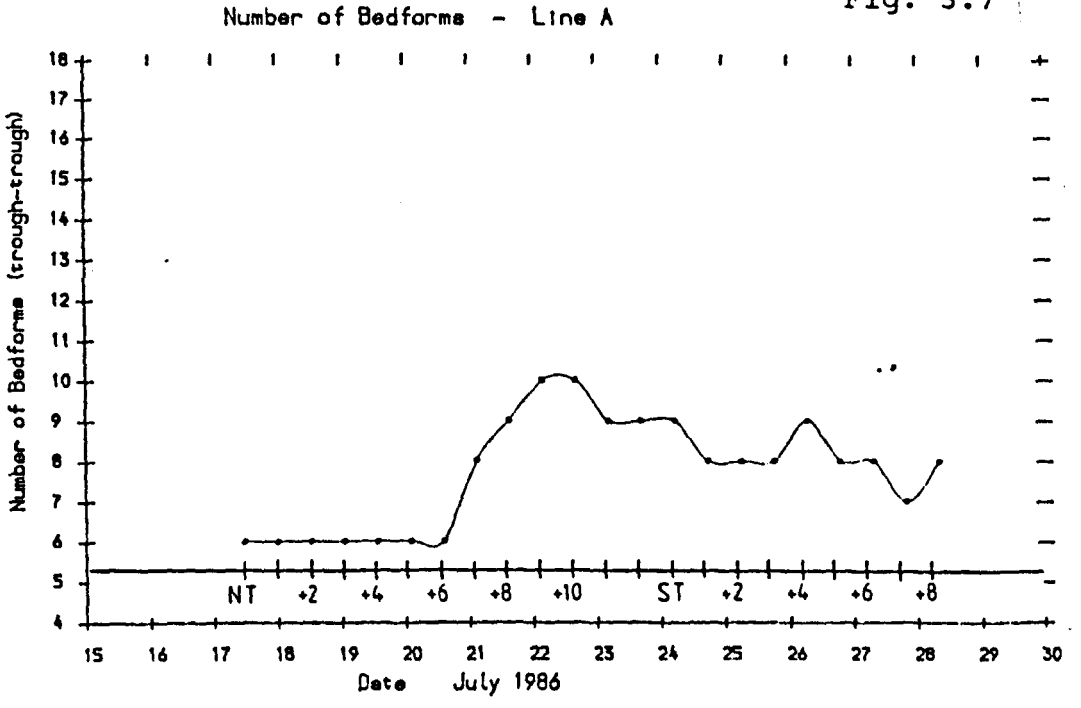
Number of Bedforms - Line A
Number of Bedforms (trough-trough)
18
17
16
15
14
13
12
11
10
9
8
7
6
5
4
NT
+2
+4
+6
+8
+10
ST
+2
+4
+6
+8
15
16
17
18
19
20
21
22
23
24
25
26
27
28
29
30
Date July 1986

Fig. 3.8

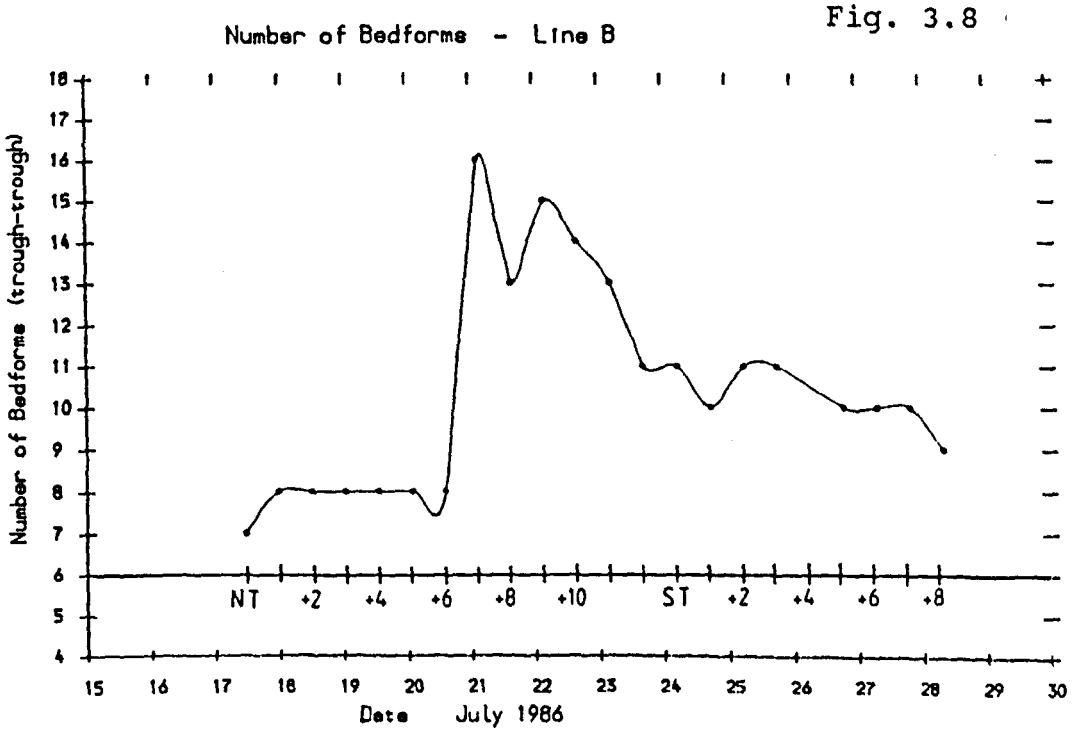
Number of Bedforms - Line B
Number of Bedforms (trough-trough)
18
17
16
15
14
13
12
11
10
9
8
7
6
5
4
NT
+2
+4
+6
+8
+10
ST
+2
+4
+6
+8
15
16
17
18
19
20
21
22
23
24
25
26
27
28
29
30
Date July 1986

3.3 Results - Bedform Dimensions - Line A

3.3.1 Variation with Time

3.3.1.1 Mean Symmetry Index (b/a) (Fig. 3.9)

The mean symmetry index varied over the study period between 0.48 and 3.57, representing flood and ebb megaripple orientations respectively. The maximum mean asymmetry occurred with ebb-orientated forms, which may be expected with surveys done at LW over megaripples which evidently change their shape considerably due to tidal action.

For 5 tides after NT, flood-orientated bedforms occurred at LW, displaying their highest asymmetry at NT+4. The bedform assemblage approached a symmetrical form at NT+6, then rapidly increased in ebb-orientation to peak at NT+9, but decreased towards ST itself. After a sustained peak of 2.7 at ST+2 - ST+4 there was a single tide decrease to near-symmetrical forms, remaining so until the end of the study period.

3.3.1.2 Mean Height (h) (Fig. 3.10)

Mean bedform height varied between 0.16m and 0.31m, at NT+10 and ST+2 respectively. Prior to ST+2 there was an increase in h of 0.08m in one tide.

From NT a general decrease in height occurred over 10 tides, with the exception of NT+5. Heights increased from NT+10 to a peak at ST+2, but as with the symmetry there was a decrease at ST itself. Following the peak at ST+2 to the end of the survey h generally decreased.

3.3.1.3 Mean Wavelength (L) (Fig. 3.11)

Mean wavelength varied between 3.52m at NT+10 and 5.91m at NT+3, although from NT+5 L was constant between 5.8m and 5.9m.

Between NT+6 and NT+7 the formation of short wavelength bedforms superimposed upon the larger forms reduced the mean wavelength rapidly to

Fig. 3.9 Mean Bedform Symmetry Index - Line A

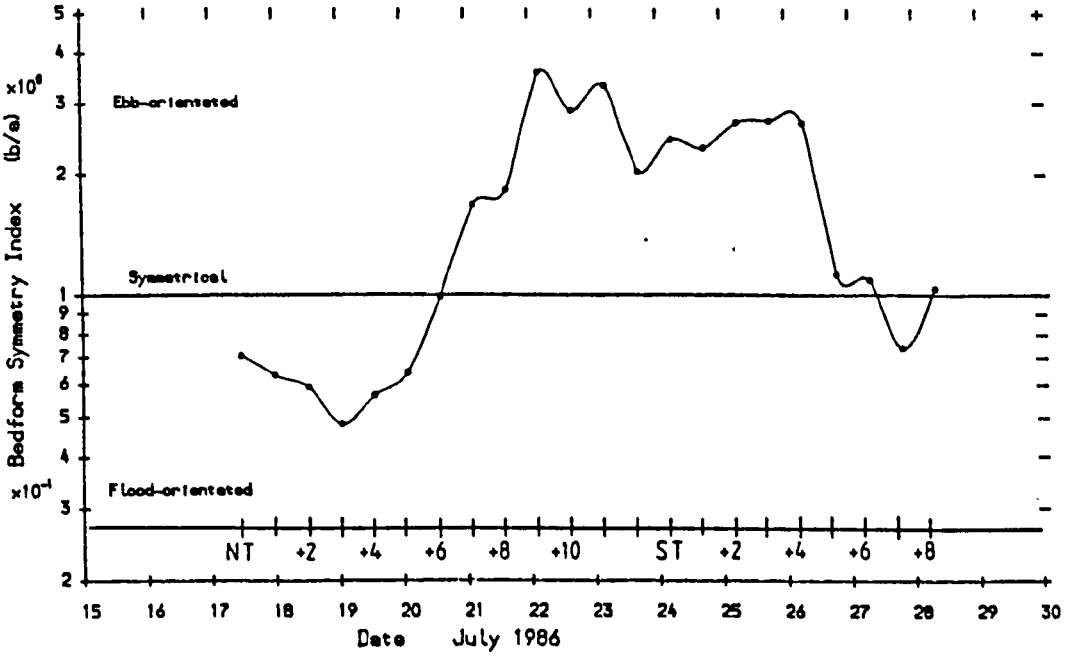

Fig. 3.10 Mean Bedform Height - Line A

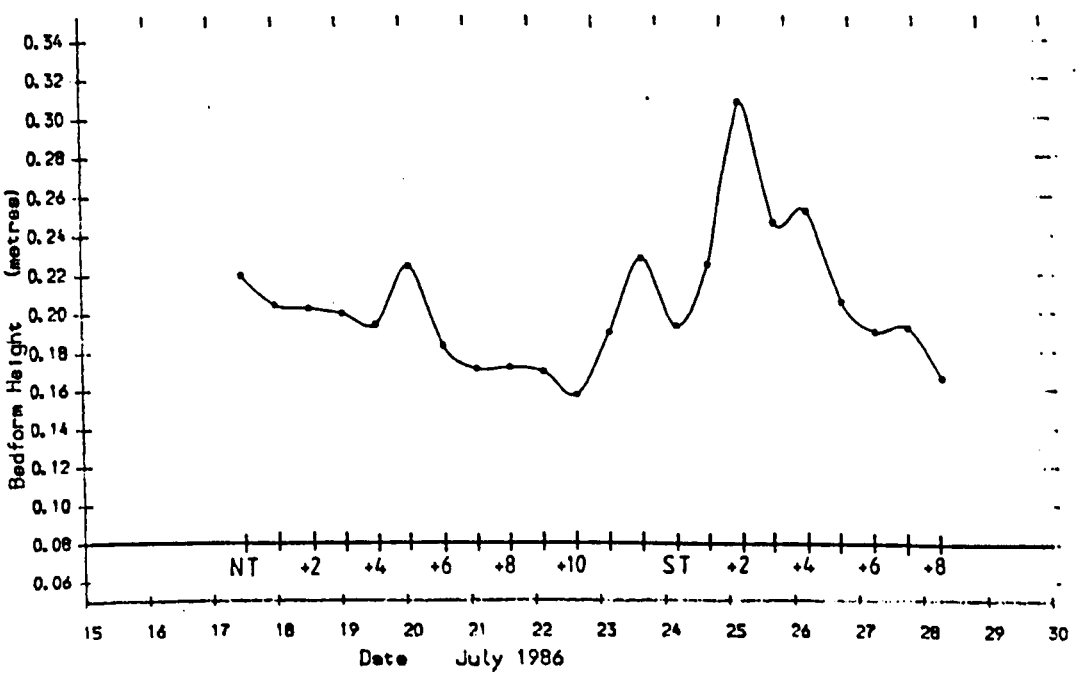

Fig. 3.11 Mean Bedform Wavelength - Line A

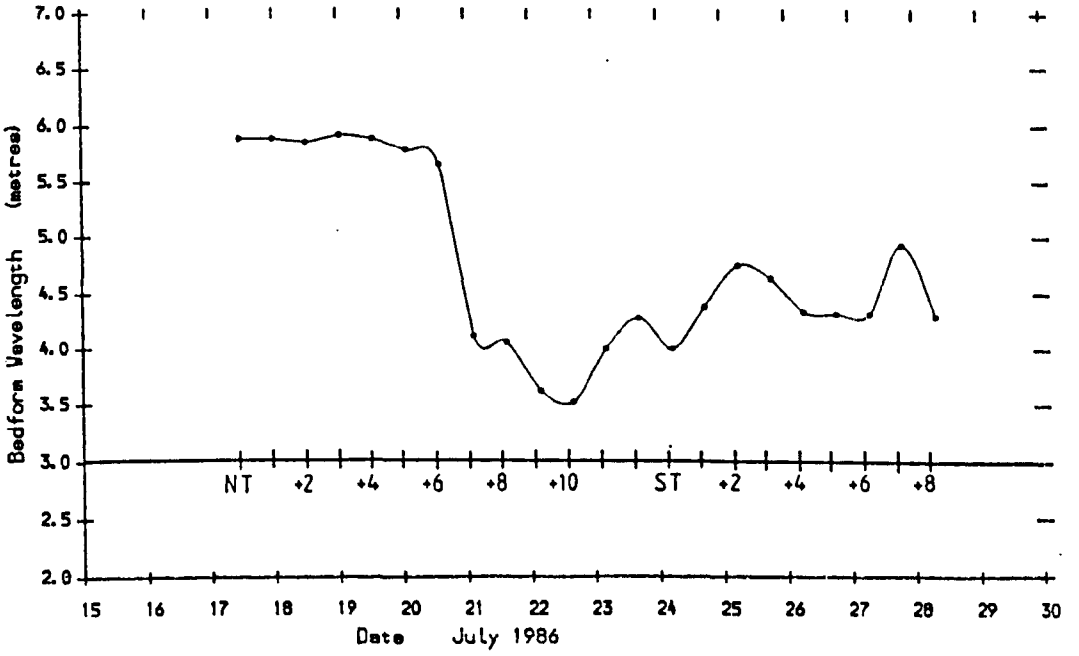

Fig. 3.12 Mean Bedform Flatness - Line A

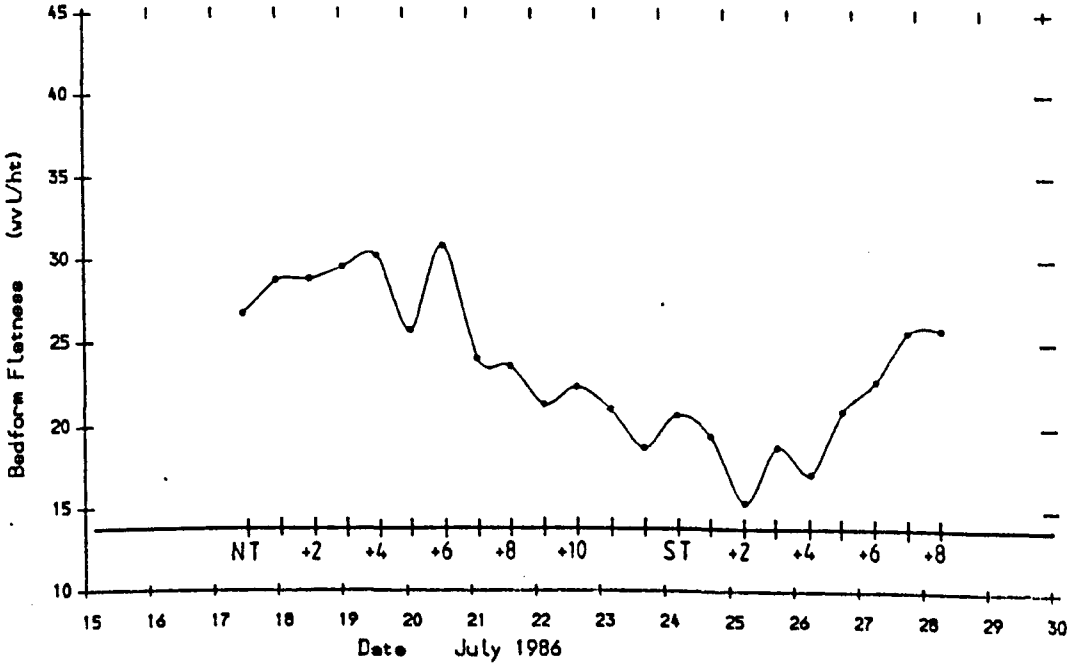

4.1m (see later discussion of bedform population structure), and this reduced further to the minimum at NT+10. In common with b/a and h, L increased to peak at ST+2, but with a decrease at ST itself. Wavelength remained between 4.3m and 4.9m until the study end.

3.3.1.4 Mean Flatness (L/h) (Fig. 3.12)

This parameter varied between 15.4 at ST+2 and 30.9 at NT+6, i.e. bedforms were steepest just after spring tides and flattest halfway between NT and ST. At NT+5, the decreased flatness was due to a 0.03m height increase. Over the following 9 tides (to ST+2) flatness decreased in a fluctuating manner, including higher values at NT+10 and ST; it then increased rapidly to the end of the study period.

3.3.1.5 Mean Bed Level (B), Crest Level (C) and Trough Level (T) (Fig. 3.13)

Mean bed level varied by up to 0.052m over the study period, being highest at ST+7 and lowest at ST+8. Bed levels increased by 0.04m from NT+7 and NT+9, and by 0.034 from ST+4 to ST+7. The only significant drop occurred prior to ST+8, of 0.052m in a single tide, and prior to this time both B and C had been gradually increasing with time.

The mean crest and trough levels must be intrinsically linked to the curve of B, but as their variation does not purely reflect that of B it is clear that they are parameters with their own developmental histories (Table 3.2 and Fig. 3.13).

There is a stronger correlation of the B curve with T than with C. The curve of T is strongly in phase with B but as expected is more variable. Crest variation C is broadly in phase with B but not in detail.

Mean trough levels increased by 0.118m between NT and NT+10, though not continuously. It then dropped through ST to the minimum at ST+2, after which it increased by 0.1m in 4 tides.

Fig. 3.13 Mean Crest, Trough and Bed Elevation - Line A

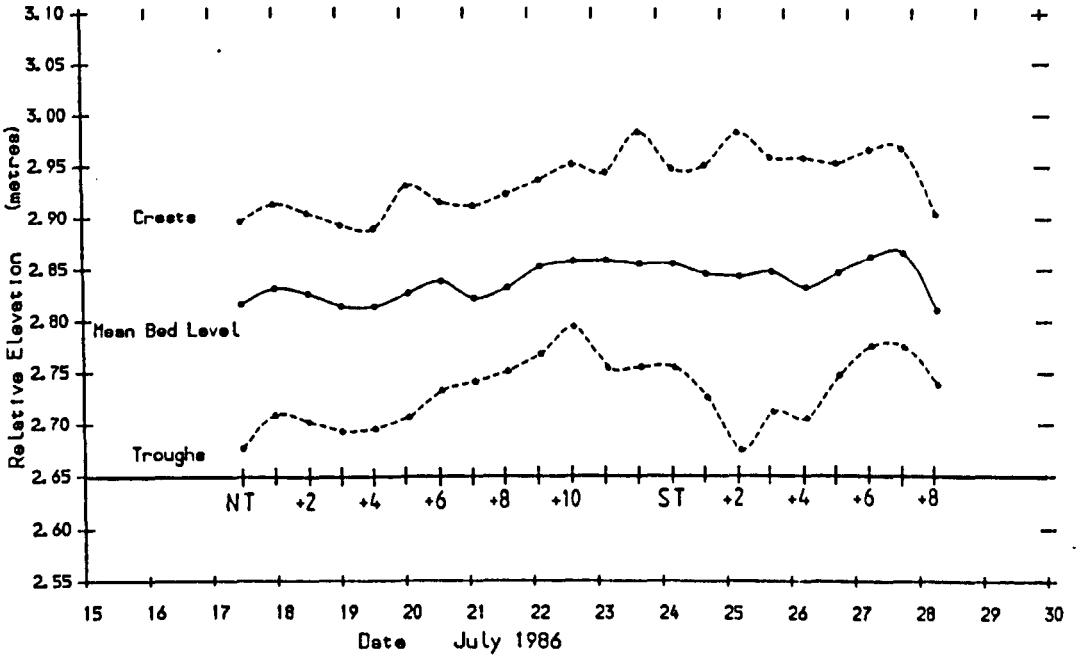

Fig. 3.14 Bedform Symmetry Index v Tidal Range - Line A

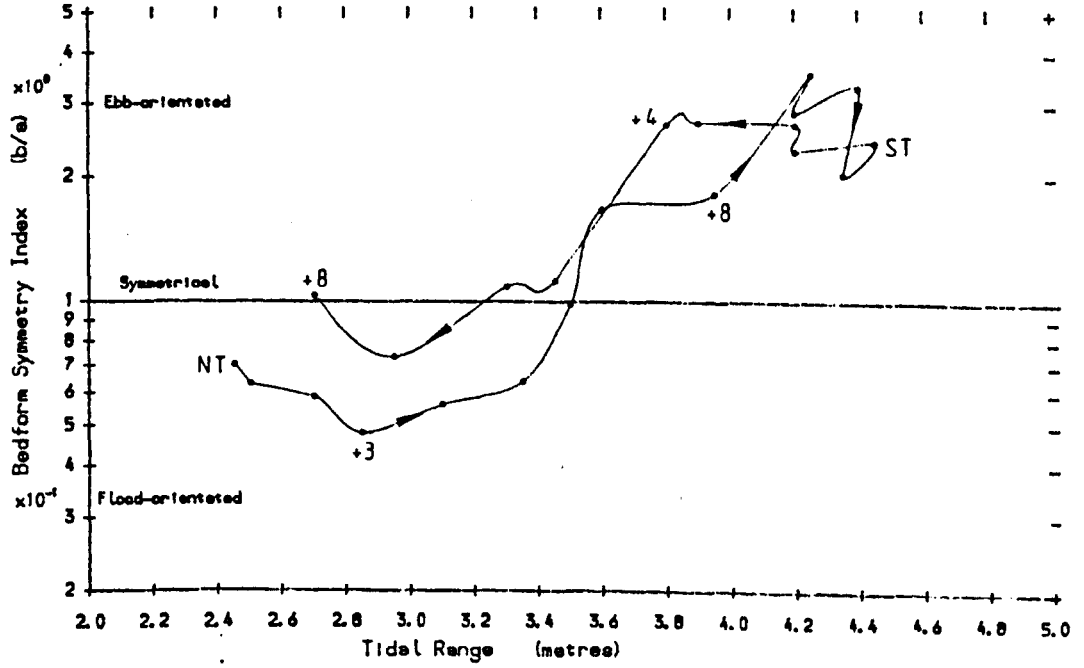

Mean crest levels showed a less clear pattern. They broadly decreased from NT to NT+4, increased to NT+12 and remained high until ST+7, where in one tide they dropped 0.063m.

Table 3.2

Times of extreme Bed Levels

Parameter	B	C	T
Highest	ST+7	NT+12	NT+10
Lowest	ST+8	NT+4	ST+2
Total variation (metres)	0.052	0.095	0.119

3.3.1.6 Qualitative Relationship between Morphometric Parameters

The curves of L and h show some similarity, with low values towards the middle of the study period on increasing tidal ranges, and increasing again with the spring tidal period. These two parameters are particularly closely-related between NT+9 and ST+3, which corresponds to a period where the surveyed megaripples displayed strong ebb orientation. Furthermore, both L/h and T were decreasing and reaching their lowest values.

Other studies have found some of these attributes to be sometimes co-related. Boersma & Terwindt (1981), Terwindt & Brouwer (1986) and Larcombe (1986) have noted increased wavelengths and heights with decreased trough elevations. Jones (1984) also found strong periodic correlation of L and h, though did not present data on trough elevation. The data presented by Allen & Friend (1976a) also show some correlation of L and h, though only around spring tides. Indeed this is a common feature; the relationships between L, h and T are strongest around spring tides, when

bedforms are most active, i.e. migration rates are highest.

However, care must be taken in the interpretation of morphometric changes and relationships as there are a number of factors which are not a simple function of the tidal conditions. For example, bedform crest elevations may be lowered, and trough elevations raised, where waves are present due to high winds (Larcombe, unpublished data), increasing flatness. In this study flatness increased when megaripples were near-symmetrical, at NT+7 - NT+9, prior to the generation of new short wavelength ebb-orientated forms.

3.3.2 Variation with Predicted Tidal Range

As an aid to interpretation of the morphological data, a series of plots have been constructed relating the measured morphometric parameters to predicted tidal range. Firstly, from these diagrams conclusions may be reached regarding the 'time-lag' of parameters, a term which, modified after Terwindt & Brouwer (1986), is here defined as the number of tides after ST or NT at which maximum or minimum values are attained. Secondly, they can help define different stages of bedform development over the lunar cycle and elucidate the dominant processes and controls acting upon the bedforms.

There follows a description of the diagrams and discussion of their interpretation.

3.3.2.1 Mean Symmetry Index (b/a) (Fig. 3.14)

The data show an overall increase in relative ebb orientation with tidal range, which may be a result of one or both of the following:

1) a systematic change with increasing tidal range of increasing ebb/flood bedload transport ratio;

2) the bedforms surveyed at each LW were flood- orientated megaripples, that have been reworked and reversed to various extents by the ebb tide.

As shown in Chapter 2 and by the current meter records in Chapter 4, there is no evidence to support the first hypothesis. It will be demonstrated below that the bedforms are flood-dominated throughout the spring-neap cycle, and are reversed by increasing amounts with increasing tidal range.

At low and medium tidal ranges, i.e. <4m, the megaripples are generally more flood-orientated on increasing tidal ranges, and there is a 3 tide lag between NT and maximum flood asymmetry. Due to a lag in 'reworking' the already flood-orientated bedforms to a reversed asymmetry by each ebb tide, hysteresis occurs in the b/a curve. This is despite the fact that at tidal ranges above 4.1m megaripples are slightly less ebb-asymmetric on falling tidal ranges. There are at least five possible explanations for this clockwise hysteresis at spring tides:

1) the data were insufficient to fully reflect the relationship between tidal range and b/a, and/or to remove the natural spread of b/a values occurring in the area;

2) at the highest flow strengths there is a natural change in megaripple form, which slightly reduces their asymmetry;

3) the ebb/flood bedload transport ratio (<1) moves closer to unity at spring tides;

4) newly created short wavelength and highly asymmetrical bedforms develop towards ST into less asymmetrical forms;

and, 5) tidal range is not a sufficiently satisfactory way of representing tidal flow severity.

The representative nature of the data can be tested by comparison of Line A data with Line B. This is done in more detail later (Section 3.6); here, it is sufficient to note that Line B megaripples also show a weak clockwise hysteresis around spring tide. A total of 19 - 25 megaripples per tide were surveyed; this would suggest that the trend is a real one.

However, analysis of the change in b/a for each individual megaripple reveals that between NT+9 and ST newly-created forms, small in both L and

h, do change significantly. From a flat almost delta-like morphology they develop a more rounded form with the crest separated from the slip face by a crestal shoulder (Allen, 1984, Vol I, Fig. 8.2) (see the different crestal zones of the 2 bedforms illustrated in Fig. 3.3). So point 4 (above) is a significant factor. The spread of b/a values co-existing at each stage of the tidal cycle will be discussed below.

To the author's knowledge, the only published field data on the changes in mean megaripple symmetry index with varying strength of flow is that of Terwindt & Brouwer (1986), who present data collected over a period of five weeks, from 27m long transects over both 2D and 3D intertidal megaripples. Each survey covered between 4 and 6 complete megaripples. The megaripples remained flood-orientated throughout the study period, and the 3D field were more symmetrical at ST than at NT. This was due to ebb cap formation at ST which resulted in more symmetrical rounded crests emerging at LW. The 2D field had quite variable b/a values, and did not show specific trends with time or tidal range.

This study is significantly different, because ebb caps or complete ebb-orientation occurred at virtually all stages of the lunar cycle; hence, the symmetry index is, throughout, strongly related to the degree of megaripple reversal. However, neither study indicates that at the highest flow strengths there is an organised decrease in asymmetry as part of a change in form.

Having noted that the pre-spring strongest ebb orientations resulted essentially from megaripple population changes, we can note that there is a 3 (-4) tide lag in peak asymmetry at both NT and ST.

3.3.2.2 Mean Height (h) (Fig. 3.15)

Height shows considerable hysteresis around spring tides, with a 2-tide lag in attaining maximum height. In two tides from ST, h increased by 0.115m to 0.308m, which suggests that the bedforms are most active around spring tides, undergoing considerable modification from their height

of only 0.16m at NT+10. Other studies (eg. Allen & Friend, 1976a,b; Boersma & Terwindt, 1981; Elliott & Gardiner, 1981; Dalrymple, 1984; Jones, 1984; Larcombe, 1986) have also shown increased heights of intertidal megaripples at spring tides, and lower heights at neaps. Larcombe (1986) reported a 2-tide lag in maximum height, and Terwindt & Brouwer (1986) a 3-tide lag, both being studies of 3D megaripples.

Data obtained from 2D megaripple fields has shown maximum height one tide before ST (Terwindt & Brouwer, 1986) and between 4 and 8 tides before ST (Jones, 1984). In both these studies, the symmetry index decreased towards ST, and in the latter case migration direction was reversed.

The plotting of height against tidal range (Fig. 3.15) reveals a 3-stage diagram, with divisions at tidal range of approximately 3.4m and 4.1m. These divisions may be interpreted in broad terms of megaripple activity thresholds. At the highest tidal ranges the ebb flow is sufficient for ebb-orientated megaripples to become active and increase their height. At the lowest ranges, mostly flood-orientated megaripples occur; these may be inferred to increase slightly their height at NT. In mid-ranges, near-symmetrical or ebb-orientated forms are either approaching or leaving the conditions of peak development of ebb forms.

3.3.2.3 Mean Wavelength (L) (Fig. 3.16)

Wavelength shows a well-defined figure of eight pattern, clockwise at low tidal ranges, anticlockwise at high. The curve crosses itself at a tidal range of 3.5 - 3.6m and L of 4.1m. Above this range megaripples were all ebb-orientated, but it is only between NT+10 and ST+2 that L is notably increased, which may indicate peak ebb-orientated megaripple activity.

Peak wavelengths lag ST by 2 tides, and NT by 3; little change occurs between NT and NT+5. That wavelength peaks both after NT and ST, where symmetries are opposite, demonstrates that the shoal-tide system comprises two parts, both of which interact with the flow in a recognisable

Fig. 3.15 Mean Bedform Height v Tidal Range - Line A

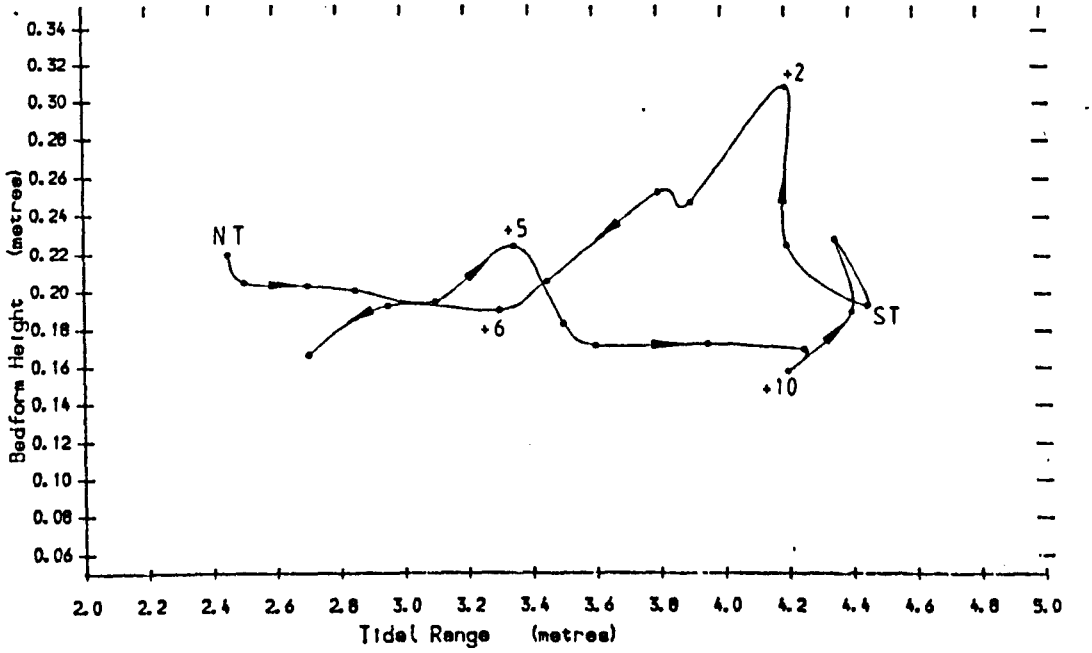

Fig. 3.16 Mean Bedform Wavelength v Tidal Range - Line A

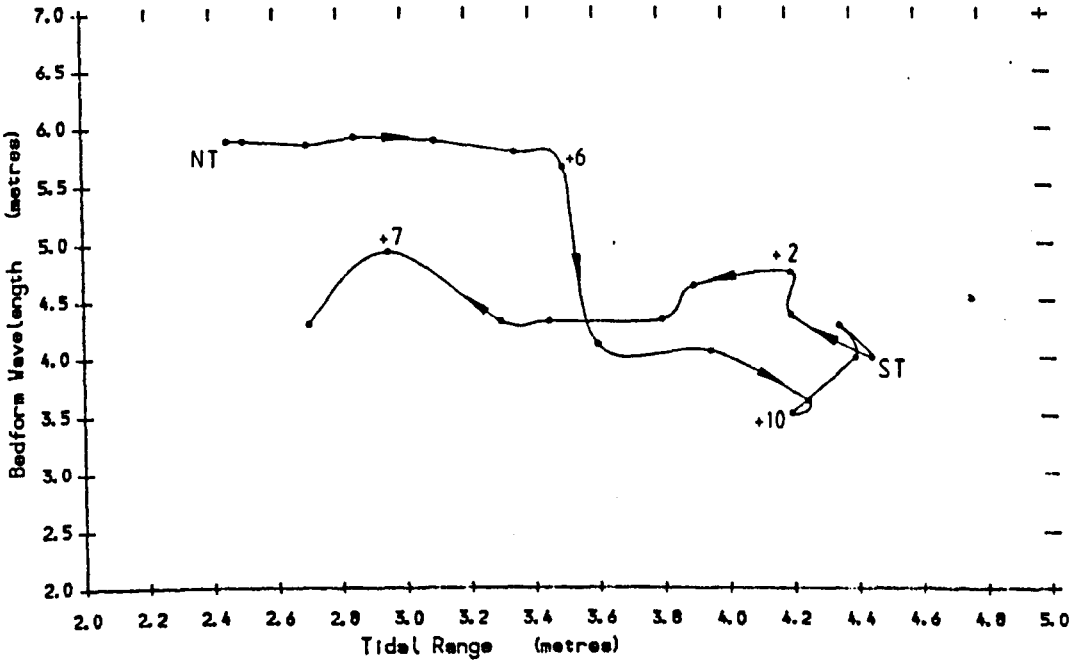

fashion. The implication is that at NT the ebb is strong enough to cause only the (observed) formation of ebb caps, whereas towards ST the ebb exceeds the threshold of megaripple 'activity', i.e. morphological change and migration. Thus, around NT the short wavelength forms are (presumably) reworked into larger flood-orientated megaripples, and around ST the newly-created short wavelength forms are reversed by successive flood and ebb currents.

In a 3D megaripple field, Terwindt & Brouwer (1986) found a 3-tide lag of maximum wavelength past both sampled spring tides. Jones (1984), in a 2D megaripple field, found that minimum wavelengths occurred 2-4 tides after spring tide.

3.3.2.4 Mean Flatness (L/h) (Fig. 3.17)

There is a very well-defined clockwise hysteresis loop, around a general trend of decreasing flatness (i.e. steeper bedforms) with increasing tidal range. This simple relationship tends to suggest that flatness may be a more fundamental property of intertidal megaripples subject to tidal flows than either wavelength or height.

The minimum mean bedform flatness occurred at ST+2, comparing with a zero or 2-tide lag (Allen & Friend, 1976a), 2-4 tides (Jones, 1984), 0-1 tides (Terwindt & Brouwer, 1986), and 0-7 tides (Larcombe, 1986).

3.3.2.5 Mean Bed Level (B), Crest Level (C)
and Trough Level (T) (Fig. 3.18)

The variation of B with tidal range is an anticlockwise loop, at it's broadest with mid to low- ranges. The implications and interpretation of this pattern in terms of preservation potential will be discussed more fully later, in Section 3.8, discussing shoal shape and volume changes.

In terms of bedform development over a lunar cycle, both C and T have been shown to be useful in interpreting periods of megaripple development

Fig. 3.17 Mean Bedform Flatness v Tidal Range - Line A

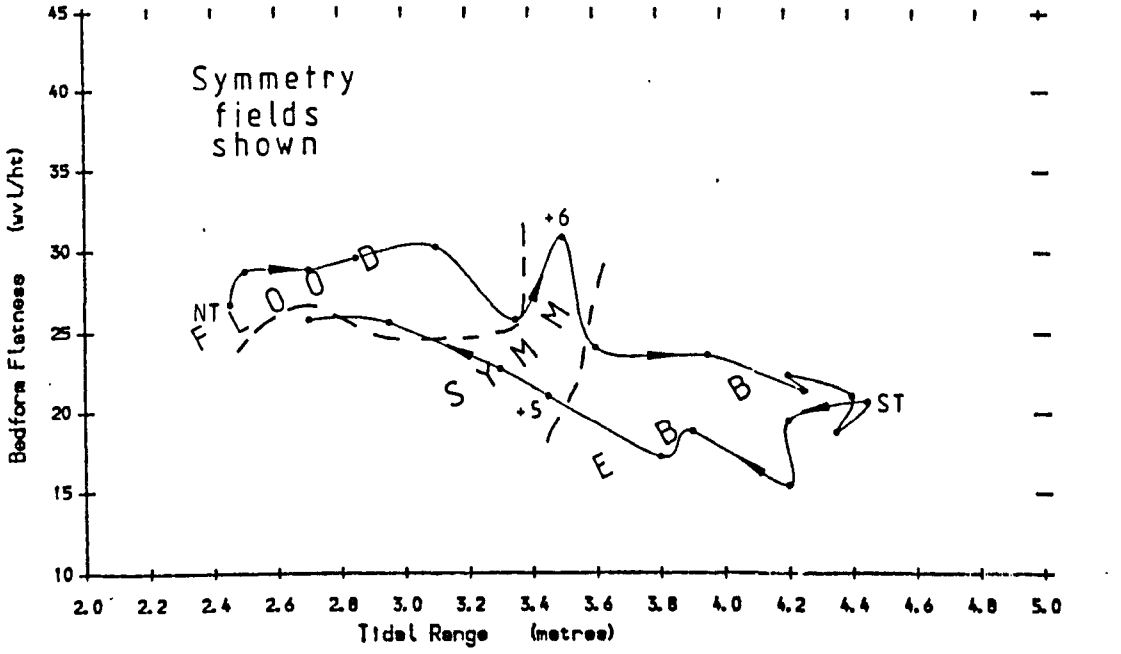

Fig. 3.18 Mean Bed Elevations v Tidal Range - Line A

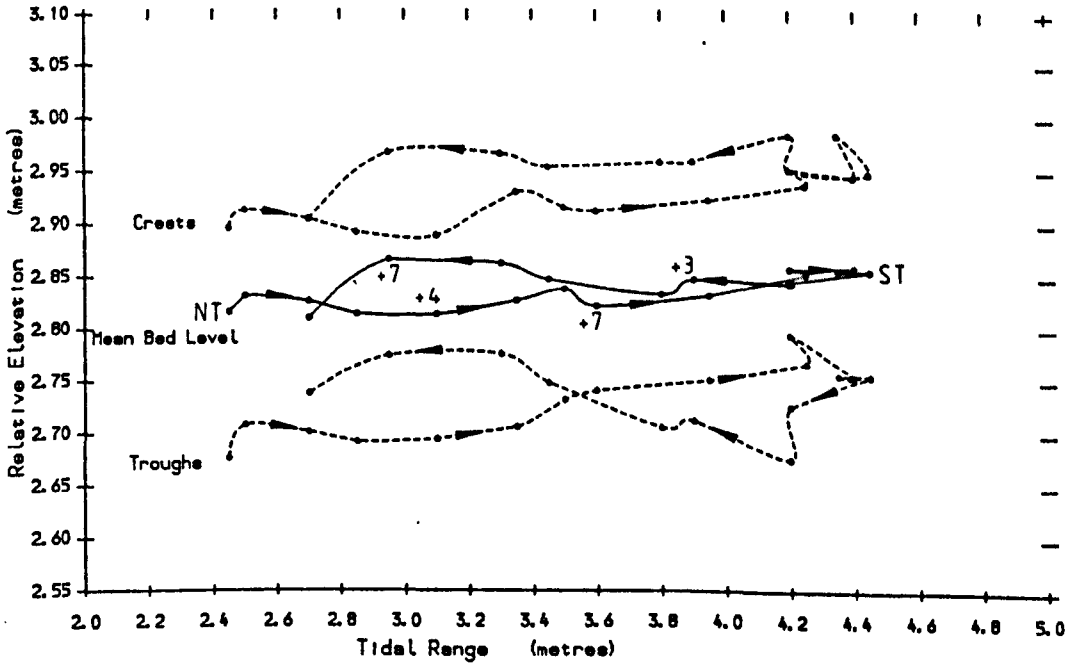

and migration, in both Recent and ancient examples (eg. Terwindt, 1981; Boersma & Terwindt, 1981; Terwindt & Brouwer, 1986; Allen & Homewood, 1984; Larcombe, 1986). Broadly speaking, their results showed that trough elevations decreased near ST, with or without increased crest elevations.

Crest elevations show strong anticlockwise hysteresis with tidal range, and the main axis of the loop has a positive slope, i.e. C is directly proportional to tidal range. In marked contrast, the curve of trough elevation has a well-defined figure of eight shape, i.e. with periods of low trough elevations at both neap and spring tides. This disagrees with the above studies, which explained lower trough levels at springs by arguing that trough levels were maintained by erosion of the stoss side of the next downstream bedform by the reattaching flow and lee-side vortex, and that fast spring tide currents produced increased erosive power and thus decreased trough levels.

This study shows that this mechanism is active at spring tides, where tidal currents reached over 1m/s, but it cannot explain the deepened troughs at neap tides. Thus the above interpretation is too simplistic, incorrectly inferring two periods of strong megaripple 'activity' on the shoal, whereas at neap tides there were only moribund forms.

The processes which caused two periods of low troughs are explained below. The first period is around ST, where the ebb currents are sufficient to fully reverse the asymmetry of flood-orientated megaripples formed by the strong flood tide, and the ebb-orientated forms migrate seawards to some degree. The second is around NT, where the bedload and migration thresholds are not exceeded by either tide, and the flood-orientated megaripples are inactive. Trough levels at springs are lowered in the latter part of the ebb tide by the action of the reattaching ebb current over the (migrating) ebb-orientated bedforms. At neaps, trough levels must be lowered by a different mechanism, possibly erosion by lateral late stage runoff currents. No current data on these possible currents was taken.

Both neap and spring megaripples have lags (with respect to minimum and maximum tidal range) in the development of low trough levels. In the case of neaps, this can be explained by the proposed late-stage runoff mechanism continuing to occur after neap tide itself when migration remained zero, but later its effects are masked by bed-level changes caused by bedform migration. At spring tides, the lag in trough level is explained by lag of the sedimentary response to the increased bedload transport competetence of the ebb tide.

3.4 Megaripple Populations

3.4.1 Introduction

Sedimentologists now recognise that populations of natural transverse sandy bedforms may exhibit modal or polymodal behaviour (Allen, 1978), in terms of their morphometric characteristics, either periodically or permanently (Collinson, 1970; Boothroyd & Hubbard, 1974; Allen & Friend, 1976a; Jackson, 1976; Zarillo, 1982; Dalrymple, 1984). An additional factor in determining the make-up of a bedform population is that of change in the population composition by a constant creation, change and destruction of individual bedforms, and by immigration to, and emigration from, the population (Allen, 1968,69,74; Allen & Friend, 1976a; Larcombe, 1986). Jain & Kennedy (1974) put forward the idea of a non-deterministic 'variance cascade' operating around a deterministic central condition.

Work in flumes, and modelling of bedform systems, have also shown that these factors are significant in determining bedform population composition (Allen 1978; Allen & Friend, 1976b; Costello & Southard, 1981; Wijbenga & Klaasen, 1983; Allen, 1976a,b). However, there are reported bedform assemblages which are apparently unimodal, found in low discharge rivers (Nasner, 1974; Stuckrath, 1969). Levey et al (1980) noted little wavelength variation, between times of flood and average discharge, in the meander bend of a river.

The data collected in this study need care in their interpretation of morphometric trends, because surveyed bedform orientation changed much during the lunar cycle (Fig. 3.19), and varied between the population being wholly flood-orientated or virtually wholly ebb-orientated, and between individual extremes of b/a of 22 and 0.07. It appears, however, that there is no modal behaviour in b/a values, so the megaripple symmetry index may be a potentially useful parameter to correlate with the flow.

Individual bedform wavelengths are shown on Fig. 3.20. Note that flood-orientated and ebb-orientated bedforms are plotted differently. At NT,

Fig. 3.19 Range of Bedform Symmetry Index - Line A

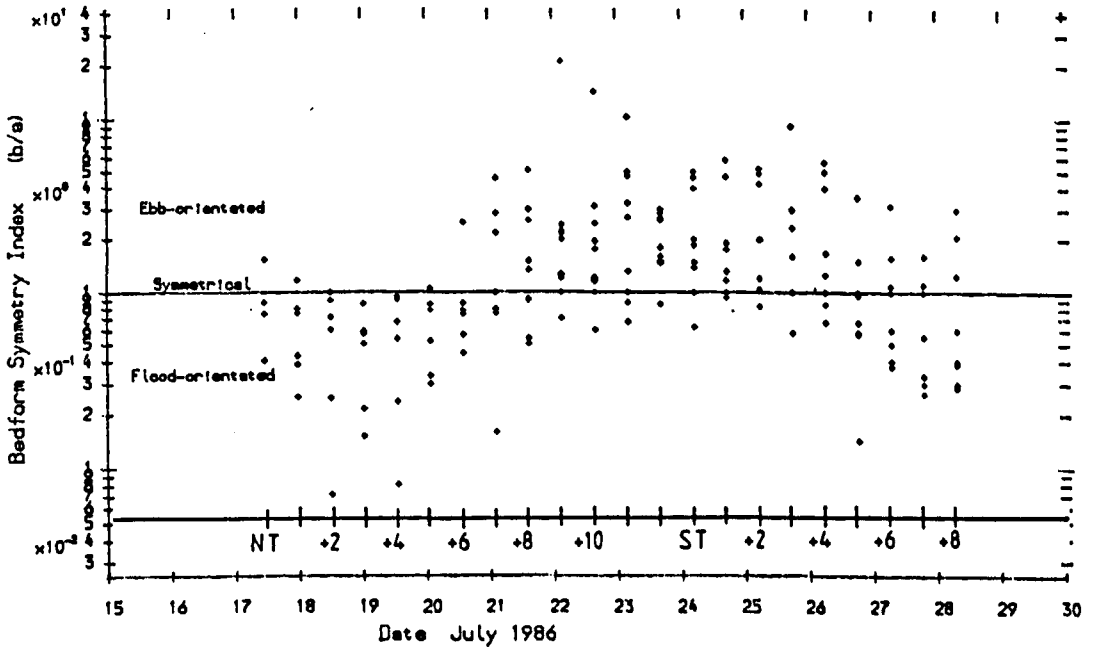

Fig. 3.20 Range of Bedform Wavelengths - Line A

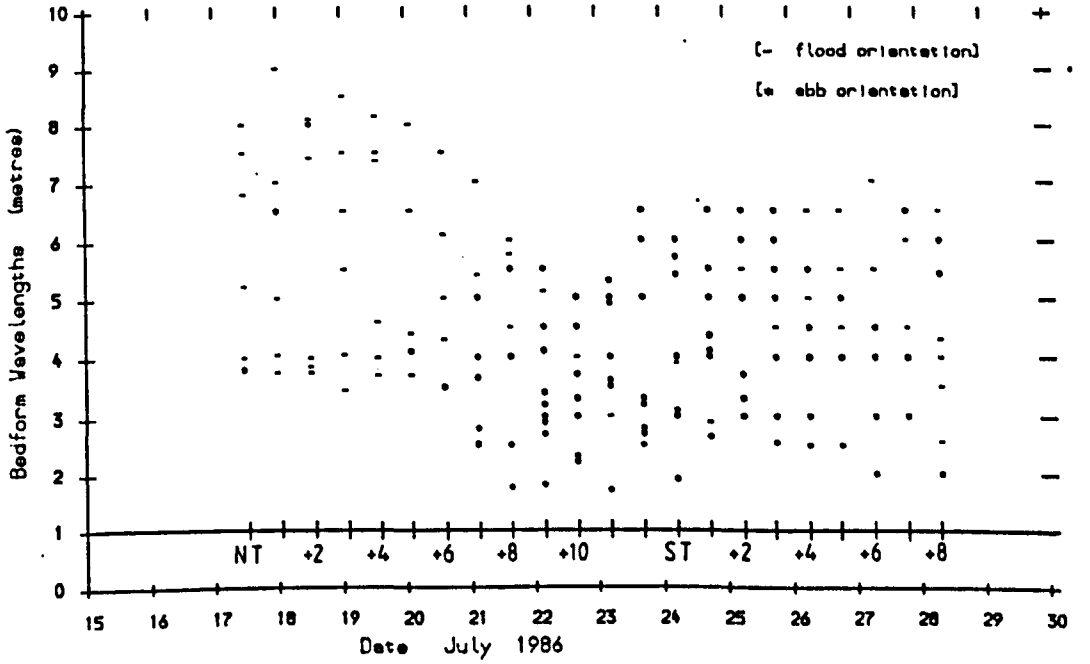

flood- orientated megaripples occurred with L of between 3.5m and 9m, in marked contrast to ST when bedforms were ebb-orientated and 1.5-5.0m in wavelength. In broad terms increased tidal ranges correlate with both lower wavelength and decreased wavelength variation. Least variation occurred at NT+10. At NT+7 short forms first appeared, which tended to be ebb-orientated; these replaced larger flood-orientated forms.

Daily maximum wavelengths were least at NT+10 at 5m; this then increased to 6.5m at ST. Minimum wavelengths were highest at ST+2, which is a second time of least wavelength variation. The significance of times of least variation may be that they represent times when the bedforms are most in equilibrium with the (?tidal) flow conditions. Bedform heights (Fig. 3.21) varied least at NT+8, but waves can also be a factor in limiting megaripple heights (Langhorne et al, 1985; Larcombe, unpublished data) and so this does not negate the postulation made above. It is also notable that heights do not appear related to bedform orientation.

Most of the surveyed megaripples were less than 0.35m in height. The maximum attained was 0.7m at ST+2 on a bedform 6m long. There was least variation at NT+8 where all megaripples were between 0.08m and 0.2m in height. Waves can cause decreased heights through erosion of crestal areas and deposition in troughs (Langhorne & Read, 1986) but there was not a period of strong winds in the estuary at this time, so a tidal cause is inferred. Unlike wavelength, where least variation is interpreted as a near-equilibrium population, the time of least variation in megaripple heights is interpreted as an effect of the relative morphological effect on the bedforms of the flood and ebb tides. At this stage in the lunar cycle the ebb tide was capable only of modifying flood-orientated megaripples to a near symmetrical form (Fig. 3.19). It was only on larger ranges that the ebb tide was capable of completely reversing the megaripples, a full lee- side vortex then forming, deepening the trough and so increasing height.

Megaripple flatness values ranged between 6 and 86 (Fig. 3.22) and variation was least at NT+12, where all values were between 10 and 33. The spread of values decreased up to ST and remained low throughout the remainder of the study period.

3.4.2 Modal Behaviour

There is little published field data, on modal behaviour within populations of transverse intertidal bedforms (Allen & Friend, 1976a; Dalrymple et al, 1978; Elliott & Gardiner, 1981; Zarillo, 1982). Morphometric modes within megaripple populations have been recognised by Allen & Friend (1976a) on the basis of wavelength. Their 'major dunes' were divided at a wavelength of 6m into a short-wavelength sub- population, with L close to 3.5m, and a long-wavelength sub-population, with L close to 9m. They also distinguished 'minor dunes' of modal wavelength 1-2m and height 0.08-0.12m.

Histograms of all megaripple wavelengths, heights and flatnesses (Figs. 3.23, 24 & 25) show, that taken over the whole study period, there was little evidence of polymodality except for wavelength, where there were five modes. The strongest was at 4-4.5m, and contained 17.6% of all measured forms, the next at 5-5.5m contained 11.8%. Overall however, the wavelength values were centred around 4-4.5m, and the population slightly skewed towards the lower wavelengths.

Figure 3.26 shows the skewness values for L and h for the study period. Positive skewness means that the median and modal values are less than the mean, negative skewness means they are greater than the mean. Thus for the final 8 tides most megaripple heights were lower than the mean, i.e. a small number of them were high. The remainder of the height curve, and the whole of the wavelength curve fluctuates markedly, showing no clear pattern. Allen & Friend (1976a) found that, disregarding short period scatter, skewness of wavelength appeared to follow a definite pattern, with larger commonly positive values during springs, whereas the smaller generally negative values were linked to neaps. It may be that the combined effects

Fig. 3.21 Range of Bedform Heights - Line A

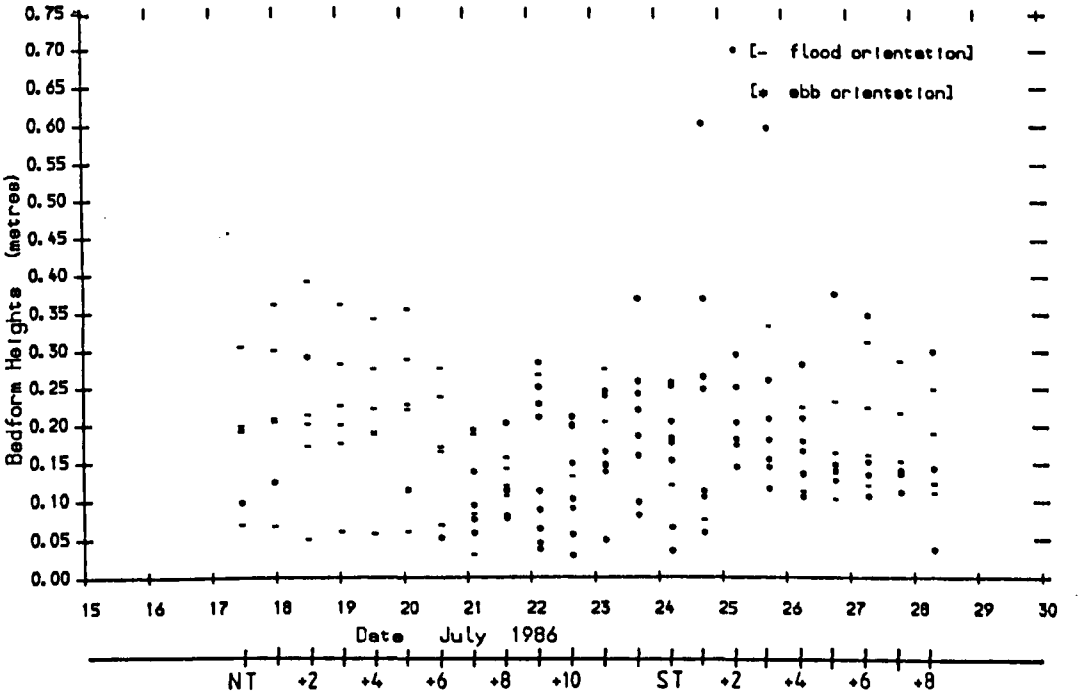

Fig. 3.22 Range of Bedform Flatness - Line A

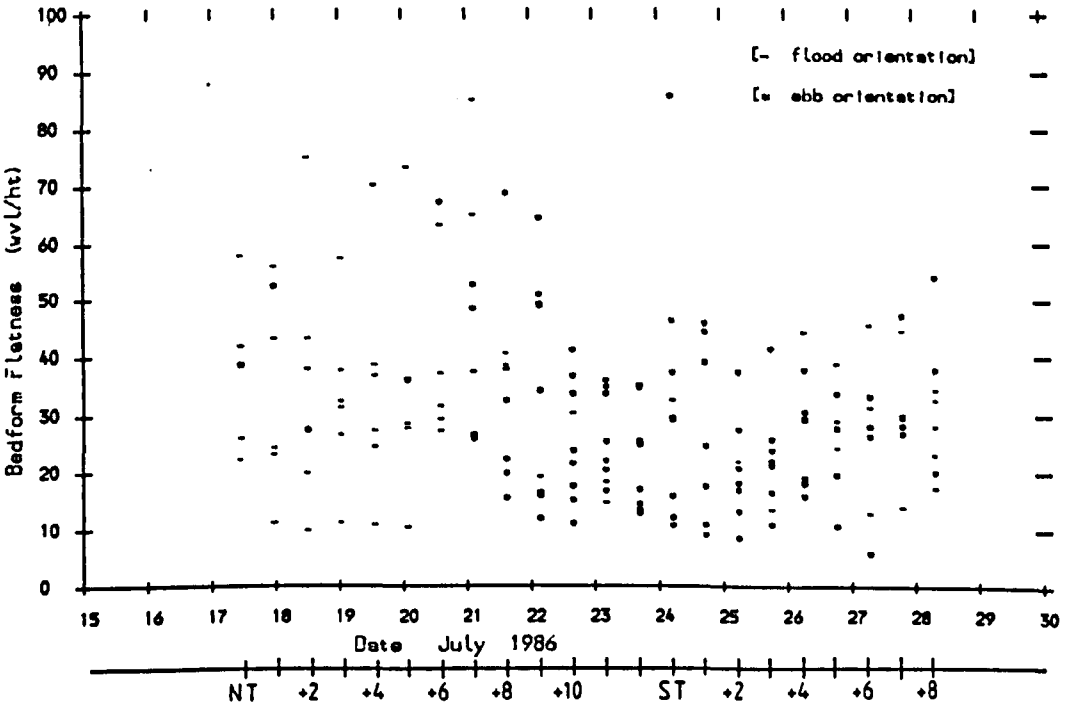

Fig. 3.23 Bedform Wavelengths - Line A (n=170)

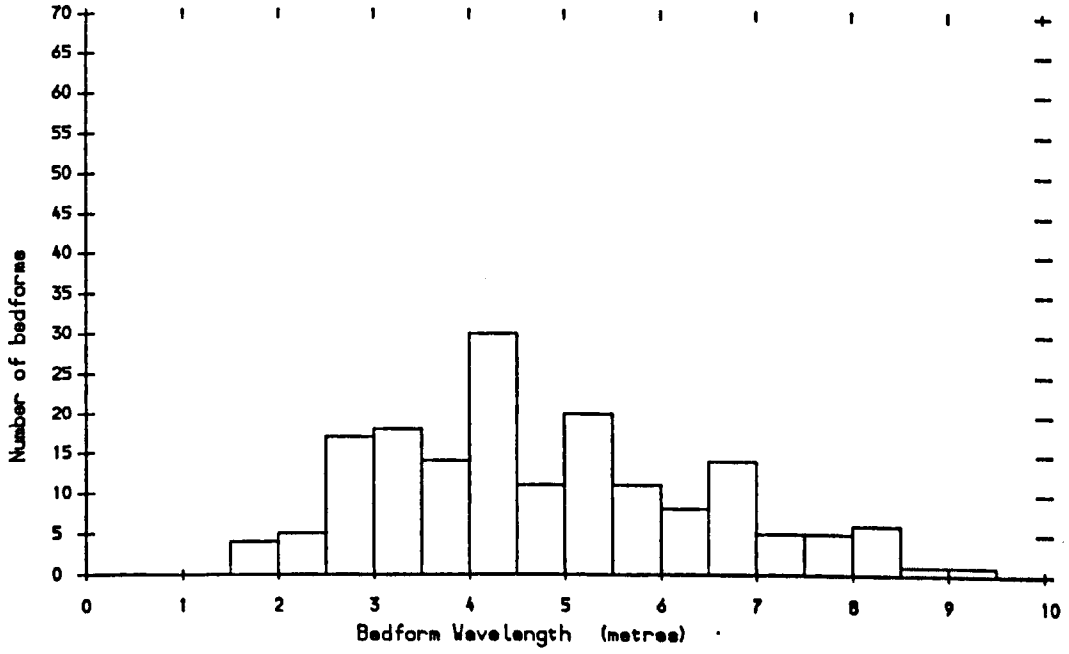

Fig. 3.24 Bedform Heights - Line A (n=170)

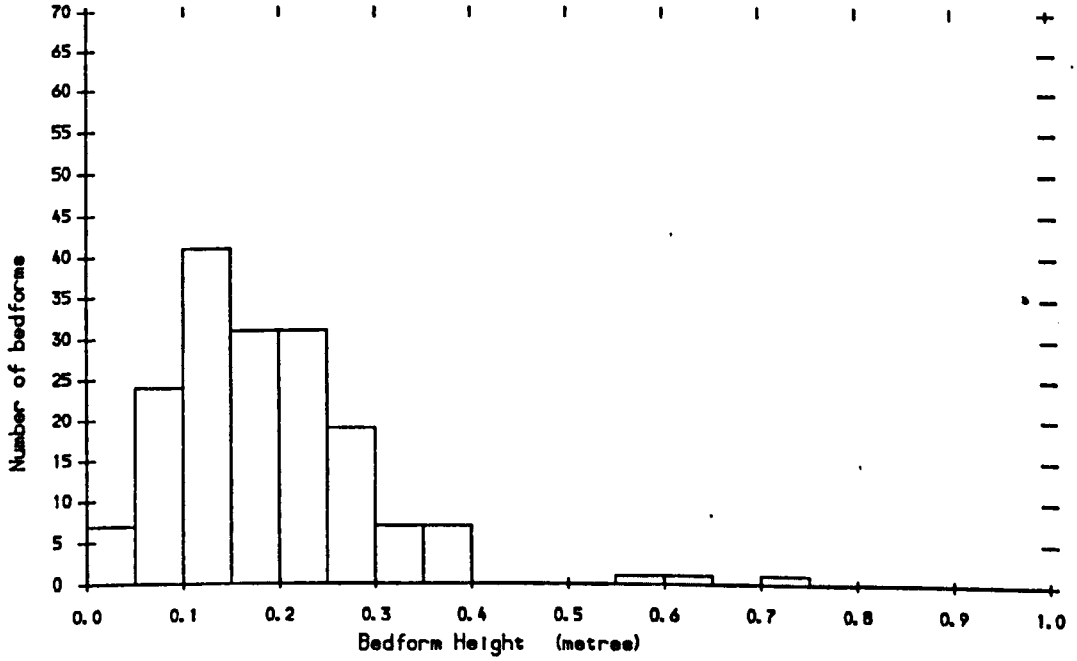

Fig. 3.25 Bedform Flatness - Line A (n=170)

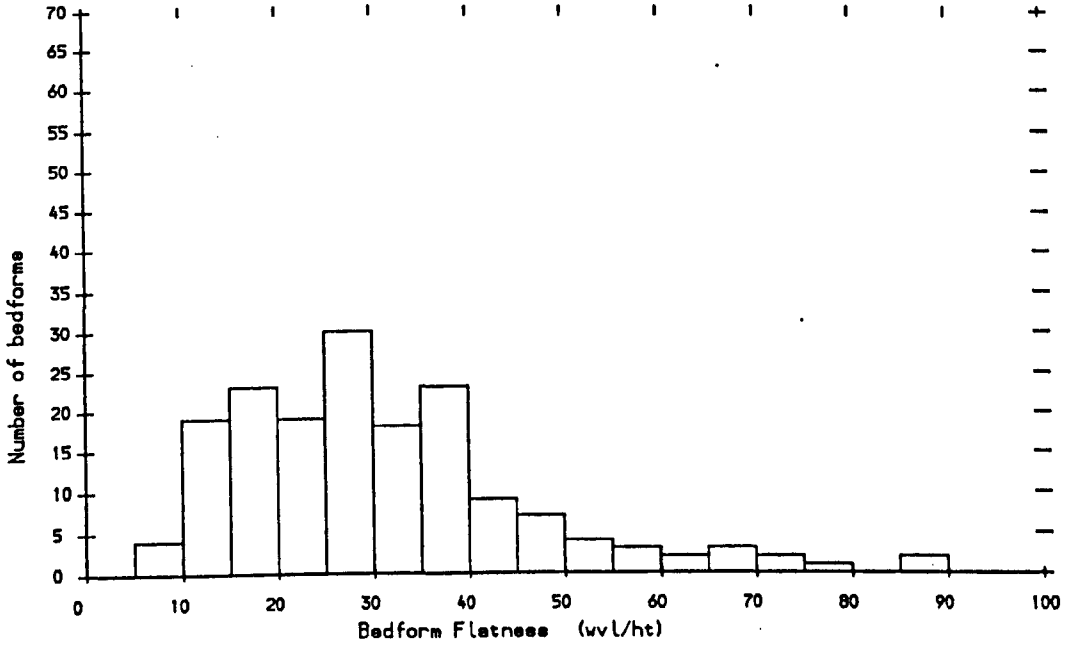

Fig. 3.26 Skewness of Wavelength and Height - Line A

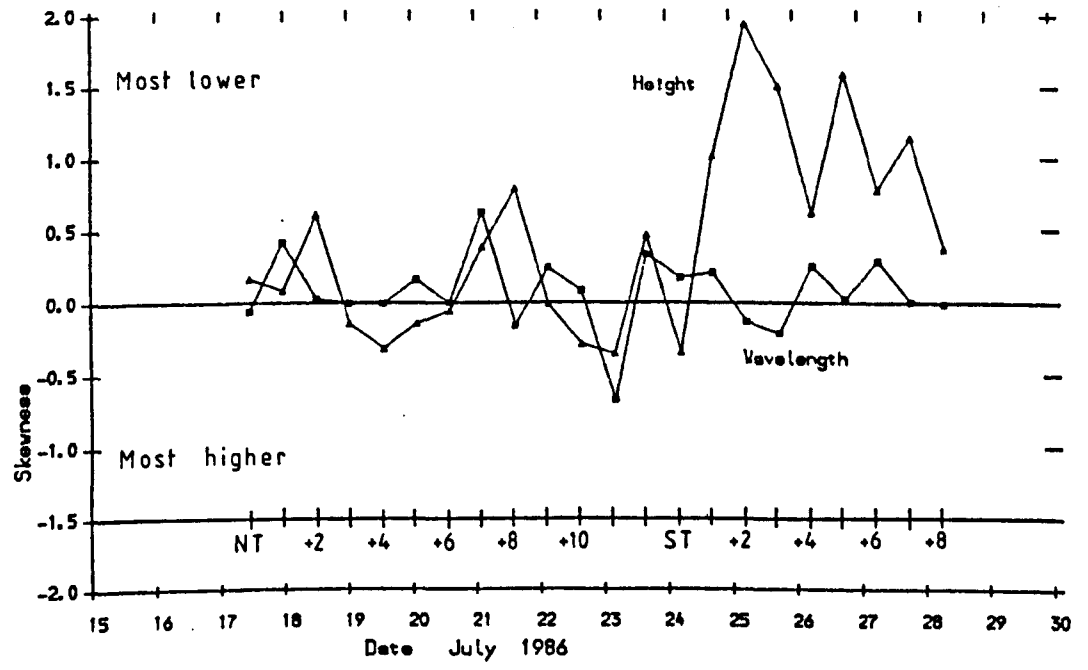

of megaripple immigration, development, emigration and sometimes reversal were too great in this relatively small sample to show such a trend, if present. Allen & Friend (1976a) found no clear pattern in the skewness of height, but this data suggests a rapid increase at ST followed by fluctuating but overall decrease. In physical terms this represents a rapid proportional increase in short-wavelength forms at ST, followed by a slower return towards a more normally-distributed population, a result also found by Allen & Friend.

At NT + 7 it was noted that short-wavelength forms became more numerous, and it is this which caused a short-lived rise in skewness of both L and H. No long- term effect on skewness of L or H resulted from the formation of these small megaripples.

There are conflicting interpretations of polymodality in meso-scale transverse bedforms (megaripples and sandwaves). Due to the prevalence of superposition many workers have considered the modes as distinct hydrodynamic forms, either explicitly, or implicitly by their classifications, eg Klein, (1970), Boothroyd & Hubbard (1975), Dalrymple et al (1978), Zarillo (1982). In contrast, in a consideration of unidirectional flows, Allen & Collinson (1974) concluded that when flows are unsteady, the members of certain classes of bedform may evolve according to a discontinuous cycle, and so large scale transverse bedforms occurring one upon the other are all the same in a hydrodynamic sense, although only one of the classes is likely to be active at any one time. In terms of the bedforms on shoals, megaripples are 'created' during particular stages of the tidal cycle, and provided there follows a suitable variation of discharge, they have the ability to evolve into active examples of the larger forms.

Neither of the two models is negated by the dynamics of the meso-scale bedforms on the Fegla Fach shoal. Allen & Collinson's (1974) concept is favoured by this data, but both small and larger megaripples are active when present together on the shoal.

3.4.3 2D - 3D Megaripple Distinctions

The division of megaripples into 2D and 3D forms has been called an arbitrary one (Dalrymple et al, 1978). No single characteristic can be used to distinguish between the two types, and a continuous gradation occurs between them, although their degree of separation in some bedform phase diagrams indicates the distinction is of potential genetic significance.

Dalrymple et al (1978) show field data (their Fig. 4), plotting current speed versus grain size and water depth. The two types of megaripples plot separately in both diagrams. Costello & Southard (1981) also show that when plotted on a depth-velocity diagram, flume and field megaripples fall together into distinct 2D and 3D areas. Boothroyd & Hubbard (1975) presented a boundary between linear and cuspate megaripples on a similar diagram.

Vanoni (1974) summarised much published flume and field data in a series of bedform stability diagrams which relate Froude number to the ratio of water depth to grain size. On one of these, Terwindt & Brouwer (1986) plotted 2D and 3D megaripple data from the Ossenisse shoal in the Westerschelde estuary, which showed a boundary at a water depth-grain size ratio of $8 * 10^3$. Data from Fegla Fach has been superimposed on this diagram (Fig. 3.27) and showing only a reasonable fit with the bedform phase boundaries.

At neap tide, where 2-D megaripples were at the threshold of movement on flood tides, the flood tide data just falls within the 2-D megaripple field, and the ebb within the current ripple field. On spring tides the flood tide falls within the 3-D field, the ebb towards the top of the current ripple field. The phase boundaries of this diagram are based on 'equilibrium' bedforms, but the bedforms on Fegla Fach Shoal are commonly lagging behind the flow, and considering this difference, the data fits the diagram quite well. Data from this study lies below the data of Terwindt & Brouwer (1986) which is outlined by dashed lines, probably as a result of the more highly skewed tide

in their study, producing high velocities in shallow water.

The surveyed megaripples in this study varied between 2D and 3D. Flood-orientated 2D forms were dominant at NT and were best developed at the seaward end of the shoal, a relationship also noted by Larcombe (1986) in the Conwy estuary. 3D forms occurred first at NT+7 as short wavelength 'scour pits'; small 3D megaripples noted for their limited positive relief (see Elliott & Gardiner, 1981) and comparable to the 'minor dunes' of Allen & Friend (1976a). These either increased in wavelength and relief, or disappeared, until after NT+11 only 3D ebb-orientated megaripples occurred on the survey line.

3.5 Bedform Migration

3.5.1 Definition of 'Migration Distance'

Studies which have included measurements of large- scale subtidal and intertidal bedforms have not been uniform in their methods of measuring migration, nor in their explicit or implicit definitions of precisely what constitutes 'migration distance'.

Klein (1970) measured the migration of intertidal megaripples and sandwaves by placing sand stained with acrylic lacquer on bedform slip-faces. Two tides later the bedforms were trenched to reveal the stained sand buried as a cross-bedded layer. Presumably the migration distance was measured as the horizontal distance between the present slip-face and the cross- bedded layer, though it is not stated.

Langhorne (1982) measured the migration of the crest of a marine megarippled sandwave approximately 200m in wavelength. Divers repeatedly examined the sediment level along lines of sea-bed reference stakes to determine the change in shape of the crestal region. Jones (1984) surveyed intertidal bedforms in the Menai Straits using a novel levelling system based upon liquid level in a flexible tube. He defined migration distance as the average horizontal displacement of three positions over each bedform on the survey line : the crest, trough, and lee slope, though the latter is not defined.

Standard levelling techniques were used by Langhorne & Read (1986) to obtain repeated cross- sectional profiles of three intertidal sandwaves. The profiles were then lag cross-correlated to compare the displacement of each wave form from its predecessor. Thus migration was averaged over the 75m survey line, and defined in terms of a wave-form rather then movement of a particular feature. This statistical technique has the advantage of providing a quantitative measure of similarity between profiles, i.e. bedform shape change, through the correlation coefficient.

Terwindt & Brouwer (1986) were rigorous in defining migration distance in their study of intertidal megaripples. It was defined as the horizontal displacement of the point halfway between crest (highest point) and trough (lowest point) (Fig. 3.3). While proving satisfactory in their study it has two disadvantages :

1 - If the surveyed bedform changes shape in its crestal region between surveys, for example in developing a crestal shoulder or an ebb cap, the position of the point under consideration for migration measurement may be considerably altered, by a process other than by migration. So this measure may be of limited use in conditions of rapid (one tide) shape change, for example, at the threshold of ebb cap formation. Late-stage runoff can also cause movement of the trough position, by undercutting the base of the lee face or by deposition in the form of a trough- parallel microdelta;

2 - For a geologist measuring a series of complex cross-bedded cosets, or large-scale foresets (Dalrymple, 1984) interpreted as migrating bedforms, it will not be possible to define where on the boundary of each tidal bundle (Fig. 3.4) to measure (in all but the most exceptional cases). The crests of intertidal bedforms have a very poor preservation potential, and are normally eroded during migration, and it is not always possible to define the trough point related to a particular tidal bundle, as many bottomset laminae may merge together at the base of a cross-bedded set.

So in terms of palaeoflow reconstructions the measurement of 'migration' by this method is not practical, and it is impossible to use the lag cross-correlation method. It appears therefore that the simple measurement of horizontal bundle spacing, as presumably used by Klein (1970), and used by Berben et al (1978) is the most useful in terms of the geological record. Many studies of ancient bedform migration have used this measure, eg Allen (1981a,b), and Allen & Homewood (1984).

However, it should be noted that this measure may be subject to variations brought about by bedform shape change, particularly if measured

near the top or base of the tidal bundle. For example, if the megaripple lee face is significantly steepened by one particular tide, the geometry of the tidal bundle will tend towards an inverted triangle, so if bundle thickness is measured near the base it will will underestimate 'migration', and if measured near the top will overestimate. This is reversed if the bedform lee face angle is reduced from one tide to the next.

Siegenthaler (1982) estimated the amount of sediment deposited in tidal bundles by assuming that there was no systematic variation in bedform height and that erosion by the lee-side eddy was negligible. Then for 2D cross strata, sediment volume is directly proportional to bundle thickness.

3.5.2 Uses of Migration Data

An important point from the above introduction is that the measure and definition of bedform 'migration distance' may be different depending on what use the data is intended for. Since the aim of the study of Terwindt & Brouwer (1986) was to investigate relationships relevant for palaeoflow reconstructions, they need not have been so rigorous in their definition of the measure of migration, as that rigour is impossible when measuring preserved sections. Their flow-bedform relationships include a good correlation between peak depth-averaged current velocity of the dominant tide and the mean bedform migration rate. However, when comparing mean migration rate with computed sand transport for the dominant tide, a set of poor correlations result. Whilst some of this non- agreement results from the reliability of the sand transport formula used and reworking of sediment by the lesser tide, a proportion may also be due to the potential imprecision of their measure of migration.

Some workers have calibrated bedload sediment transport equations by simultaneously measuring bedform migration and the transporting flow, eg Kachel & Sternberg (1971), Langhorne (1982). However this assumes that the whole volume of each tidal bundle was transported as bedload, which

may not be the case. Jopling (1966) proposed that, in addition to avalanching, an important process in the formation of foreset laminae was grain fall-out from suspension. Hunter & Kocurek (1985), in a flume study using 0.33mm diameter sand, found that this process formed up to 8% of the lower slipface deposits. Yang (1986) discussed the contribution of intermittent suspended load to the development of cross-bedded deposits, and advised that the sediment transport rate measured from bedform migration be designated as 'bed material' transport rate. This bed material is moved by sliding, rolling, saltation and intermittent suspension (Blatt et al, 1980) and transport rates thus defined are directly comparable with bedform migration rates.

Van den Berg (1987) noted that for medium - coarse grained sands, bedform migration was probably equivalent to bedload transport, but that for fine sands there were two complications :

1 - near the brinkpoint of the bedform some bedload may become suspended and be transported across the trough on to the next stoss slope rather than being deposited on the lee face and incorporated into the tidal bundle;

2 - some settling from suspension of fine grains may occur in the lee of the bedform, therefore increasing apparent bedload transport (see above).

However, he concluded that in his study (with grain sizes of 210um and flow velocities up to 1.15m/s), either the two processes were not important or they approximately balanced each other.

Mean migration rates have been correlated with flow strength parameters and bed material transport rates, eg Terwindt & Brouwer (1986), and this is possible if migration is measured by either displacement of individual lee faces or by a lag cross- correlation method. However it may be important to know the range of migration values within a population, for example the upper and lower limits of migration rate in an area considered to have spatially near- constant flow conditions. This is easily found if the mean migration rate is the result of many individual lee face displacements, but if

migration is measured by lag cross-correlation it is only found if the technique is employed on a number of portions of the population, and this may give very variable results due to shape and size change of individuals within a portion.

Below are presented results from lag cross- correlation of the whole profiles (Lines A and B). Emphasis is placed upon data from Line A as it was on this line that detailed current measurements were taken, but comparisons are made with the Line B data.

3.5.3 Results - Lag Cross-Correlation

The information obtained from lag cross- correlation of successive profiles is :

1 - The maximum correlation coefficient obtained by lagging one of each pair of profiles incrementally in both directions. The correlation coefficient (CC) has a range between 1 and -1, with 1 indicating an identically-shaped pair of profiles in phase, and -1 identical profiles 180 degrees out of phase. The coefficient may be used as a quantitative measure of form change between profiles (Langhorne & Read, 1986). The profiles were lagged incrementally in steps of 0.01m;

2 - The direction (flood or ebb) and magnitude of net bedform migration averaged over the whole profile, for each LW - LW period. The magnitude is defined as the lag at which the correlation coefficient is highest.

The mean migration per tide (M) for Lines A and B over the study period is shown in Fig. 3.28. The y- axis runs from 0m upwards, as there were no values indicating net migration in the ebb direction. All values of M were either zero or flood-directed.

From NT to NT+4 values of M were essentially zero, but with M = 0.14m on Line A at NT+3. The threshold for net migration was exceeded on both lines by NT+5 and throughout the remainder of the study. On Line

Fig. 3.27 Fegla Fach bedform and flow data plotted on the bedform stability diagram of Vanoni (1974). (Modified after Terwindt & Brouwer, 1986).

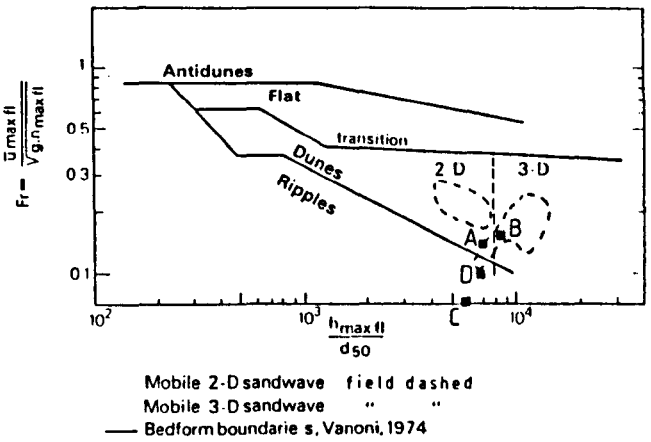

Fegla Fach data:

A	Flood	neap
B	"	spring
C	Ebb	neap
D	"	spring

Fig. 3.28 Mean Bedform Migration - Lines A and B

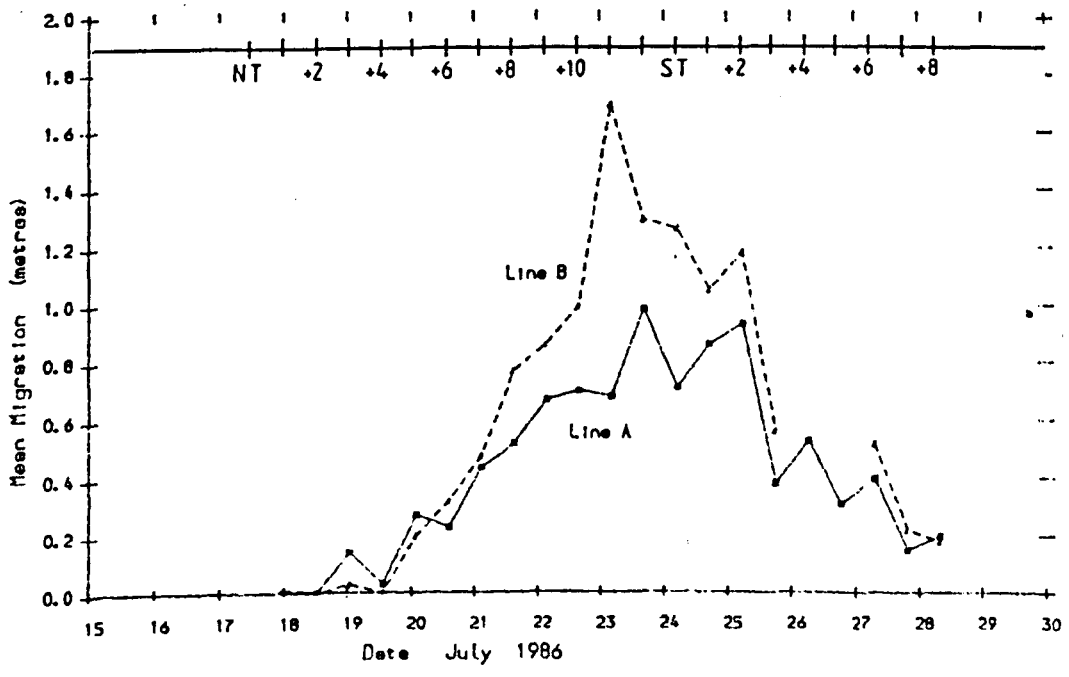

A, M increased steadily from NT+5 to NT+11, and peak migration occurred at NT+12 and ST+2, with M = 0.98m and 0.93m respectively. After ST a diurnal variation on M was present, attributed to the diurnal variation in tidal heights and currents.

The variation of correlation coefficient CC (Fig. 3.29) has a very close negative relationship with M, i.e. with an increase in M, CC decreased, and vice- versa. On Line A, CC decreased steadily from 0.944 at NT+4 to a minimum of 0.812 at NT+12, i.e. there was a gradual increase in rate of form change as tidal ranges increased. For four tides there remained a constant low CC, but a rapid one tide increase occurred from ST+1 to ST+2 and CC remained high for a further tide. Following this CC was variable but increased overall.

Both M and CC are plotted against tidal range in Figs. 3.30 and 3.31. For Line A, at both at low and high tidal ranges (<3.5, and >4.1m) M was up to 0.2m higher on decreasing ranges than on increasing ones, though data points are arranged around a near-linear positive relationship. The curve of CC was clockwise overall, with higher correlations on increasing tidal ranges, but with the marked exceptions of the profiles at ST+2 and ST+3.

The potential use of tidal range for prediction of migration and sediment transport rate is briefly discussed in Chapter 7.

3.5.3.1 Discussion

Migration rates measured in this study compare well with published data on sandwave and megaripple migration rates in tidal environments (Table 3.3).

Fig. 3.31 Correlation Coeff. v Tidal Range - Lines A and B

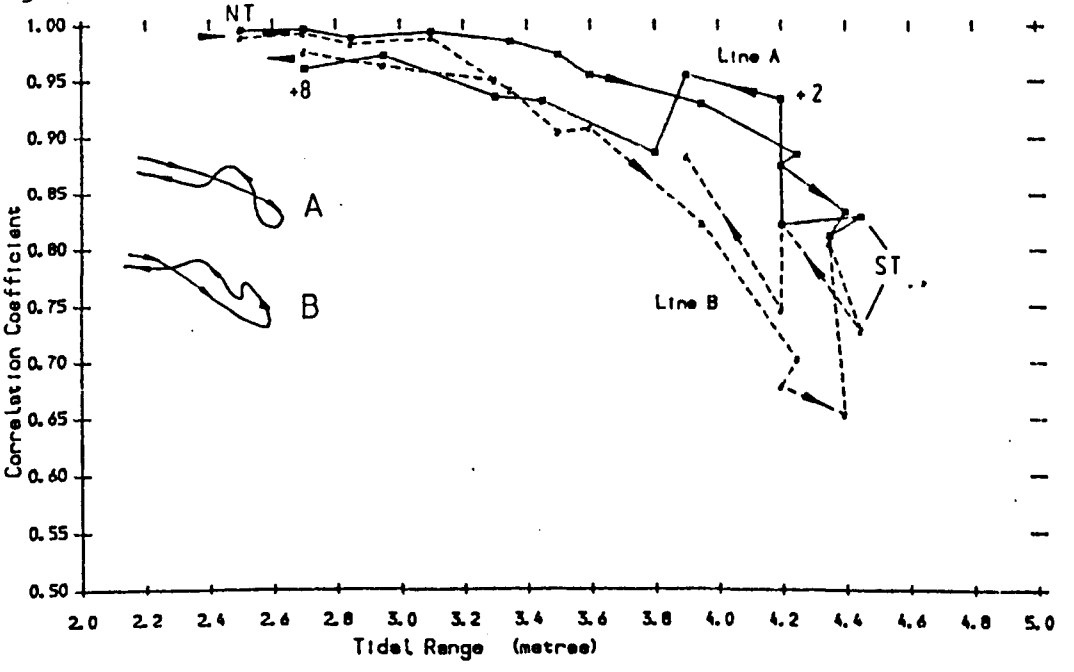

Table 3.3

Some Published Tidal Bedform Migration Rates
Modern and Ancient examples

Source	Modern or Ancient M A	Bedform type and measurement method	Migration Rates m/tide
Klein 1970	M	Dunes & Sandwaves Emplacement of stained sand	mean 0.12
Boothroyd & Hubbard 1975	M	Megaripples & Sandwaves Surveying at LW swaves spring 0.2 - 0.4 megaripples < 4.5	swaves neap 0.01 - 0.05
Berben et al 1978	M	Megaripples Surveying at LW	0.09 - 0.395
Visser 1980	A	Sandwaves Tidal Bundle Thickness perpendicular to cross-beds	0.04 - 0.8
Allen 1981a	A	Sandwaves Tidal Bundle Thickness	0.03 - 1.8 (0.35)
Van den Berg 1982	A	Sandwaves Echo Sounding	Lunar Month mean 0.22
Siegenthaler 1982	A	Sandwaves Tidal Bundle Thickness	< 0.3
Dalrymple 1984	M	Sandwaves (Method not specified)	short term -0.65 - +1.5 (0.9) long term net 0.01 - 0.31 (0.11)
Allen & Homewood 1984	A	Sandwaves Tidal Bundle Thickness	0 - 0.3
Jones 1984	M	2D Megaripples Surveying at LW	-0.5 - +0.5
Langhorne & Read 1986	M	Sandwaves Surveying at LW	0 - 2.25
Larcombe 1986	M	Megaripples Surveying at LW	-2.2 - +1.8
Terwindt & Brouwer 1986	M	2D and 3D Megaripples Surveying at LW	2-D 0.01 - 0.42 3-D 0.01 - 1.69

cntd over ....

Table 3.3 cntd.

Source Modern or Ancient	M A	Bedform type and measurement method	Migration Rates m/tide
This study	M	Megaripples Surveying at LW Lag cross-correlation	Line A 0 - 0.98 (0.43) Line B 0 - 1.69 (0.61)
		Mean of Crest and Trough	Line A -0.03 - +1.34
		Mean of Brink and Toe	Line A -0.04 - +1.29

Note : figures in brackets are mean values

Points of particular interest in the migration data include :

1 The interpretation of the change in correlation coefficient;

2 Why migration peaked prior to ST, what effect bedform population changes had upon migration, and whether there were any effects attributable to biological processes?

3 What reasons were there for differences in the data of Lines A and B?

Interpretation of Variation in Correlation Coefficient

The pattern of change in CC is very important as a basis for the interpretation of the migration data. Prior to ST the relatively steady fall in CC implies a gradual increase in form change with increasing tidal range. At and just after ST, CC increased indicating a reducing rate of change of form. This pattern is similar to that found by Langhorne & Read (1986) who found that correlation continued to increase with decreasing tidal ranges. Their data shows very smooth trends throughout but they only used data from alternate tides, thus reducing the short-term variation that may occur due to the diurnal tidal variation. In this study, diurnal variation in CC was most evident from ST+2 to ST+8.

The detailed nature of this data presented have revealed a sharp increase in correlation, from 0.822 to 0.934 in one tide from ST+1 to ST+2, which increased further to ST+3. This may be interpreted as bedforms reaching a near-equilibrium state with the spring tidal ranges, despite both decreasing migration rates and tidal ranges. Following this, CC decreased for one tide then gradually increased towards the study end. It is notable that the curves of CC of Line A have a two-tide leap at ST+2 and ST+3, then return to the general trend of the curve. This may be explained in terms of the 'spring tidal form' of Langhorne & Read (1986) but with significant differences, due to the smaller scale of the bedforms in this study (see below).

Langhorne & Read (1986) surveyed a 75m transect across bedforms approximately 20-25m in wavelength and up to 2m in height, which were not subject to a reversal in orientation during the lunar tidal cycle. However, similar rates of sediment transport over smaller bedforms, such as on this shoal, are capable of producing much larger relative form changes, for example the flow can fully reverse flood-orientated megaripples. (This is the reason that CC in this study varies down to 0.812 on Line A, and 0.653 on Line B, whereas Langhorne & Read found correlations down to just 0.88).

In this study the post-ST short period of high correlation on Line A coincided with :

1 a 3-tide sustained peak in ebb-orientated mean symmetry index (Fig. 3.9);

2 the 1-tide maximum of mean height (Fig. 3.10);

3 a small peak in mean wavelength (Fig. 3.11);

4 minimum values of mean flatness (Fig. 3.12);

5 minimum mean elevation of bedform troughs (Fig. 3.13);

6 a time of least variation in wavelength and height (Figs. 3.20 and 3.21).

(Although CC varied more tide-tide on Line B, broadly similar trends were noted, with the exception of a peak in height.)

So there is ample evidence to suggest that at this time the bedforms were at some sort of morphological equilibrium with the spring tidal flow, i.e. they had developed a 'spring tidal form'. However it should be noted that the precise nature of this 'equilibrium' is unclear, because although measured on well-developed ebb-orientated megaripples, the morphological parameters and thus the CC are a product of the interaction of a number of flood and ebb tidal flows, not just the ebb current of that specific tide. In the same way, migration of the bedforms was always in a net flood direction, yet is a product of a complete flood- ebb cycle, not just the flood current.

The data of Langhorne & Read (1986) did not show at what stage of the tidal cycle the bedforms reverted to the expected original 'neap tidal form'. This data suggests that on this shoal the bedforms cease being 'spring tidal forms' at ST+4, although because they are small ebb-orientated forms in a flood-dominated environment their life span may be different or shortened compared to large sandwaves.

An important difference with Langhorne & Read (1986) is the relationship over time between CC and tidal range. Their data shows well that CC is lower on increasing tides than at the same range on decreasing ones, and they state that this apparently contradicts their migration data, which decreases between ST and NT. However, for this to be contradictory there is an inherent assumption that the period of maximum migration, through maintenance of the 'spring tidal form', is solely responsible for increasing correlation, whereas in reality increasing CC is also a function of decreasing sediment transport and migration in the post-spring period.

The data from Line A show that on tidal ranges below 3.8m, CC is higher on increasing ranges, opposite to the results of Langhorne & Read. A more complex relationship occurs with higher ranges. Line B shows a well-developed anticlockwise trend at the highest tidal ranges (>3.9m), but like Line A shows higher correlations on low but increasing ranges. That both lines show this feature is significant. Taking into account the interpretations

of the bedform morphological changes, one possible explanation is that developed on the shoal over a lunar cycle there are both 'spring tide forms' and 'neap tide forms', both with a lag, or 'relaxation time' (Allen & Friend, 1976b) shown by the open curve of CC at high and low ranges. Between extremes of tidal ranges intermediate forms occur which may or may not display lag.

Interpretation of Migration Rates, and the Influences of Bedform Population Changes and Biological Factors

Mean migration rate M peaked both at NT+12 (at 0.98m) and at ST+2 (0.93m), as shown in Fig. 3.28. Below is a consideration of this pattern, and why there was not a single peak at ST itself.

It was shown earlier that some curves of measured mean morphometric parameters were strongly influenced by bedform population changes. Mean bedform height H at NT+11 and NT+12 was considerably less than at ST+2 (Fig. 3.10). For particular volumes of bed sediment to be transported along the bedform train, migration rates (i.e. the streamwise tidal bundle thickness) will be greater for low height bedforms than for higher ones, so one proposal could be that migration was high at NT+12 due to the geometry of the tidal bundle formed on bedforms of low height.

Table 3.4 shows that values of M for NT+11 and ST are very similar, yet approximately 30% more sediment transport (HnM in Table 3.4) occurred on ST. Migration at NT+12 was greater than at ST+2 despite less sediment transport, and M at NT+11 was 73% of M at ST+2 with only half the sediment transport. All these effects may be explained in terms of the mean bedform height H, with higher values of M with lower H, thus suggesting that bedform height is a major factor upon migration.

So migration is inherently linked to the history of flows over the bed, which control bedform size and shape, as well as to the last tidal cycle before observation, i.e. the same flow acting over a different shape of megaripple will probably produce different shaped megaripples. That the

understanding of bed-flow interactions requires study of the flow history, simultaneously with the bedforms, was also noted by Allen & Collinson, 1974). So an analysis of the trends of M must also consider H, which in turn is intimately related to the make-up of the bedform population.

Table 3.4

Heights and Migration Rates around Spring Tide, Line A

Tide	H (m)	n	Hn (m)	M (m)	HnM (m^2)
NT+11	0.174	9	1.564	0.68	1.064
NT+12	0.209	9	1.882	0.98	1.845
ST	0.211	9	1.899	0.71	1.348
ST+1	0.209	8	1.672	0.86	1.438
ST+2	0.267	8	2.133	0.93	1.984
Ratio NT+12/ST+2	1/1.28	-	1/1.13	1.05	1/1.07
Ratio NT+11/ST	1/1.21	-	1/1.21	1/1.04	1/1.27

Note : n = no. of surveyed megaripples.

Langhorne & Read (1986) speculated that maximum sediment transport, indicated by maximum migration, occurs only when the bedform population has attained an equilibrium with the spring tidal flow, i.e. bedforms are the 'spring tidal form'. Once the effects of a changing bedform morphology have been noted (above), this data appears to confirm that idea. As shown later, the maximum measured total bed material transport occurred at ST+2, and so the lag in migration at high tidal ranges is due to the time taken for bedforms to adjust to a changing flow, i.e. the 'relaxation time' of Allen & Friend (1976b). That maximum sediment transport occurred elsewhere than on ST itself shows that the capability of the flow to transport sediment may be highly dependent on the shape of the bed surface.

The Line A data shows lag effects, limited to <30% at ranges >4m, (Fig. 3.30). Proportionally larger effects occur at ranges <3.5m, and in mid-

ranges no lag effect was shown. Allen & Friend (1976a) noted a thin crust of algae and mud on the surface of an intertidal sandbank, and proposed it was responsible for a difference in threshold conditions for movement of current ripples. On decreasing tides the threshold maximum velocity at 0.6m above bed was 0.14m/s, and on increasing tides it was 0.23m/s. Such an effect was demonstrated by de Boer (1981) who showed that sudden erosion of a part of an intertidal megaripple occurred after it had been poisoned with a Copper Sulphate solution.

Frostick & McCave (1979) noted seasonal changes of about 5cm in the level of tidal mud flats, with accretion in summer and erosion in winter. When living algae were present deposition occurred, when dead or absent, erosion took place. Grant (1988) demonstrated sediment stabilising effects of benthic microalgae in both flume and field, and showed a negative correlation between wave ripple index and concentration of chlorophyll at the ripple crest, but was unable to determine a cause-effect relationship. Vos et al (1988) showed that benthic diatom mats decrease the bed grain size (because of trapping of fine sediment) and bed roughness. they found that diatom concentration was inversely related to the maximum wind velocity and wave height in the 4 days previous to sampling dates.

Thus care is needed in interpreting intertidal sedimentation and bedforms purely in terms of a physical background. At NT, the eastern (landward) end of survey Line A had a well-developed layer of green algae on the surface. This was only weakly present or absent elsewhere on the shoal. No mud drapes were present on the shoal at any stage of the lunar cycle. The algae is considered responsible, at least in part, for the difference in migration at similar low tidal ranges before and after NT, and, because the layer was better developed at the eastern end, is a factor in causing differential migration rates along the survey line (see below).

3.5.4 Migration Variation

An assumption inherent in correlations of bedform migration with sediment transport or flow strength is that migration approximates to being constant along the length of the transect considered. Terwindt & Brouwer (1986) showed no data on the subject, but Figs. 3.32 and 3.33 show that in this study there were significantly lower migration rates at the landward (eastern) end of the transects. This has been quantified using the lag cross-correlation method of measuring migration. In the migration calculations presented in the previous sections, correlation coefficients were calculated as averages of the whole survey line; below they have been calculated (for Line A data) as averages of successive 10m sections.

Migration from 10m sections is shown in Fig. 3.34, the four plotted points representing 0-10m, 10-20m, 20- 30m and 30-40m intervals. It is clear that at all stages of the tidal cycle there is a migration gradient along the line. This gradient is most pronounced at NT+7 - NT+9, when there was up to 0.95m difference between migration in the 10-20m and 30-40m sections. Table 3.5 shows the mean migrations over 4 tides for these two sections, at neaps, intermediate tides and springs.

Table 3.5

Four Tide Mean Lag Migrations (m) for 10m Sections of Line A

	NT-NT+3	NT+7-NT+10	ST-ST+3	ST+5-ST+8
10-20m	0.04	1.10	0.66	0.59
30-40m	0.04	0.44	0.52	0.02

Fig. 3.32

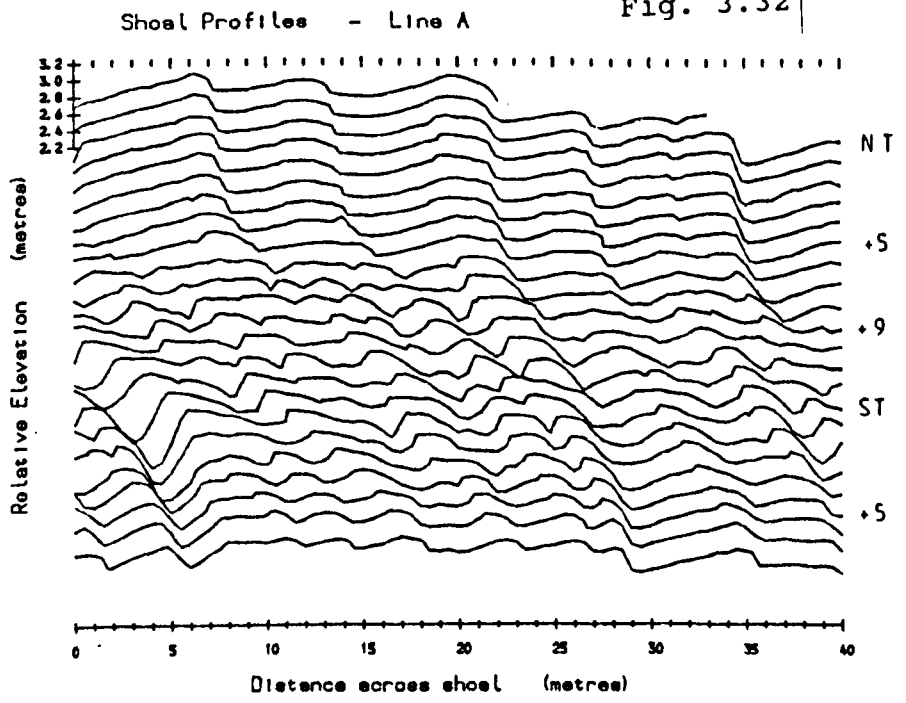

Fig. 3.33

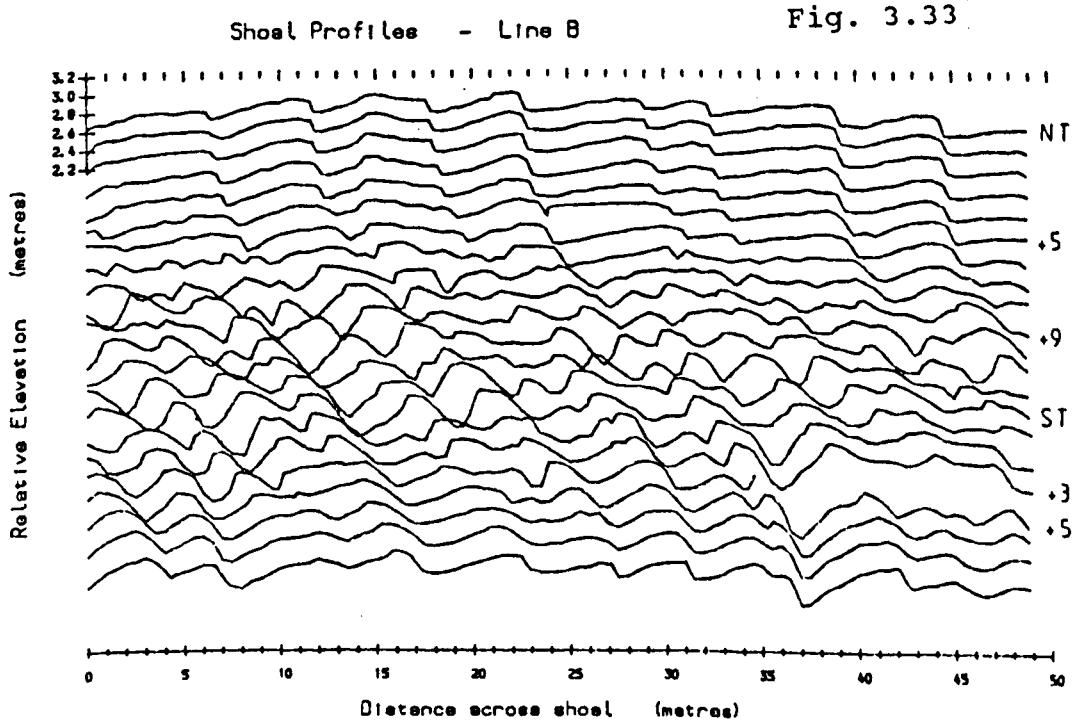

Fig. 3.34

Lag migration of 10m long sections- Line A

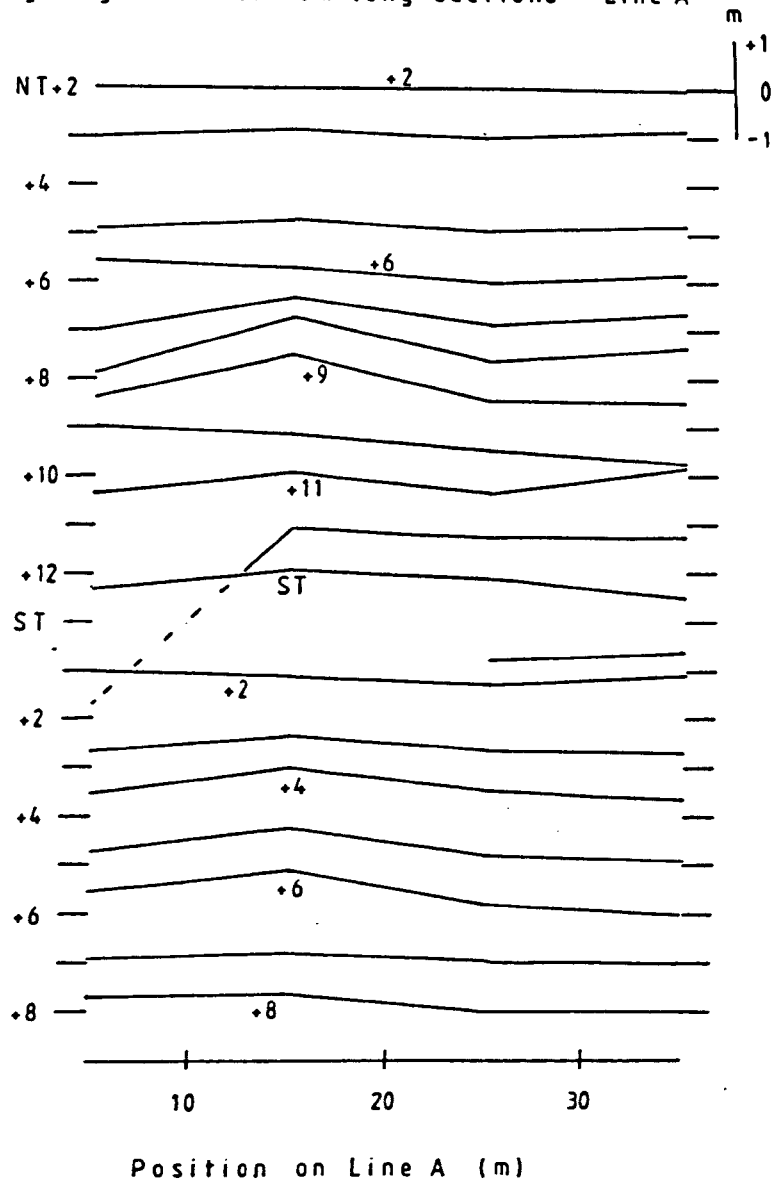

Fig. 3.35

Correlation coefficient of 10m long sections - Line A

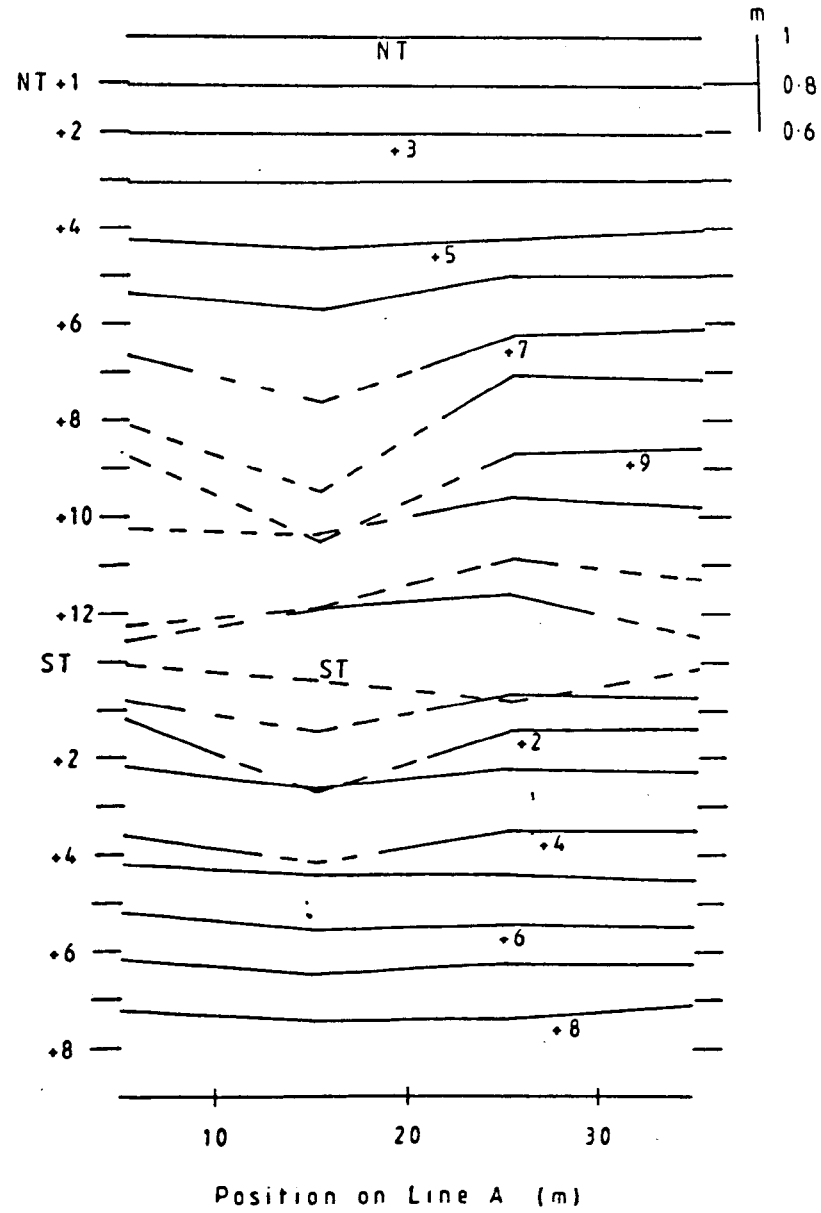

It is notable that throughout the lunar cycle the 10-20m section showed the highest migration rates, and this was most pronounced 7-5 tides before, and 4-6 tides after spring tide. This is related to the pre- spring initiation and post-spring degredation of low height bedforms which were more common in the seaward (western) half of the transect (Figs. 3.32 and 3.33). As discussed above, low height bedforms tend to show relatively high migration rates. That migration rates were relatively even over the transect length at spring tide reflects the development of these small bedforms into taller forms, which have lower relative migration rates. (To attempt to obtain further detail by taking 5m long sections proved unsuccesful, because the section size was equivalent to a wavelength, and scatter in the data was much increased).

It is useful to consider also the variation in correlation coefficient CC between the same 10m sections from one tide to the next (Fig. 3.35). CC is very variable over the transect length, and CC values are mostly less than the CC values calculated from the whole transect; this is expected as with 10m long sections, a change in form of a single bedform of approximately 4-7m wavelength will drastically reduce CC. The diagram also emphasises the form changes which occurred in the seaward half of the transect after NT+6. Form changes all along the line decreased after ST; further indicating the development of the 'spring tide form' megaripples.

This brief analysis clearly demonstrates that assumptions of constant migration rates in a particular area are unjustified. It may be that mean values are useful in flow and sediment transport relationships, but from the geologists point of view it is also very important to be aware of the within population variation of migration rates (and form changes) that occur in modern environments.

3.6 Comparison of Line A and Line B Data, and Interpretation

Table 3.6 shows some data from all simultaneous surveys of Lines A and B. It is notable that, by chance, the two lines have the same mean bed level averaged over the study period. This means that differences in morphometry and sediment transport on the bed are unlikely to have been caused by different elevations and thus periods of tidal inundation. It implies that differences between the lines are most likely to have been caused by their lateral displacement (15m) with respect to the main direction of the tidal currents. The variations in mean bed level B, of and between the lines is briefly discussed in terms of shoal dynamics in a later section.

3.6.1 Height Comparison

The mean bedform height H was 1.7cm greater on Line A than B, a result of both higher crests and lower troughs. The standard deviation (SD) of C was greater for A than B, yet the total variation was 1.8cm less than B, with both a higher minimum and a lower maximum. T was more variable on A than B, expressed by both the SD and total variation.

In terms of short term variation with time, mean crest levels showed least similarity from NT to NT+6, and NT+12 to ST+3, i.e. broadly during times when bedforms were consistently strongly asymmetrical, and most similarity when more symmetrical (compare Figs. 3.13 and 3.36). Trough levels T of A and B show broadly similar trends in the short term, but the longer period trend is far better established on A than B. Both curves of T peaked at NT+10, and Line B has more short term variation.

Fig. 3.36 Mean Crest, Trough and Bed Elevation - Line B

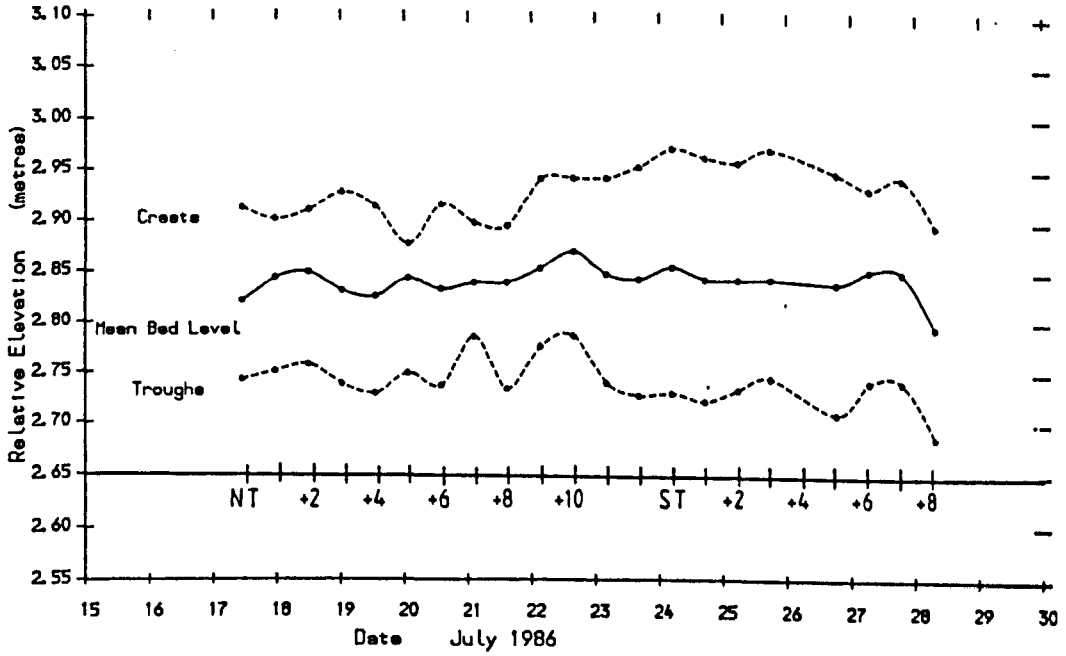

Fig. 3.37 Bedform Heights - Line B (n=219)

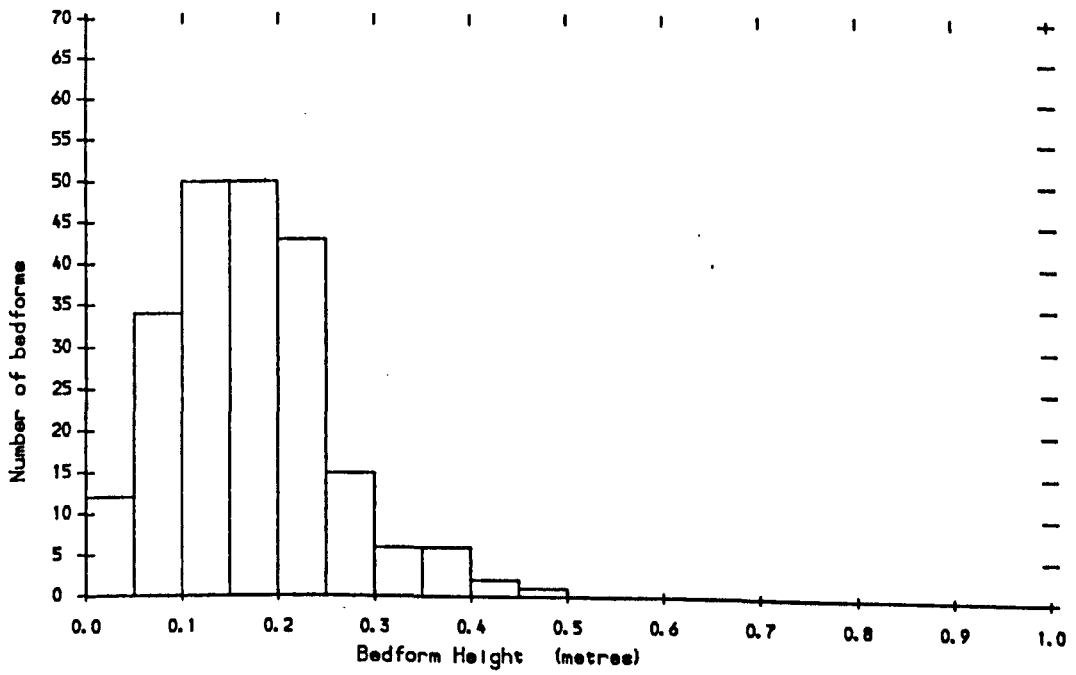

Table 3.6

A comparison of some morphometric parameters.
Data from all simultaneous surveys of Lines and B.

Survey Line A	Survey Line B		Survey Line A	Survey Line B
Bed Level B (m)			**Crest Level C (m)**	
2.840	2.840	Mean	2.936	2.929
0.018	0.015	SD	0.029	0.027
2.863	2.870	Max.	2.968	2.972
2.811	2.794	Min.	2.890	2.876
0.052	0.076	Variation	0.078	0.096
Trough Level T (m)			**Height h (m)**	
2.732	2.741	Mean	0.205	0.188
0.024	0.023	SD	0.034	0.037
2.795	2.786	Max.	0.308	0.240
2.676	2.686	Min.	0.158	0.128
0.119	0.100	Variation	0.151	0.128
Wavelength L (m)			**Flatness L/h**	
4.744	4.378	Mean	23.56	24.34
0.825	1.001	SD	4.43	8.34
5.917	5.713	Max.	30.85	43.40
3.520	2.833	Min.	15.41	15.97
2.397	2.880	Variation	15.44	27.44
Symmetry b/a			**Migration M (m)**	
1.384	1.141	Mean ! Mean	0.43	0.61
0.699	0.439	-1SD ! SD	0.43	0.49
2.741	1.750	+1SD ! Max.	0.98	1.69
3.571	4.033	Max. ! Min.	0.00	0.00
		Ebb !		
*2.083	*1.953	Max. !		
		Flood !		

Notes :
1 - * designates reciprocal of Flood value
2 - M values obtained by lag cross-correlation
3 - Variation = Max - Min
4 - SD = Standard Deviation

The distribution of heights of the two lines is shown on Fig. 3.24 and 3.37. Line A showed a tail of high forms, with 10% >0.3m and 1.8% >0.4m. Line B had 6.8% >0.3m and 1.4% >0.4m, but had none above 0.5m. Bedform height curves were only very broadly in phase (compare Figs. 3.10 and 3.38) and short term trends were sometimes opposite. However, significantly, 10 out of 21 data points coincided to within 0.5cm. Line A bedforms were higher at neap tide and at ST+2/3. Skewness of height over time is shown in Figs. 3.26 and 3.39; positive skewness values indicate that most values are lower than the mean. Much high-frequency scatter is present, but when this is ignored, on Line A from ST+1 onwards there was a high positive skew which gradually decreased. Line B data was more variable and was generally positive prior to ST.

Crestal variation with tidal range (Figs. 3.18 and 3.40) of Line A was slightly different to B, firstly in having no lag effect at ranges above 4.2m, and secondly in having most lag, i.e. the widest hysteresis loop, at low tidal ranges, below 3m. In contrast the Line B loop is widest at mid-ranges. Variation of T is very well ordered for A, but unclear for B. The sum of these variations in shown in Figs. 3.15 and 3.41, the curves of height against tidal range. The Line B curve shows hysteresis at all ranges, Line A only above a range of 3.5m.

3.6.1.1 Interpretation and Conclusions

Some conclusions and interpretations can be made from this comparison. Mean trough levels were more directly related to tidal currents than crest levels, where non-tidal factors such as wave action may have been an important control, introducing short-period scatter in these parameters. The Line B parameters h, T and C are less directly related to tidal range than on Line A. It is considered that wave-activity reduces crest heights, particularly at neap tides, and sediment is deposited in the troughs. As a consequence, being closer to the main channel at low water, (and thus closer to the source

Fig. 3.38 Mean Bedform Height - Line B

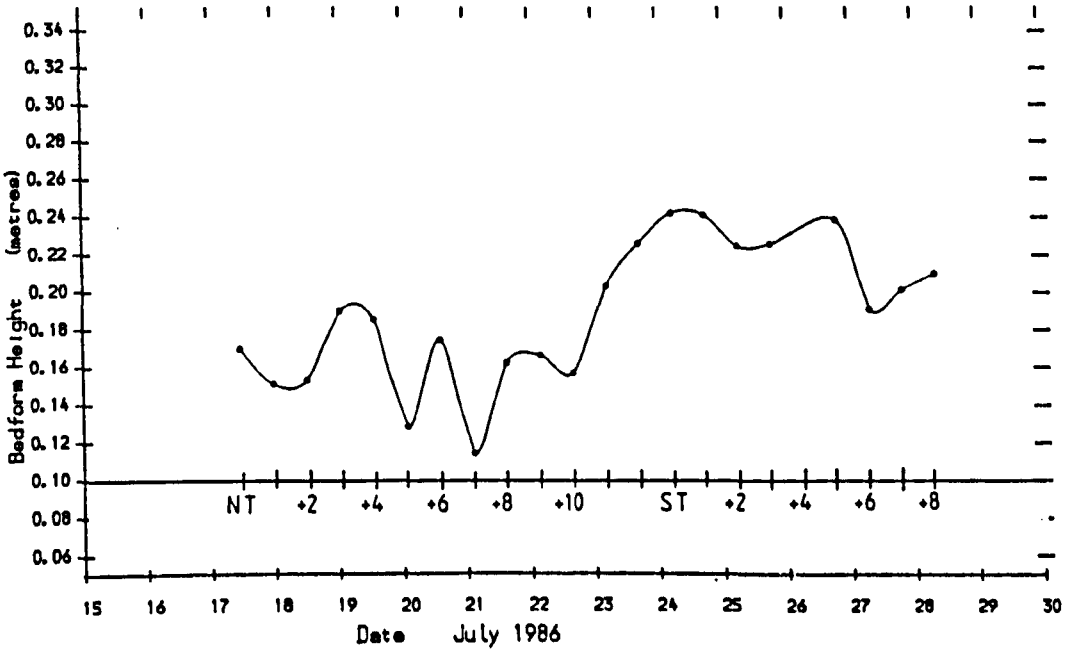

Fig. 3.39 Skewness of Wavelength and Height - Line B

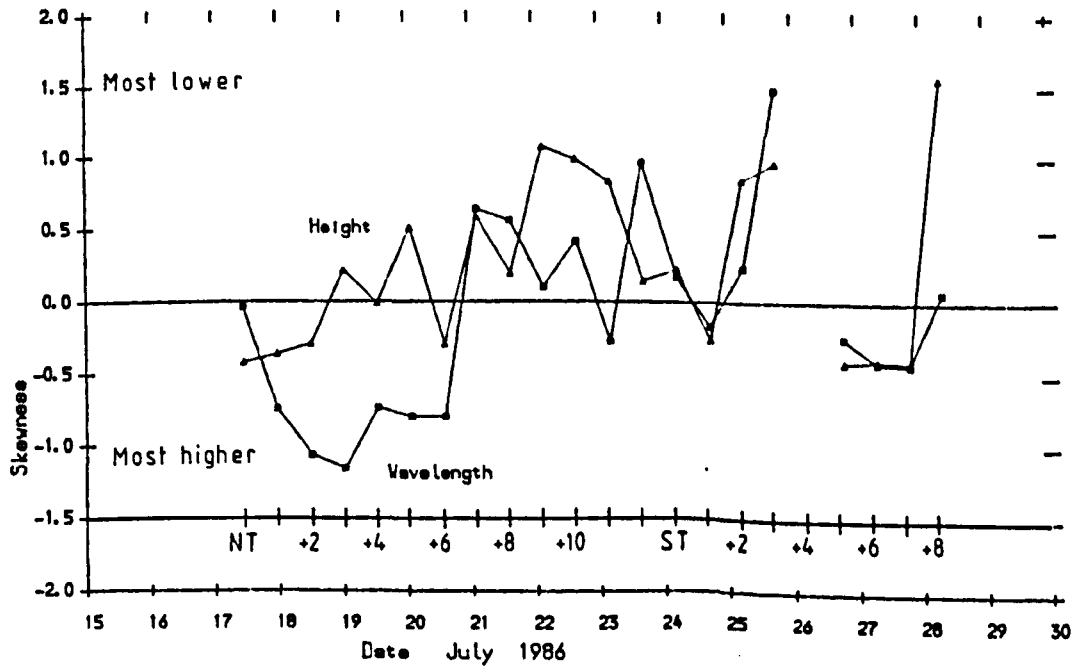

Fig. 3.40 Mean Bed Elevations v Tidal Range - Line B

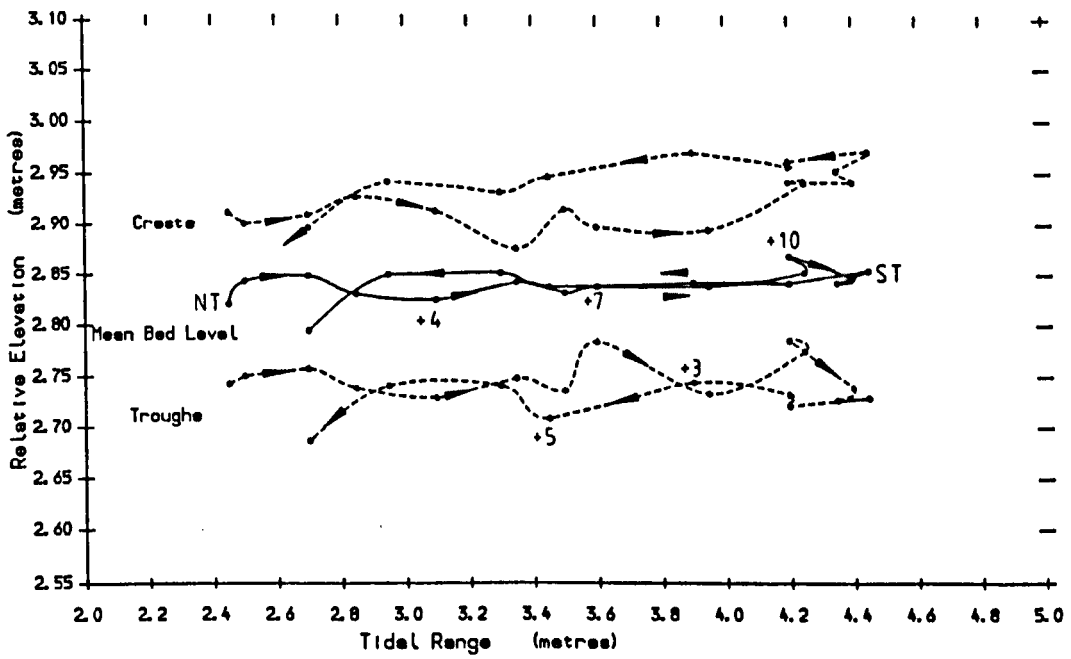

Fig. 3.41 Mean Bedform Height v Tidal Range - Line B

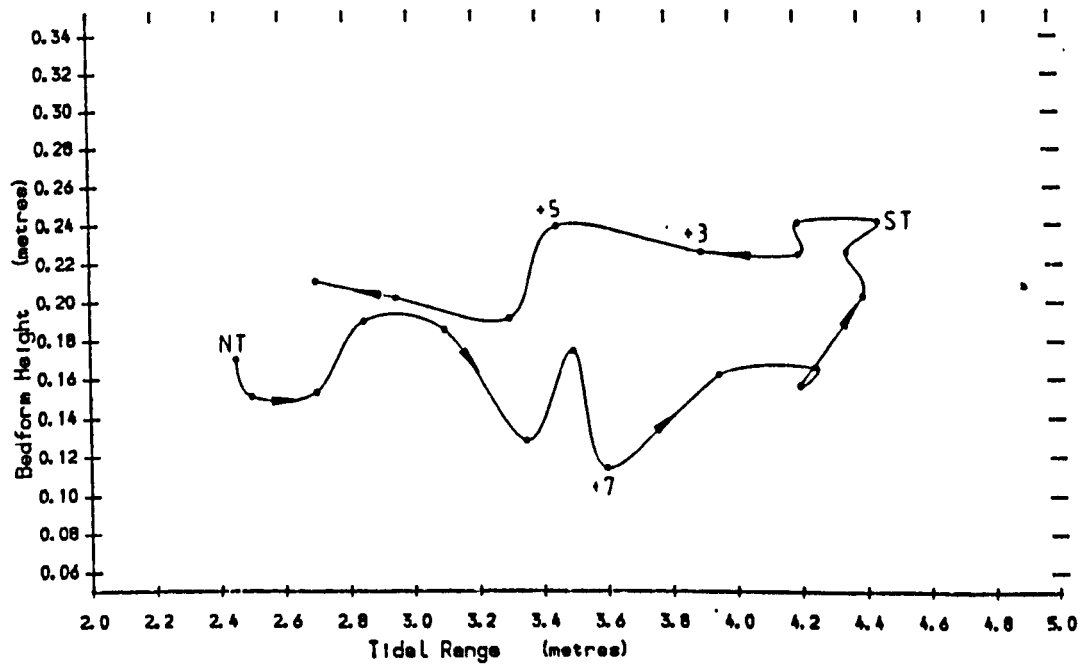

of the waves), this effect is greater towards the shoal edge, i.e. Line B. However crest parallel flows may also be important in varying trough levels; evidence for this is the 3cm drop in trough elevation on Line B between NT+2 and NT+4, despite a total mean migration of only 3cm over that period. Crest elevations on Line A at ST reach equilibrium with the tidal flows, Line B crests not so.

Line A skewness of height showed the effect of an increased proportion of low height forms at ST, due to the initiation of bedforms, whereas Line B showed a similar population change prior to ST, which may be interpreted more as an effect of waves than of tidal flow alone.

3.6.2 Wavelength Comparison

The mean wavelength L on Line A was 8% greater than on Line B, and the SD was 18% less. Line A had both a larger maximum and minimum than B. The Line A population was multimodal (Fig. 3.23) but overall normally distributed, in contrast to B (Fig. 3.42) where there was a more even spread in L. Both populations had a largest mode at L = 4-4.5m.

The long term trends of L are identical and in phase, and in the short term are very similar. At ST+2 L of Line A was 1m greater than Line B (Figs. 3.11, 3.43). Between NT+7 and NT+11, L on Line A was greater than B by up to 1.3m, due to the generation of small forms on Line B one tide before A. Skewness of L on Line A (Figs. 3.26, 3.39) showed no clear pattern with much short period scatter whereas Line B showed a post-neap negative skew (i.e. most wavelengths were higher than the mean) and generally positive around springs, in common with Allen & Friend (1976a, his Figs. 4 and 8).

There are remarkable similarities in the curves of L against tidal range (Figs. 3.16 and 3.44) with the crossover in the curves occurring between the same tides. At ranges >3.6m L on Line A was up to 1m greater than Line B, but at NT+12 to ST+1 was almost identical.

Fig. 3.44 Mean Bedform Wavelength v Tidal Range - Line B

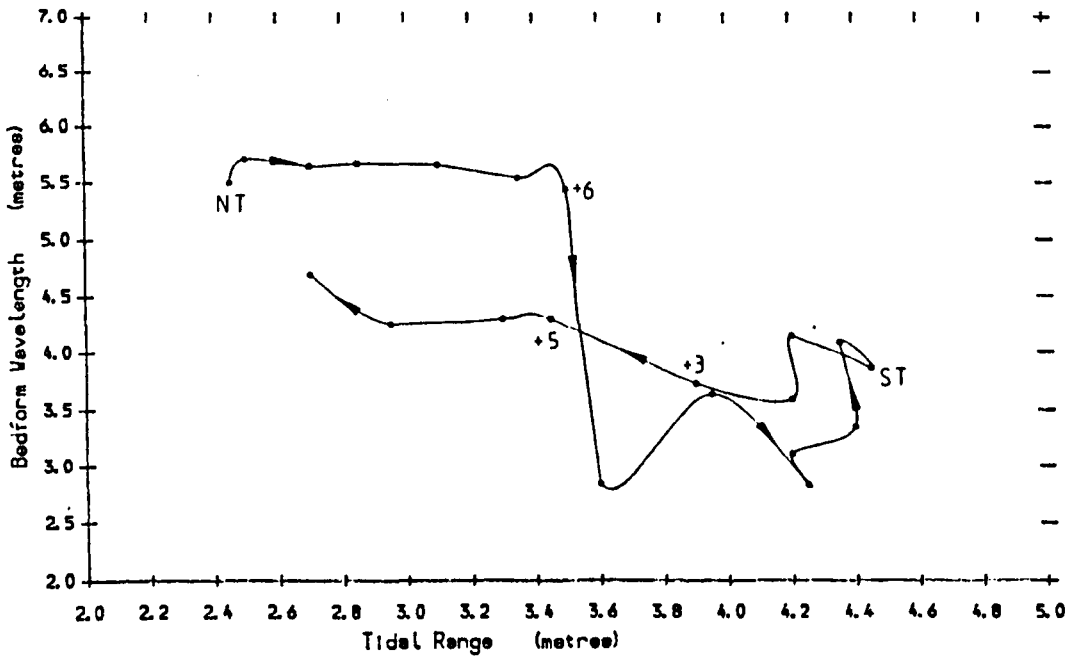

Fig. 3.45 Bedform Flatness - Line B (n=219)

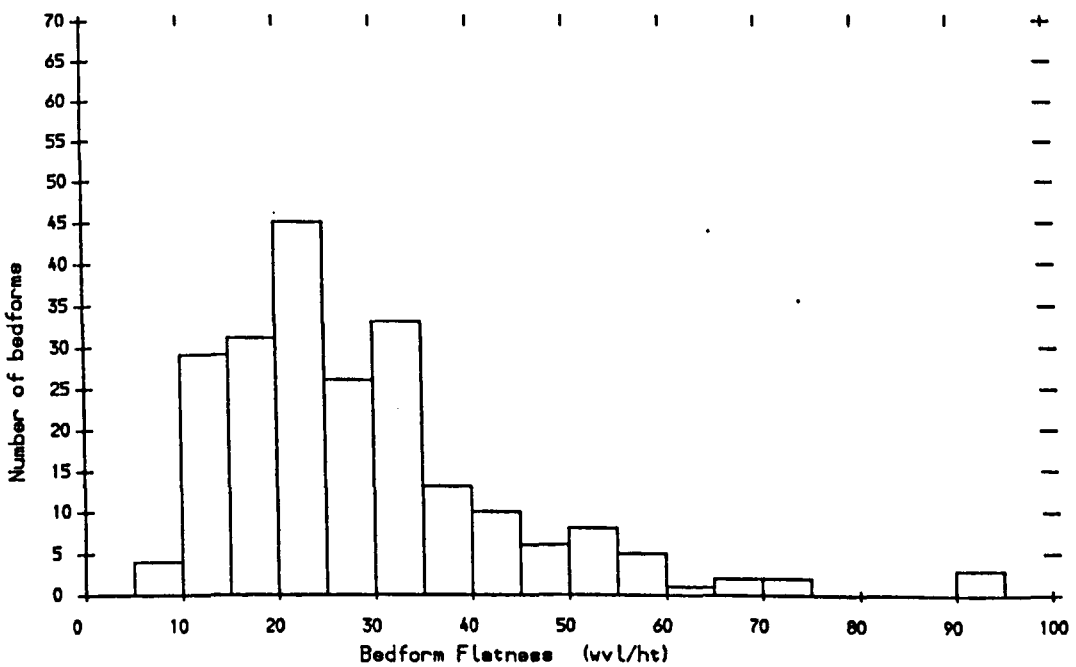

3.6.2.1 Interpretation and Conclusions

Scour pits and the associated short 3D megaripples were better and earlier developed on B, which implies that the nature and speed of the currents may vary significantly across the shoal, despite its limited size. Possible variables include tidal current velocities, flood-ebb velocity ratio, and wave influence, and if these occur, they may explain why the SD of Line B is the greater. One reason against a wavelength difference is that they are subject to exactly the same depth variation curve.

The near coincidence of points at ST implies that both lines were near an equilibrium form, and also that at ST there was more spatial uniformity in megaripple wavelengths. The pattern of skewness of L on Line B shows that the high tidal ranges correlate with the predominance of short forms in the population.

3.6.3 Flatness Comparison

Flatness values are very similar, but Line A had both a lower SD and maximum value. Flatness distribution plots (Figs. 3.25, 3.45) show that both populations appear to be one skewed distribution; both have 10% of forms with L/h >50. The steepest bedforms, i.e. lowest flatness, occurred simultaneously at ST+2. Their long term trends are the same and in-phase, however short term variation was higher on Line B during the post-neap period (Figs. 3.12, 3.46). From NT+9 to ST+1 L/h on line A was consistently higher than B, and generally lower between ST and ST+8. A total of 8 points out of 21 are coincident. There are few notable differences in the curves of flatness against tidal range (Figs. 3.17, 3.47) with both lines showing a single clockwise loop. Little variation occurs above ranges of 4.2m.

Fig. 3.46 Mean Bedform Flatness - Line B

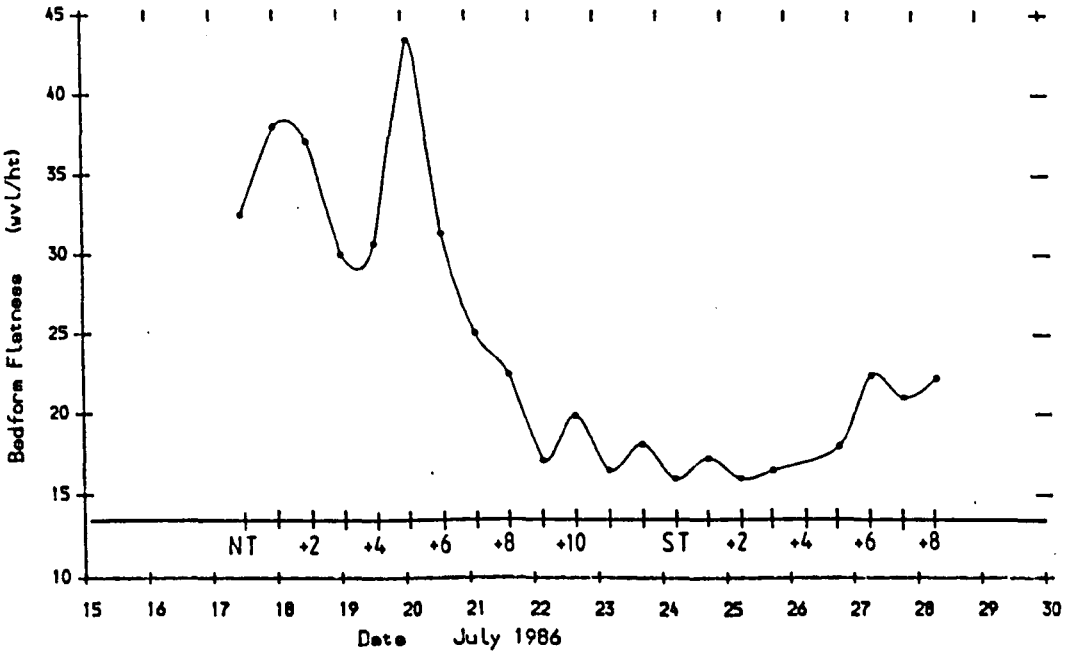

Fig. 3.47 Mean Bedform Flatness v Tidal Range - Line B

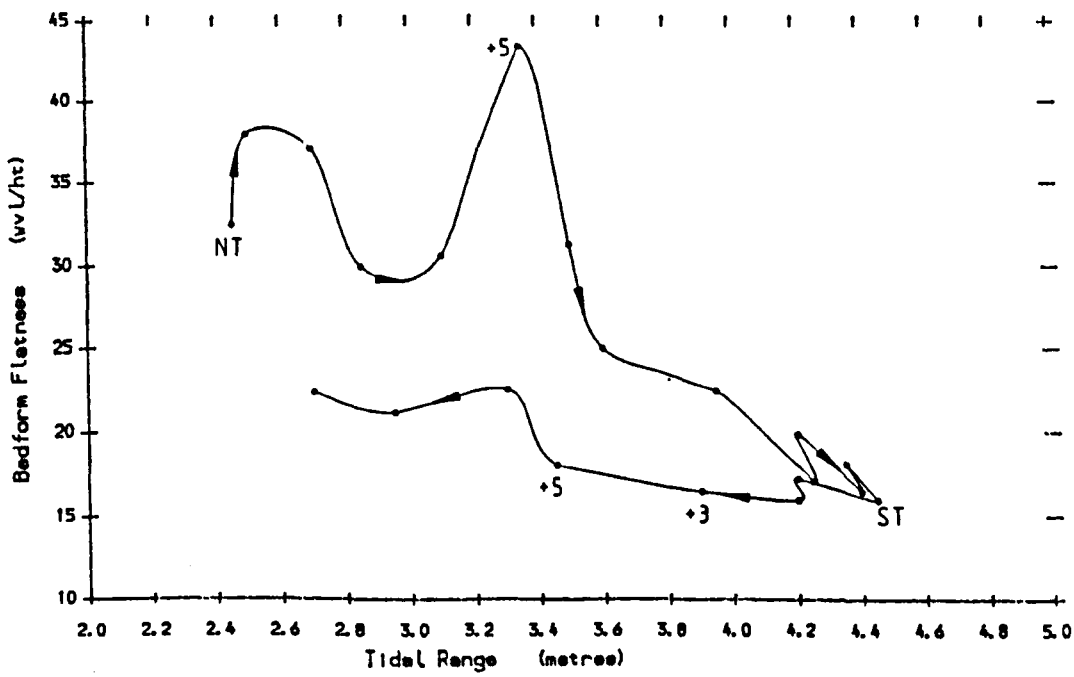

Fig. 3.48 Mean Bedform Symmetry Index - Line B

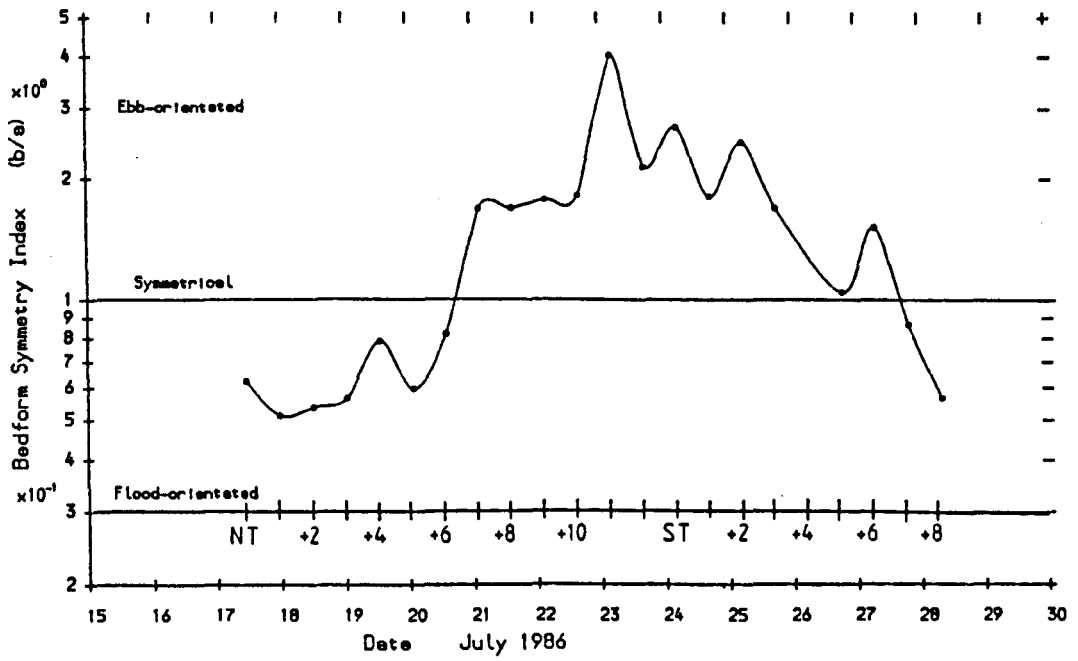

3.6.3.1 Interpretation and Conclusions

As with the wavelength data comparison, it appears that at ST both lines reached an equilibrium with respect to the tidal currents. That Line B values were more variable is interpreted as effects of wave action and/or lateral runoff. Maximum flatness on Line B occurred at NT+5 when mean symmetry was still flood- orientated, but on Line A the maximum was with symmetrical bedforms implying non-tidal factors to be important. In addition, maximum flatness occurred immediately prior to the first appearance of short wavelength scour-pits, i.e. it appears that flat long- wavelength bedforms are unstable at these times.

The post-neap period of higher and more variable L/h values on Line B is interpreted as being due to the interplay of megaripples close to their migration threshold, and non-tidal factors such as wave action and late-stage runoff. The flatness population distribution indicates that the two lines are very similar, and this may indicate that flatness is a fundamental response to the tidal current regime.

3.6.4 Symmetry Comparison

Line A bedforms were, on average and in terms of their SD, more ebb-orientated than B, and on both lines maximum mean ebb-orientations were greater than the maximum attained flood values. Their overall trends were similar, with reversed surveyed symmetry at NT+6/7, and both showed the effects of the greater diurnal tidal variation between NT+9 and ST+3, with higher ebb-symmetry values on ST, ST+2, +4 etc. (Figs. 3.9, 3.48). Both lines showed that at tidal ranges below 3.6m bedforms were more flood-orientated on rising ranges, and that at spring tides an ill-formed clockwise hysteresis occurred.

3.6.4.1 Interpretation and Conclusions

With a survey programme taking place at LW, it is to be expected that in an area of strong tidal currents, peak surveyed ebb-symmetry is greater than

peak flood-symmetry. To explain why the Line A bedform population was more ebb-orientated than B, a number of factors may be considered. Firstly, the relative strength of the ebb current may be higher along Line A, perhaps caused by the local coastal morphology and bed topography. Secondly, if the previous inference that wave action is significant is correct, waves may affect the late stages of the ebb flow over the edge of the shoal, i.e. Line B. As has been previously discussed, ebb-caps are important in determining b/a, and if waves disrupt ebb-cap formation, or rework ebb-caps, then b/a values are likely to be less ebb-orientated. It was noted that ebb-caps were better formed on the topographically high parts of the shoal, i.e. the mid- parts of Line A, compared to most of Line B (Figs. 3.32, 3.33).

However there are possible effects acting against the fact that Line A symmetries are greater than B. One is that of mean bedform size in relation to sediment transport. Both mean heights and wavelengths on Line B are smaller, and thus equivalent amounts of ebb-directed sediment transport along both lines may be expected to produce Line B bedforms more fully orientated with the ebb.

A second possible effect is that of different net bed material transport directions on the surface of estuarine shoals. There are two causes :

1 - With an asymmetrical tide such as exists in the estuary, a shoal may only be inundated near the end of the flood tide when the high flood velocities may cause significant flood-directed sediment transport. The longer duration but weaker ebb tide may not exceed the threshold for sediment entrainment and transport, or may not exceed it by much. As bedload transport is a power function of flow velocity, over a single tidal cycle there may be a net flood-directed bed material transport over a shoal. By contrast, channels may have a greater relative ebb-transport component due to late stages of the ebb tide being confined in them, and velocities thus increased;

2 - Under certain conditions local estuarine topographic effects may cause a particular direction flow may be deflected towards or away from the shoal.

No direct evidence for cause 1 would be expected due to the limited relief differences along and between the survey lines. However, Fig. 3.28 shows that there is a considerable lateral gradient of net sediment transport rate across the shoal, with greater net flood-directed transport on Line B, near the shoal edge.

From the above consideration, it is concluded that the disruption and/or reworking of ebb caps, and possibly local topographic effects on tidal flow direction, are the causes of the greater ebb asymmetry of the bedforms on Line A.

3.6.5 Migration Comparison

Total migration distance over the 21-tide period from NT to ST+8 was 9.13m for Line A, 12.86m for B, i.e. tidal averages of 0.43m and 0.61m repectively. The long and short term variation of M was virtually identical, but whereas M on Line B peaked very markedly at NT+11 then again weaker at ST+2, Line A values peaked twice, at NT+12 and ST+2 (Fig. 3.28). In terms of variation with tidal range (Fig. 3.30) limited lag occurred on Line B except at low ranges.

3.6.5.1 Interpretation and Conclusions

At virtually all stages of the tidal cycle M was higher on Line B (near the shoal edge), implying flood- tidal velocities were relatively higher at B, and ebb at A. Like the symmetry comparison, this may be related to greater flood-directed residual flows at the shoal edge compared to the centre. In the case of Line B, the decreased heights around NT+10/11 may have been a factor in the high M at NT+11. Binding of sediment at neap tides may have been important in determining the sediment threshold on rising tidal ranges.

3.7 Palaeoflow Reconstruction from Megaripple Deposits

3.7.1 Introduction

There follows a look at 'geological measures' of bedform migration (i.e. those features of ancient deposits that may be measured in the field) to see how they compare with the lag cross-correlation measure of migration, and with the calculated total bedload sediment transport. The likely effects on the accuracy of palaeoflow calculation are also discussed.

3.7.2 Geological Measures of Megaripple Migration

As a comparison with the lag cross-correlation measure of migration M, two geological measures of megaripple migration are used here :

1 - Crest and trough migration (Mct)

Crest and trough points from successive profiles were normally identifiable as the same features of the same bedform, and therefore their horizontal offset (migration) could be measured throughout the lunar cycle. The measure of migration used is the average migration rate of these two features on each bedform;

2 - Brink and toe ('slip face') migration (Msf)

Brink and toe positions of each bedform were also recognised from one tide to another, and their movement quantified. The measure of migration is the average migration rate of the brink and toe of each bedform, which is an approximation of the horizontal width of the tidal bundle which a geologist may measure.

(This method gave no measure for Line A at NT+7 and NT+8 when slip faces were absent. This was related to the presence of near-symmetrical megaripples which were insufficiently developed as either flood or ebb-orientated forms to show slip faces).

3.7.3 Comparison of the Migration Measures

The mean migration over the length of Lines A and B was calculated by the three methods and is shown in Figs. 3.49a & b. These clearly show that the three measures show similar overall trends, but are very different as short term or individual measures of 'migration'.

Line A - After neap tide the three measures show similar magnitude and diurnal variation, but increased tidal ranges produced differences between M and Mct of greater than 0.5m at NT+8. Only immediately after ST were all measures equal.

Line B - All three migration measures were broadly similar throughout the study period, and were particularly close from NT+12 to ST+3.

It is concluded from this comparison that in this study, the three different measures of megaripple migration tend to be equivalent at spring tides, when net migration was strongly in the flood direction and bedforms were totally re-orientated to an ebb-asymmetry by the ebb tide. The spring tide equivalence of the different migration measures is explained by the fact that despite net flood migration, the flood-orientated megaripples were reworked to a common shape over this period, i.e. full re-orientation of the bedforms produced an 'equilibrium form' of ebb megaripple, so that relative positions of crest, slip face and trough on each megaripple were little changed from one LW to the next.

Comparison of short-term averages of simultaneous measures provides a very useful insight into the use of the geological measures (Table 3.7). The three measures give similar results for the initial neap tide period where migration rates were very low, however at spring and intermediate tides there is a large difference between the lag result M and the other two; for example Mct and Msf are very close at spring tides and are 20% greater than M, but are respectively 96% and 150% greater then M during post-spring intermediate tides. An explanation for this is given below.

Fig. 3.49 (a) Line A - Three measures of megaripple migration; (b) Line B - Three measures of megaripple migration

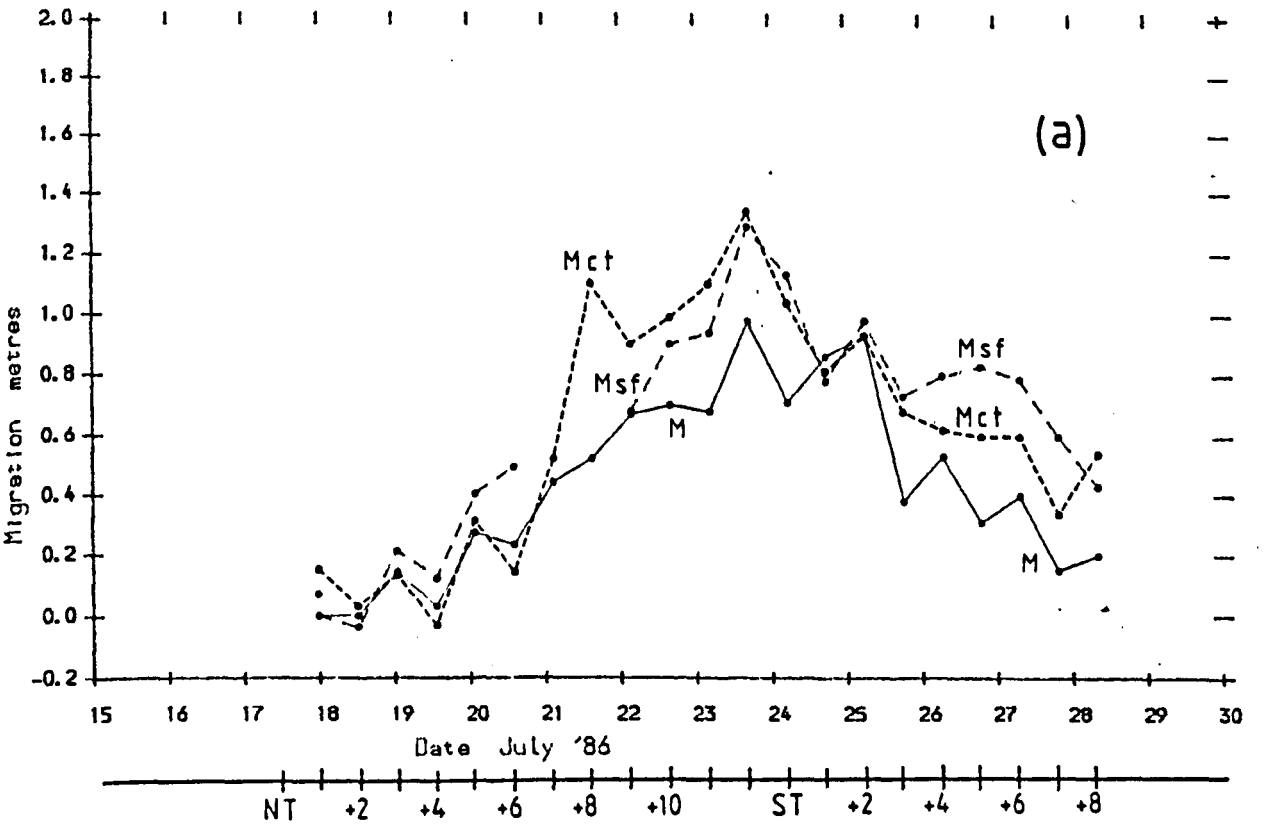

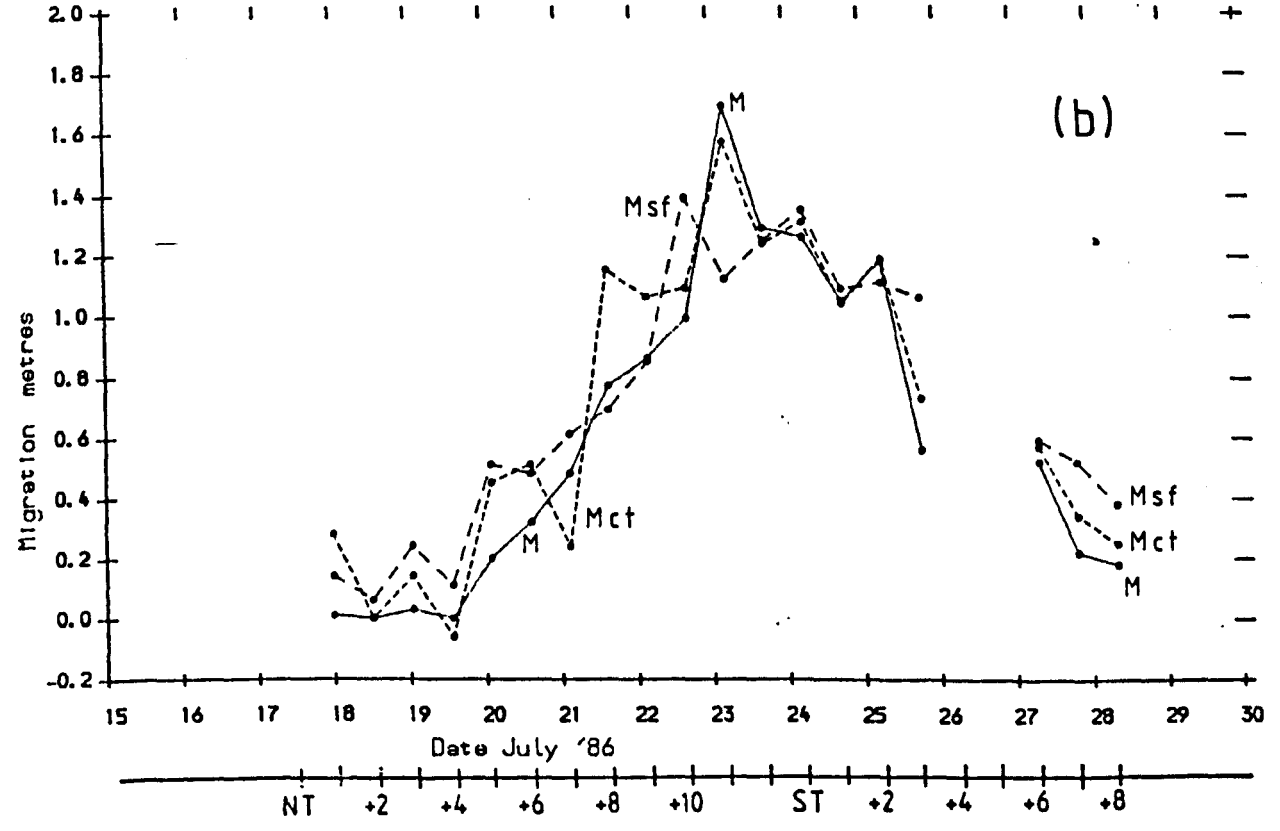

Table 3.7

A comparison of three measurements of migration
Four-tide mean migrations (m)
Data from Line A

Migration Measure	NT+1-NT+4	NT+7-NT+10	ST-ST+3	ST+5-ST+8
M	0.043	0.583	0.72	0.26
Mct	0.07	0.878	0.865	0.52
Msf	0.09	-	0.9	0.663

3.7.4 Geological Implications

Taking all comparable data over the whole survey period shows that for Line A, Mct and Msf are larger than M by 34% and 87% respectively. For Line B, the equivalent figures are 43% and 76%. So on average, Mct and Msf are approximately 40% and 80% larger than the lag cross-correlation migration M. The reasons for this are most probably due to the effects of merging or decaying bedforms. When megaripples are merging or decaying, they tend not to have a well-defined morphology, i.e. they do not display a slip face, or an obvious trough-crest-trough form. Thus, the measures Mct and Msf tend to be applicable to the more 'active' megaripples, i.e. those which are migrating. In this way, these two measures are inherently likely to be lower than the lag cross-correlation method of measuring migration. This also explains why Msf is the largest of the measures, as a megaripple brink and toe are only identifiable on the most actively migrating forms.

If we make the simple assumption (shown below to be true) that the lag cross-correlation measure of migration (M) most closely approximates bedload sediment transport (by virtue of being a measure of movement of the whole bedform rather than of specific points), then a geologist measuring

tidal bundle width on the ideal exposure of perfectly preserved megaripple cross-beds, sectioned perpendicular to the palaeocrestline, would systematically overestimate net weekly/monthly sediment transport rates over the preserved bedform. There are of course many simplifications and assumptions contained in this statement, not the least of which is that merging and decaying bedforms tend to have relatively high trough levels and low migration rates, and so the preservation potential of sedimentary structures produced in these situations is in any case very low.

The reasons for short term differences in M, Mct and Msf are related to megaripple shape in the vertical plane; for example, if a symmetrical form develops into a strongly asymmetrical megaripple, or if an ebb cap is developed or lost. Using the above assumption regarding sediment transport measured by M, is clear that the best estimates of palaeo-transport rates would be obtained from those tidal bundles deposited at times in the lunar cycle when megaripple morphology was most stable i.e. :

1 - from measurements of tidal bundles formed at and just after spring tides (broadly speaking the largest bundles);

2 - from measurements of post-neap tidal bundles.

The precise times in the lunar cycle when the geological measures of migration are most 'accurate' would depend greatly on the particular dynamics of the flows and bedforms in the area of deposition; for example, in this study the particular set of tidal velocities and asymmetries meant that at rising intermediate tidal ranges there was a change in the population structure of the megaripples, resulting in greatly increased differences between migration measured by lag cross-correlation and by 'geological' means. However, if these velocities had only been achieved at spring tides then Mct and Msf would have been <u>least</u> reliable measured from the largest bundles. This would be the case on the Lifeboat Station Bank at Wells-next-the-Sea (Allen & Friend, 1976a) where the 'minor dunes' were active for only 1 or 2 tides per lunar cycle.

Studies like this one give greater understanding of the possible range of sedimentary structures produced over the lunar cycle. With this better information, it should become easier for geologists to identify those tidal bundles within the lunar cycle which will potentially provide most useful information.

3.7.5 Correlation of Flow with Sediment Transport and Megaripple Form

The flow data collected over the shoal at Fegla Fach has been correlated with various transport parameters derived from the megaripples. The flow parameters considered were : Tidal range; Maximum depth; Umaxflood; U100maxflood; and V.A.I. (= U100maxflood/U100maxebb).

The bedform morphological measures used were : the 3 migration measures, M; Mct; Msf; and volumes of Erosion (E); Accumulation (A); and Transport (T).

3.7.5.1 Megaripple Migration as a Measure of Bed Material Sediment Transport

To determine which of the 3 migration measures above is best suited for use as a measure of bed material sediment transport, T was correlated against each one, by using a least squares fit linear regression. Figure 3.50 shows:

1 - the raw data for lag cross-correlation migration M; the regression line is drawn with a solid line (three points of lowest migration were removed prior to the regression calculation, as they were far removed from the strong trend of the other points and had migrations below the survey resolution);

and 2 - the regression lines for Mct (short dashes) and Msf (long dashes), both similarly amended.

Fig. 3.50 Relationships between sediment transport and the three measures of migration.
(Data points shown for lag migration data M only).

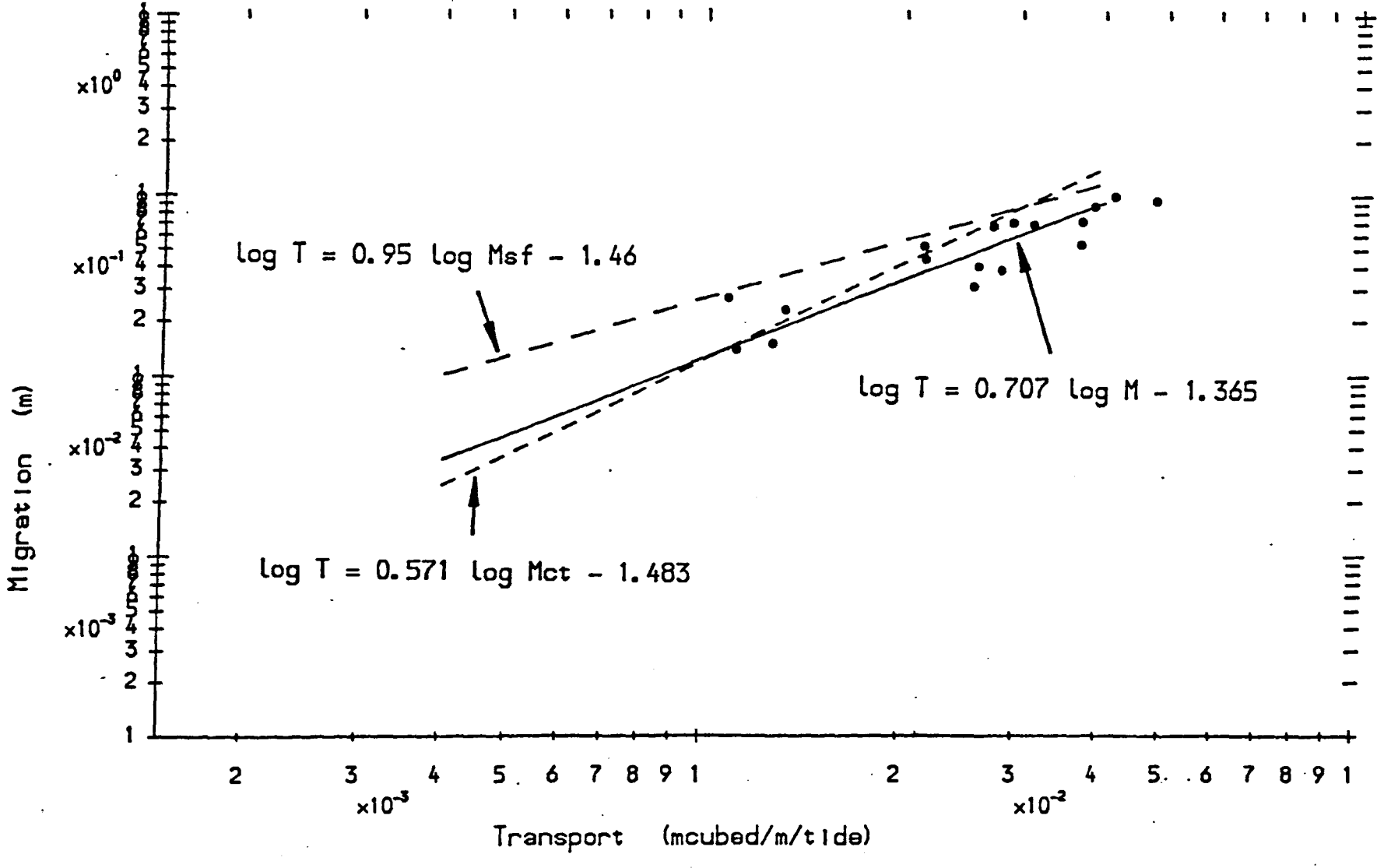

With migration in metres/tide, the regression equations obtained are :

$\log T = 0.707 \log M - 1.365$ $m^3/m/tide$ (7.1)

with correlation coefficient CC = 0.903

and number of data points n = 17

$\log T = 0.571 \log Mct - 1.483$ $m^3/m/tide$ (7.2)

CC = 0.836, n = 17

$\log T = 0.95 \log Msf - 1.46$ $m^3/m/tide$ (7.3)

CC = 0.865, n = 15.

As expected from the morphological considerations explained above, the lag-cross correlation measure of migration is strongly related to sediment transport, and the Mct and Msf measures are less well correlated. The steep gradient of T with Msf may reflect post-neap steepening of slip faces towards an avalanche slope, rather than migration of already steep lee slopes, i.e. Msf may be systematically lower then M or Mct at low transport rates because a certain volume of sediment transport is required to steepen lee slopes before they migrate.

The measured transport volumes (and hence these equations) probably represent a lower limit to the actual volume moved in one tidal cycle, firstly because some sediment is moved by the ebb tide, and secondly because some bed material may be temporarily suspended in the crestal region and move over the trough onto the stoss slope of the next downflow megaripple. Van den Berg (1987) also noted that some suspended grains may be incorporated into the lee face deposits, hence apparently increasing bedload transport.

Measured flood tides give 14 data points from which to obtain relationships of flood flow to migration. The correlation coefficients for the derived expressions are low, below 0.55. For the maximum flood velocity at 1m above the bed U100maxflood, in m/s

$$\log M = 4.173 \log U100maxflood + 0.017 \qquad (7.4)$$

$$CC = 0.526, n = 14$$

$$\log Mct = 3.685 \log U100maxflood + 0.096 \qquad (7.5)$$

$$CC = 0.497, n = 14$$

$$\log Msf = 3.44 \log U100maxflood + 0.145 \qquad (7.6)$$

$$CC = 0.470, n = 12.$$

Regression equations for Umaxflood, the maximum depth mean flood velocity are presented below. These are based on fewer data points (n = 9, or 8 for Msf). With relatively few points as the base for these expressions, these may have limited use in terms of palaeoflow analysis.

$$\log M = 1.291 \log Umaxflood - 0.162 \qquad (7.7)$$

$$CC = 0.438, n = 11$$

$$\log Mct = 1.747 \log Umaxflood + 0.005 \qquad (7.8)$$

$$CC = 0.441, n = 11$$

$$\log Msf = 1.099 \log Umaxflood + 0.063 \qquad (7.9)$$

$$CC = 0.41, n = 9.$$

Terwindt & Brouwer (1986) also used linear regressions between flow and migration or transport parameters. For 3-D megaripples, they obtained the relationship

$$\log U_{maxflood} = 0.194 \log M_{sf} + 0.018 \qquad (7.10)$$

$CC = 0.88, n = 32.$

For 2-D megaripples their relationship had a correlation coefficient of only 0.63. Equations 7.9 and 7.10 are compared in Table 3.8.

Table 3.8

Comparison of Predictive Migration Equations

Velocity (m/s)	Msf (m) Eqn.7.9 This study	Msf (m) Eqn.7.10 Terwindt & Brouwer (1986)
0.1	0.09	0.00
0.2	0.20	0.00
0.3	0.31	0.00
0.4	0.42	0.01
0.5	0.54	0.02
0.6	0.66	0.05
0.7	0.78	0.12
0.8	0.90	0.25
0.9	1.03	0.46
1.0	1.16	0.80
1.1	1.28	1.33

The equation of Terwindt & Brouwer (1986) suggests a migration threshold velocity of 0.4-0.5m/s., broadly in agreement with their observed threshold of 0.5- 0.6m/s. The equation derived here suggests a threshold velocity of less than 0.1m/s, under a quarter of the approximate threshold from observations (see below). The results suggest that at equivalent peak flood depth mean velocities, net megaripple migration would be greater on Fegla Fach. This may be an effect of a longer flood tide duration in the Mawddach Estuary than over the shoal studied by Terwindt & Brouwer (1986). The ebb tide is also longer in Fegla Fach, so that net ebb transport effects are likely to be greater (see also below). However, observations show that the flood threshold for migration in the two studies were approximately equal, and the few data points used to derive equation 7.9 are considered insufficient to reflect the actual relationship present.

By far the strongest relationships of 'flow' and megaripple migration are found with the indirect measures of flow strength, i.e. predicted tidal range and maximum water depth. These two measures form linear regressions with similarly high correlation coefficients. For predicted tidal range R

$$M = 0.466\,R - 1.254 \quad m \qquad (7.11)$$

$$CC = 0.924,\ n = 18$$

$$Mct = 0.599\,R - 1.57 \quad m \qquad (7.12)$$

$$CC = 0.897,\ n = 18$$

$$Msf = 0.503\,R - 1.18 \quad m \qquad (7.13)$$

$$CC = 0.864,\ n = 16$$

and for maximum depth over the shoal D

$$M = 0.672\,D - 1.571 \quad m \qquad (7.14)$$

$$CC = 0.914,\ n = 18$$

$$Mct = 0.841\ D - 1.911\ m \qquad (7.15)$$

$CC = 0.864, n = 18$

$$Msf = 0.748\ D - 1.593\ m \qquad (7.16)$$

$CC = 0.885, n = 16.$

The high correlation coefficients for these indirect measures of flow strength may be due to four possible factors :

1 - errors in the flow measurement process and subsequent reduction to 10 minute velocity averages. Errors of the current meters themselves are considered negligible; as discussed in Chapter 4 the data was filtered for bad data prior to use. The use of 10 minute averages means that most short period turbulence is averaged out;

2 - the assumption of rectilinear tidal currents, and therefore sediment transport over the shoal. This is unaccounted for in this study;

3 - the inadequacy of the flow parameters U100 and U to represent fully the sediment transport capabilities of the flood tide. Tidal range and flow depth may average out long-period unsteadiness within each individual flood tide, which may affect U100 and U;

4 - sediment transport by the ebb tide may be sufficient to significantly decrease the apparent sediment transport of the flood tide, particularly at spring tides.

The ratio of maximum flood to ebb current speeds V.A.I. did not correlate well with any megaripple or sediment transport measure.

3.7.6 Intra-Population Variation of Migration

When a geologist measures preserved megaripple cross-beds, he has little knowledge of the extent to which the measured bundle reflects characteristics of the general population or the variation of that individual

bedform; for example, in measuring tidal bundle width (i.e. migration) is he likely to obtain a migration rate value applicable to a substantial part of the hypothesised bedform population, or purely to that bedform? In short, how representative are individual measures of migration, and can they be quantified? How big are the error bars on derived sediment transport rates? These questions are addressed below.

A statistical measure of the spread of values of a variable within a population is the standard deviation, and this has been calculated for the migration measures Mct and Msf for each tide. This gives a value of variability of migration rates over each flood-ebb cycle, and therefore a measure of the potential difference of an individual migration rate and that of the population mean.

The standard deviations of Mct and Msf for each tide over Lines A and B are shown in Figs. 3.51a & b. The diagrams show the mean value with error bars of +/- 1 standard deviation (i.e. forming a 68% confidence envelope). In general, the standard deviation of migration is higher around spring tides than neaps. On Line A, Mct attained a standard deviation of 0.8 at NT+11, and Msf a maximum of 0.66 at ST+1. Minimum standard deviations were 0.2 and 0.05 for Mct and Msf.

Relatively high but variable SD occurred prior to springs, when the bedform population was undergoing change. Table 3.9 gives four-tide averages of standard deviations of migration. As an average over the study period, the standard deviation of Mct on Line A was >0.1m greater than the other data in Table 3.9. Line A megaripples showed more variation in L and h than Line B forms, and this would be a possible cause of higher standard deviation of migration on Line A. It does not however explain why Mct and Msf on line B are the same.

Line A migration measure Mct, showing +/- 1 S.D. Fig. 3.51 (a)(i)

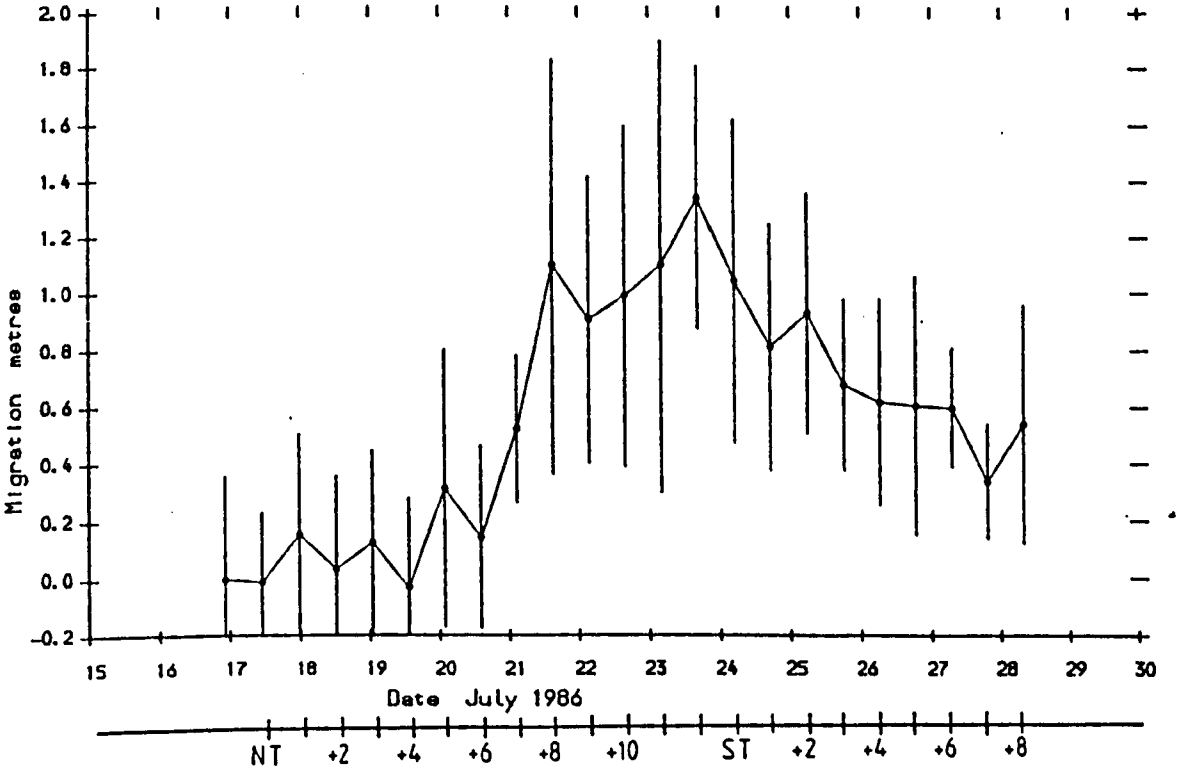

(a)(ii)

Line A migration measure Msf, showing +/- 1 S.D.

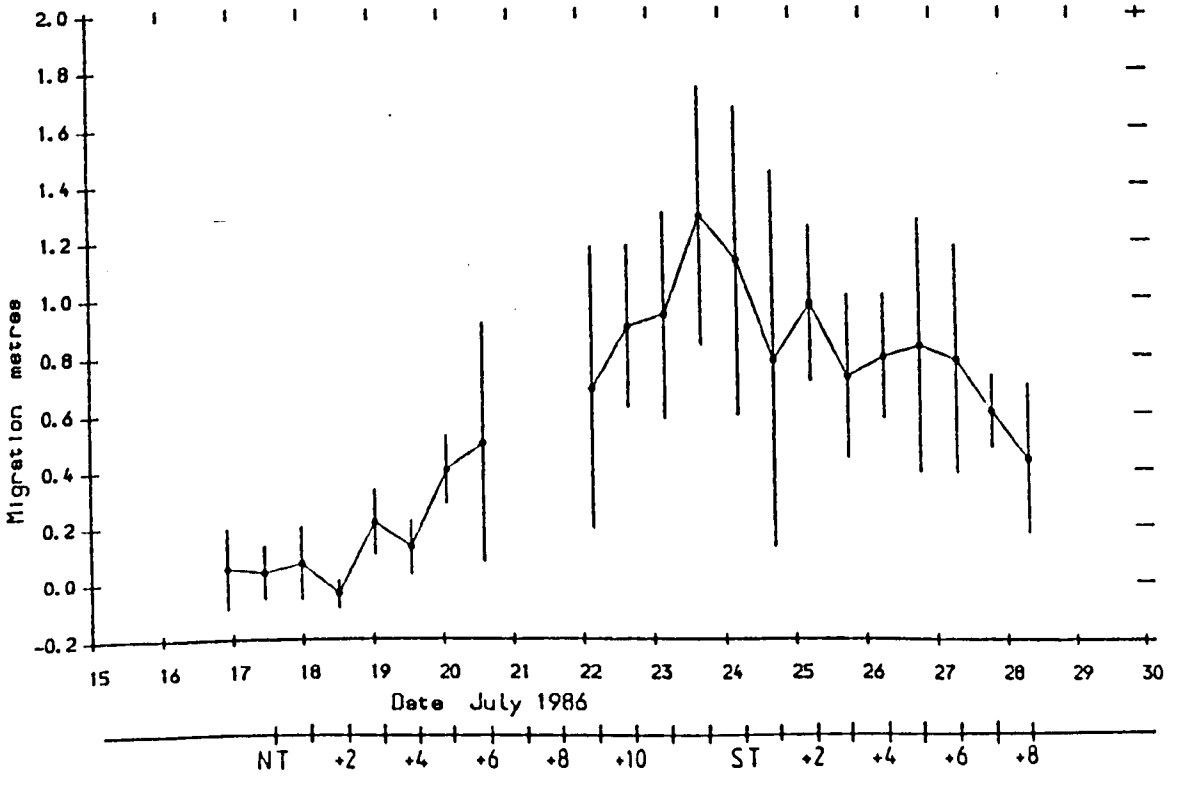

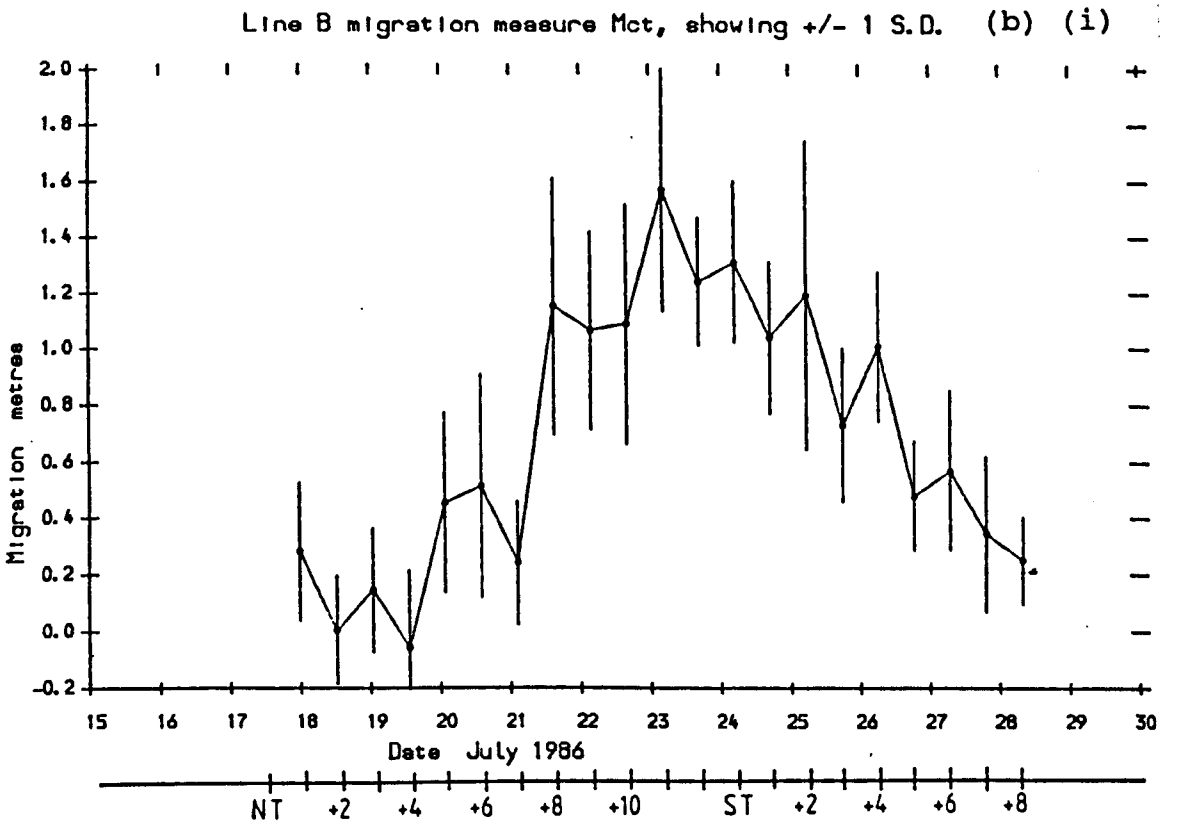
Line B migration measure Mct, showing +/- 1 S.D. (b) (i)
Migration metres
2.0
1.8
1.6
1.4
1.2
1.0
0.8
0.6
0.4
0.2
0.0
-0.2
15 16 17 18 19 20 21 22 23 24 25 26 27 28 29 30
Date July 1986
NT +2 +4 +6 +8 +10 ST +2 +4 +6 +8

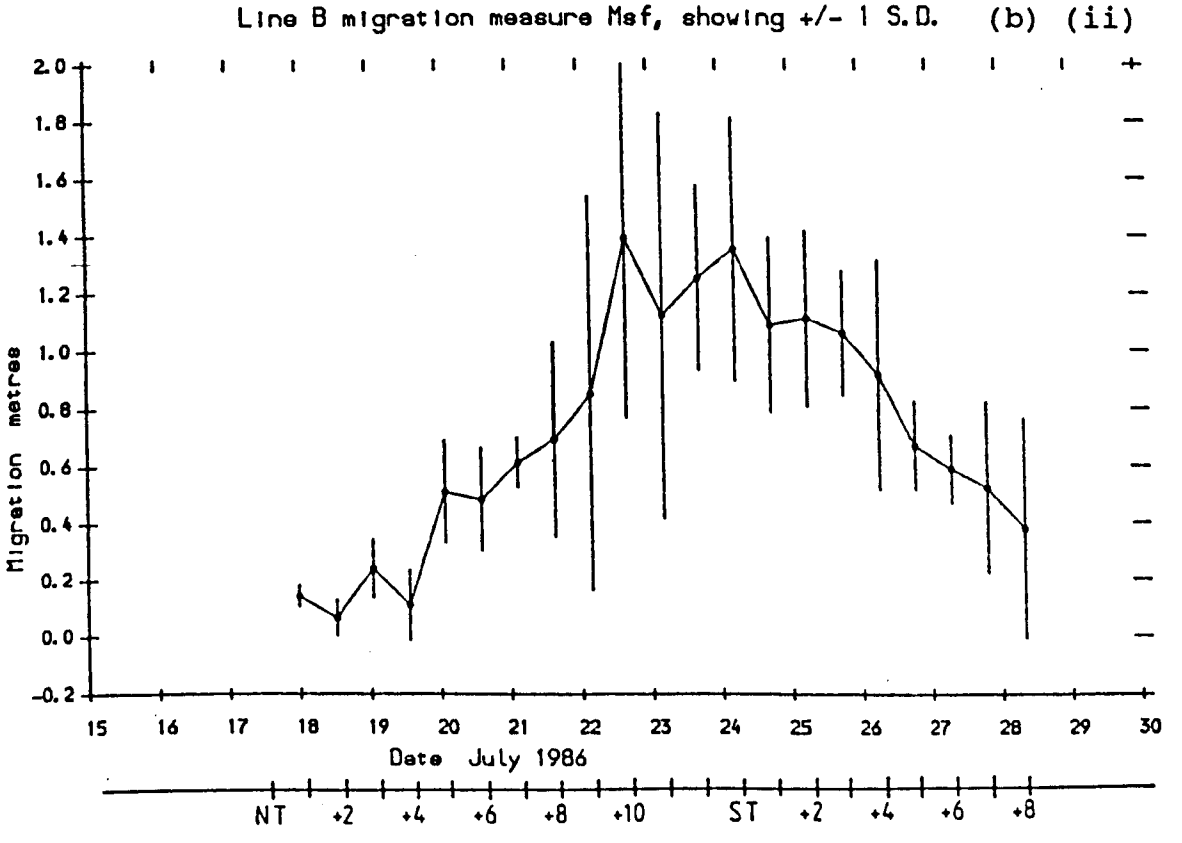
Line B migration measure Msf, showing +/- 1 S.D. (b) (ii)
Migration metres
2.0
1.8
1.6
1.4
1.2
1.0
0.8
0.6
0.4
0.2
0.0
-0.2
15 16 17 18 19 20 21 22 23 24 25 26 27 28 29 30
Date July 1986
NT +2 +4 +6 +8 +10 ST +2 +4 +6 +8

Table 3.9

Four-Tide Mean Standard Deviations of Megaripple Migration (m)

Migration Measure		NT+1 -NT+4	NT+7 -NT+10	ST -ST+3	ST+5 -ST+8
Line A	Mct	0.325	0.535	0.432	0.32
Line A	Msf	0.095	-----	0.437	0.306
Line B	Mct	0.229	0.364	0.345	0.226
Line B	Msf	0.083	0.433	0.320	0.238

Note : On Line A between NT+7 and NT+10 few slip faces were present.

3.7.7 Megaripple Form and Sediment Transport: Palaeoflow Indicators ?

3.7.7.1 Introduction

The importance of the type and shape of sedimentary bedforms in terms of their use for estimating palaeoflow conditions has been of increased interest over recent years. Of most relevance to the study of intertidal megaripples undertaken in this study in the work of various Dutch workers, summarised in Terwindt (1988). A question posed by Terwindt & Brouwer (1986) is whether bedform shape is important in palaeoflow analysis, i.e. is it possible to derive bedform shape from preserved sedimentary structures, and from the shape information to interpret a range of possible palaeoflow conditions. The first step in this process is to determine the nature of the shape-flow relationship. Due to the factors emphasised in Chapter 3, of the intra-population variation and lag of morphological parameters, it is necessary to use parameters averaged over the length (or parts of) of the survey lines.

3.7.7.2 Megaripple Morphological Threshold Conditions

Sediment transport occurs on intertidal shoals, under flow conditions which may or may not be sufficient to cause megaripple migration. On comparing successive transects surveyed over the shoal, up to 0.016 m^3/m/tide of accumulation and 0.008m^3/m/tide of erosion occurred prior to any net migration, at NT+1 and NT+2 respectively. (It should be noted here that these volumes represent sediment movement across a metre width of the shoal, as an average of the whole survey line. Hence, the figures quoted by Terwindt & Brouwer [1986] should be divided by 27m, the length of their survey line, to be comparable with the Fegla Fach data. In figures equivalent to those presented here, Terwindt & Brouwer found up to 0.198 m^3/m/tide of accumulation and 0.182 m^3/m/tide of erosion in a field of 3-D megaripples, and 0.034 m^3/m/tide and 0.061 m^3/m/tide respectively, in a field of 2-D megaripples).

Published flow thresholds related to megarippled shoals are limited to intertidal situations, and include a number of form changes, for instance the start of megaripple migration, full megaripple reversal by ebb currents etc. Table 3.10 summarises the threshold conditions and the associated flow parameters, based on this study and that of Terwindt & Brouwer (1986).

The threshold velocity for megaripple migration found in this study is comparable to that found by Terwindt & Brouwer (1986). This is not entirely unexpected as grain size (~250um), megaripple size (wavelength 5-6m) and the flood tide period of inundation (~3.5hrs c.f. 3.5-4hrs in this study) are all similar. Their Umax threshold for the 2-D and 3-D megaripple transition is close to that for the formation of scour pits on Fegla Fach. The scour pits either disappeared or grew rapidly into larger forms, 3-D in nature. Thus the study provides evidence confirming the findings of Costello & Southard (1981), Boersma & Terwindt (1981) and Terwindt & Brouwer (1986), i.e. that 2-D and 3-D megaripples appear separated in bedform phase diagrams by a depth-mean velocity of the dominant tide of 0.75- 0.8m/s.

Table 3.10

Velocity Thresholds for Intertidal Megaripples

Form Change	FLOW PARAMETER m/s			
	T & B (1986)		This study	
	Umax	Umax	U100max	U*max
* Migration	0.5-0.6	~0.53-0.57	0.56-0.6	~0.04
* Shape change	0.75-0.8	----	----	----
** Ebb cap formation	0.45	~0.24	0.3	~0.033
** Partial reversal	----	NT+6 0.34 ST+6 0.22	0.4-0.45	ST+6 0.051
** Full reversal	0.85	0.31	0.5-0.55	0.067
* 2-D to 3-D transition	0.8	----	---- ----	
* Scour pit formation	----	>0.76	>0.8	>0.056

Notes :
* = Flood tide flow parameters
** = Ebb tide flow parameters

It is notable that the velocity thresholds for the formation of ebb caps and for full reversal of the megaripple by the ebb tide are lower in this study than those quoted by Terwindt & Brouwer (1986). In considering whether the difference is real or not it must be noted that there is some subjectivity in deciding whether ebb caps are present or not. There may also be differences related to the morphology of the megaripples and the shoal upon which the megaripples occur, because on Fegla Fach shoal, ebb caps are better formed on the topographically high parts of the shoal, i.e. the mid-parts of Line A, compared to Line B. Hence wave and depth effects may be controls on ebb cap formation.

In this study, two thresholds regarding bedform reversal are identified, Umaxebb for partial reversal, which produces symmetrical bedforms (as defined by b/a ~1.0), and Umaxebb for full megaripple reversal. However, there are important points regarding the 'validity' and usefulness of these velocities:

1 - the threshold for 'partial reversal' may vary because of the sensitivity of the b/a parameter to megaripple morphology changes in the crestal zone, and the development of small strongly asymmetrical bedforms prior to ST. Is is notable that the Umaxebb of NT+6 and ST+6 both of which produce symmetrical megaripples, are very different, with a threshold 50% higher at NT+6. This may be related to the physical size of the megaripples; all other things being equal, it would clearly require greater volumes of sediment transport to partially reverse a larger bedform. Mean megaripple height and wavelength at NT+6 were 0.18m and 5.65m respectively, compared to 0.19m and 4.31m at ST+6. Part of the reason for the higher partial reversal threshold prior to spring tide is therefore considered to be the longer megaripple wavelength, and thus this threshold velocity may only be of use in relating flow to bedform if bedform size is known. (A further factor is ebb flow duration, see below);

2 - The same factor of megaripple size will be of importance in terms of full megaripple reversal, but as there is only one data point (NT+9), there is no direct evidence for this.

There is great disagreement between the threshold condition for full reversal in this study, Umaxebb = 0.31m/s, and that found by Terwindt & Brouwer (1986), 0.85m/s. There is no doubt that the low values obtained here are not erroneous, as ebb velocities did not attain Umaxebb >0.6m/s at any stage of the lunar cycle, and megaripples were clearly reversed for 6-7 tides either side of ST. At least part of the explanation for this difference may lie in the shape of the ebb velocity curve with time, and the time for which the flow exceeded bedload threshold. Transport thresholds over the

Dutch shoal were exceeded for 70minutes of the 120minute ebb tide (their Fig. 6), compared to >140mins of the ~400min ebb tide over Fegla Fach shoal (using a transport threshold of $U^* = 0.053m/s$).

3.7.7.3 Conclusion

From the above, it is clear that tidal duration is a very important factor in controlling megaripple morphology, and that this precludes the use of certain thresholds derived from studies of this nature. In particular, the flow threshold velocities related to the ebb tide, i.e. ebb cap formation, and partial or full megaripple reversal, may only be applicable in tidal and sedimentary conditions similar to those on the studied shoal.

In contrast, the flood thresholds found by the two studies are very similar, and this may indicate a greater potential use in palaeoflow analysis. There is, however, a need for research in environments where the flood tide has a significantly different duration from this study.

3.8 Sediment Transport on Fegla Fach Shoal

Comparison of surveyed transects over the shoal also allowed the determination of the volume of erosion E, and volume of accumulation A (Chapter 3). The total volume of bed material transport is given by

$$j = (E + A) / 2 \quad m^3/m/tide \qquad (7.17)$$

where E and A denote a volume of sediment transport per metre of the survey line, i.e. a mean value. Hence the measure of sediment transport j is the transect mean net volume of sediment transported across a metre width of the shoal in one flood-ebb cycle.

Results - Line A

Values of j varied between $0.0048m^3$/m/tide and $0.048m^3$/m/tide, i.e. within one order of magnitude, with minimum and maximum values having occurred 2 tides after predicted NT and ST respectively. The lunar cycle is evident in the curve (Fig. 3.52a), but the diurnal variation is absent. At ST+8, j attained $0.031m^3$/m/tide, 65% of the peak value measured at ST+2. This is due to the high volume of erosion E, $0.059m^3$/m/tide. In contrast, the corresponding A was only 5% of this value. The weather conditions at this time were heavy rain and a strong up-estuary wind, creating waves within the estuary, some of which were breaking onto the shoal, and it is concluded that such conditions cause great net erosion of the shoal, presumably with deposition in adjacent channels. (Kohsiek et al (1988) found that during storms, the total sand transport on a large (6.5x2.5km) shoal in the Oosterschelde increased by 3-8 times, and the net sediment transport was directed off the shoal). The calculated volume of erosion is 20% higher than the maximum fair-weather E, which occurred at ST+2. Hence such conditions are likely to have a significant effect on the sedimentary structures formed, and their preservation potential.

Fig 3.52 Sediment transport j

= (erosion + accumulation) / 2

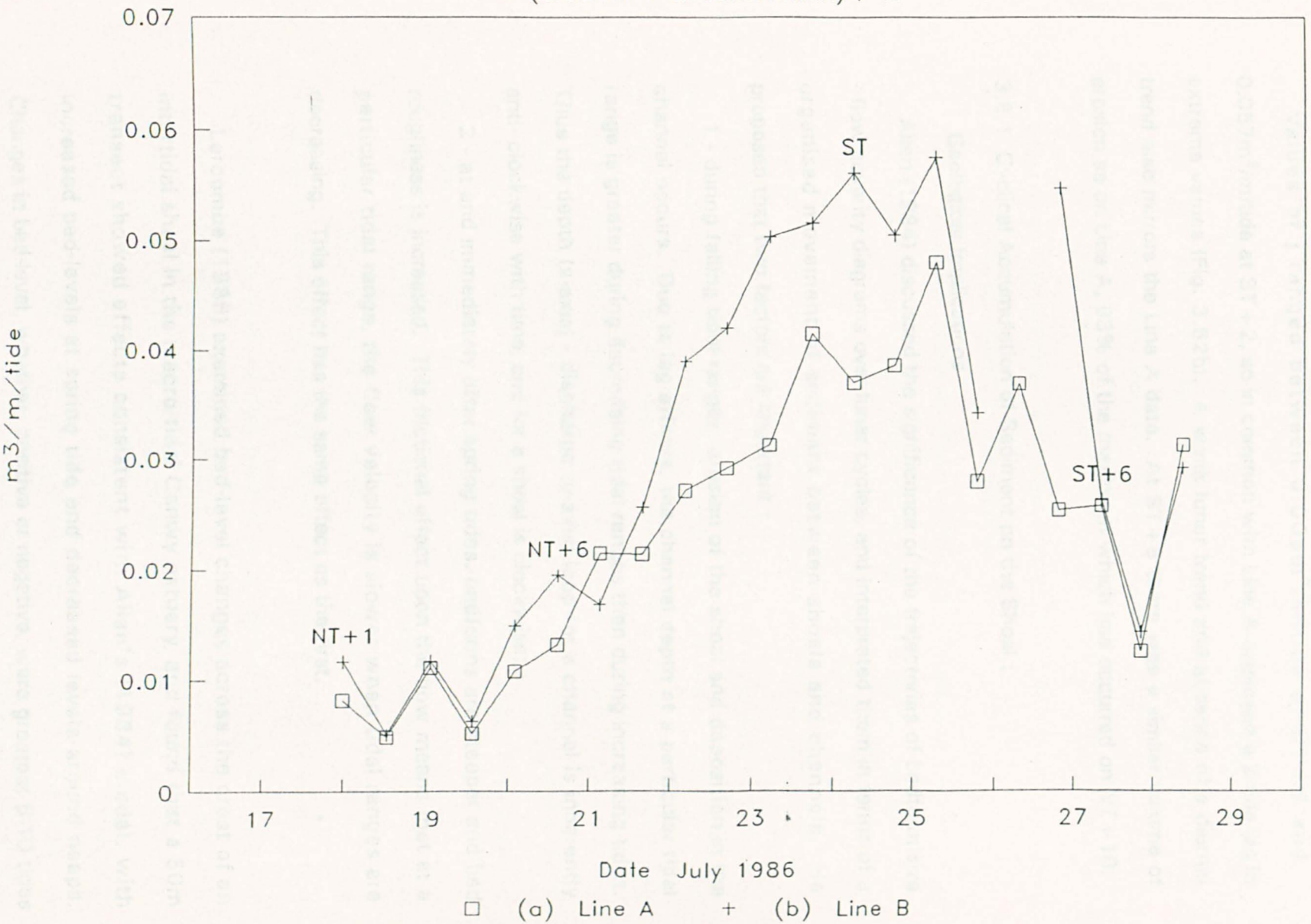

Results - Line B

Values of j ranged between 0.005m^3/m/tide at NT+2 and 0.057m^3/m/tide at ST+2, so in common with Line A displayed a 2-tide lag in extreme values (Fig. 3.52b). A weak lunar trend and absence of a diurnal trend also mirrors the Line A data. At ST+8 there was a similar volume of erosion as on Line A, 93% of the maximum which had occurred on NT+10.

3.8.1 Cyclical Accumulation of Sediment on the Shoal :

Geological Implications

Allen (1984) discussed the significance of the trajectories of bedform size - flow severity diagrams over lunar cycles, and interpreted them in terms of a organised movement of sediment between shoals and channels. He proposed that two factors are important :

1 - during falling tidal ranges, erosion of the shoal and deposition in the channel occurs. Due to lag effects, the channel depth at a particular tidal range is greater during decreasing tidal ranges than during increasing tides. Thus the depth (x-axis) - discharge (y-axis) loop for a channel is inherently anti- clockwise with time, and for a shoal is clockwise;

2 - at and immediately after spring tides, bedforms are steeper and bed roughness is increased. This frictional effect upon the flow means that at a particular tidal range, the flow velocity is slower when tidal ranges are decreasing. This effect has the same effect as the first.

Larcombe (1986) examined bed-level changes across the crest of an intertidal shoal in the macro-tidal Conwy estuary, and found that a 50m transect showed effects consistent with Allen's (1984) model, with increased bed-levels at spring tide and decreased levels around neaps. Changes in bed-level, whether positive or negative, were greatest 6-10 tides either side of spring tide. Larcombe & Lowe (unpublished data) repeated the

survey on the upstream flank of the same shoal, and found bed-level variation intermediate between the ideal shoal and channel variation. It thus seems that the model of Allen (1984) is a valid first approximation to shoal behaviour.

Allen's (1984) model appears to apply reasonably to the data collected on Fegla Fach shoal, with Figs. 3.18 and 3.40 showing high bed-levels around spring tides. Near-constant levels at spring tides, are interpreted to represent an 'equilibrium spring tide shoal'. However, the highest bed-levels are actually on intermediate tides after spring tide, at ST+6, prior to the major erosive episode caused by bad weather.

The results of this study are shown in Fig. 3.53, in terms of the variation of net sediment accumulation and erosion averaged over the lengths of the two survey lines. This reveals a regular alternation over both lines of accumulation and erosion, with each complete cycle 4-5 tides in length. These cycles do not correlate with the immigration or emigration of individual megaripples from the survey lines, and are therefore considered to be changes in shoal volume relatively independent of the superimposed bedforms. Volumes of deposition and erosion both reached ~0.02m^3/m/tide, and both lines showed very similar trends and transported volumes. Both Lines A and B (Chapter 3) showed similar trends, with times of net sediment accumulation at NT+1, NT+5, NT+9/10, and ST+5/6.

It is unclear why there was an increase in bed- level at ST+5/6, though it is possible that a 'pulse' of sediment unrelated to tidal effects was transported onto the shoal at that time. The apparently cyclical nature of accumulation and erosion on the shoal is more difficult to explain. 'Channel erosion' during rising tidal ranges is likely to involve both increased depth and changes in 'width'. It is speculated that there are fluctuations in the channel shape during this period which cause the shoal to systematically vary between acting as part of the channel side and part of the shoal, i.e. respectively erosive and depositional in nature. This fluctuation may depend on the changing strengths and directions of flood and ebb currents in the

Fig. 3.53 Bed level change A - E - Lines A and B

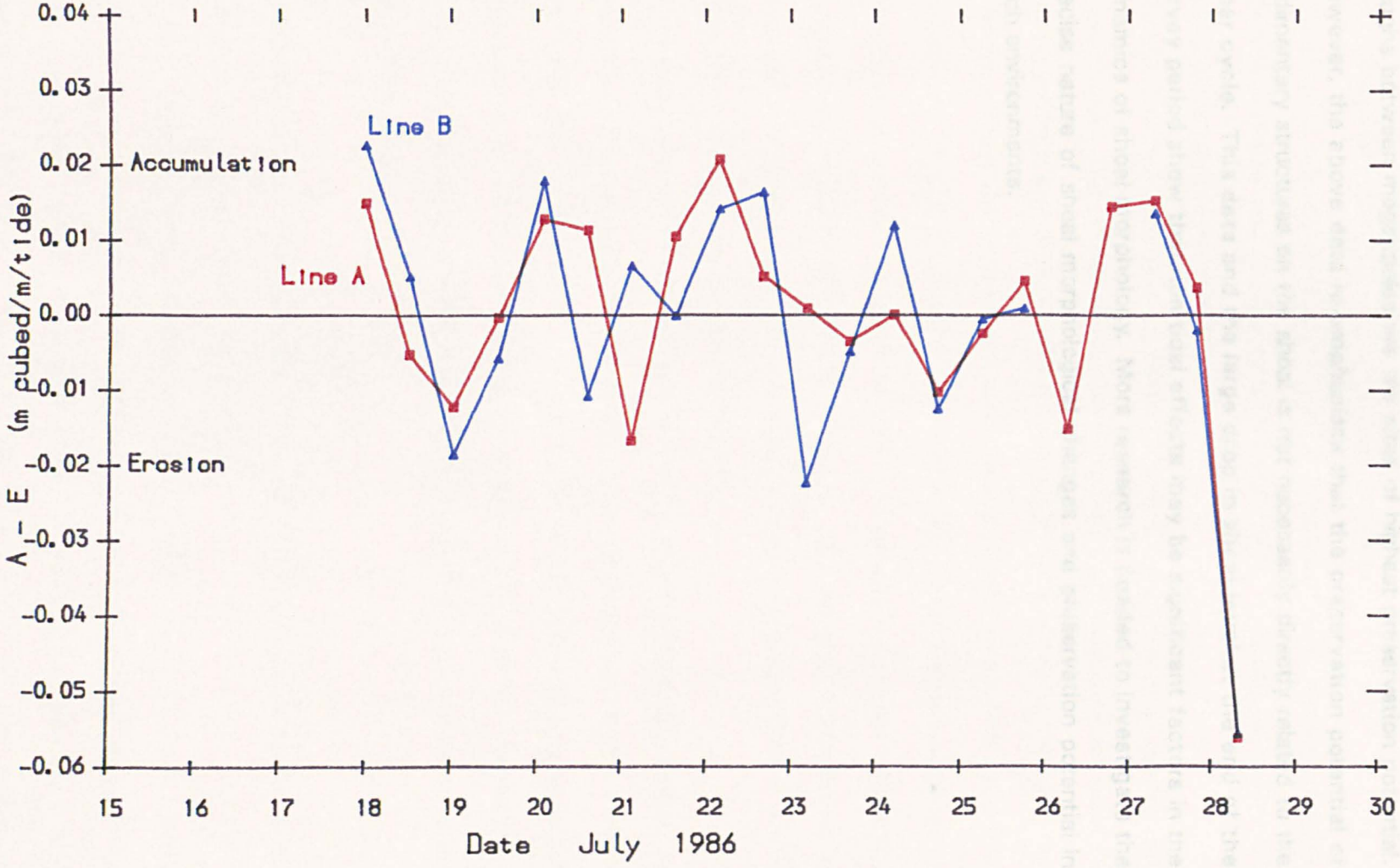

area of the shoal margins.

In the light of the above, there are consequences in terms of preservation potential of sedimentary structures. Preservation potential relates to the variation of trough levels as well as mean bed levels, as the troughs between megaripples are the sites of highest preservation potential. However, the above data re-emphasises that the preservation potential of sedimentary structures on the shoal is not necessarily directly related to the lunar cycle. This data and the large drop in shoal level at the end of the survey period show that non-tidal effects may be significant factors in the dynamics of shoal morphology. More research is needed to investigate the precise nature of shoal morphological changes and preservation potential in such environments.

3.9 Summary and Conclusions

Linearly-defined populations of intertidal megaripples show that temporal variation in their morphology; their dynamics is related strongly to the lunar cycle. This is of importance in three main contexts :

1 - in allowing the inference of probable sediment transport vectors, in areas where no detailed measurements have been made - this has relevance for coastal engineers and navigation;

2 - as part of the process of palaeoenvironmental reconstruction carried out by geologists. The preserved internal structures of megaripples are used to infer palaeoflow and other environmental conditions, likely to increase the understanding of the depositional environments of the geological sequence concerned. This is of interest to those seeking exploitable mineral or hydrocarbon reserves, and to the academic research community. However, it should be remembered that there is high spatial variability in morphodynamic and hydrodynamic conditions around intertidal shoals, which limits the usefulness of such reconstructions;

3 - as part of studies of bedform stability, dynamics and population structure, not necessarily of tidal bedforms or megaripples. Some work is related to the prediction of resistance to flow in alluvial channels, of importance to those concerned with the supply of water, or flood-prevention. This, and much other work, forms part of the background research to the two points above.

Spatial variation in megaripple dynamics has also been considered, an aspect as yet unquantified in the literature.

Two parallel linear transects over the shoal at Fegla Fach, were repeatedly surveyed at low water for a period of 24 consecutive tides, covering a neap - spring - neap lunar cycle. Transect Line A was 40m long, Line B was 48m long, and Line B was 15m nearer the main estuarine

channel. On both lines, at neap tides flood-orientated 2-D megaripples were found, and at springs, ebb-orientated 3-D megaripples.

Mean megaripple heights varied between 0.16m and 0.3m, maximum heights lagging peak tidal range by 2 tides. Mean wavelength ranged between 3.5m and 5.9m, and showed a complex variation with time, with maxima after both neap and spring tides. The mean flatness was lowest (i.e. megaripples were steepest) at 15.4 at ST+2, and highest mid-way between neap and spring tide, reaching 31 at NT+6. The megaripple symmetry index varied between 0.48 and 3.6, where values >0 represent flood-orientation, and <0 an ebb-orientation.

The temporal variation of megaripple morphometry is intricately linked to the formation at NT+6/7, and subsequent development of short-wavelength 3-D megaripples. This rapid change in the population structure is related to the following changes in the mean morphometric parameters :

1 - a decrease in height, which continued for 5 tides;
2 - a decrease in wavelength, which continued for 4 tides;
3 - a decrease in flatness, which continued for 8 tides;
4 - a rapid increase in ebb-orientation;
5 - an increase in elevations of megaripple troughs,
which continued for a further 5 tides.

Examination of these temporal morphological changes plotted against tidal range elucidates the data. The trajectories of these curves often show a figure-of-eight form, defining different megaripple development trends at high and low tidal ranges. The megaripples are interpreted as having distinct neap tide and spring tide 'equilibrium forms', which may have different processes causing similar morphological change. At neap tides, the ebb tide is only sufficiently strong to cause the formation of ebb caps on the flood-orientated forms, and trough levels are lowered probably by trough-parallel

late-stage runoff. The flood tide causes small quantities of sediment transport, sufficient just before neap tides to rework the small spring tide forms to a flood orientation. The spring tides bring considerable sediment transport and morphological change, reversing the megaripples every half tidal cycle. The surveyed ebb-orientated forms increase in height at spring tide due to erosion of the trough by the lee-side eddy of the ebb- orientated form.

The definition of the measure of megaripple migration depends on the reason for measurement. Lag cross-correlation of successive shoal transects is an effective measure when deducing net bed material sediment transport rates. Mean migration rates on Fegla Fach Shoal are always in a flood direction. Migration began at NT+5 and attained a maximum of 1m/tide at ST+2. The diurnal tidal variation was visible in the migration data following ST. Megaripple population changes also significantly affect megaripple migration rate and form change; in particular, heights affect migration rate. A pre-spring peak in migration is caused by the dominance of low height megaripples at that time. The maximum correlation coefficient CC, obtained by incremental displacement of one transect against the next, is useful as a measure of megaripple shape change, and reveals that from ST and ST+4 there is a period of stable megaripple morphology. This correlates with other morphological variation interpreted as indicating that 'equilibrium' bedforms were present.

After recognising the effects of the changing bedform population, migration lags tidal range by two tides, and it is suggested that the capability of the flow to transport bed sediment is dependent on bed shape. The tidal range at which megaripple migration is initiated is higher on rising tidal ranges, and it is tentatively attributed to the adhesive effects of algal mats developed at neap tide.

The time-averaged population of megaripples on Fegla Fach shoal shows a polymodal structure only in terms of wavelength, with the most common modes at 4- 4.5m (containing 17.6% of all measurements), and 5-5.5m

(containing 11.8%). Overall however, the wavelengths were centred around 4-4.5m, and the population was slightly skewed towards the lower wavelengths. The data tends to favour the conclusions of Allen & Collinson (1974) that different-sized members of a certain class of bedform are hydrodynamically equivalent. However, this study shows that both small and larger megaripples are active when present simultaneously on the shoal, contrary to the ideas of Allen & Collinson (1974).

There is a gradient of migration rate along the two transect lines, and a difference between them. There is up to 0.95m difference between migration within the 10-20m and 30-40m sections, most apparent 7- 5 tides before and 4-6 tides after ST. This is related to the preferential pre-spring development and post- spring degradation of small bedforms on the seaward-facing flank of the shoal.

A comparison of data from the two survey lines shows that :

1 - presumed greater wave effects on megaripple morphology near the main estuary channel (i.e. Line B) may be the cause of a weaker morphological - tidal range relationship;

2 - scour pits and associated 3-D megaripples are developed earlier in the lunar cycle on Line B, possibly a result of higher tidal velocities (suggested by greater migration rates), and/or different flood-ebb velocity ratio;

3 - megaripple flatness may be a fundamental response to the tidal current regime;

4 - megaripple symmetry at low water is less strongly ebb-orientated on Line B, nearer the main channel, possibly caused by waves reworking or disrupting the formation of ebb caps, and/or local topographic effects on net bed material sediment transport direction;

5 - migration rates on Line B were on average 40% higher than on Line A, despite only 15m separating them.

Megaripple migration rate on an intertidal shoal in the Mawddach has been studied with reference to three different measures of migration, the first two of relevance to geologists :

1 - Mct, the mean migration of the crest and trough of individual megaripples;

2 - Msf, the migration of megaripple slip faces, i.e. the mean migration of brinkpoints and slipface toes;

3 - M, the migration measured by lag-cross correlation of the bedforms over the survey line.

The measures Mct and Msf show closest values immediately after spring tide, particularly from NT + 12 to ST + 3, despite the fact that the megaripples had net flood-directed migration but were reversed completely by the ebb tide. There are however significant differences between these geological measures of migration and the lag cross-correlation measure M. On average, Mct and Msf are respectively 40% and 80% greater than M. At spring tides Mct and Msf are 20% greater than M, and during post-spring intermediate tides are respectively 96 and 150% greater.

Geologists using measurements of the width of preserved megaripple tidal bundles to calculate palaeo- transport rates would obtain most reliable estimates from those tidal bundles deposited at those times in the lunar cycle when megaripple morphology was most stable. The errors depend heavily on the presence and timing of rapid changes in the megaripple population within the lunar cycle. In the case studied, this means measurements would be best made :

1 - at and immediately following spring tides, i.e. the largest tidal bundles;

2 - immediately following neap tide.

This is not valid for all instances, for example the shoal studied by Allen & Friend (1976a), would produce the least reliable estimates measured from the largest tidal bundles.

Further errors in the deduction of palaeo- transport rates from measurements of tidal bundles would be caused by the variation within a megaripple population of morphology and migration rate. The standard deviations of Mct and Msf for each tidal cycle range up to 0.8m and 0.66m respectively.

Simple velocity threshold values (maximum depth, mean velocity, Umax) for the production of various morphological changes related to intertidal megaripples have been presented. These thresholds are crude but have applications for palaeoflow analysis. The Umax of the flood (dominant) tide (Umaxflood) required to initiate megaripple migration, is in good agreement with values found by other workers, and Umaxflood for the 2-D to 3-D transition is also implied to be valid. In contrast, velocity thresholds for morphological changes related to sediment transport by the ebb tide (i.e. Umaxebb for ebb cap formation, and megaripple reversal) are much lower than published data. This is due mainly to the different duration for which the ebb tide exceeds threshold. There is also an effect caused by the physical size of the megaripples; greater volumes of sediment transport are required to reverse large bedforms.

Topographic differences between successive surveys of the megarippled shoal have been used to determine volumes of bed material transported by each tidal cycle, j. A weak lunar trend is present in the data, but with a two tide lag of extreme values compared to predicted tidal range. The diurnal variation is absent. Values of j vary by one order of magnitude over the lunar cycle, reaching a maximum of $\sim 0.05m^3$ at tide ST+2. A regular cycle of net accumulation and erosion exists over the shoal, 4-5 tides in period and $0.04m^3$ in amplitude. Very poor correlations exist between flood tide measures and net tidal sediment transport.

The results of this bedform research, in terms of the geological products of estuarine sediment accumulation, are incorporated into Chapter 8.

Chapter 4

Bedform - Boundary Layer Interactions

4.1 Introduction

This chapter details the structure of the tidal currents over the Fegla Fach megarippled shoal described in Chapter 3. Following a review of the factors which influence the vertical form of tidal velocity profiles, there is a detailed description of the method of flow measurement used in this study.

Neap and spring tidal currents are then compared, and there is an analysis of the effects of the underlying megaripples upon flow parameters. There is also a detailed appraisal of the relationship between shear velocity and roughness length, within each tidal flow. The flow data is then analysed to deduce the strength of the lunar tidal signature in various flow parameters, with reference to their use as palaeoflow measures useful to geologists.

In addition to being an integral part of the process study of the megaripples on Fegla Fach shoal, the data is further detail on the nature of the tidal currents in the lower estuary.

The major aims of this process-orientated flow study are integral with those stated in the previous chapter, relating to the study of the morphology and dynamics of intertidal megaripples. Repeated briefly, these are :

1 - to define the detailed hydrodynamic regime over intertidal megaripples, and to provide a quantitative study of the subject;

2 - to investigate the feasibility and accuracy of making palaeoflow inferences from bedform morphology;

and 3 - to correlate measures of sediment transport with flow parameters, measured over the megaripple field.

Throughout the period of study of megaripple morphology on Fegla Fach Shoal (Fig 4.0), the tidal flow in the middle of survey line A was measured using a Velocity Gradient Unit (V.G.U.). This array of current meters provided detailed data on the velocity profiles of the tidal flows over the shoal. The data elucidates the relationship between bedform morphometric parameters such as size and migration rate, and flow parameters such as peak velocities, shear velocities and roughness length. Topics under examination include how the various flow parameters vary if measured in the field over different parts of a megaripple, and how they vary over the tidal cycle.

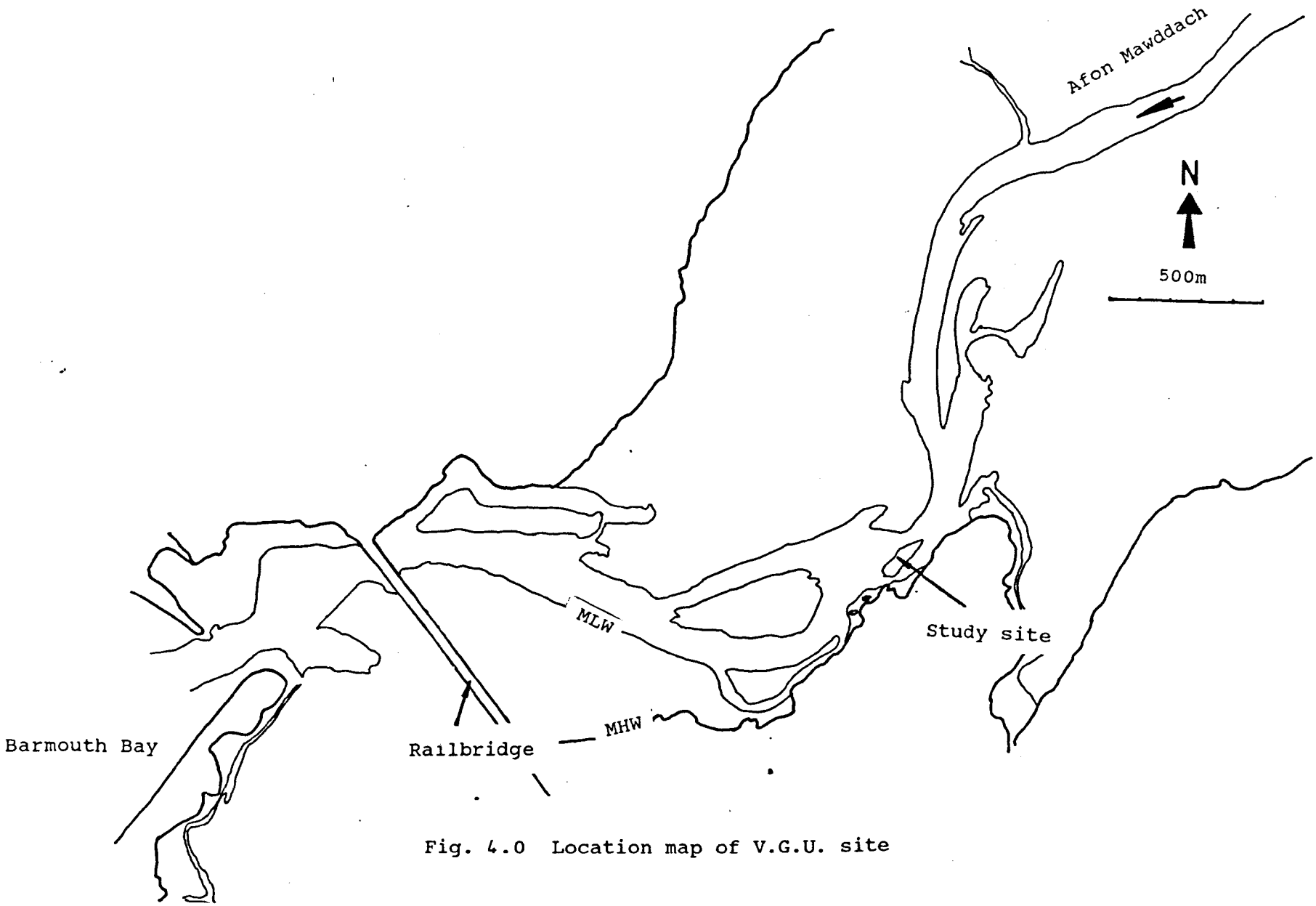

Fig. 4.0 Location map of V.G.U. site

4.2 Tidal Current Velocity Profiles : General

4.2.1 The Logarithmic Profile

The velocity profile near the sea bed can be represented by the von Karman - Prandtl equation

$$Uz = (U^* / K) \ln (Z/Zo) \qquad (4.1)$$

where Uz is the mean flow velocity at height Z above the bed, K is von Karmans constant (0.4), U* is the shear velocity and Zo the roughness length, the theoretical height above the bed where the velocity is zero. (This height is usually derived from extrapolation of velocity profiles downwards towards the bed). This equation is valid if the following conditions are satisfied :

- the flow is steady, and uniform unstratified;
- Z is much larger than Zo, but much smaller than the total boundary layer thickness (Soulsby & Dyer, 1981).

The shear stress at the bed To is given by

$$To = (U^*)^2 roe \qquad (4.2)$$

where roe is the density of the water. Both mean and instantaneous bed shear stress are important flow parameters controlling sediment transport.

With height plotted logarithmically on the y-axis, the slope of the velocity profile is equal to K / U*, and the intercept at U = 0 is equal to the roughness length Zo. However, there are a number of factors which may cause the velocity profile to deviate from this simple form; these are outlined below.

4.2.2 Factors Influencing Velocity Profile Form

Bedforms

(i) Form Drag

For flat beds of a uniform grain size, the roughness length Zo is given by

$$Zo = D / 30 \qquad (4.3)$$

where D is the bed grain diameter (Dyer, 1980). However, where the bed is made up of ripples or larger bedforms, Zo is greater due to form drag over the bedforms. Thus, the total force on the bed is equal to the skin friction (the drag caused by the bed grains) plus the form drag.

Form drag arises because bedforms create an internal boundary layer in the flow (Fig. 4.1), within which there is flow acceleration over the bedform crest and deceleration near the trough. There is, thus, a net horizontal force on the bedform profile due to the pressure difference across the bedform - the form drag. (Krugermeyer & Grunwald (1978) found that this effect in the atmosphere above sea waves is limited to 2 or 3 times the wave height above the water). In tidal flow, at heights greater than a ripple wavelength, form drag is the major source of roughness felt.

Where there is a hierarchy of bedforms, common in regions of strong sediment transport, each type of bedform acts as roughness at heights greater than the order of a wavelength, and as topography at heights only a small fraction of bedform wavelength. This results in a segmented velocity profile, with each straight-line section (on a log plot) related to a different roughness element (Smith & McLean, 1977a,b). Thus, in Fig. 4.2, the slopes 1, 2, and 3 and their intercepts, give the U* and Zo values for the different roughness elements present (e.g. grains, ripples, megaripples).

This is highly significant when choosing which rotors to include in the fitting of a log profile to the data; it must be realised that a fit which includes points throughout the flow depth does not provide flow parameters related

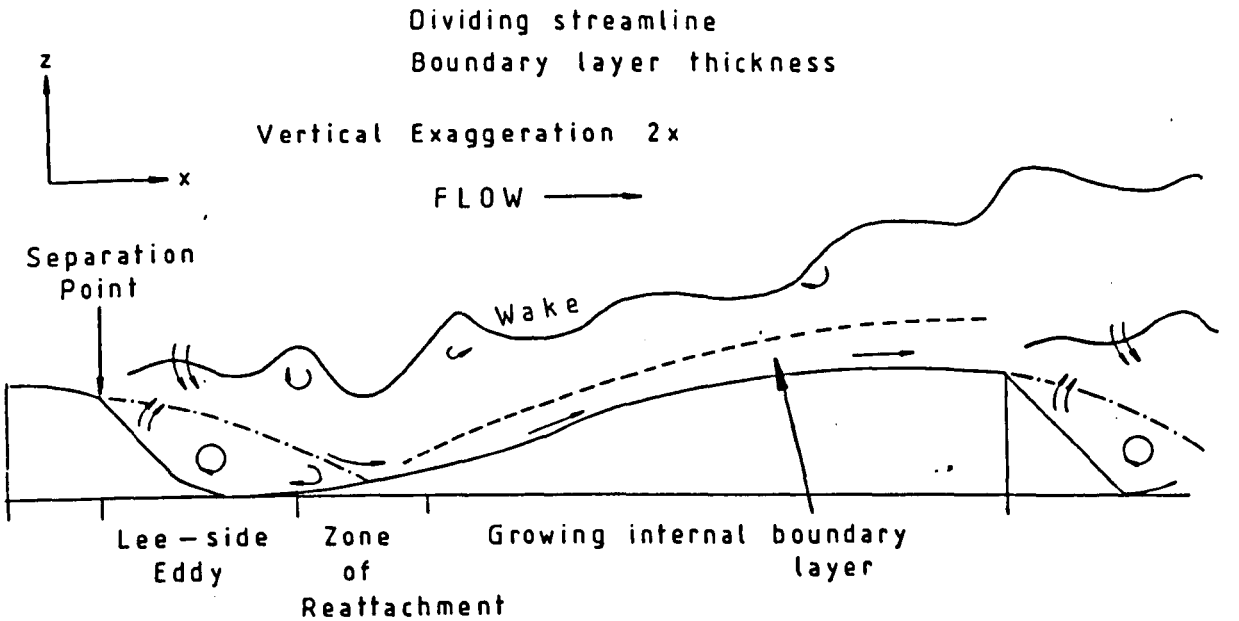

Flow separation over a megaripple Fig. 4.1

Spatially averaged velocity measurements over a sand wave field where flow did and did not separate

Fig. 4.2

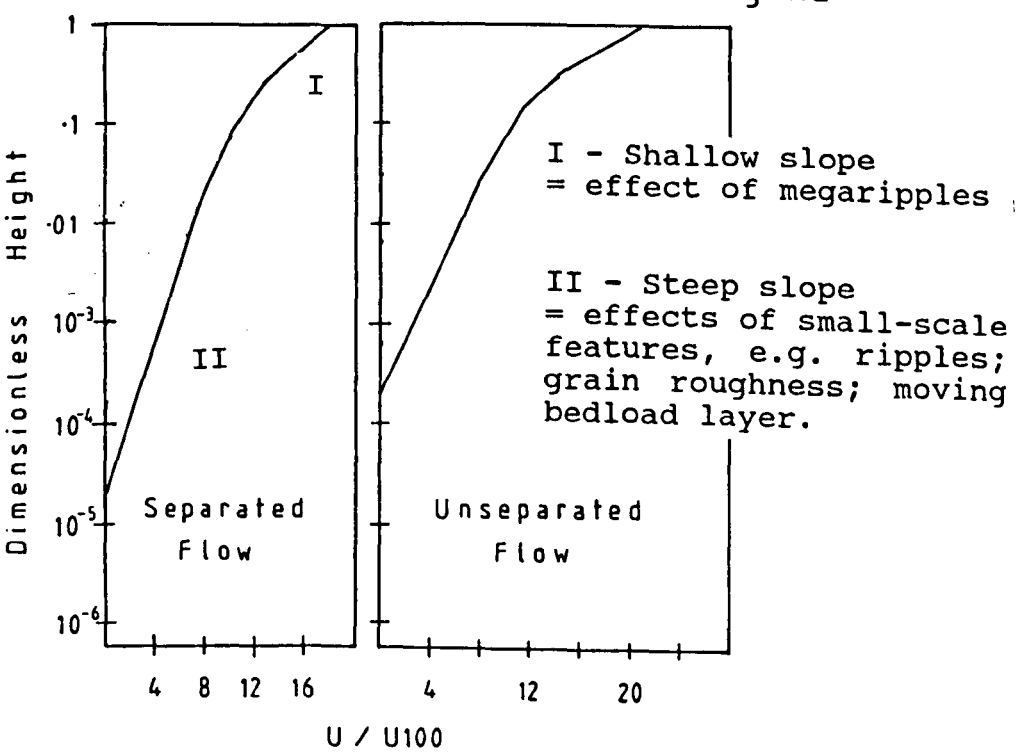

(After Smith + McLean, 1977a)

solely to the bed. Rather, it will give parameters related to a combination of bed friction and form drag, and the nature of this combination may be different depending on the statistical method of calculating a line of 'best fit'. A fit to velocity data taken wholly above the boundary layer caused by ripples will provide velocity parameters containing very limited effects due to grain size and ripples. In contrast, if the fit is made from data taken from within the boundary layer of ripples, the dominant bed controls upon the parameters are from the grain size and ripples only. Thus, if used for sediment transport estimates in predictive equations, data should be manipulated to remove form drag effects, to represent a measure of skin friction alone. This is not a simple process.

In this study, the second lowest rotor was never closer than 0.23m to the bed, and for 23 of the 27 sampled tides it was greater than 0.3m above bed. At each tide, the lowest rotor was either 0.15m or 0.2m below the second. Current ripple size was typically 0.15 - 0.25m in wavelength and 0.015 - 0.03m in height, and they were both 2D and 3D in plan form. Their flatness was approximately between 7 and 12. It is therefore clear that flow parameters derived from the lowest two rotors would be inclusive of form drag from the current ripples as well as skin friction.

Fredsoe (1975) discussed form drag over bedforms, and showed how curves fitted to measured friction factors over megaripples alone are not accurate in cases of megaripples with superimposed ripples.

(ii) Spatial variation

The differences in velocity profile over bedforms and the distributions of bed shear stress have been measured by Raudkivi (1966). Buckles et al (1984) measured mean and fluctuating velocity over a solid sinusoidal wave surface having a wavelength of 0.05m and a height of 0.01m. Mean velocity was 0.51m/s, and the experiments showed a large separated region, extending from 0.14 to 0.69 wavelengths downstream of the crest (their Figs. 3 and 4). Mean velocity profiles suggested the formation of a thin,

growing boundary layer originating at the point of flow reattachment; it continued to the separation point of the next bedform downstream.

Dyer (1970) has distinguished four groups of velocity profile, each related to the mean flow regime at different positions over tidal gravel waves in the West Solent (Fig. 4.3). These profiles were measured at heights between 0.15 and 6.86m above the bed. The profile groups were :

Group 1 - Profiles taken from the lower stoss slope of the gravel waves. These exhibited significant correlations with logarithmic velocity profiles over almost the entire measured depth range. Calculated roughness lengths (0.0001 - 0.005m) were interpreted as realistic over the coarse sand to gravel bed;

Group 2 - Profiles taken on the upper stoss surface of megaripples, and on flat beds. These velocity profiles are composed of two sections of equal linear slope, but the lower one is generally less than 1m thick and relatively slower. Between the two sections is a zone of reduced current shear. The profile is interpreted as being due to a reduction in bed roughness upstream of the measurement position. Grant & Masden, 1986, in comments on future boundary layer work (16 years after Dyers paper) consider it no longer acceptable to explain large roughness by 'unobserved upstream bumps', so on this basis Dyer's interpretation is no longer satisfactory. However, Paola (1985) has shown that flow in the bottom boundary layer at height above bed Z may be influenced by changes in bottom roughness in a zone extending from 10-200Z upstream of the measurement position;

Group 3 - Velocity profiles measured above the lee slope of megaripples. These show opposite effects to Group 2, i.e. between the fast flowing upper portion and the slower lower portion (which is generally less than 2m thick) lies a zone of high current shear. These profiles will result in overestimates of near bed U* and Zo;

Group 4 - Profiles taken over flat beds, which show a power law relationship of velocity with height. Most profiles had the bottom 2 - 3m

Fig.4.3

The four groups of velocity profiles over gravel dunes (Dyer 1970)

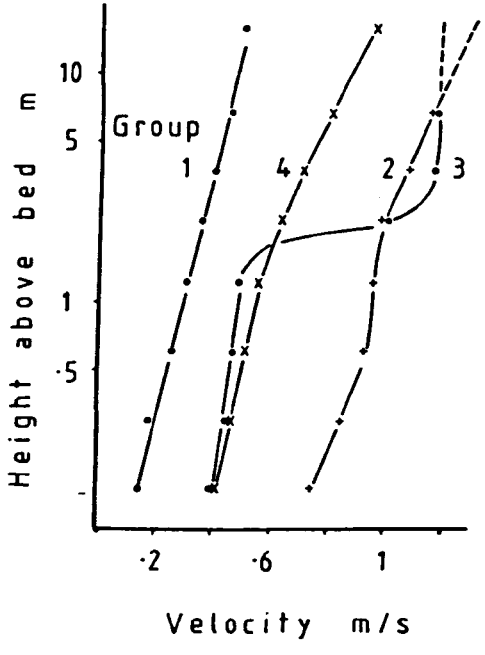

Fig.4.4

Curvature of the log-profile produced by acceleration and deceleration (Soulsby + Dyer 1981)

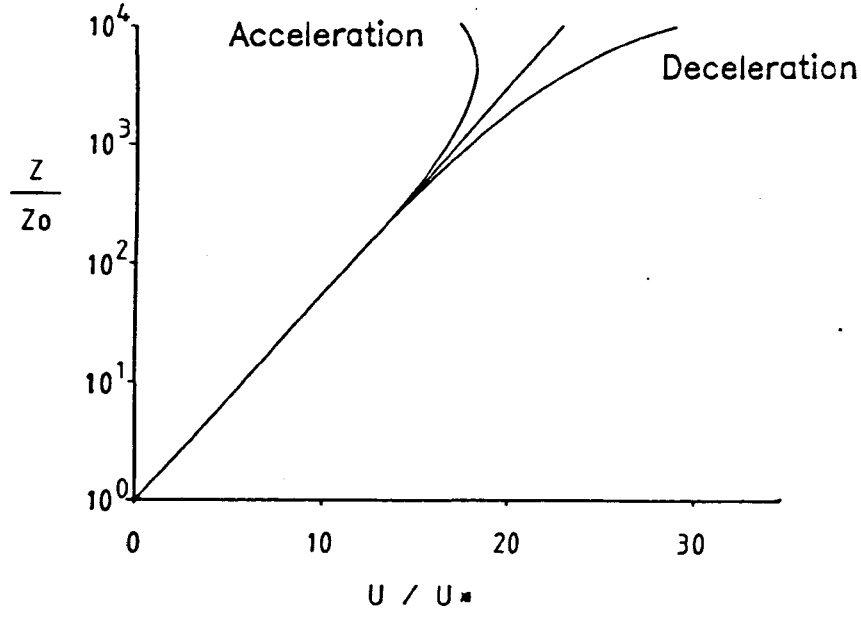

equally near to a logarithmic velocity profile, and and those profiles with the lowest exponent (~1/7) could equally have been placed in Group 1.

Dyer (1970) found that the most consistent one minute averages of U* and Zo were obtained by using only the bottom two rotors, which were at 0.15 and 0.3m above the bed. These values of U* and Zo were interpreted as relating to the skin friction, and the higher rotors were measuring flow affected by form drag from the dunes.

The bedforms in the Mawddach are comprised of fine sand, which, unlike gravel, is developed into current ripples under currents exceeding threshold. Thus the lower two rotors in this study would not be measuring skin friction alone, but also form drag caused by current ripples.

Nelson & Smith (1989) modelled the velocity and boundary stress fields over 2-D asymmetrical bedforms, and compared their model to flume data taken over immobile bedforms of 0.8m wavelength and height 0.04m. A lee face angle of 30degrees was used, comparable with natural megaripples during migration. They predict the length of the flow separation region over well- developed 2-D megaripples to be 3.5-4.5 megaripple heights, varying with megaripple steepness.

Nelson & Smith (1989) noted also the difficulty of making accurate measurements of boundary shear stress above bedforms, particularly due to the systematic accelerating nature of the internal boundary layer; they found that errors result from use of a uniform boundary layer theory to obtain bottom-related flow parameters over bedforms. Since the internal boundary layer is accelerating, near-bed shear is increased relative to the shear at the top of this layer. Shear stress calculated from points including the upper parts of the internal boundary layer (or above in the 'free stream'), would be underestimated by 10-20%, and roughness lengths would also be underestimated. Such systematic errors may have affected the results presented below. The actual errors due to this effect are probably higher, due to the 3-D nature of the megaripples during much of the lunar cycle.

Stratification by Suspended Sediment

At current velocities above the threshold for bedload sediment transport, the threshold for suspended sediment transport may be reached. In a theoretical model, Taylor & Dyer (1977) showed that suspended sediment may stabilise the near-bed velocity profile, a density stratification inhibiting vertical exchange by turbulence. Smith & McLean (1977a,b) also modelled these effects, and from field measurements gave an equation predicting roughness length modified by suspended sediment,

$$Zo = \frac{\text{roesed alpha } (U^{*2} - U^{*}crit^{2})}{g\ (\text{roesed} - \text{roe})} \qquad (4.4)$$

where alpha is a constant equal to 26.3, U*crit is the bedload threshold shear velocity, and roesed is the sediment density.

Dyer (1980, his Fig. 6) broadly agreed with this formula for low sediment transport rates, although he also found that the constant alpha could be >300 at neap tides. He explained this by increased bed roughness and observed higher movement thresholds at neaps. Bed roughness was decreased at peak spring currents by the intensity of sediment movement, decreasing ripple heights, and presumably also by the stabilising effect of suspended sediment. Ripples were also lower and flatter at spring tides. Values for alpha varied during periods of ripple shape and size change, and it was unclear if the bed roughness was predicted accurately (Grant & Masden, 1986).

Heathershaw & Hammond (1979) found some evidence for modification of near-bed velocity profiles by suspended sediment. In fitting a log profile (eqn. 4.1) to their data, they found U* and Zo were systematically overestimated (see also below).

Adams & Weatherly (1981) suggest that turbulent kinetic energy and bed shear stress are reduced by about 40% and 45% respectively, so the slope

of the velocity profile is diminished. Also, the thickness of the boundary layer is decreased by up to 50%. They, in common with other some other workers (eg McCave, 1973) consider that suspended sediment may alter the von Karman constant to below 0.4. However, Coleman (1981) points out this is a misrepresentation of the physics, designed to get around the problem of measured concentration data disagreeing with concentration profiles calculated from use of the Rouse (1937) equation with (unsatisfactory) velocity profile data.

Temperature-Induced and Salinity-Induced Stratification

Strong, stable, salinity-induced stratification periodically occurs in the estuary (Chapter 2). The effects of stable stratification on the mean and turbulent structure of boundary layer flows are well understood (Grant & Masden, 1986). Vertical mixing is damped, boundary layer thickness is reduced, and for the same external driving velocity the boundary shear stress is also reduced.

In Chapter 2, it was shown that stratification affects velocity profiles, particularly near HW and LW slack. Its effects are also perceptible from time- averaged velocity profiles. Such effects on the V.G.U. data are quite possible, although due to the extreme width of the estuary at this point, the less saline surface layer (if present) would be very thin at HW. The strong vertical mixing that occurs on the flood tide would decrease the chances of such stratification being present. Early on the flooding tide, the surface layer would have a relative seaward velocity compared to the underlying water.

These effects are also unlikely to be measured by the V.G.U., because the likely thickness of the surface layer is small compared to the rotor spacing - so only one rotor would be subject to the surface layer at any one time. Secondly, each OTT impellor is 0.12m in diameter, so the rotor would only be fully in the thin surface layer for a short time; if the layer was <0.12m thick, it would only be measuring the integrated velocity of a combination of surface and lower layers. Such short term, fine resolution

effects are not likely to be detected in the velocity records; they would not be distinguishable from other causes of variation in the velocity profiles.

Wind and Waves

A strong wind blowing over the water column may entrain a surface layer; hence, the free surface of the water may be accelerated or decelerated relative to the flow beneath. Such a wind would also cause waves, producing a component of oscillatory flow, maximum at the surface. The current meters produce the same electrical pulse regardless of the direction of impellor rotation; thus, waves will always increase the apparent surface flow velocity. It is, therefore, impossible from the V.G.U. data to quantify the effects of wind and waves on the velocity structure of the tidal flows.

Flow Acceleration / Deceleration

One condition required for the logarithmic profile equation to hold is that currents are steady. However, tidal currents are accelerating or decelerating for large proportions of the tidal cycle, and so flow parameters calculated from fitting data to a log profile will be in error. Soulsby & Dyer (1981) state that (relative to friction) the importance of inertia increases away from the bed, so that in an accelerating current the velocity is less than that predicted by the log profile, and this error increases upwards into the flow. Thus, flow parameters U* and Zo are underestimated. Conversely, in a decelerating flow, U* and Zo are overestimated.

They proposed that the log profile be replaced by

$$U = \frac{U^*}{K}\left(\ln(Z/Zo) - \frac{Z}{\text{gamma } A}\right) \qquad (4.5)$$

where A is an acceleration length scale (in cm) expressing rate of change of U* (see below), and gamma is an empirical constant (~0.04).

$$A = \frac{U^* \, |U^*|}{dU^* / dt} \qquad (4.6)$$

where $|U^*|$ = modulus of U^*.

For a semidiurnal sinusoidal tide, with peak U^* of 0.03m/s, Zo of 0.005m and velocity measurement height of 0.5m, they found that one hour into the flood tide (i.e. conditions of accelerating flow) U^* and Zo will be underestimated by 20% and 60% respectively. One hour before HW, they will overestimated by 20% and 83% respectively.

When plotted in the form ln Z against U, accelerating profiles are concave upwards, and decelerating profiles concave downwards (Fig. 4.4).

4.3 Tidal Current Velocity Profiles : Measurements

4.3.1 The Velocity Gradient Unit (V.G.U.)

The velocity gradient unit consists of an array of ten OTT rotors, fixed at various heights to a steel mast standing vertically in the bed. The mast has support and rigidity provided by a set of four guy ropes (each 4m long), attached to stakes driven into the bed. The current meters are unable to swing freely with the tide; thus, they are pointed into the face of the current they are to record.

No directional information is thus gained from the V.G.U., so no data were gained regarding changes in flow direction during tidal inundation. Consequently, all flow data is treated as rectilinear. The mast reaches 2.5m above bed, and current meters may be placed at any of over 30 positions on it, and their alignment or height altered as required at each low water.

The current meters are all connected by cable to a pre-programmed data logger. The data logger is contained within a waterproof stainless steel cylinder (length 0.62m, diameter 0.2m), which is held in position on or under the sediment surface by a weighted frame. The logger was placed 5-6m away from the middle of the survey line, to avoid interfering with the measured bedforms or flow. The logger was programmed (via an interface with a BBC microcomputer), to record the number of pulses produced by each current meter (i.e. number of impellor revolutions) during successive time intervals. About every third day, the data were down-loaded onto floppy disc, and in this study they were then transferred to the U.C.N.W. VAX mainframe computer, for storage and subsequent analysis.

4.3.2 Fegla Fach Site - V.G.U. Deployment

V.G.U. deployment took place between the 16th and 30th July 1986, covering 27 continuous tidal cycles, to coincide with the study of the intertidal megaripples. Tide number 2 was the predicted neap tide NT, and

tide number 15 Spring tide ST. The shoal was uncovered at low water so current data did not cover an entire flood or ebb period. Fig 4.0 shows the location of the study site.

Initially, at NT-1, 8 OTT rotors faced the flood tide, and were spaced at intervals between 0.08m and 1.99m above the bed. After two tides, at NT + 1, OTT orientation was reversed so that 8 rotors faced the ebb and 2 faced the flood. Following this, OTT reversal continued to take place every 2 tides. Every low water, and before and after reversal of OTT facing directions, the height above bed of the centre of each OTT rotor was recorded.

Past experience (Larcombe, 1986) suggested that, for significant periods of time during each tidal cycle, up to half the current meters would not provide useful data. This had been due to fouling of rotors by seaweed, or by failure of some part of the electrical connection between current meter and data logger. Thus, given a maximum of 10 rotors operating simultaneously (a limit imposed by the data logger) the above 8:2 facing strategy was designed to ensure good detail of at least one of the flood or ebb tides, whilst having at least a single measure of the opposing tide. In the past, data loss had meant little useful data on vertical current structure had been obtained from either flood or ebb, and in this study it was considered essential to define flow parameters such as shear velocity or roughness length with reasonable accuracy for at least either flood or ebb.

The logger was programmed to record the total number of revolutions of each rotor over successive periods of 60 seconds (R), i.e. data were time-averaged. The calibration provided by the OTT manufacturers gives the 60 second average flow velocity (U) as

$$U = (4.158 \times 10^{-3} R) + 0.003 \text{ m/s} \qquad (4.7)$$

which is applicable in flow velocities which vary above and below 0.17 m/s.

4.3.2.1 Initial Data Processing

Computer programs were essential, to analyse the great quantity of data obtained. However, due to the irregularity of periods of useful data from various rotors, it was necessary to manually look through the data to identify when rotors produced good data. It was possible to recognise when each rotor was covered by the rising tide and uncovered by the ebb; thus, water depth curves (up to 2.2m depth) were calculated. The time of HW was taken as the slack water from the current meter records, and the maximum depth was obtained from use of the interpolated tidal curves, predicted heights from tide tables, and two water level curves obtained by sighting onto the V.G.U. mast with a theodolite.

The times of useful data, rotor heights and facing directions, and the water depth curves were put onto computer files. The main current analysis program (VGU.FOR) used data from these files to control its actions and output.

4.3.2.2 Rotor Heights

In order to draw vertical tidal velocity profiles and accurately derive flow parameters from them, it is necessary to know accurately the height of the rotors above the bed. This is a problem in studies of this nature. Where a piece of equipment, in this case the V.G.U., is fixed in position by being attached to a stake driven deep into the sediment, the surface layers of sediment may undergo erosion or accumulation. Thus the instrument attached to the stake will vary in height above the bed as bed level varies. On Fegla Fach shoal, megaripples of amplitude up to 0.4m migrate across the shoal, and this migration may bring about bed level changes of several decimetres in a single flood/ebb cycle.

Previous attempts to tackle the problem and measure the bed level continuously throughout the tide, have included the development of acoustic bed level monitors which monitored the varying distance of the bed from a

fixed downward facing acoustic transducer. Thorne et al (1984/5) described a compact self- recording high frequency echo sounder, with a resolution of a few millimetres. This was partially successful, but the acoustic definition of the bed level was unclear with suspended sediment near the bed, and especially after the threshold for bed sediment transport was exceeded.

A mathematical way of tackling this problem was presented by Jackson (1981) in terms of the 'displacement height' (dZ) (the height difference between actual bed level and the datum used). It is obtained by fitting measured velocity profile data to a modified von Karman equation of the form

$$U = \frac{U^*}{K} \ln \frac{Z + dZ}{Zo} \qquad (4.8).$$

The parameters U* and Zo and dZ are obtained by finding the value of dZ which results in the best straight line fit to the data (Dyer, 1986).

However, using data collected over gravel in the Solent, Heathershaw & Langhorne (1988), obtained values for dZ of 0.15 - 0.22m, an order of magnitude larger than Zo values calculated from an unmodified von Karman equation; they considered them unrealistically large in the generally level gravel bed field site. Dyer (1980) has calculated displacement heights of the order of 0.1m over ripples of just 0.003m height; he did not correct his flow data for this displacement, concluding the effect was a product of flow acceleration and the occasional larger bedform. In a detailed consideration of the structure and measurement of velocity profiles, he further concluded (Dyer, 1986) that corruption of the velocity profile due to the displacement height was insignificant compared to other effects such as bedform topography or tidal flow acceleration.

In this study, the assumption was made that rotor height (i.e. bed level) varied linearly with time between bed inundation and exposure. This is not

fully satisfactory as bed height change would only be possible during periods when the bedload transport threshold was exceeded, and would be intimately related to the migration of the megaripples below the V.G.U.. The assumption would be least valid around spring tides when height change due to flood-directed bedform migration may be reversed by the strong ebb currents. However, lacking intratidal bed level information, it was considered a useful assumption in this study, and in the data interpretation (see later), due account was taken of V.G.U. position relative to megaripple morphology.

4.3.2.3 Description of Program, VGU.FOR

This computer program was written for this study, to analyse the current meter data. It is briefly described below.

The main operations which the program does are :

1 - reads a data file of 60 second rotor counts, finds slackwater, and converts data to velocities;

2 - reads data file of water depths (obtained from identification of submergence and emergence times of each rotor);

3 - averages velocities over 10mins, and calculates mean water depth for each 10minute point;

4 - calculates the best fit line through a plot of log height .v. velocity, and hence boundary-layer flow parameters (U*, Zo, Shields theta etc.);

5 - calculates 95% confidence limits for U* and Zo, using the method of Wilkinson (1984);

6 - if the correlation coefficient for the best fit line is <0.8, it ignores the top rotor reading and recalculates the fit (i.e. returns to stage 4);

7 - if the number of data points on a velocity profile is below 3, flow parameters are not calculated;

8 - outputs the calculated data for each period of tidal inundation as a graphic display.

4.3.3 The Data Obtained

4.3.3.1 Number of Points on each Profile

The number of rotors providing useful data at any particular time varied between 0 and 8. Only when 3 or more were working was it possible to fit a logarithmic curve to the data. If the calculated value of U* was >0.2m the U* and Zo values were disregarded. However, the U100 values calculated from such profiles showed consistency with surrounding values, and were used in subsequent analysis. Tabulated below in Table 4.1 are the proportions of the U* data 'disregarded', and proportions of the values obtained by different numbers of rotors.

Table 4.1

Percentage of Flow Parameter Data Obtained
by Curve Fits to 'n' Rotors
10 minute average profiles

Number of rotors n	Flood tide % of profiles	Ebb tide % of profiles
3	19.1	20.9
4	21.8	21.7
5	24.0	20.9
6	18.2	19.7
7	6.2	5.2
8	3.6	5.2
% of profiles disregarded	7.1	6.4

Thus of all the data with more than 2 rotors working simultaneously, 6.8% of the data was disregarded according to the above criteria.

There are no significant differences between flood and ebb tides in the proportions of data derived from profiles of the same number of rotors, so there is no overall bias in the likely accuracy of the calculated flow

parameters. Therefore, overall, all flood and ebb parameters derived in this way are directly comparable, with no inherent bias in favour of either flow.

4.3.3.2 The 'Averaging Time'

Time-averaging is part of the process of reducing the large volume of current data to a manageable level, and also of obtaining a physically meaningful and useful measure of velocity. Too short an averaging time and random errors in the data will be large, due to the intermittence of the turbulent bursting process (Dyer, 1986). Some of the turbulent energy will not be measured and bed stress may be underestimated. In contrast, too long an averaging time means some tidal energy will be included in the measurements and overestimates will result.

Soulsby (1980) defined tidal record lengths as stationary between 8 and 12 minutes, and later (Soulsby, 1983) he measured bursts in the marine environment with a periodicity of 18 seconds. A 10 minute averaging time as suggested by Gross & Nowell (1983) would include about 30 such bursts. They found that averaging over longer periods produced no further reduction in errors of U* or Zo.

The raw data collected in this study consisted of one minute averages; thus it was not possible to determine the characteristic bursting period of the tidal currents - so an averaging time of 10 minutes has been used. Examples of the raw data are shown in Figs. 4.5 - 4.8, covering neap and spring flood and ebb tides.

4.3.3.3 Were Velocity Profiles Logarithmic ?

In using U* and Zo to define the tidal flows, the assumption is made that the velocity profiles can be approximated to a logarithmic form (eqn. 4.1). The common measure of whether this approximation is justified is the correlation coefficient (CC) of the data to a log curve (e.g. Dyer, 1980). For the 10 minute averaged profiles presented in this study 81% of the flood profiles had CC >0.95 and 25.5% had a CC of >0.99. Ebb currents

Fig.4.5 Tidal currents - Fegla Fach Shoal

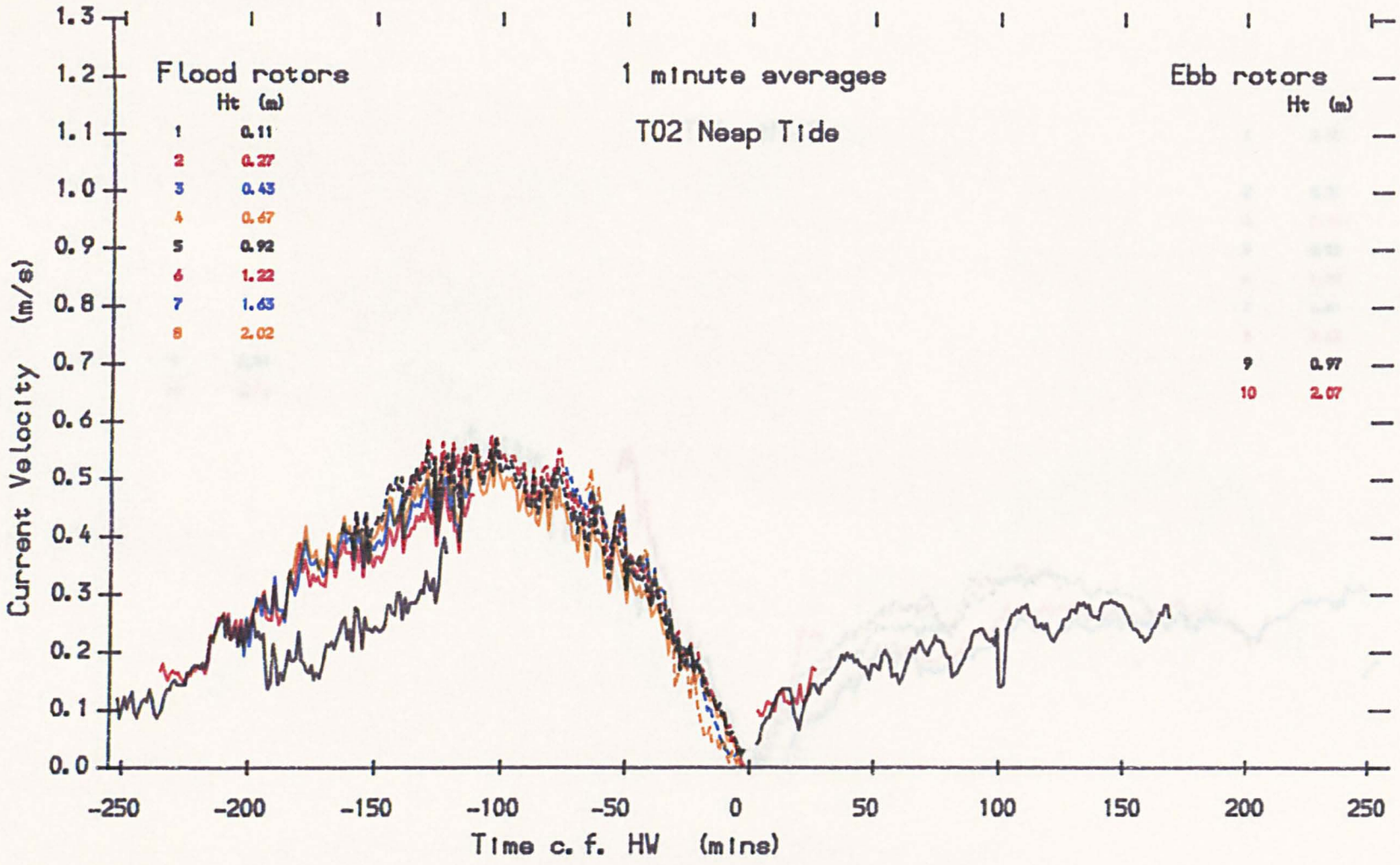

Fig. 4. 6 Tidal currents - Fegla Fach Shoal

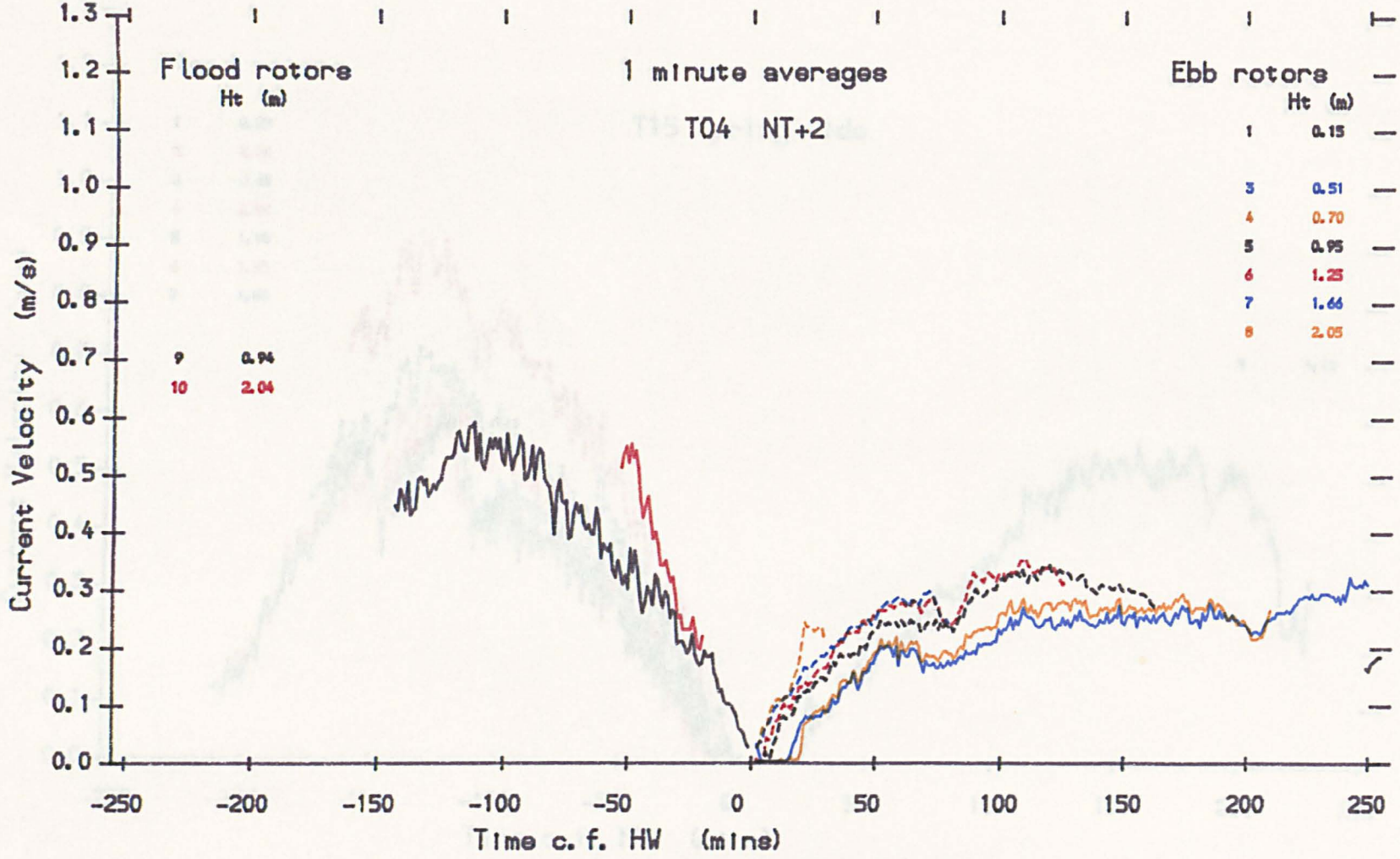

Fig. 4.7 Tidal currents - Fegla Fach Shoal

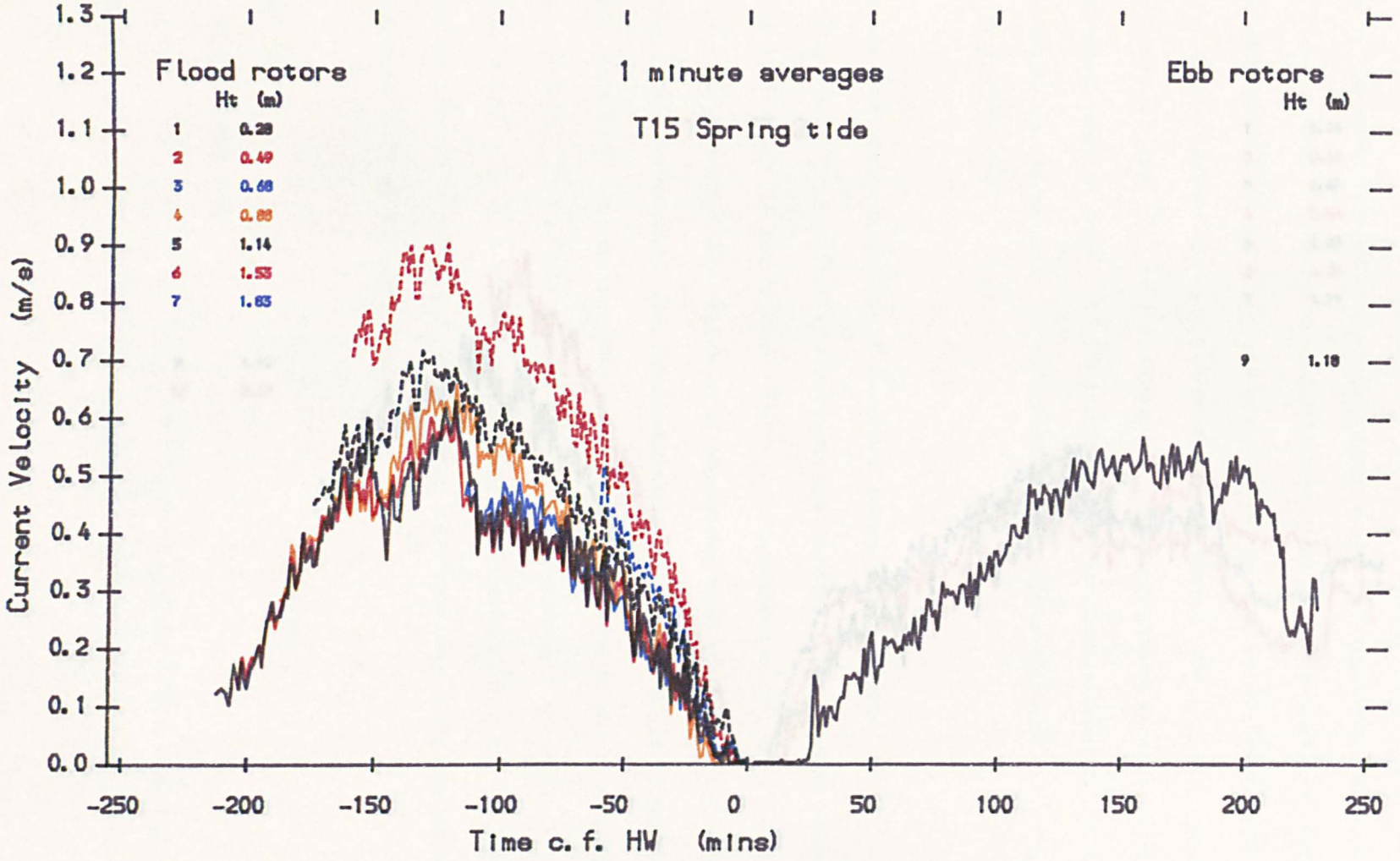

Fig. 4.8 Tidal currents - Fegla Fach Shoal

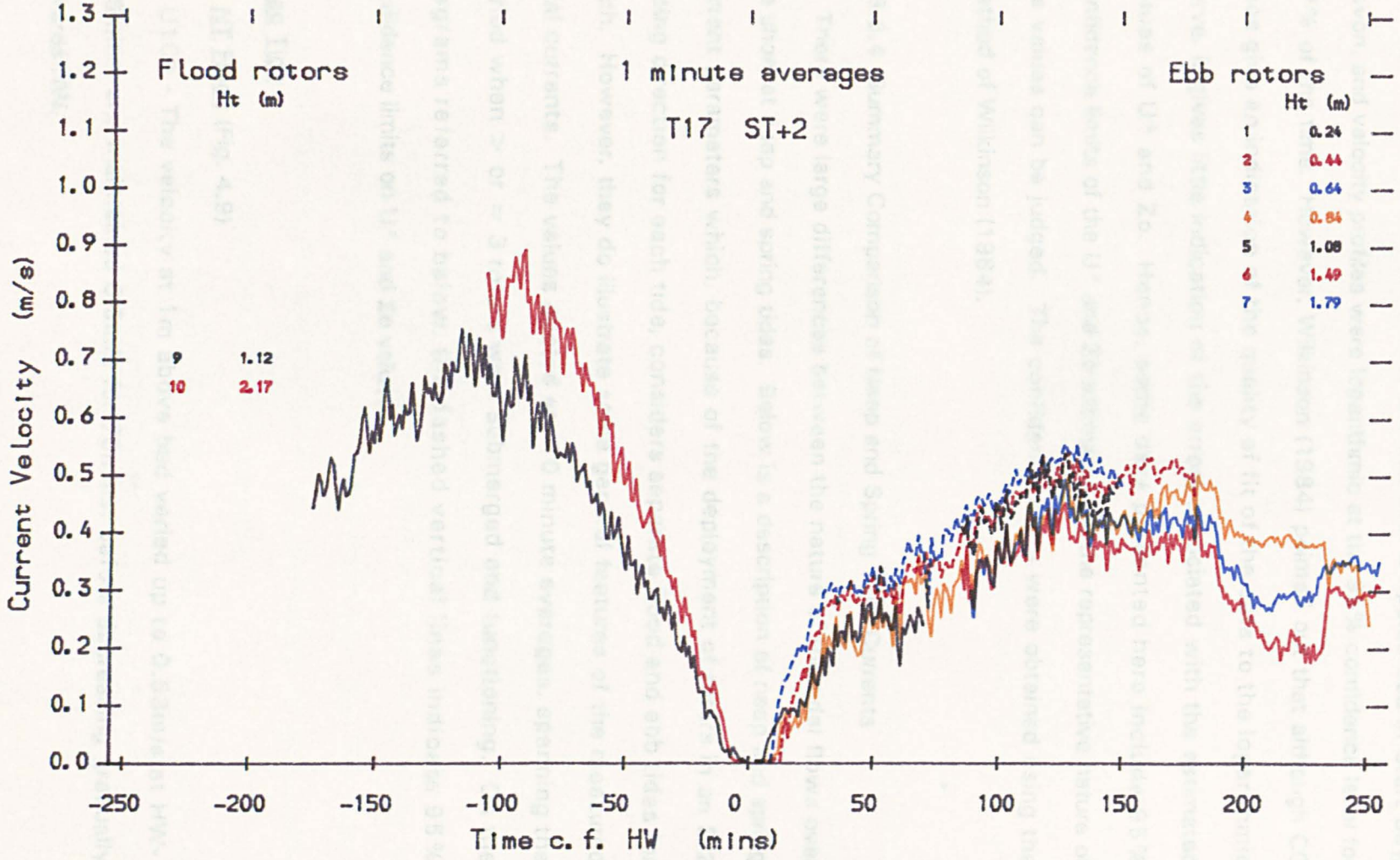

showed 75.3% of profiles with a CC >0.95 and 15.3% with a CC of >0.99. There were 9.3% of flood profiles which fitted a log form with a CC of <0.8, one criterion for rejection, and 4.2% of ebb profiles were similarly rejected.

Dyer (1980) measured velocity profiles over a rippled bed in Start Bay, Devon, and velocity profiles were logarithmic at the 95% confidence level for 87% of the time. However, Wilkinson (1984) pointed out that although CC does give an indication of the quality of fit of the data to the logarithmic curve, it gives little indication of the errors associated with the estimated values of U* and Zo. Hence, some data presented here include 95% confidence limits of the U* and Zo estimates, so the representative nature of the values can be judged. The confidence limits were obtained using the method of Wilkinson (1984).

4.3.3.4 Summary Comparison of Neap and Spring Tidal Currents

There were large differences between the nature of the tidal flows over the shoal at neap and spring tides. Below is a description of neap and spring current parameters which, because of the deployment of rotors in an 8:2 facing direction for each tide, considers separate flood and ebb tides for each. However, they do illustrate some general features of the measured tidal currents. The values quoted are 10 minute averages, spanning the period when > or = 3 rotors were submerged and functioning. On the diagrams referred to below, the dashed vertical lines indicate 95% confidence limits on U* and Zo values.

Neap Tide

NT Flood (Fig. 4.9)

U100 - The velocity at 1m above bed varied up to 0.53m/s at HW-105mins, and maintained 0.5m/s for 70mins, before decreasing gradually towards HW.

U* - Calculated U* values varied between 0.005 and 0.041m/s, peaking at HW-175mins, when flow depth was ~0.9m.

Zo - Roughness length was maximum at 0.0139m (coinciding with U*max) though for much of the flood tide it was below 0.005m.

NT+2 Ebb (Fig. 4.10)

U100 - This gradually increased with time, reaching 0.33m/s at HW+125mins, but at HW+75mins did show velocities decreased by 2-3cm/s. (A rotor at 0.5m above bed showed the velocity continued to increase with decreasing depth).

U* - The shear velocity varied between 0.019 and 0.056m/s, reaching maximum at HW+125mins, at a flow depth of ~1.25m, although it was of similar magnitude for the previous 50mins also, when depths were decreasing from ~1.6m.

Zo - Zo varied between 0.0145 and 0.56m, but 95% confidence limits were very large, most being >0.1m. Values were very variable and do not suggest a general trend with time.

Spring Tide

ST Flood (Fig. 4.11)

U100 - This increased rapidly to 0.71m/s at HW-125mins, and decreased more slowly towards HW. However, this decrease included at HW-95 to -85mins a period where velocity remained constant.

U* - Shear velocity varied between 0.004 and 0.077m/s, increasing rapidly to its maximum at HW-135mins, when depth was ~2m. For 70mins U* was >0.058m/s, but note that all U* data had large error bars, greater than 0.05m/s. 90 minutes of data was discarded.

Zo - Roughness lengths also had large error bars, of greater than 0.1m. Zo varied up to 0.13m, and showed a small minimum of 0.009m at HW-125mins.

Fig. 4.9 Velocity parameters for flood neap tide (NT)

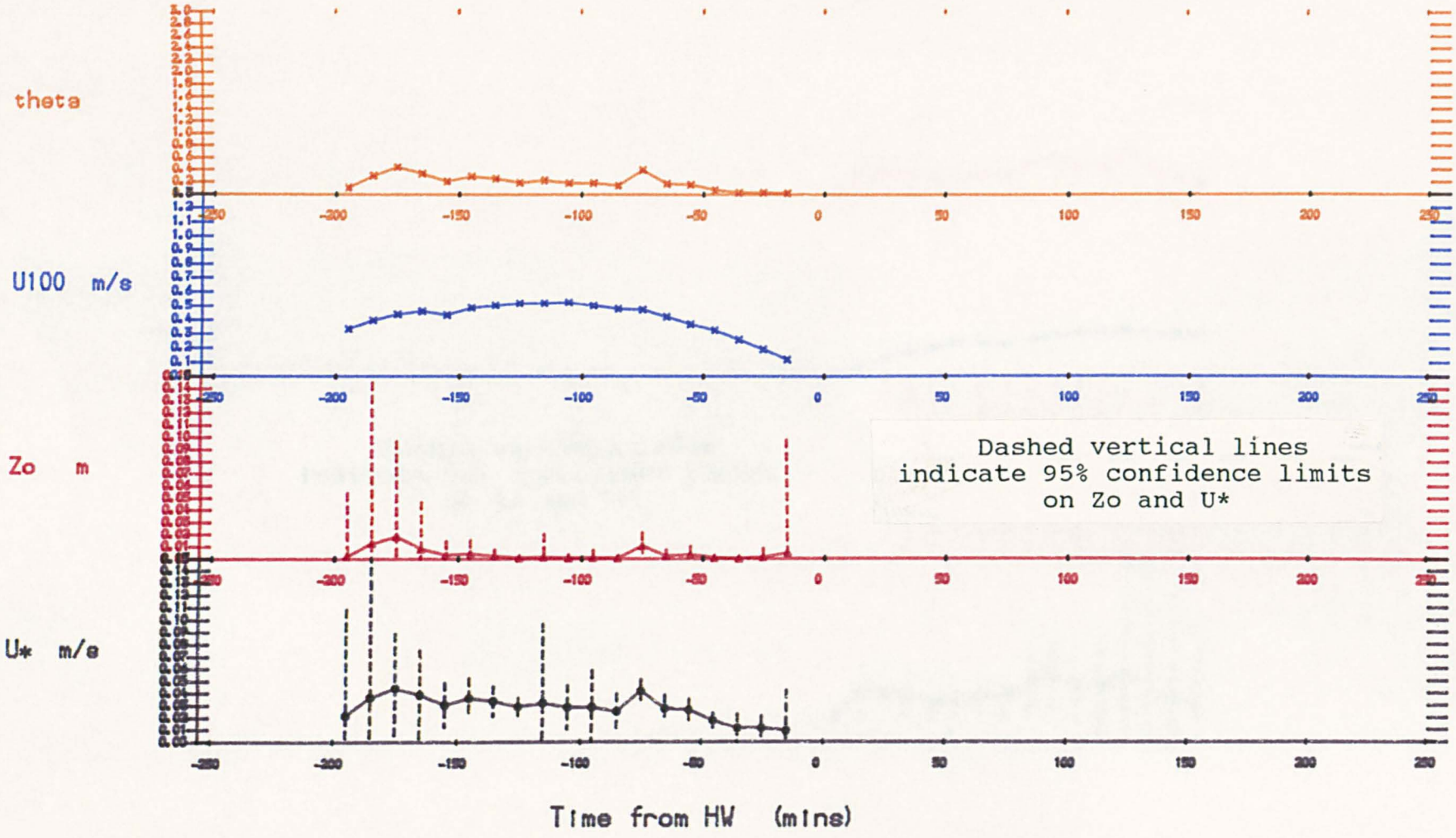

Fig. 4.10 Velocity parameters for ebb neap tide (NT+2)

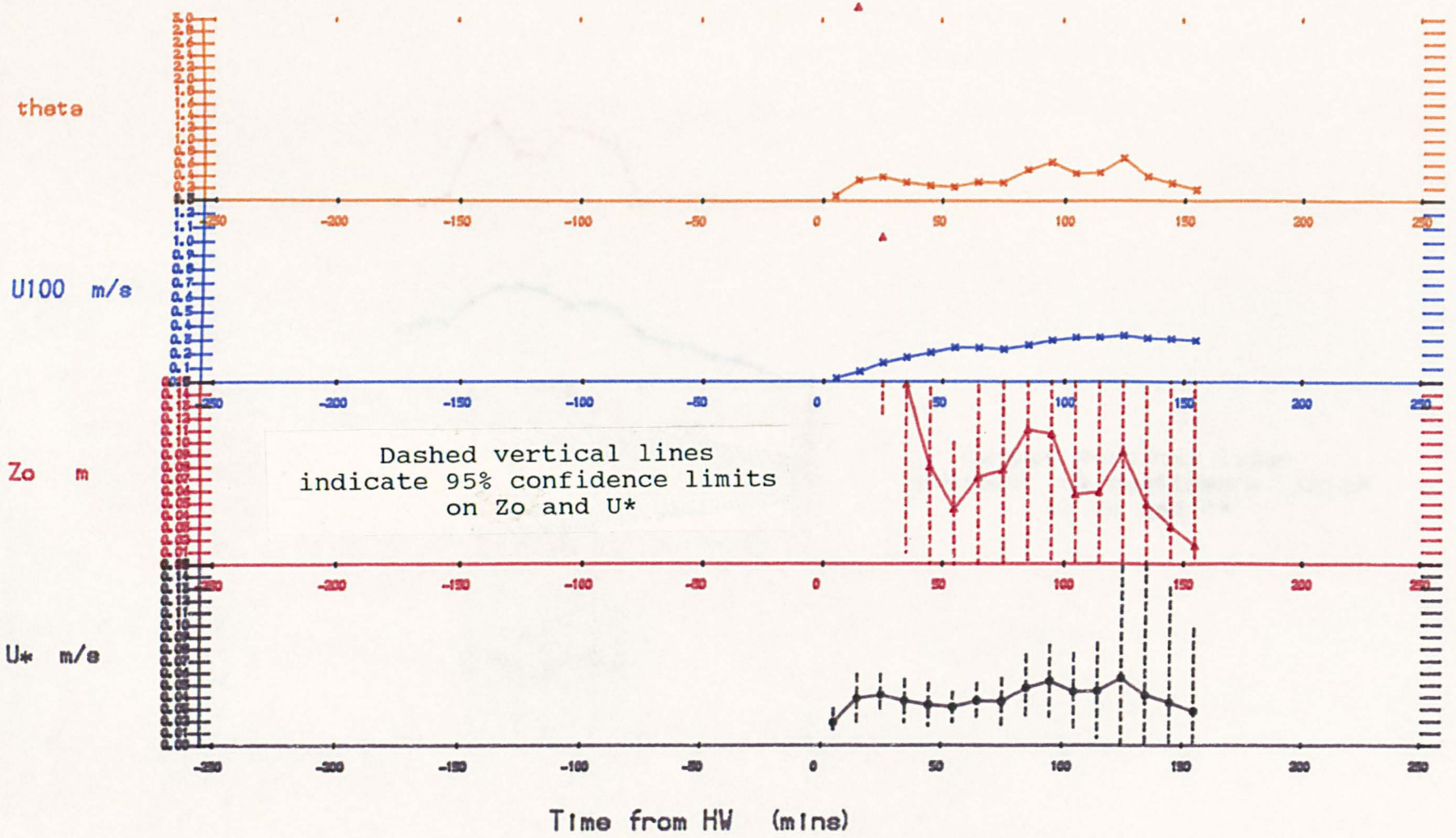

Fig. 4.11 Velocity parameters for flood spring tide (ST)

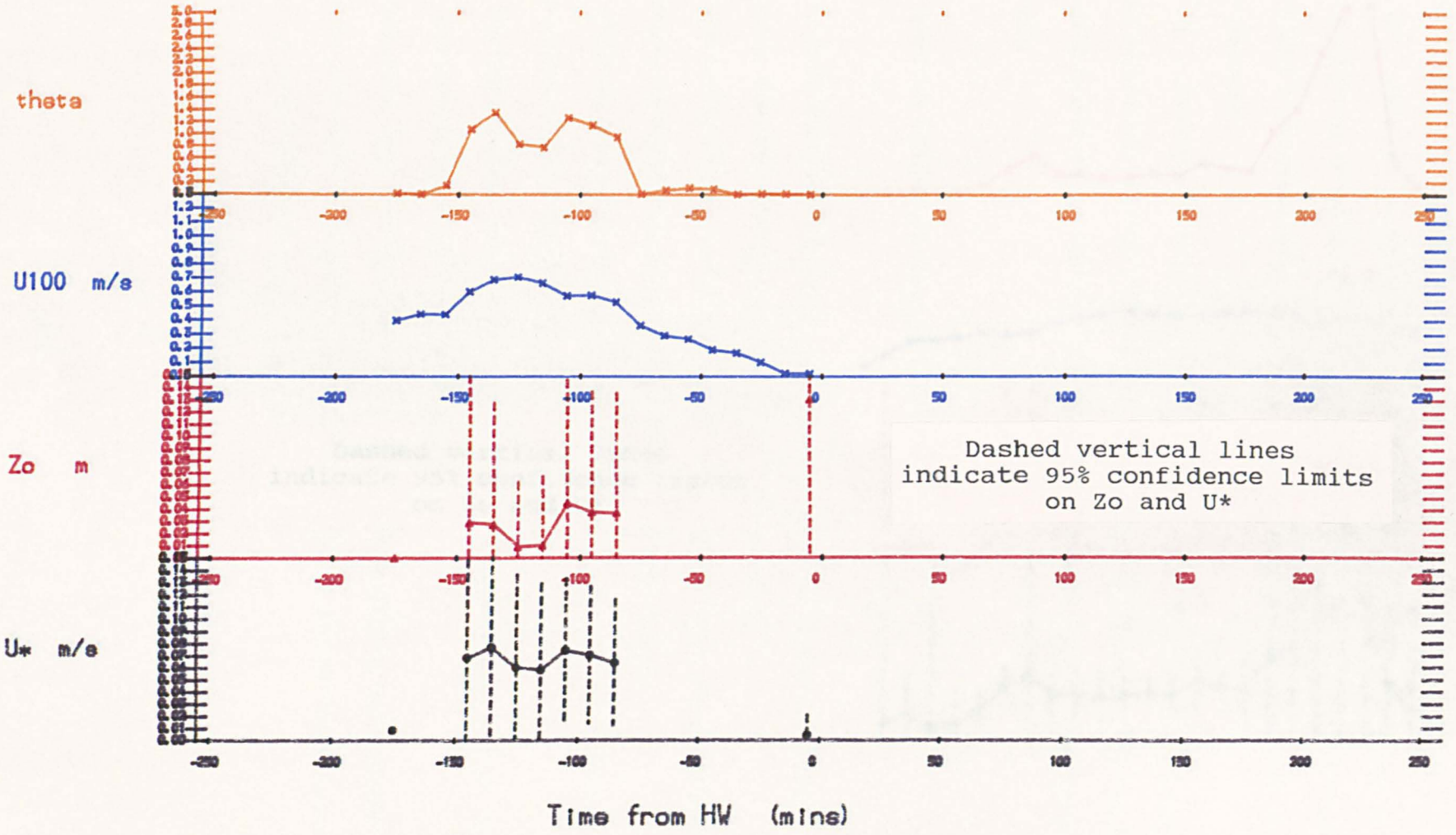

Fig. 4.12 Velocity parameters for ebb spring tide (ST+2)

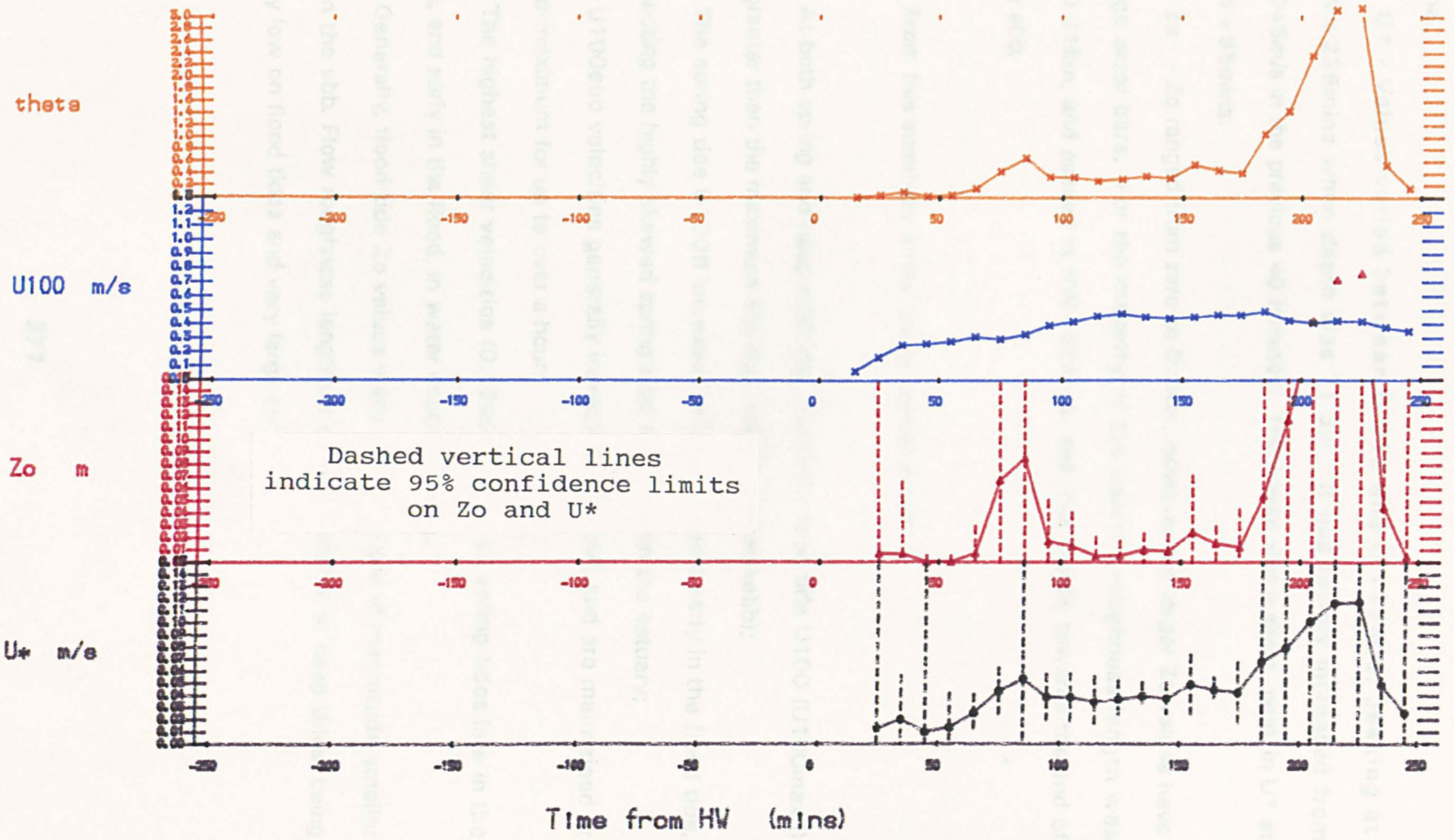

ST+2 ebb tide (Fig. 4.12)

U100 - This reached 0.49m/s at HW+185mins, but was broadly constant for the previous 80 minutes. Overall, the velocity increased with time.

U* - Values varied between 0.013 and 0.117m/s, peaking at HW+225mins when depth was ~1.3m. It had rapidly increased from 0.045m/s in the previous 40 minutes. There was also a slight peak in U* at HW+85mins.

Zo - Zo ranged from zero to 0.24m, however the larger Zo values have large error bars. For the majority of the tide the roughness length was <0.015m, and peaked at HW+85mins, and rose rapidly towards the end of the ebb.

From this summary a few points can be noted :

1 - At both spring and neap tides the maximum flood tide U100 (U100maxfl) is greater than the maximum ebb tide value (U100maxebb);

2 - The spring tide U100fl increases to its maximum early in the flood tide, reflecting the highly skewed spring tidal wave within the estuary;

3 - U100ebb velocities generally increase with time, and are maintained at near-maximum for up to over a hour;

4 - The highest shear velocities (0.12m/s) occur on spring tides late in the ebb, and early in the flood, in water depths of ~1m;

5 - Generally, flood tide Zo values were 1 or 2 orders of magnitude smaller than the ebb. Flow roughness lengths are most variable at neap tides, being very low on flood tides and very large on ebbs.

4.4 Relationship of Flow to Megaripple Form

As discussed above, Dyer (1970) distinguished 4 groups of velocity profile measured in different places over tidal bedforms. In this study the V.G.U. remained fixed in position and megaripples migrated past it, so at different tides the current profiles were measured at different places over a megaripple. In this way the flow data collected for this study is unlike that of Terwindt & Brouwer (1986), who moved their array of 6 OTT-Minor current meters at each LW to ensure that measured velocities remained indicative of the bedform crestal zone. Whilst being a disadvantage in some ways, for example in terms of judging precise sediment threshold velocities, it enabled the flow data to be examined in terms of measured velocity profiles over different parts of intertidal megaripples.

From the bedform profiles measured at each low water, the position of the V.G.U. (which was mid-way along Line A) with respect to the megaripples was placed into one of the following three groups :

Group 1 - 'crest'; defined as the upper part of the megaripple upstream flank;

Group 2 -'flank'; the lower part of the megaripple upstream flank;

Group 3 - 'trough'; the lee of a bedform, i.e. where the V.G.U. was above the slip face or over a megaripple trough.

The category into which each tidal record has been placed in given below in Table 4.2.

Table 4.2

Categories of Tidal Flow Measurements
With Respect to Position of Measurement Over Megaripple
(see text for explanation of groups).

Tide	Flood	Ebb	Tide	Flood	Ebb
NT-1	1	1	NT+11	2	3
NT	1	1	+12	2(3)	3
NT+1	1	1	ST	3	3
+2	1	1	ST+1	3	2
+3	1	1	+2	3	2
+4	1	1	+3	3	1
+5	1	1	+4	1(2)	1/3
+6	1	1	+5	2	3
+7	2	3	+6	2	3
+8	2	3	+7	2	3
+9	3	3	+8	2(3)	2/3
+10	3	1			

Notes :
- 1(2) denotes alternative grouping
- 1/2 denotes uncertain grouping because of high migration rates
- In both cases the former group was used in the calculations below

There are three points to be made regarding the validity of these groups :

1 - it is a subjective distinction between groups, eg. precisely where does the 'trough' finish and the 'flank' begin? Similarly, where does the 'flank' become the 'crest'?;

2 - there is no information on the precise location of the megaripple beneath the V.G.U. except at LW, so with high megaripple migration rates such as on flooding spring tides, there may be very hydrodynamically significant changes in the relative position of the V.G.U.. An example; if the V.G.U. at LW was underlain by the lee slope of a flood-orientated megaripple, and hence the tidal flow was placed in Group 3, at some time during a strong flood tide, high migration may cause the megaripples crest to reach and pass the V.G.U., so the flow should then be placed in group 1. Boothroyd &

Hubbard (1975) reported short term migration rates of intertidal megaripple slip faces of up to 0.08m/minute, so that in just 15 minutes the relative position of a fixed current meter could have been changed by over 1m! Migration rates in this study reached up to a net 0.98m/tide on NT+12 (see Chapter 3). Allowing for no ebb migration (to obtain a minimum value) this is equivalent to a minimum mean migration rate on the 3 hour flood tide of 0.33m/hour. Peak rates would be substantially higher due to the power relationship between flow velocity and sediment transport (and therefore migration rate). Clearly megaripple migration is a large potential factor in blurring the boundaries of the defined groups;

3 - because flood and ebb currents are opposite in flow direction, a V.G.U. position that on the flood tide is in group 3 (trough), on the ebb tide would be more appropriately placed in group 2 (flank). Megaripple migration increases the difficulty in assigning a particular tidal flow to a group, and emphasises the inherent subjectivity of the divisions.

Dyer (1970) found that velocity profiles measured over troughs of subtidal megaripples produced overestimates of both U* and Zo. This has yet to be established for the intertidal regime.

4.4.1 Results

In Table 4.3 are tabulated values of U* and Zo for all the flows designated as belonging to each of the three groups described above. All U* values are peak measured 10 minute averages; Zo values are those at the time of peak U*. The suffix '3' indicates that the value is an average of three such profiles, the one at the time of peak U*, and the two adjacent ones, i.e. it is a 30 minute average.

Table 4.3

Peak Shear Velocities and Associated Roughness Lengths Measured over Different Parts of Megaripples.

Units : U* in m/s, Zo in m.
N = No. of 10 minute values averaged.

		N	Zo	Zo3	U*	U*3
Group 1 'Crest'	Flood	5	.0123	.0078	.0441	.0398
	Ebb	6	.0814	.0717	.0659	.0616
Group 2 'Flank'	Flood	5	.0094	.0075	.0635	.0602
	Ebb	1	.2381	.1721	.1173	.0942
Group 3 'Trough'	Flood	3	.0235	.0121	.0745	.0614
	Ebb	3	.0903	.0554	.0563	.0443
Averages of all data regardless of V.G.U. position						
	Flood	13	.0226	.0166	-	-
	Ebb	10	.1476	.1125	-	-

4.4.2 Shear Velocity

In interpreting the U* and U*3 velocities shown above it should be remembered that shear velocity does show a weak systematic variation over the spring-neap cycle; so results within and between groups are not fully comparable. However, the tides with crestal profiles (Group 1) were measured over a similar spread of tidal ranges, so provide comparable flood and ebb data. Here the ratio of ebb/flood U* and U*3 is ~1.5. The flood - ebb difference for the trough profiles (Group 3) is interpreted as being largely due to the spring-neap variation of U*, and no conclusions are drawn.

Ebb and flood shear velocities over the flank of megaripples (Group 2) appear the same order of magnitude, with perhaps ebb velocities approximately twice that of the flood; as only a single ebb data point exists, however, the conclusions are unreliable. The single ebb data point is from ST+2, at HW+225mins when depth was just 1.3m. The reason for the large shear velocities at this time is unclear, because the megaripples found after this ebb flow were fully ebb- orientated; it would, therefore, not be unreasonable to consider that form drag would be relatively low and, thus, the shear velocity would be smaller than for the same flow over megaripples of flood orientation. However, when calculating shear velocity in shallow currents the depth of measurement Z and the roughness length Zo will become close; hence, U* will be increased (see eqn. 4.1). It is concluded that rapidly decreasing depths are a large (but unquantified) factor in causing the large U* on spring ebb tides.

4.4.3 Roughness Lengths

The grouped data are more successful in elucidating the meaning of roughness lengths measured over the megaripples, mainly because of the lack of a coherent spring-neap variation of Zo. The crestal (Group 1) measured roughness lengths show very well that flood lengths are approximately an order of magnitude smaller than ebb lengths, in common with the results of Terwindt & Brouwer (1986) obtained at the crests of 2D and 3D flood-dominated megaripples. (See more detailed discussion below). The data from megaripple flanks also suggest relatively large ebb roughness, and profiles over troughs (Group 3) show a similar result, with ebb/flood ratios of ~0.5.

Both Zo and Zo3 (30 min. average) parameters show that for the flood tide, measured roughness is largest over megaripple troughs, a confirmation of Dyer's (1970) findings in the subtidal zone. However, for the ebb tides there is a less clear distinction. Ebb roughness lengths suggest a relationship

with depth, rather than being strongly position specific.

4.4.4 Comparison with Predicted Roughness

Wooding et al (1973) gave a predictive equation for roughness lengths over bedforms

$$Zo = 2h\,(h/L)^{1.4} \qquad (4.10)$$

for Z/Zo of 15-1000. This is applicable for the conditions on the Fegla Fach shoal.

Using the minimum, mean and maximum megaripple dimensions which occurred over the lunar cycle, this equation predicts the following roughness lengths:

minimum Zo 0.0026m

mean Zo 0.0048m

maximum Zo 0.0134m.

These values are of the same magnitude as the measured roughness (Fig. 4.13) on flood tides over megaripple crests and flanks. On this and subsequent similar diagrams the following notation is used :

C = flow data measured over a megaripple crestal zone

F = measured over a megaripple flank

T = measured over a megaripple trough

U = measured over an unknown position.

UPPER CASE letters indicate FLOOD tide

Lower case indicates ebb tide.

They seem to show general validity of Woodings equation in these conditions, but only (although not exclusively) for the flood flow over flood-

Fig. 4.13 Flow roughness lengths at peak velocities for the study period. (C = flow measured at megaripple crest, F = at megaripple flank, T = at megaripple trough. Capitals denote flood tide data; lower case denotes ebb tide data; dots denote predictions using the equation of Smith & McLean, 1977a).

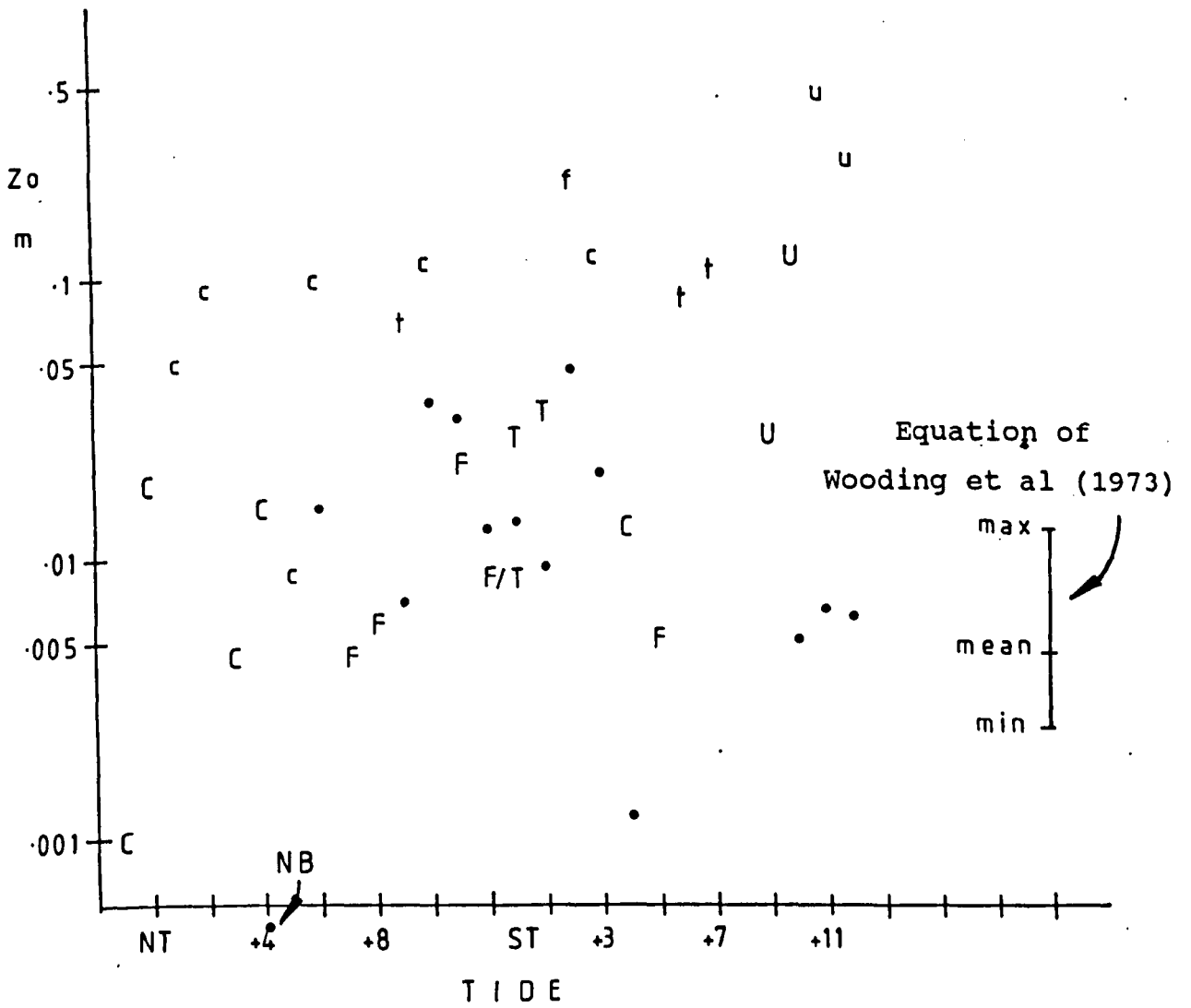

orientated megaripples. Only one ebb tide roughness measurement falls within the predicted range, despite the fact that at spring tides the ebb Zo occurred over strongly ebb- orientated forms.

The predictive equation of Smith & McLean (1977a,b) takes into account the modifying effect of suspended sediment on the roughness length. Predictions have been calculated for each measured tide, using a bedload threshold U* value (U*t) of 0.053m/s, and the relevant peak U* value. The results are plotted in Fig. 4.13, marked by dots, based on a threshold U* value of 0.053m/s (obtained by the method of Black & Healy, 1986, and using the flood tide mean Zo of 0.0266m). Tides for which no prediction is made are tides where the 10 minute averages of U* did not exceed threshold.

The flow data upon which Black & Healy (1986) tested their method of calculating U* was taken between 0.5m and 9m above tidal megaripples, and so their method calculates the critical shear velocity for a megarippled bed; thus, the predicted Zo values should not contain large errors caused by the presence of the megaripples. Fig. 4.13 clearly shows that most of the predicted roughness lengths are below the measured Zo at the time of maximum shear velocity, i.e. the dots are below the corresponding letters for each tide. This is discussed below. The predictions are most accurate around spring tides, where they are within a factor of 4 of the measured value, and least accurate at neaps, where they are generally an order of magnitude too low. This is possibly related to the development of an 'equilibrium' megaripple population around spring tides (Chapter 3), where it is implied that the flow-bed relationship is fully in equilibrium. A predictive equation describing the structure of tidal flow over bedforms, would be most applicable at this time, consistent with these results.

The consistent underestimation of roughness, together with the trend of accuracy varying with the spring-neap cycle suggests a systematic error in the predicted values. One possibility is that there was more suspended sediment present than the equation predicts, and/or that the threshold shear

velocity used was inappropriate. The use of a threshold parameter which is a time-averaged measure is likely to underestimate sediment transport because it will not predict transport at times when the current may only fluctuate above threshold. Therefore, the amount of sediment in suspension will also be underestimated. This would have the effect of decreasing predicted roughness lengths because of the lower flow-stabilising effect of suspended grains on the near-bed flow (Dyer, 1986) and thus could be partly responsible for the disagreements. Dyer (1980) found that threshold shear velocities vary over the lunar cycle.

A further possible source of error in the above predictive method is its reliance on a measure of grain size to calculate U*t. A single grain size cannot be sufficient to describe the complex transporting action of a flow over a bed comprising a mixture of grain sizes. The mean grain size may relate to the concentration of suspended material in different ways depending on the skewness of the distribution of the bed material, i.e. the local 'availability' of material sufficiently fine to be suspended near-bed. With a fine-skewed bed, more material may be available for suspension at the site of flow measurement than with a coarse-skewed bed of equal 'mean grain size'.

4.5 Intra-Tidal Relationship of Roughness Length with Shear Velocity

The data collected here provide an opportunity to investigate the relationship of Zo with U*, within individual tides. Dyer (1980) measured these parameters over subtidal rippled sand (1.75phi, ~300um) for >20 tidal cycles. Depth was 14m, and the tides produced U* up to 0.05m/s. He found a broadly consistent variation in the Zo - U* relationship over time, which he related to changes in ripple shape and the effects of sediment transport at spring tides. His findings, relating to a spring ebb tide, were :

1 - Zo decreased at the start of the ebb tide, due to flow acceleration;

2 - the lowest Zo coincided with the sediment threshold, and visible flow separation over ripples;

3 - ripple asymmetry reversed from flood to ebb, height increased and migration began. During the period of ripple height increase, Zo was proportional to the 4th power of U*. (Heathershaw & Hammond [1979] found a similar relationship). It was estimated that half the Zo increase was due to sediment transport and half to form drag changes;

4 - with flow deceleration, Zo increased briefly, then rose rapidly after sediment movement ceased.

On neap tides Dyer (1980) found an approximately constant Zo; this was probably related to the minimal sediment transport observed. As he did not present any neap tide Zo data, the quantitative meaning of 'approximately constant' is unknown.

This study allowed the investigation of whether the U* - Zo relationships observed by Dyer (1980) occur in a macrotidal and intertidal setting, where mean grain size was 1.84phi (280um), and where U* varied up to 0.11m/s. Another significant difference between the studies was that the new data were taken above a field of megaripples. It was thus possible to categorise the tidal flows depending upon the position of flow measurement above a

bedform (see above), and to investigate the influences of this factor upon the Zo - U* relationship. The new data comprised both flood and ebb tides, rather than purely ebb in Dyer's study.

There were distinct differences in the morphology and dynamics of the megaripples, between neap and spring tides. The neap tide data were measured over strongly flood orientated (b/a ~0.5), relatively flat (L/H ~30), non-reversing megaripples; these were barely altered by the successive flood-ebb cycles. The intermediate tidal range data was measured over slightly steeper (L/H 20-30) megaripples, which were near-symmetrical at low tide, having partly reversed symmetry during the ebb tide; these had migrated up to a net 0.44m over one flood-ebb cycle. By contrast, the spring tide data presented here refers to flow over steep (L/H 17-22) bedforms, fully reversed by both flood and ebb tides; these migrated in the flood direction, by a net distance of <0.7m per tide. Hence, there are complications likely to be present in the data from intermediate and spring tides related to changing bedform morphology and position.

4.5.1 Results

A series of Zo v U* plots were constructed (on log-log paper, as Dyer, 1980) for each tides time series of 10 minute averages of U* and Zo. The discussion of results will first concentrate on flow data measured above megaripple crests, except where none exists, when data from megaripple flanks is used.

Flood Tides (Figs. 4.14 - 4.18)

Neaps - NT+3 and NT+4 showed very similar curves. From an initial low Zo at HW-135mins, Zo increased towards peak U* values, than it fluctuated around a general increasing trend as the flow decelerated.

Intermediates - the only data (NT+7, ST+5) refers to megaripple flanks. The lowest Zo values occurred at about HW-145mins, and this was followed by an irregular increase in both U* and Zo. Following peak U*, Zo increased by approximately 5 times. Tide ST+5 shows a 40 minute decrease in Zo towards HW.

Springs - a 40 minute rapid increase in Zo was followed by a 50-60 minute period of near constant Zo and U* (ST+4) . A constant decrease in both U* and Zo followed, down to a Zo of <0.00001m at HW-45. There then occurred a rapid increase in both parameters, Zo by over 1000 times.

So the simplest pattern is shown by the neap and intermediate tides data, with an overall increase in Zo while U* rose to a peak and subsequently fell. Spring tide data was significantly different, with much variation in both U* and Zo at the beginning and end of the data set.

Ebb Tides (Figs. 4.19 - 4.23)

Neaps - both data sets (NT+1,+2) showed an initial decrease in Zo, reaching a minimum around HW+50mins. Both U* and Zo then rose; at and subsequent to peak U* the two parameters appeared to be closely related.

Fig.4.14 T05 NT+3 Flood tide

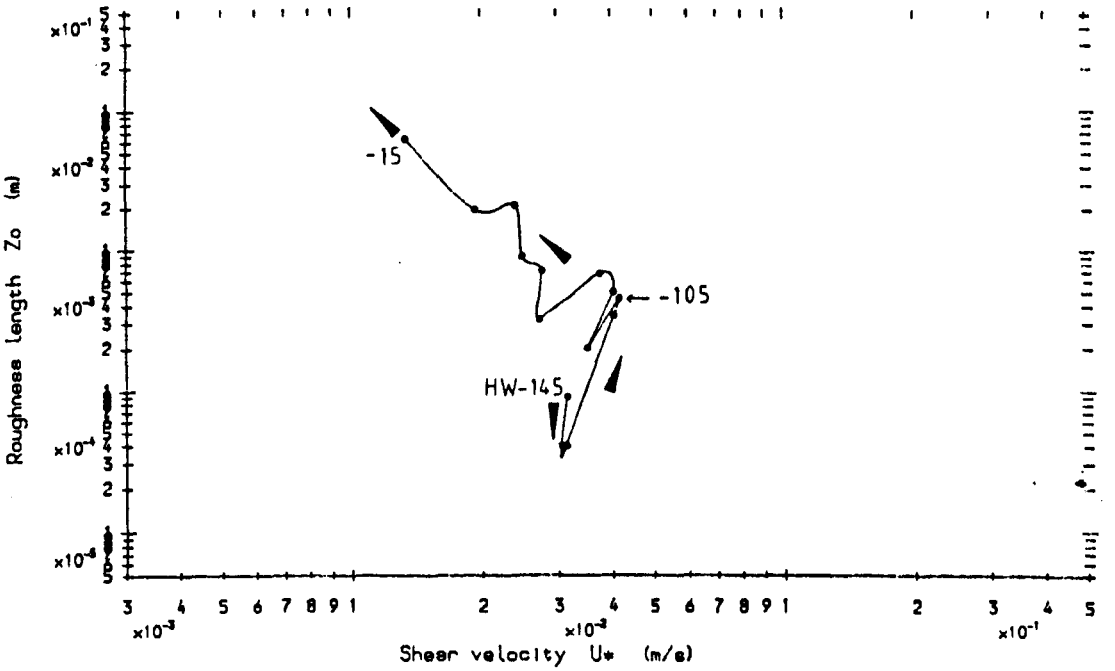

Fig.4.15 T06 NT+4 Flood tide

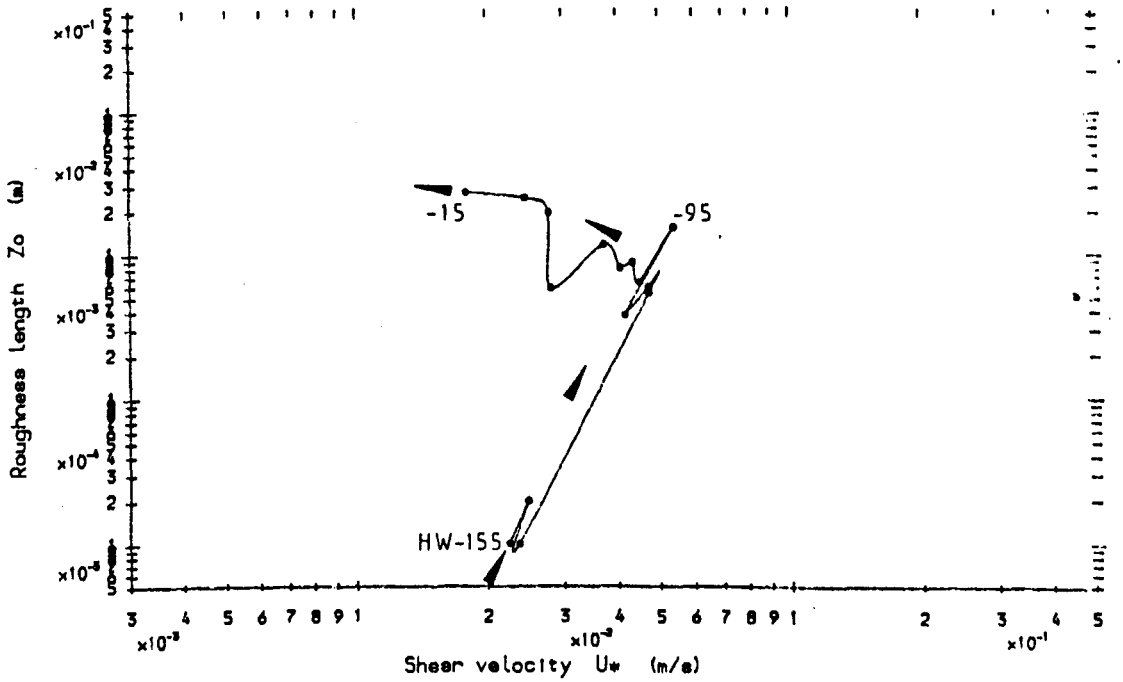

Fig. 4.16 T09 NT+7 Flood tide

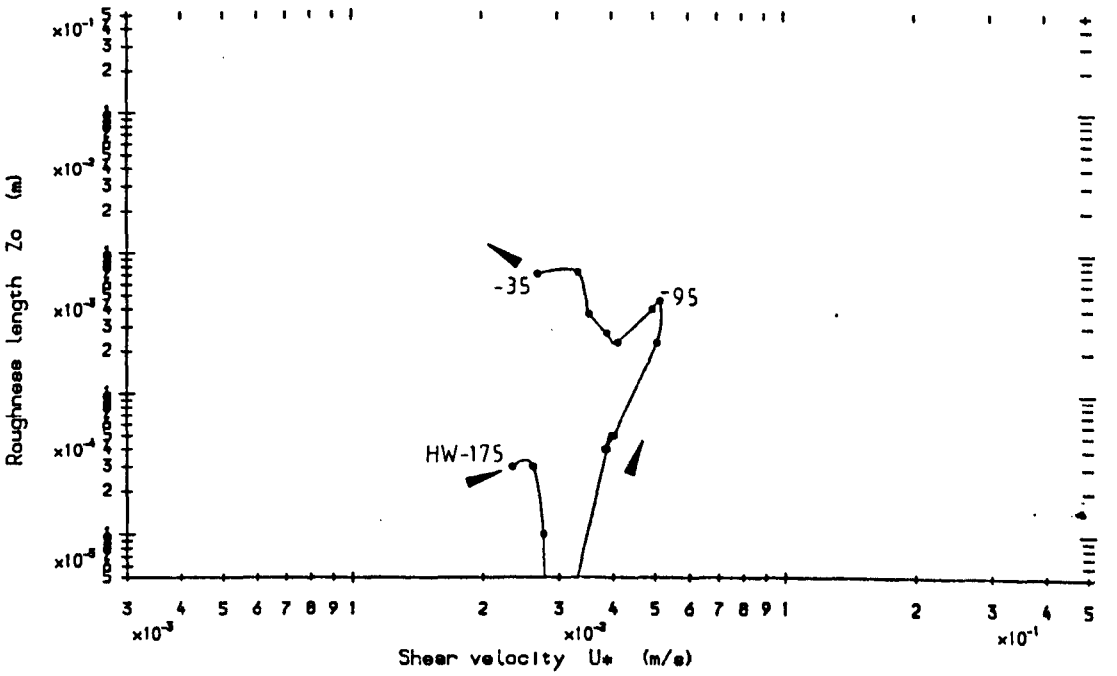

Fig. 4.17 T20 ST+5 Flood tide

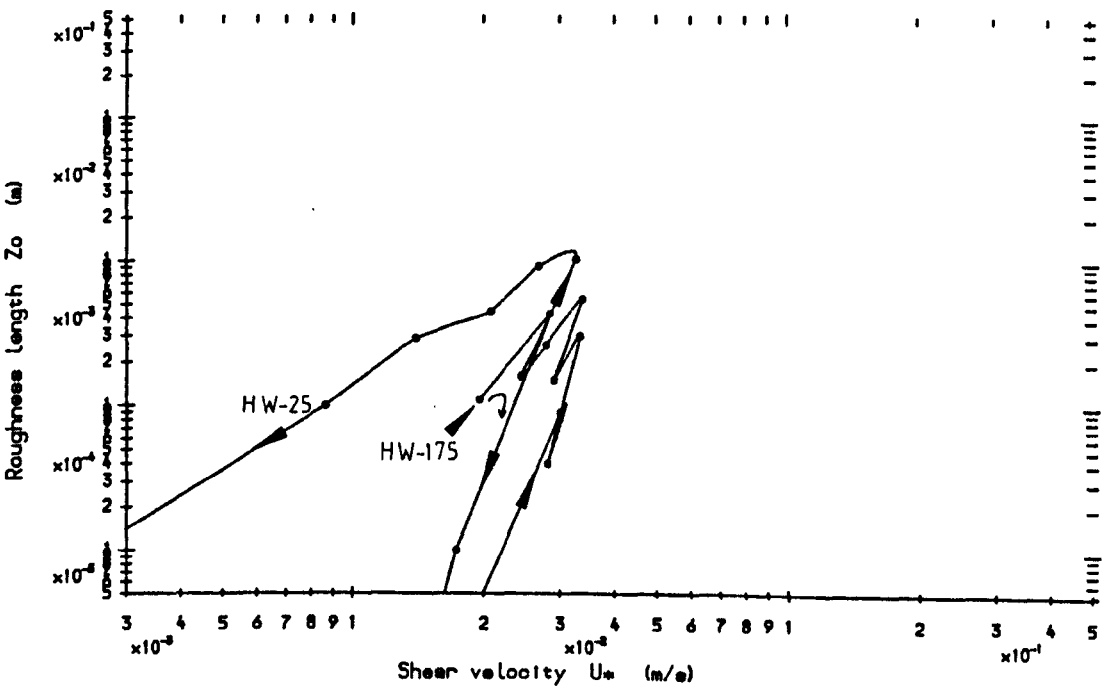

Fig. 4.18 T19 ST+4 Flood tide

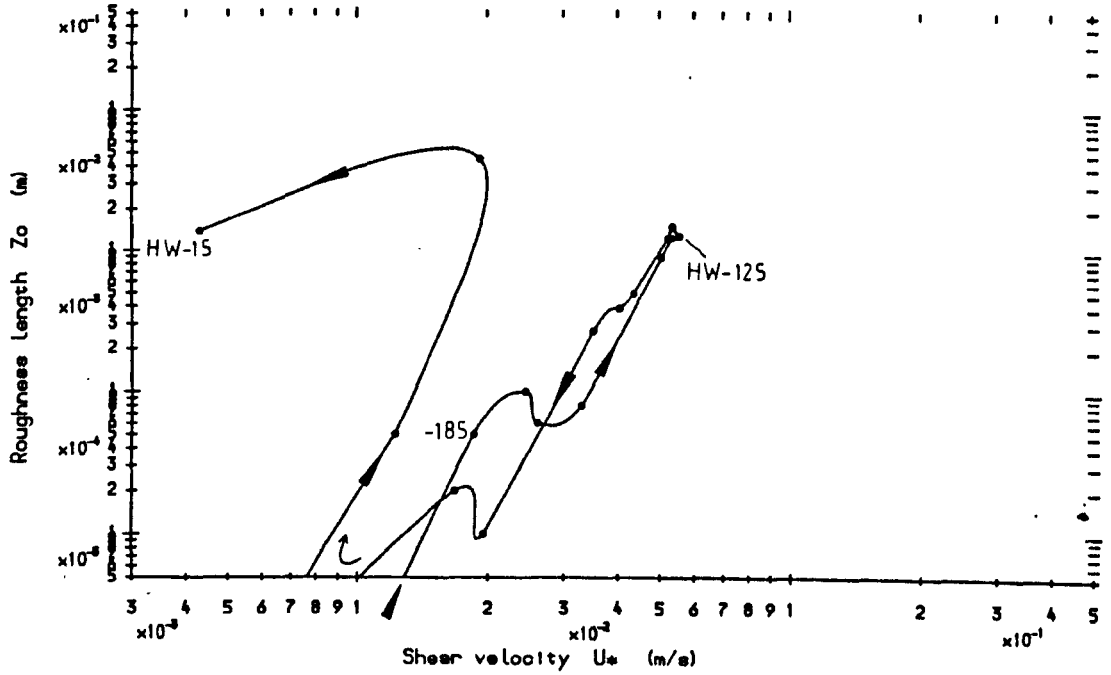

Fig. 4.19 T03 NT+1 Ebb tide

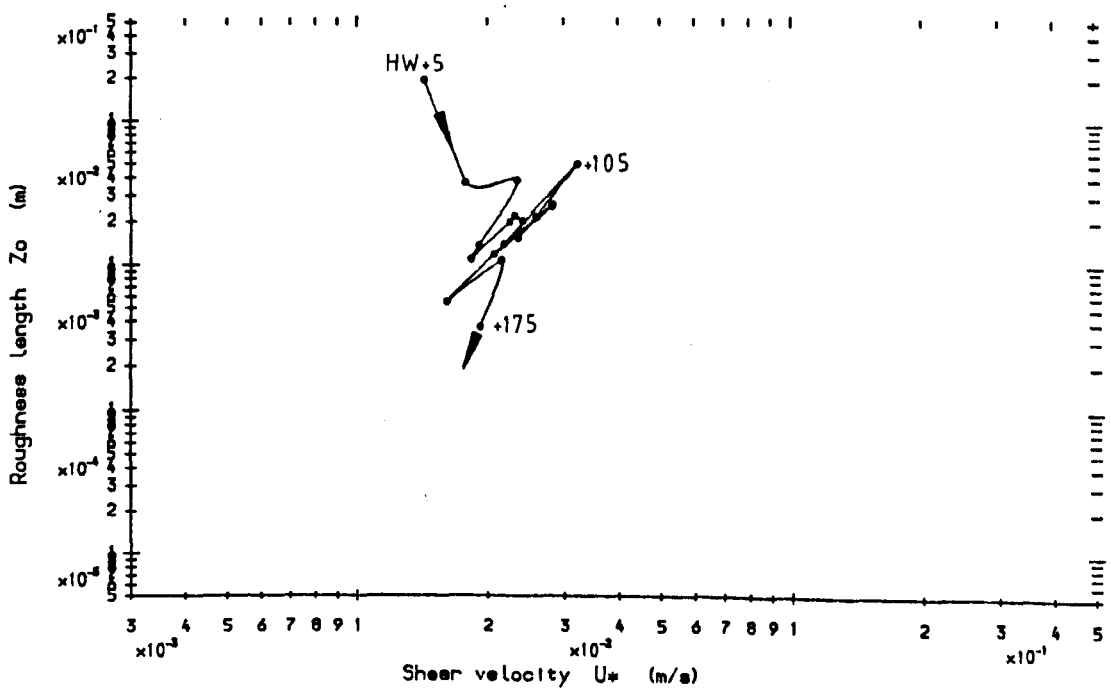

Fig. 4.20 T04 NT+2 Ebb tide

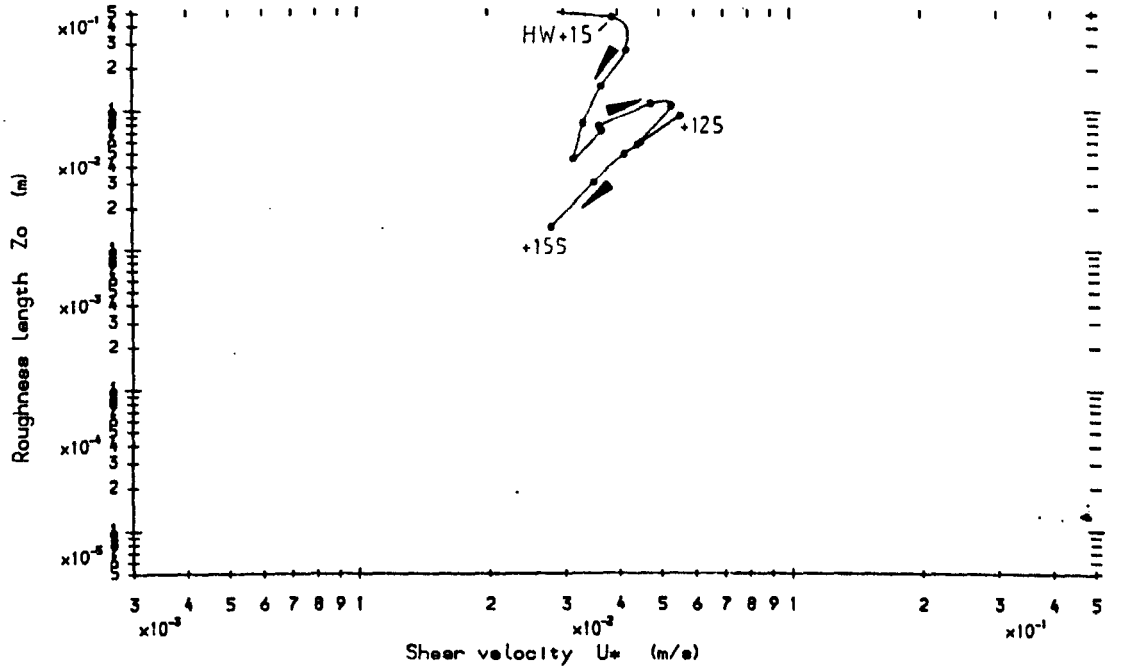

Fig. 4.21 T08 NT+6 Ebb tide

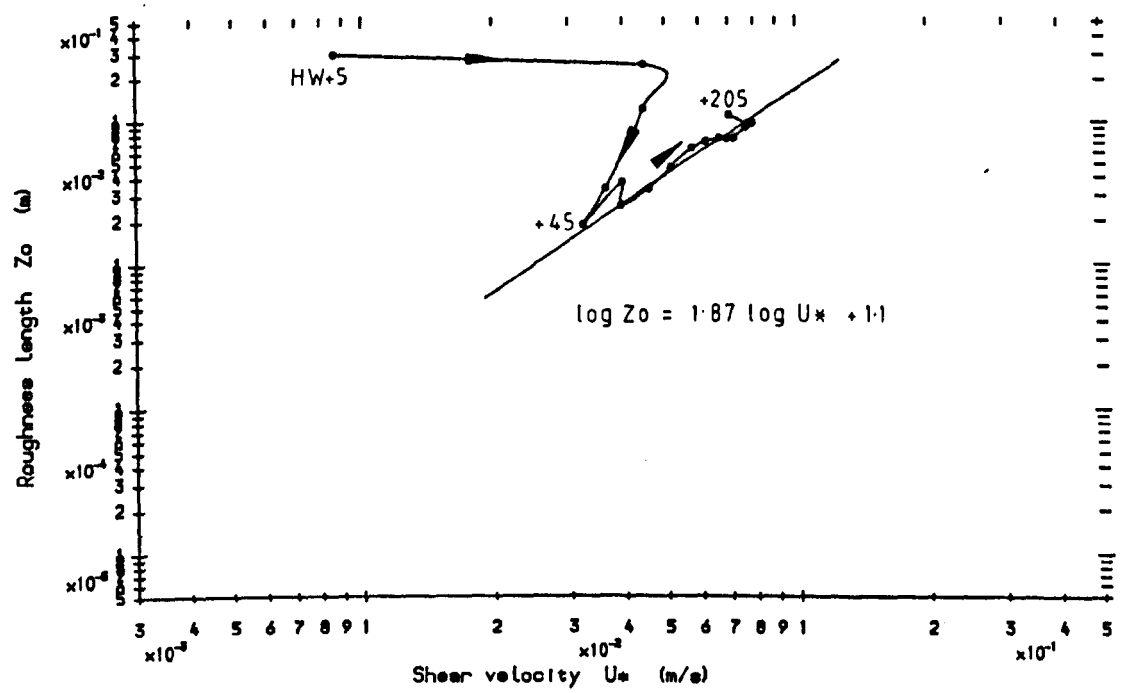

Fig. 4.22 T12 NT+10 Ebb tide

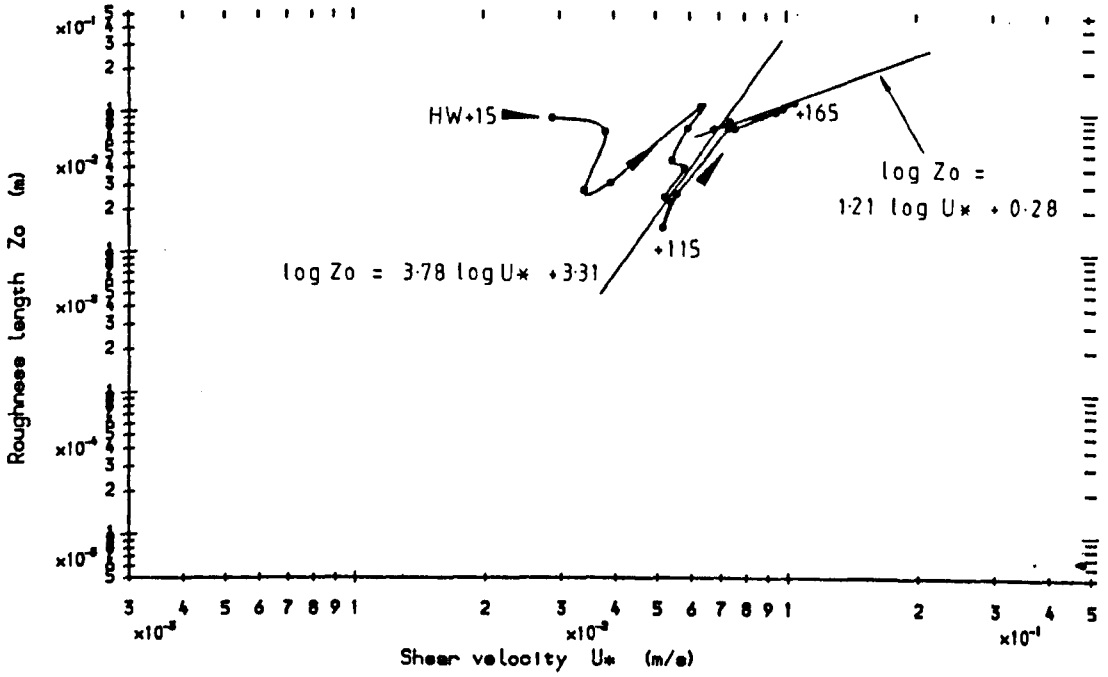

Fig. 4.23 T18 ST+3 Ebb tide

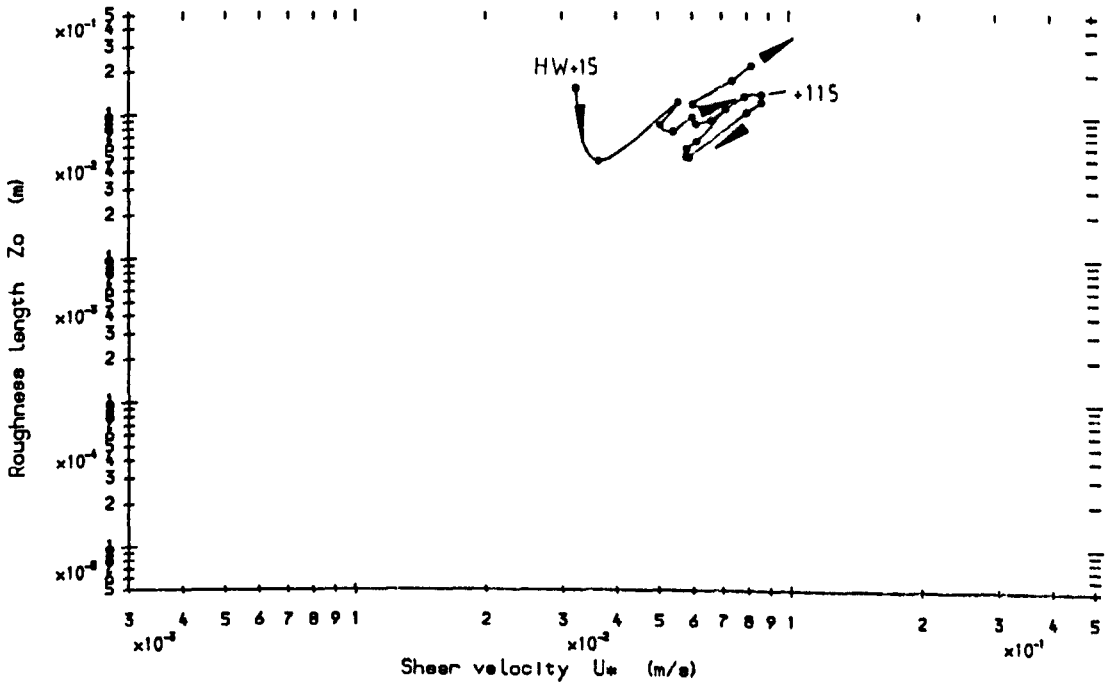

Intermediates - NT+6 shows high values of U* and Zo until HW+25, thereafter there was a general rise in U* and Zo towards the end of the data set at HW+205.

Springs - both NT+10 and ST+3 showed that Zo remained within one order of magnitude between HW+15 and HW+195mins. Both also show a similar trend, of two Zo minima followed by points plotting along a single line.

There appears a similar trend in the data, regardless of tidal range. An initial Zo decrease is followed by a fairly well-grouped set of points aligned around a positive Zo - U* relationship. Zo decreases around this trend towards the end of the ebb. The spring tide data from the megaripple flank show a similar form curve, but with exaggerated loops.

4.5.2 Interpretation and Discussion

Dyer's (1980) observations suggested that Zo was least when sediment threshold was attained. Using the method of Black & Healy (1986) to calculate the sediment threshold over megaripples, U* of ~0.05m/s is required for sediment movement over the shoal. (This value was calculated using a representative Zo of 0.0226m). This would predict a change in the form or slope of the Zo - U* plot at U* = 0.05m/s, as sediment transport would affect both Zo and U* parameters (see above). There is a trend of a lower slope of the curve at U* values above ~0.05m/s (NT+6,+10,+11,+12,ST+2,+3), suggesting that the effect of sediment transport over the megaripples is to change the U* - Zo relationship; possibly variation of Zo is decreased by near-bed concentrations of suspended sediment stabilising the boundary-layer. As the change in slope of the curves is not sufficiently well-defined, and the plotted parameters not independent of other factors influencing their calculated value, it is not possible to comment on the accuracy of the assumed U* threshold value.

Few patterns in the Zo - U* relationship are attributable to changes in megaripple morphology. The high Zo (0.25m) attained during the ebb tide of ST+2 and ST+3 may be related to the development of steep (L/H 15-19) ebb-orientated megaripples; thus, above a U* of 0.04m/s the curve may represent megaripple reversal and growth. During the period of initial current ripple growth, Dyer (1970) found

$$Zo = 0.0017\ U^{*4}\ cm \qquad (4.11)$$

or

$$Zo = 170000\ U^{*4}\ m \qquad (4.12)$$

which was valid for U* <0.05m/s, and which, over the range of values found is equivalent to

$$\log Zo = 1.889 \log U^* + 1.119 \quad m \quad (4.13).$$

Dyer (1970) stated that the gradient of this line (the power of U* in equation 4.11) was consistent from tide to tide. The constant of proportionality changed with tidal range. Few tides measured on Fegla Fach showed periods where there was a linear relationship between log Zo and log U*. Of the velocity profiles measured over megaripple crests, the ebb tides NT+6 and +10 showed such a feature (Figs. 4.21 & 4.22). On NT+6, the trend shown was followed for virtually the whole data set after HW+35mins. Between U* of 0.03 and 0.08m/s, the relationship is approximated by

$$\log Zo = 1.872 \log U^* + 1.103 \quad m \quad (4.14)$$

or

$$Zo = 10.344\ U^{*1.8} \quad m \quad (4.15)$$

For the spring tide NT+10 there were two distinct straight line sections. For U* between 0.05 and 0.07m/

$$\log Zo = 3.778 \log U^* + 3.309 \quad m \quad (4.16)$$

or

$$Zo = 4054\, U^{*4.17} \quad m \quad (4.17)$$

and for U* of 0.07 - 0.117m/s

$$\log Zo = 1.21 \log U^* + 0.278 \quad m \quad (4.18).$$

It is interesting that, with large U*, the power 4 relationship is succeeded by one of a lower power, i.e. shallower gradient. This occurs at a U* of 0.07m/s, where U100 velocities were about 0.5m/s, and depths were decreasing from ~2.6m at HW+135mins to ~1.7 at HW+ 185mins. Values of Shields theta rose from 1.3 to 3.5, then fell back to 1.3 during this period.

Clearly this was a period of high rates of both suspended and bed material transport. For sediment of grain size ~0.00028m, at U* values above 0.04m/s, the approximate suspension threshold is exceeded (Fig. 4.24) and at all U*max values found in this study. The effect of suspended sediment will be to decrease Zo, i.e. it will be systematically underestimated (Dyer, 1986, p.165). However, at U* >0.07m/s, (i.e. Shields theta >~1.11), the effect of a reduced Zo is lessened; if there were a change in slope on the U* v Zo curve, one may expect it to be increased. The fact that the slope actually decreased may indicate reduced form drag. If we interpret the low U* linear section, with its power 4 Zo - U* trend, to be related to ripple height increase (as Dyer, 1980), then the succeeding lower slope section may reflect the destruction of ripples at high U* - combined with a possible lowering of megaripple height. The Zo would then relate only to suspension effects and (reduced) form drag from the megaripples alone.

The bedform phase diagram presented by Allen (1984, his fig 8-23) shows that these conditions of Shields theta (1.3 - 3.6) and grain size (0.00028m) lie across the transition zone between megaripples and upper-stage plane beds (Fig. 4.25). Current ripples are certainly not equilibrium forms under these conditions, and would be rapidly destroyed under such flows. Megaripples, by virtue of their large volume, would not be destroyed in such a short time; the possible morphological effect may be planing off of megaripple crests at peak values of theta. Megaripple heights may be increased again during the later flow deceleration stages, which also reinitiate current ripples.

The flood tide data is interpreted thus :

- neap and intermediate tides have a low Zo early in the flood tide, caused by flow acceleration. Somewhat surprisingly, this is not as well seen on the spring tide;
- there is then a substantial (x10-100) increase in Zo lasting for ~30 minutes at neaps and ~50 minutes at springs. Whilst it would not be unreasonable to relate the neap tide pattern to changes in current ripple morphology, it is highly unlikely that under spring tidal currents it would take 50 minutes to reverse current ripples and cause them to grow. Therefore, effects of megaripple morphological change should also be considered. It is possible that, at spring tides, the roughness length increase is related to the reversal, growth and migration in a flood direction of previously ebb-orientated megaripples. During this period, roughness length rose from 0.0006-0.0152m, where it remained for around 40 minutes, at U* of ~0.054m/s. Spring tides were capable of producing steep megaripples (L/H ~15) which Davies (1980) noted offer the greatest resistance to flow. It is reasonable to suggest also that the spring flood tides produced steep bedforms, which may explain the large roughness lengths towards the mid and late flood tide. Net migration of >0.5m/tide occurred during this tide, suggesting that sediment transport definitely occurred at U* <0.05m/s. Hence, the threshold shear velocity of 0.053m/s calculated for the megarippled sediment is not

Fig. 4.24

Effect of suspended sediment on the stratification of velocity profiles

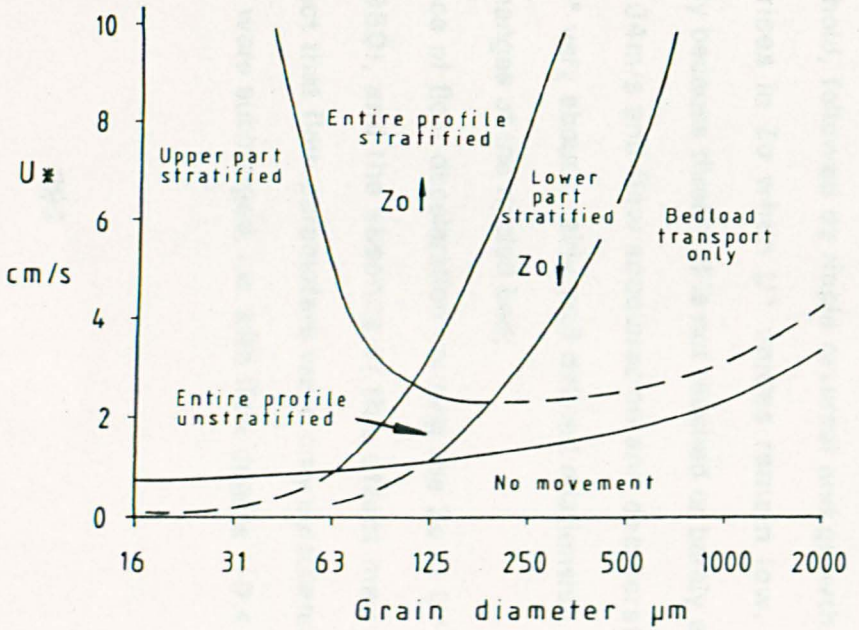

(After Soulsby + Wainwright, 1987)

Fig. 4.25

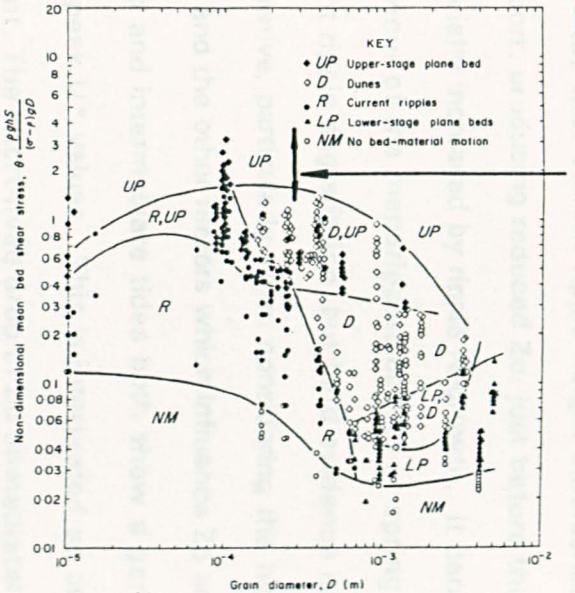

NT+10

Ebb peak flow

Experimental existence fields for aqueous bedforms under equilibrium conditions, shown in the non-dimensional mean bed shear stress (wall-corrected)-grain size plane at 25°C. A total of 595 observations is represented, but many data points (except critical or limiting ones) have been omitted for clarity of presentation. Data as listed for Fig. 8-22 with the addition of the set of Chabert and Chauvin (1963, $D = 9.6 \times 10^{-4}$, 2.48×10^{-4} m). The stress values are wall-corrected (method of G.P. Williams, 1970) and the grain diameters plotted are adjusted to water at 25°C.

After Allen (1984)

necessarily accurate;

- on the spring tide, the subsequent decrease in both Zo and U* is problematic - in terms of megaripple morphology alone. Dyer (1980) speculated that current ripple height diminished at high rates of sediment transport, producing reduced Zo; just before the cessation of transport, Zo was briefly increased by ripple re-growth. It cannot be ruled out that similar behaviour of the megaripples occurs at spring tides, possibly along with current ripple degradation, but hard evidence is absent. This idea remains speculative, particularly when considering the high migration rates on spring tides, and the other factors which influence Zo and U*;
- neap and intermediate tides both show a general Zo increase with time after peak U* values. This is interpreted as due to a slowly decelerating current. The short-lived drop in Zo immediately following the peak U* of 0.04-0.05m/s may be due to effects of sediment transport.

The ebb tide data shows some differences to the flood, and is interpreted thus :

- flow acceleration reduces Zo from high values around HW;
- the brief (10-30 minutes) increase in both Zo and U* may represent the exceeding of threshold, followed by ripple reversal and growth. There are less pronounced rises in Zo when U* values remain low, <0.04m/s (NT+1,+5) possibly because threshold is not reached or barely exceeded;
- where U* is >0.04m/s and flow acceleration and deceleration are not apparent, Zo and U* vary about a fairly well defined relationship, interpreted as morphological changes of the rippled bed;
- there is no evidence of flow deceleration causing the Zo or U* increase as found by Dyer (1980), and the absence of this effect may (in part) be attributed to the fact that flow parameters were only calculated when 3 or more current rotors were submerged, i.e. with flow depths >0.4 - 0.8m.

The effect of underlying megaripple morphology upon the intratidal variation of Zo can be gauged from a comparison of data from adjacent tides of the same direction, which were placed in different groups (Table 4.2, above). There are three of these comparisons which can be made :

1 - Ebb Tide NT+9 (trough) and NT+10 (crest).

The data from NT+9 (Fig. 4.26) produces a cluster of Zo values during mid tide of 0.01-0.03m; this is lower than the crestal data (Fig. 4.22) which has a cluster between 0.015 and 0.04m at U* below 0.06m/s, and at ~0.08-0.1m above it. The expected effect is of increased roughness lengths over troughs (Dyer, 1970). Even when comparing only the data with similar U*, no such effect is discernible. The megaripples surveyed after these ebb tides were of very similar size and shape;

2 - Ebb Tide ST+2 (flank) and ST+3 (crest).

The flank Zo values (Fig. 4.27) are generally lower, and very much more variable than those measured over the crest (Fig. 4.23). Its high variability may be related to greater near-bed flow unsteadiness over bedform flanks (Buckles et al, 1984). However the lower Zo is surprising, considering that Zo may be decreased at megaripple crests, due to a better formed internal boundary layer (Nelson & Smith, 1989). Thus these field measurements are only in partial agreement with flume experiments;

3 - Flood Tide ST+4 (crest[-flank]) and ST+5 (flank).

The crestal data (Fig. 4.18) shows a well ordered Zo and U* rise towards mid tide, in marked contrast to the highly variable nature of both parameters over the megaripple flank (Fig. 4.17). Towards the end of the flood, there were exactly opposite trends shown, with both parameters increasing when measured over the crest, and decreasing over the flank.

Due to the limited nature of comparable data, few solid conclusions can be made. However, some valuable points can be made :

- on ebb tides, there are no easily discernible differences in the relationship

Fig. 4.26 T11 NT+9 Ebb tide

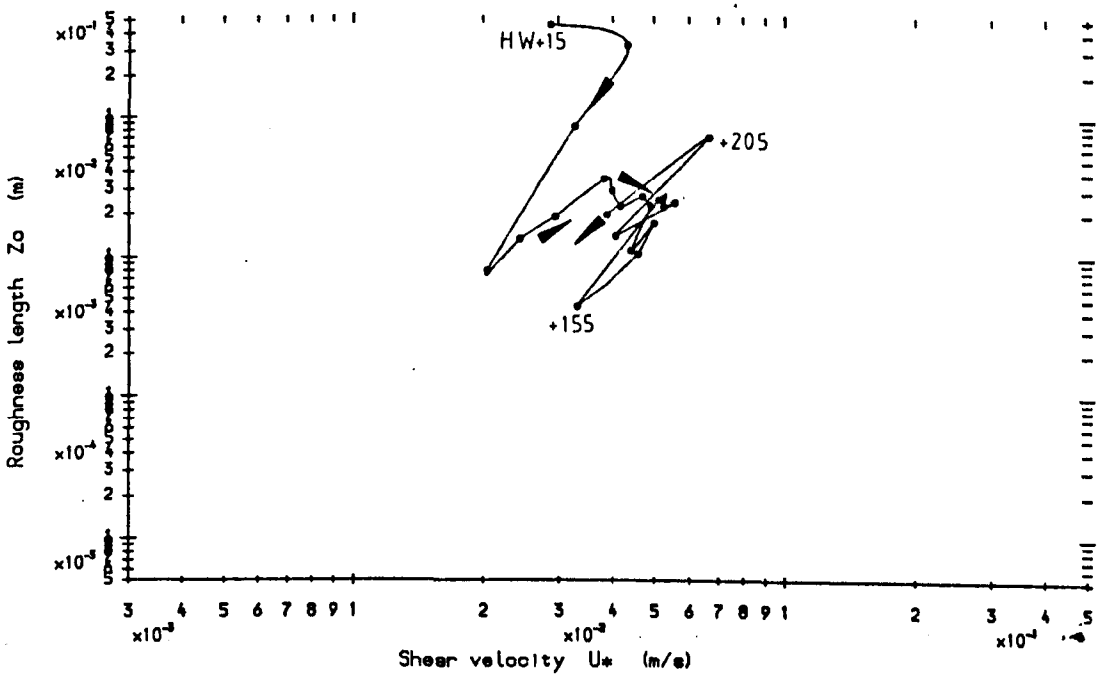

Fig. 4.27 T17 ST+2 Ebb tide

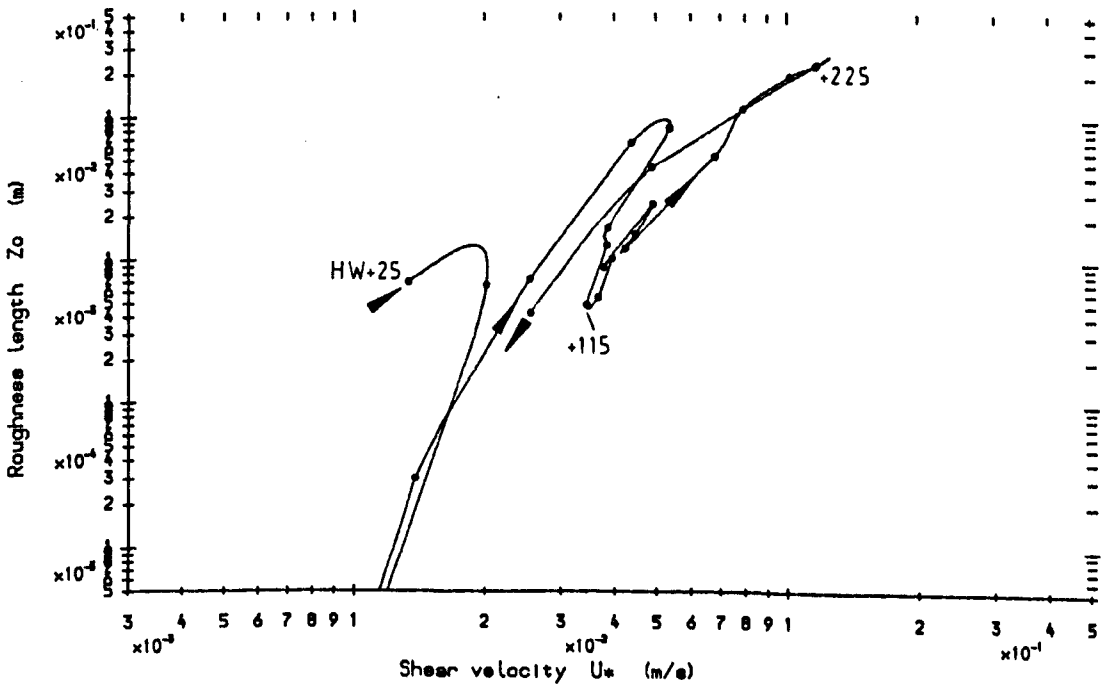

of U* and Zo between velocity data measured over megaripple crests and troughs. The expected increase in roughness length over troughs is not obvious. This agrees with the conclusions from taking Zo values at times of peak U* (Section 4.4.3);

- on both flood and ebb tides, flank Zo values are more variable than those measured above crests;
- on ebb tides flank roughness lengths may be lower than those measured above crests by a factor of < 10.

4.5.3 Conclusions

This study tentatively confirms Dyer's (1980) postulation that the 'approximately constant' roughness lengths on neap tides were found because of limited quantities of sediment transport. During mid tides, when flow parameters were dominant over acceleration or deceleration effects, Zo varied less during tides with lower shear velocities. However, some spring ebb tides also showed little Zo variation.

In general, the full interpretation of Zo v U* curves taken in high shear intertidal environments will not be possible until simultaneous real time observations of megaripple behaviour are taken. However, the intra-tidal observations and interpretations of Dyer (1980) over a rippled bed in the subtidal environment can tentatively be extrapolated to the megarippled intertidal situation of Fegla Fach Shoal, where U* v Zo graphs are interpreted in terms of megaripple morphological changes. This is a promising area for future research, probably combining field and flume observations.

4.6 Spring-Neap Variation of Tidal Flow Parameters

4.6.1 Introduction

Also of interest was to investigate whether there were systematic variations in flow parameters over the lunar spring-neap cycle. Terwindt & Brouwer (1986) presented flow data over intertidal megaripple fields which showed that many parameters did not relate to tidal range. The spring-neap cycle was strongly seen in the peak flood velocity curve, and to a lesser extent in the peak ebb velocity curve. It was hardly apparent in the curve of shear velocity over a 3-D megaripple field, and absent over 2-D megaripples. The diurnal inequality of the tide was well established in the peak flood velocities over 3-D megaripples. Shear velocity did not show such a trend. Tidal dominancy is strong in the peak velocities and Velocity Asymmetry Index (VAI), was present in the curve of shear velocity over 3-D megaripples, but faint over 2-D megaripples. Roughness length was very variable, showing only very general trends of increasing at peak velocities and at spring tides. In contrast, Dyer (1980) found that roughness length was generally higher at neap tides, as did Harvey & Vincent (1977).

In this study, it was not particularly easy to discern trends of various tidal flow parameters over time because of the element of change of the flow measure brought about by the megaripples migrating beneath the V.G.U. (see above), and because with the rotor facing strategy adopted, there was no continuous detailed profiling of either flood or ebb. However, some useful comments on various aspects can be made, and these are discussed below as sections each relating to a particular flow parameter.

4.6.2 Velocity at 1m above the Bed

Peak tidal velocities 1m above bed varied between 0.28 and 1.03m/s. The spring-neap cycle is strongly evident in the flood data, less so in the ebb tide (Fig. 4.28), in common with Terwindt & Brouwer (1986), but unlike their

Fig. 4.28 Variation of U100max over the lunar cycle. (. = flood, x = ebb).

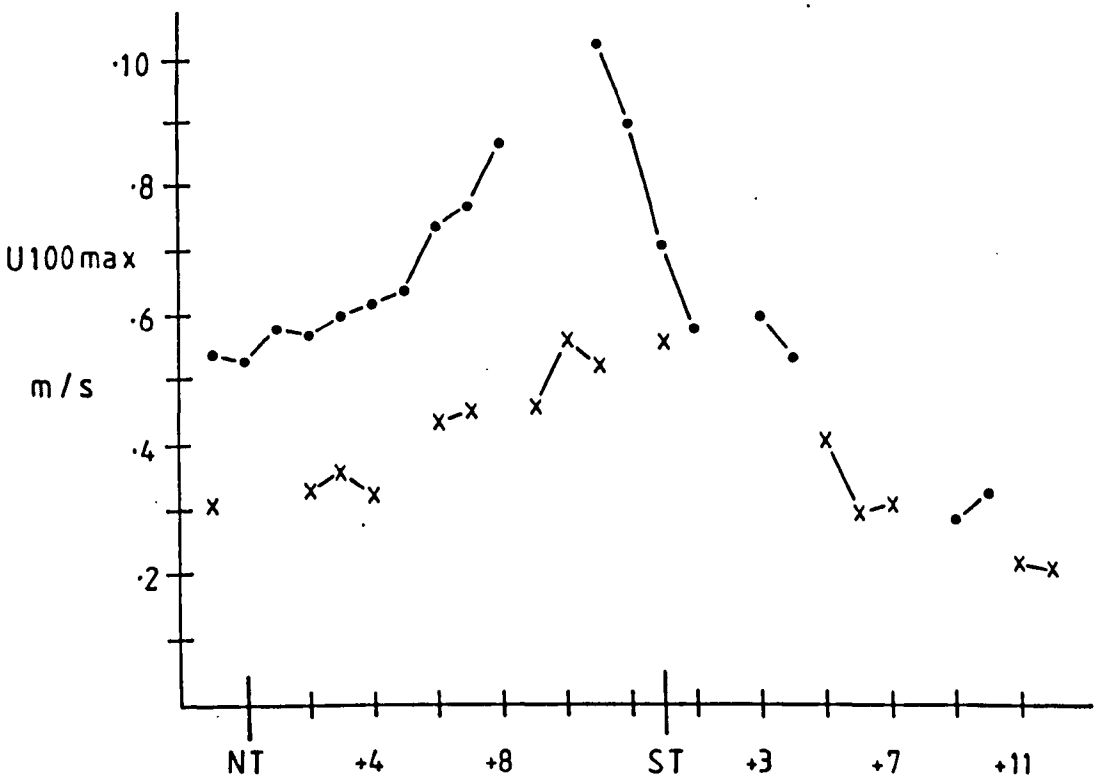

Fig. 4.29 Variation of U100max with maximum flow depth. (. = flood, x = ebb).

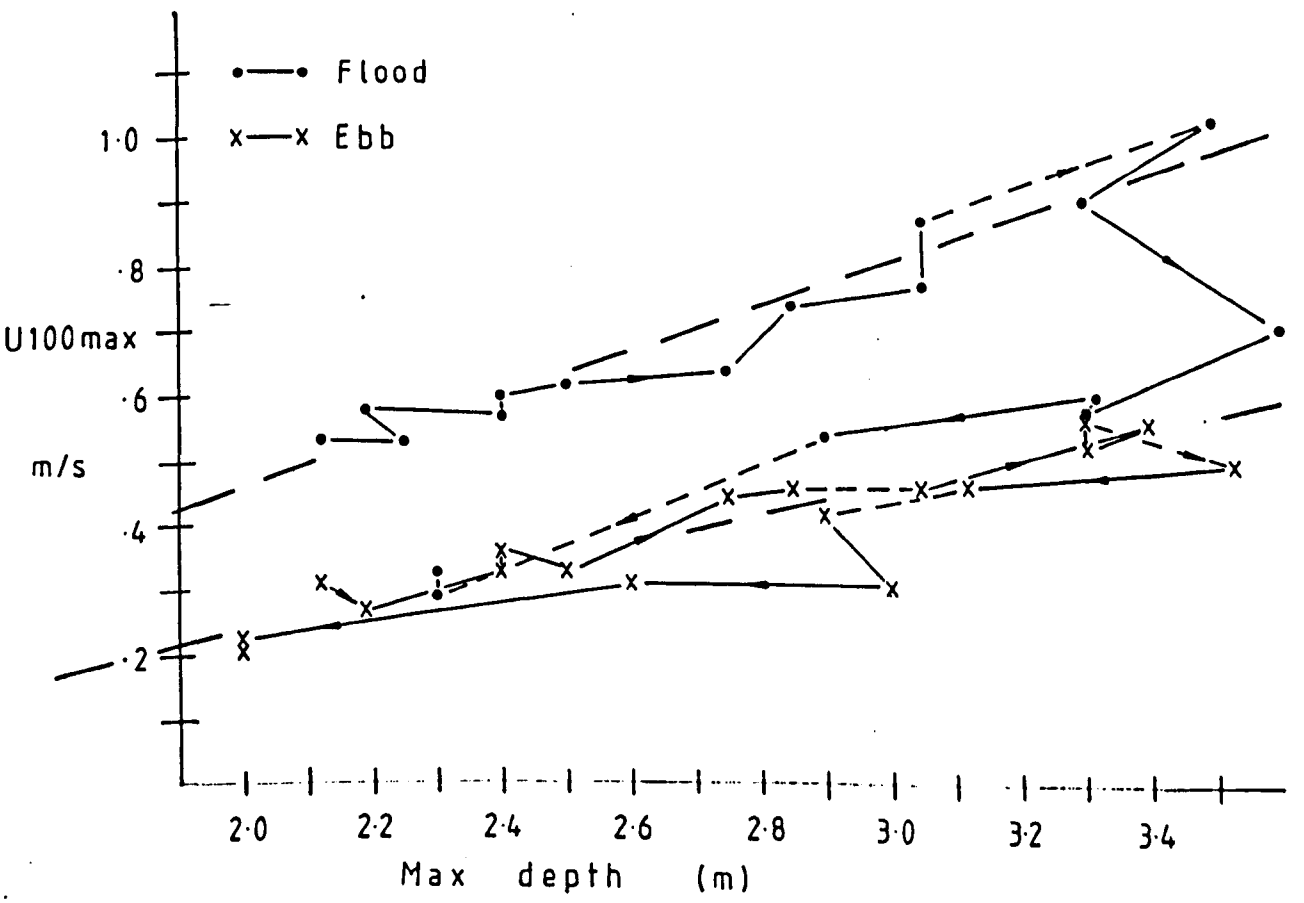

Fig. 4.30 Variation of U*max over the lunar cycle. (. = flood, x = ebb).

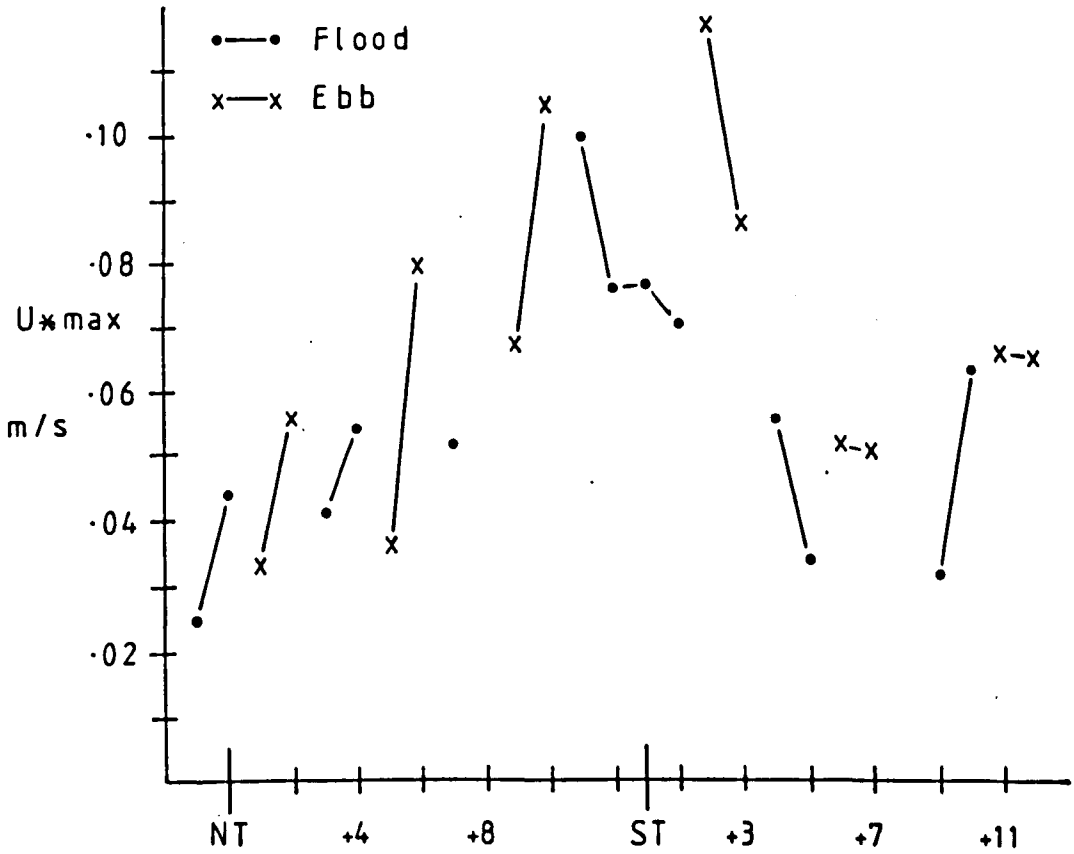

Fig. 4.31 Variation of U*max with maximum flow depth. (. = flood, x = ebb).

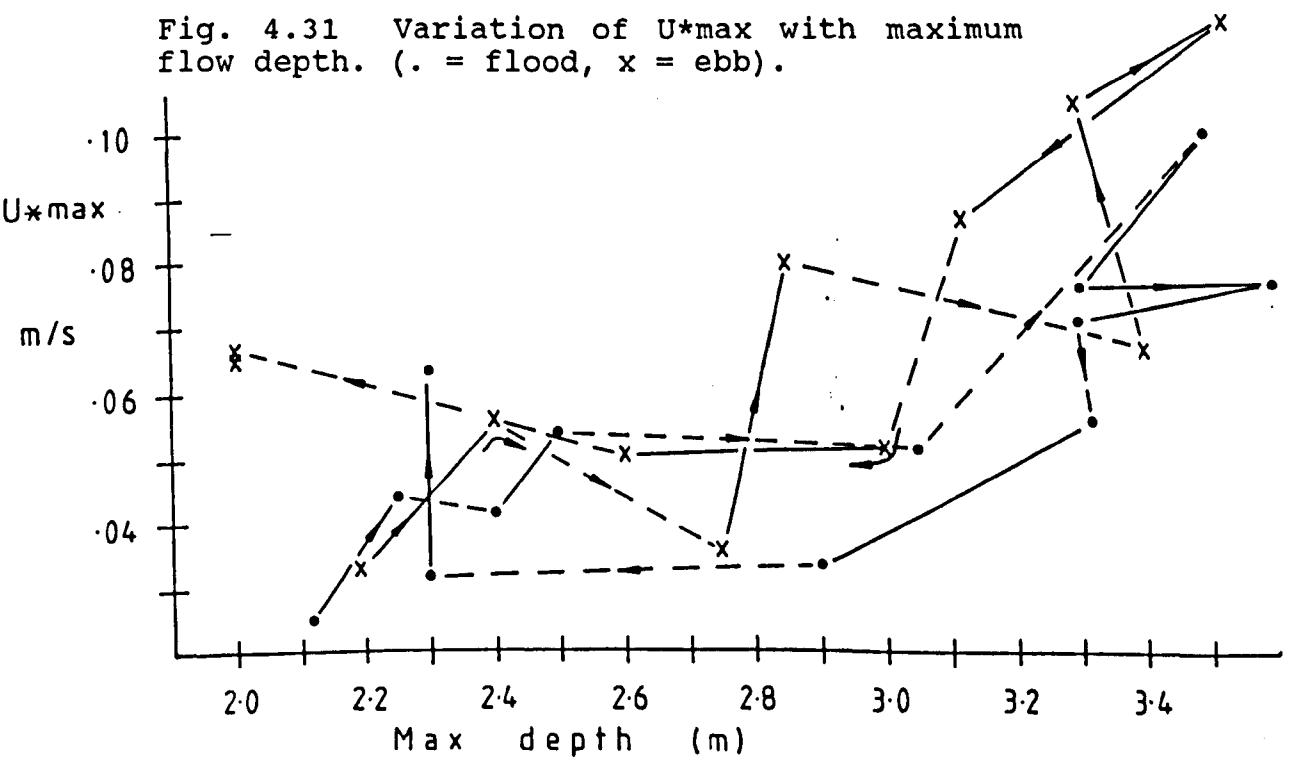

Fig. 4.32 Variation of U100*max with tidal range. (. = flood, x = ebb).

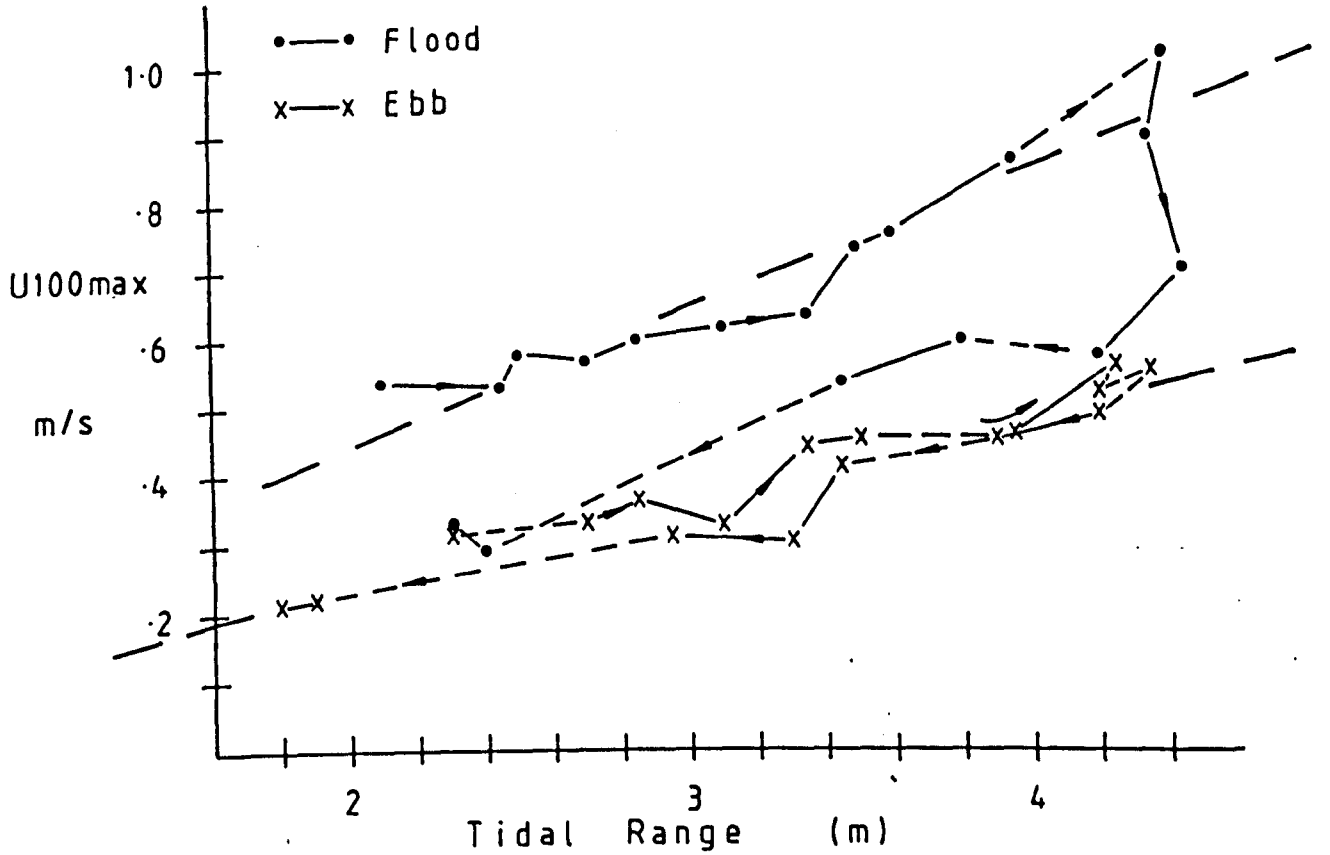

Fig. 4.33 Variation of U*max with tidal range. (. = flood, x = ebb).

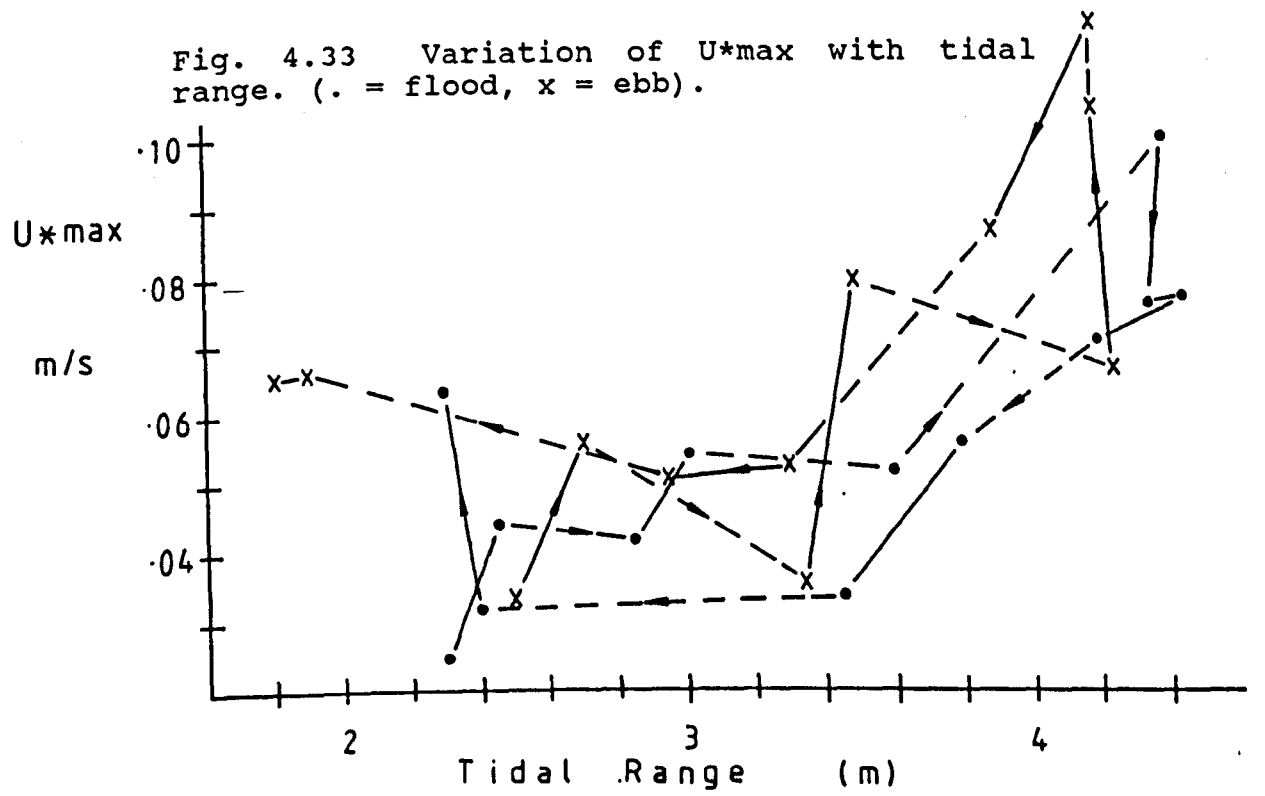

data, the diurnal variation is absent from both flood and ebb measurements. This is possibly due to the variation in the data, caused by the measurement position varying with respect to the underlying megaripples. However, the dominancy of the flood tide is well shown, with variation in the Velocity Asymmetry Index (V.A.I.) of between 1.2 and 2.2, where

V.A.I. = U100maxfl / U100maxebb (4.19)

(modified after Terwindt & Brouwer, 1986). Thus, in all cases the flood U100max exceeded that of the ebb. There is no discernible effect on the data caused by the underlying bedform morphology.

There are strong relationships of U100max with both predicted tidal range (Fig. 4.32) and maximum depth (Fig. 4.29). For the ebb tide, the relationship with predicted tidal range R may be approximated by

U100maxebb = 0.123 R m/s (4.20)

and with maximum depth MD by

U100maxebb = 0.223 MD - 0.21 m/s (4.21).

The flood tides results show considerable hysteresis. Velocities on rising tidal ranges are ~0.2m/s higher than those on falling tides. The relationships with R and M on rising tides are

U100maxfl = 0.206 R + 0.03 m/s (4.22)

U100maxfl = 0.35 MD - 0.24 m/s (4.23).

On falling tides, the flood values are closer to the ebb velocities.

The strong hysteresis shown by U100maxfl suggests that the faint hysteresis of U*maxfl is indeed real. The reason why the flood tide should display such a trend in velocity is unclear, but it may be related to a

particular combination of tidal components during the study period, resulting in shorter, faster rising tides prior to springs.

4.6.3 Shear Velocity

Peak tidal shear velocity (U*max) varied between 0.025 and 0.117m/s. Fig. 4.30 shows that the spring- neap cycle is apparent in the measured U* curve. The data did not provide continuous measures of either flood or ebb U*max, so it is not possible to study its detailed tide-tide variation. However, when plotting U*max against a measure of position in the lunar cycle, such as predicted tidal range or maximum depth over the shoal, some patterns emerge. Both Figs. 4.33 and 4.31 show similar trends, with a large spread in U*max at all times.

The final two U*maxebb values, of over 0.06m/s, occurred at neap tides during a period of high freshwater runoff, and may have been raised by the increased ebb discharge. However, the U100max data (Fig. 4.28) does not show this apparent anomaly. It is suggested that the high U*max values were due to flow stratification. A fast, seaward flowing, surface freshwater layer overlying relatively low, more saline water would cause both both U* and Zo to be overestimated. Reference to the roughness lengths of the tides involved (0.49 and 0.28m) and the 1 minute average velocity data tends to support this contention. No salinity profile data was taken, but on ebb tides and with high runoff the lower estuary may be strongly stratified (Chapter 2).

The flood tide peak U* values lie in a field broadly matching the ebb data, but towards spring tide U*maxfl is apparently lower than equivalent ebb values. At spring tides, there is no systematic bias in terms of measurements taken over different parts of a megaripple, but the few available data points preclude the definite identification and quantification of this feature. Also weakly displayed is a clockwise hysteresis of U*maxfl.

Diurnal variation is strongly evident in the shear velocity data, in marked contrast with the findings of Terwindt & Brouwer (1986) over 2-D and 3-D megaripples. The change in peak shear velocity of consecutive flood or ebb

tides in all cases, except one, matches the expected direction of change from both tidal height predictions and maximum water depth over the shoal. The exception is the ebb data of NT+9 and NT+10, which produced a difference of greater than +0.035m/s with predicted differences of HW and maximum depth respectively of -0.05m and -0.1m. These water height differences are very small, and it is considered that any effect would have been overcome by the fact that ebb tide NT+9 was measured over a megaripple trough whereas NT+10 referred to conditions in the crestal zone. This study and others (eg. Dyer, 1970) have shown roughness lengths are likely to be higher measured over troughs, which would mean U*max would be increased. As explained above, it was not possible in this study to directly demonstrate this effect.

4.6.4 Roughness Length

The variation of Zo (a 10 minute average) is shown in Fig. 4.13 (~page 358). In common with Terwindt & Brouwer (1986), the variation of roughness length (at the time of peak shear velocity) is seen to be virtually random over a lunar cycle. Although the plotted roughness lengths include varying effects of form drag from the underlying migrating megaripples, no general relationship with tidal range is shown. However, the Zo values found in this study compare well with those found in similar megarippled environments (Table 4.4).

Fig. 4.36 shows the relationship of Zo to U100 on the shoal (i.e. using U100 as a measure of tidal conditions). For the complete data set, a negative relationship is seen, i.e. roughness lengths tended to be lowest when U100max was high. However, when taken as separate flood and ebb data (as demanded by their consistent difference), the apparent relationship disappears. Flood U100 velocities are generally greater than ebb ones, and as flow conditions (eg. depth, relative bedform orientation) are systematically different between flood and ebb tides, any general difference in Zo between

the two will tend to suggest an overall relationship between Zo and U100. The apparent overall relationship is probably spurious.

Table 4.4

Roughness Lengths over Megaripples (m)

		Roughness length Zo (m) mean	median
Black & Healy 1986			
Flow measured 0.5-9m above bed			
Site S1 -			
Grain size 300um, mean depth 9.3m			
Bedform ht 0.17m, wvl 7.5m		0.0025	0.0005
Site S4 -			
Grain size 320um, mean depth 3.4m			
Bedform ht 0.15m, wvl 4.6m		0.0044	0.0016
Terwindt & Brouwer 1986			
Flow measured 0-1.5m above bed			
2-D megaripples -			
Grain size 200um			
Bed elevation 0.4m above MSL			
Bedform ht 0.14-0.2m, wvl 6m	Flood	0.0072	
	Ebb	0.0486	
3-D megaripples -			
Grain size 230um			
Bed elevation 0.7m below MSL			
Bedform ht 0.2-0.4m, wvl 6m	Flood	0.0193	
	Ebb	0.6908	
Larcombe 1986			
Flow measured 0-2m above bed			
Bed elevation ~MSL			
Bedform ht 0.13, wvl 3.7m	Flood	~0.013	
Larcombe, this study			
Flow measured 0-2m above bed			
Bed elevation ~MSL			
Bedform ht 0.2m, wvl 3-6m	Flood	0.023	
	Ebb	0.148	

An inherent concept in some equations is that flow roughness is directly related to the morphology of the underlying bedform, for example the equations of Lettau (1969), Wooding et al (1973), Yalin (1977). Three-dimensional bedforms cause greater roughness lengths than 2-D forms. Although qualitatively not unreasonable, the predicted roughness lengths

(Fig. 4.13) demonstrate the wide gap between the predictions from the inevitably over-simplified theory and the immensely complex field situation in a study such as this. Figs. 4.34 and 4.35 show plots of Zo, against mean megaripple height and flatness. There is no systematic relationship of Zo with height, although the 7 data points interpreted as being from 'near equilibrium' megaripples (circled data points; based on a combination of the morphological parameters discussed in Chapter 3, including deep troughs, peak heights and high correlation coefficients) suggest a very weak trend of increased Zo with increased height (dashed line). This would agree with theoretical considerations. Roughness lengths of flood and ebb tides both show well-developed (and broadly parallel) negative trends with flatness, also in agreement with theory, and demonstrating conclusively that the measured velocity profiles were affected to different degrees by different megaripple morphologies.

Davies (1980) has shown that the resistance to flow caused by bedforms (i.e. form drag) is largest when bedform flatness is 10-15. The relationship of Zo with mean megaripple flatness (L/h) found here is consistent with this, with a weak increase in Zo with steeper megaripples shown by the whole data set, but a clearer trend shown by points representing 'near- equilibrium' megaripples. This trend can be compared with the predicted Zo using the Wooding et al (1973) equation (eqn. 4.10). From Figs. 4.34 and 4.35, for a known Zo, the corresponding 'equilibrium' megaripple height h and flatness L/h can be found by using the approximate relationships represented by the dashed lines. When put into the Wooding equation, these parameters give predicted roughness lengths 5-10 times smaller than those derived from Figs. 4.34 and 4.35, demonstrated below.

Zo(m)	h(m)	L/h	Zo(m)	Zo difference
	------->		------>	
0.14	0.285m	14	0.014	x10
0.012	0.175	32	0.0027	x5
via Figs. 4.34, 4.35		via Wooding eqn.		

Fig. 4.34 Roughness length plotted against mean megaripple height. C = flow measured at megaripple crest, F = at megaripple flank, T = at megaripple trough. Capitals denote flood tide, lower case denote ebb tide.

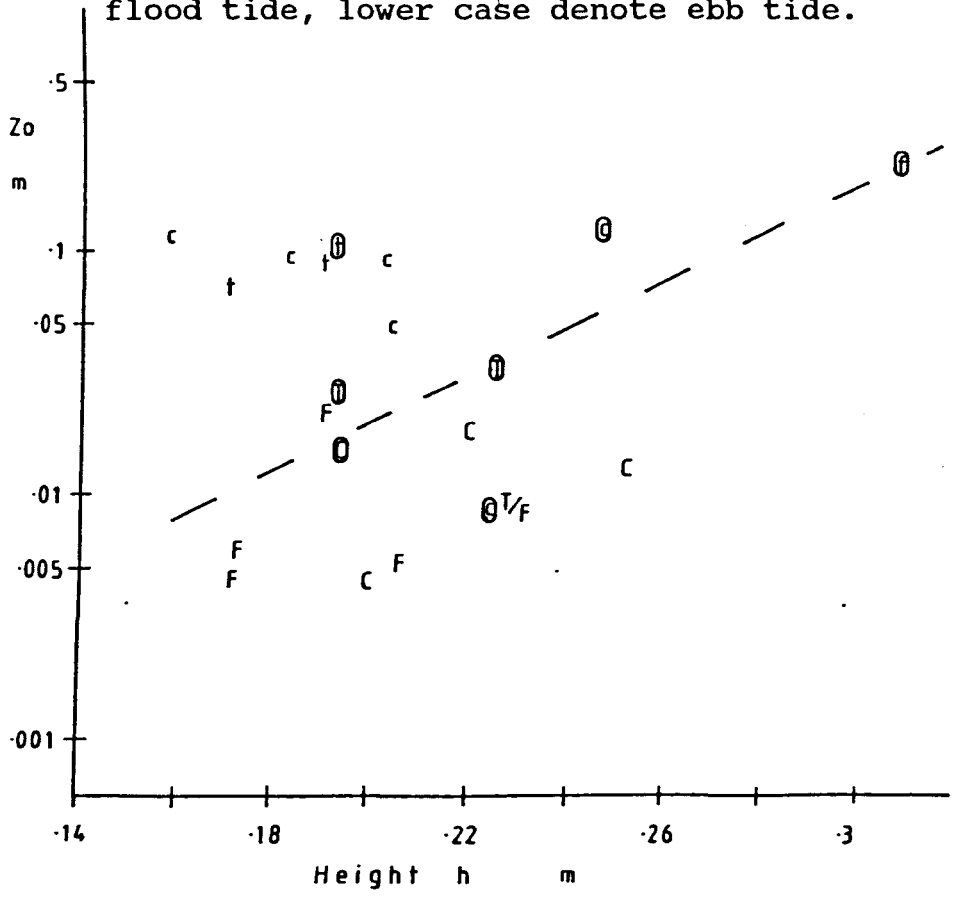

Fig. 4.35 Roughness length plotted against mean megaripple flatness. C = flow measured at megaripple crest, F = at megaripple flank, T = at megaripple trough. Capitals denote flood tide, lower case denote ebb tide.

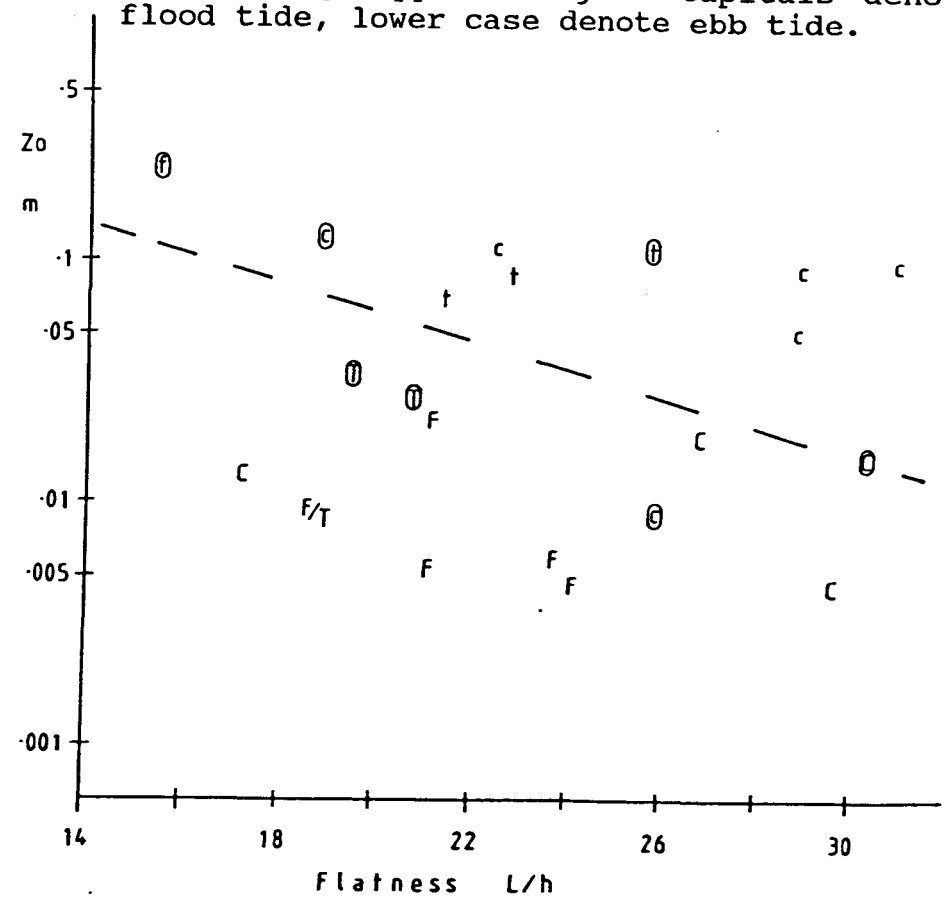

Fig. 4.36 Roughness length v U100max. C = flow measured at megaripple crest, F = at megaripple flank, T = at megaripple trough. Capitals denote flood tide, lower case denote ebb tide.

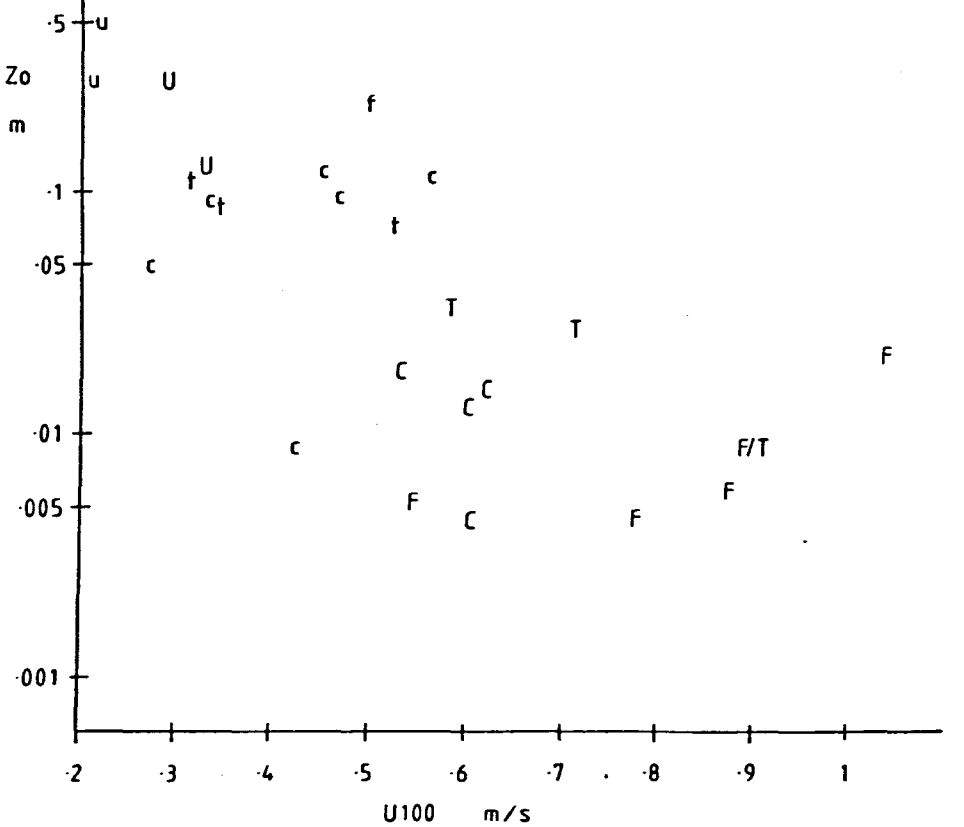

This predictive capability is similar to that of Smith & McLean (1977a,b) above. For the flow conditions measured over Fegla Fach megaripple shoal roughness lengths are underestimated by up to an order of magnitude by Yalin's (1977) equation, which is based purely on bedform morphology; also by the formula of Smith & McLean (1977a,b), which takes account of the modifying effect of suspended sediment on Zo. This is despite the effects of the accelerating internal boundary layer (Nelson & Smith, 1989), which would cause decreased roughness lengths. This layer extends up to one bedform height in thickness, in the crestal zone of the bedform i.e. between 0.16m and 0.31m over the lunar cycle. Hence, the basal rotor (occasionally the lower two rotors) was theoretically within this layer, during the majority of the measured tides.

4.7 Summary and Conclusions

A total of 481 ten-minute average velocity profiles, measured over a lunar cycle at the intertidal megaripple shoal at Fegla Fach have been analysed. 81% of flood profiles fitted a logarithmic form with a correlation coefficient CC >0.95, and 25.5% with a CC >0.99. Of ebb profiles, 75.3% had CC >0.95 and 15.3% fitted with a CC >0.99. It was therefore justified to use the shear velocity U* and roughness length Zo to describe the profiles.

Flood tides attain a maximum of 0.53m/s at 1m above bed (U100) at neaps, rising to 0.71m/s at spring tides. Shear velocities reach 0.041m/s at neap tides, and 0.077m/s at springs. Maximum flood tide U100 velocities are reached early in the flood tide, between HW-105 and HW-125mins, and rapidly decline towards HW.

Ebb tides attain 0.33m/s at neap tides, and 0.49m/s on spring tides. Shear velocities peak at 0.056m/s and 0.117m/s respectively. The ebb tide U100 velocities tend to increase with time, maintaining near-peak values for up to >80mins on spring tides.

Peak flood tidal shear velocities show a weak clockwise hysteresis effect when plotted against tidal range or maximum depth, but both flood and ebb U*max display considerable scatter. Ebb values may be increased by flow stratification at time of high freshwater runoff.

Flow roughness lengths on flood tides vary up to 0.014m on neap tides, and up to 0.13m on spring tides. The respective ebb tide values are 0.56m and 0.24m. Generally, roughness lengths on the flood tide are 10- 100 times greater than on the ebb. The spring - neap cycle is absent from the Zo curve.

The spring - neap cycle is strongly evident in the U100max data, and is seen in the U*max data also. Diurnal variation is absent in the U100max curve, but present in the variation of U*max. Flood tidal dominancy is well shown, with a Velocity Asymmetry Index of 1.2 - 2.2.

The underlying megaripples have a large effect upon the calculated velocity profile parameters. Flood tide roughness lengths measured over megaripple troughs are nearly twice those measured over flanks or crests; however, the ebb tide does not show such a difference. Intra-tidal variation of Zo above megaripple flanks is greater than above crests; this is probably related to flow unsteadiness in the zone of flow reattachment.

These brief considerations confirm the expected conclusion; that Zo is not a useful parameter in palaeoflow construction from deposits of similar environments to the Fegla Fach shoal. Roughness length does not scale to megaripple size on a basis sufficient to allow a useful conversion from a known bedform size to a palaeohydraulic parameter.

Predicted roughness lengths for the flows over the megaripples, calculated by the formulae of Wooding et al (1973) and Smith & McLean (1977a,b) systematically underestimate the measured roughness lengths at times of peak U* values, by up to a factor of 10. This is despite the effect of the internal boundary layer developed over the bedforms, which should decrease measured Zo values (Nelson & Smith 1989). A probable factor is inaccuracy of the method of Black & Healy (1986), in predicting threshold shear velocity over a megarippled bed.

The conclusion of Dyer (1980), that roughness lengths are relatively invariable when sediment transport is limited, is only partially confirmed, as some spring tides also showed this tendency.

The relationship of Zo to U*, within a tidal flow, over an intertidal megarippled bed, is more complex than as found by Dyer (1980) over a rippled sub-tidal bed. There appears a similar trend, regardless of tidal range; this is related to flow acceleration or deceleration effects, and the modification of ripples and megaripples as the flow condition pass through different bedform stability fields :

- For the ebb tides of NT+6 and NT+10, Zo is proportional to U* to the power 1.8 and 4.2 respectively, probably related to the development of current ripples;
- It is suggested that when flow conditions approach the upper limit of the stability field for megaripples, Zo becomes proportional to a lower power of U*; this is related to the disappearance of current ripples and incipient formation of upper-stage plane beds on megaripple crests. Further research is needed on this matter.

The estimated 20% underestimate of true bed shear stress, and resultant overestimate of roughness length, due to the accelerating nature of the growing internal boundary layer (Nelson & Smith, 1989), is unresolvable in this study.

The relationships of tidal range and maximum depth to U100max for ebb currents at Fegla Fach shoal are :

$U100maxebb = 0.123\ R$ m/s

and

$\bar{U}100maxebb = 0.223\ MD - 0.24$ m/s.

Flood velocities show hysteresis, with velocities ~0.2m/s higher on equivalent ranges and depths before spring tides. On rising tides the relationships are :

$U100maxflood = 0.206\ R + 0.03$ m/s

and

$U100maxflood = 0.35\ MD - 0.24$ m/s.

Chapter 5

Grain Size Investigations - The Fall Tower

5.1 Introduction

There are many different ways of defining grain size, and many ways of measuring it. Therefore, before description and interpretation of the grain size distributions of the surficial sediments of the area, it is necessary to first describe the method of grain size measurement (in this case, a grain settling method), and to define the factors which constrain the accuracy and representative nature of the results obtained.

Therefore, this chapter contains, firstly, a detailed appraisal of various factors which influence the usefulness of the grain settling method; secondly, there is a description of the empirical conversion process, from settling velocity to grain size, and an assessment of the repeatibility of the system. Finally, the framework used to describe and compare grain size distributions, is introduced. The reasons for analysis of sediment size, mode of sampling, and results are discussed in the next chapter, Chapter 6.

The study of the grain size of transported and deposited sediments has been a major feature in many geological studies of modern sedimentary systems in a range of environments, including aeolian, alluvial, estuarine, shelf, slope and deep ocean basin. For cohesionless sediments, much information on the hydrodynamics of the environment of deposition may be obtained from a study of grain size and the proportions of grains in different size fractions (Dyer, 1986); this uses the general concept that, when subject to a fluid shear stress, finer particles are more mobile than coarser ones. Hence, grain size may reflect in some way the level of the forces causing movement. Whilst such a simple concept is useful, it cannot be used without a consideration of other factors involved in the control of grain size

distributions.

The pattern of variation in grain size parameters is used to aid interpretation of the geological record; in particular, to determine the environment of deposition of sedimentary rocks. This is of great significance to geologists, and to mining or hydrocarbon industries seeking exploitable deposits or reservoirs.

5.2 Grain Size - Definitions

The size of real sediment particles is difficult to define, but is usually expressed as a length term. Only exact spheres have a known size, as their diameter is the same in all orientations - making the sphere useful as an 'ideal' particle (Allen, 1984). Real sedimentary particles are rarely spherical; most derived from rock weathering can be considered triaxial ellipsoids with a long, median and short diameters. However, many grains (particularly fragmented bioclastic debris) present grave problems in particle size analysis because of their shapes (Leeder, 1982); they cannot be rationally compared to particle sizes of more ellipsoidal grains. Allen (1984b,c) has studied the hydrodynamic properties of various biogenic particles, particularly whole shells, in an attempt to relate their behaviour to those of terrestrial origin. Nash (1987, and in prep.) has studied the settling velocity and transport threshold of shell fragments using a laboratory flume.

In practice, the measurement of grain sizes means one of three things (Allen, 1984) :

1 - The length of either the short, intermediate or long grain diameter, or a mean of any two or all of these. The standard process of sieving dry sediment samples to obtain 'sieve diameters' (Leeder, 1982) is routinely taken to sort particles depending on their intermediate particle diameter. However, there are two basic problems with sieve data (Kennedy, Meloy & Durney, 1985). Firstly, sieve dimensions may not be perfect when manufactured nor consistent with time. Secondly, and more importantly, the probability of passage of a grain through any sieve is a function of grain shape as well as size (Ludwick & Henderson, 1968).

These lengths may be measured by optical means, such as by measuring many individual grain diameters on a universal stage - either down a microscope or projected onto a large screen or TV monitor. This is a very slow measurement method, and when measuring grain size from thin sections of sedimentary rocks requires corrections to allow comparison with

sieved samples (see Folk, 1974; Harrel & Eriksson, 1979);

2 - The diameter of the sphere having the same volume, i.e. the 'volume diameter' of Leeder (1982);

3 - The diameter of the sphere of the same density having the same fall velocity as the grain in question in a given fluid, the 'free-fall diameter' of Leeder (1982), or 'equivalent fall diameter'. The method involved is the measurement of settling duration of particles through a known distance in a fluid; these are subsequently converted to settling velocities and then, through an empirical calibration, to sphere diameter.

In this study, the third definition of grain size is used but with a significant amendment. Shape and surface roughness are major controlling factors upon the fall velocity of particles (see below), so that natural sand grains and spheres of the same 'equivalent fall diameter' have different sizes measured through sieves. By conversion of fall velocities to a grain size through an empirical relationship based upon natural sand samples, rather than spheres, this study aimed to reduce to a minimum those errors in the conversion process related to grain shape and roughness effects. The fall velocity - size relationship used is based upon sieved natural sand samples, so the technique produced, via a grain settling method, distributions of 'sieve diameters'.

These diameters are discussed, compared and named using the Udden-Wentworth scale, in which the various grades are separated by factors of two. This scale adapts easily to the phi logarithmic transformation,

$$\phi = - \log_2 (d/do) \qquad (5.1)$$

where grain size d is measured in mm, and do is the 'standard' grain diameter of 1mm.

5.3 The Grain Settling Method : The Fall Tower

A fall tower (or settling tube, or sedimentation column) is a device to measure the distribution of settling velocity of particles in a bulk sample. When a sample of grains are introduced at the top of the tower, the grains rapidly become vertically sorted in the fluid column (usually water) according to their terminal fall velocity. The most common way to measure the fall velocity is to allow the particles to accumulate on a pan at the base of the fall tower, and continuously measure pan weight with time (eg Gibbs, 1972; Rigler at al, 1981; Slot & Geldof, 1986); thus, the frequency distribution obtained is one of particle weight faster (coarser) than a given velocity (size).

5.3.1 Apparatus

The fall tower at the School of Ocean Sciences, U.C.N.W., Menai Bridge, comprises four main parts :

1 - The water-filled tube itself.

The plastic tube has an inner diameter of 28.5cm and a length of 2m;

2 - A sample introduction mechanism.

This comprises a shallow conical opening 9cm in diameter with a large plug in the centre. The sample is evenly distributed in the water around the plug, and is wetted by a few drops of detergent solution. Sampling is begun by pulling a lever which raises the plug allowing the sediment to begin falling through the water. The lever simultaneously activates a microswitch to set the timing system to zero and begin the recording sequence. The distance between the sample hopper (at water level) and the balance pan, i.e. the fall distance, is 1.87m. Each sample weighed between 2.5g and 5g dry weight;

3 - A digital electronic balance.

The balance (Oertling model no. HB63) is housed above the tube, and the balance pan is suspended at the base of the tube by three nylon threads, each connected by a low strength spring via a frame to the under-side of the balance. The springs act as a damper on vibrations from the threads

affecting the balance reading;

4 - An accompanying microcomputer.

The time-weight data is recorded and simultaneously displayed by a Commodore 4032-32N microcomputer, using the program 'RECORD'. Details of the sample identifiers and the recorded data are placed onto floppy disc, and may be later processed on the same microcomputer or transferred onto the U.C.N.W. VAX mainframe. In this study all data was transferred onto the VAX where advantage could be taken of the greater storage space, computational speed, software and hardware facilities.

5.4 Previous Work on Grain Settling

The fall velocity of a sand grain is a function of its volume, density, sphericity and roundness. Hence, in order to relate 'grain size' to hydrodynamic and depositional environments, fall velocity may be a more meaningful parameter than other dimensional parameters (Reed, Le Fever & Moir, 1975; Taira & Scholle, 1974). To allow hydrodynamic interpretation, it is standard practice to convert the fall velocities to a 'grain size' distribution, although (Reed et al, 1975) consider that fall velocity distributions are themselves profitably analysed as a measure of size.

There have been many studies which attempt to relate settling properties of grains to a measure of its physical size. One extreme of simplicity is the relationship of Migniot (1977),

$$w = 125d \qquad (5.2)$$

in c.g.s. units, for quartz sands of diameter d between 0.02 and 0.1cm, and water at room temperature, where w is the fall velocity.

Hallermeier (1981) used 115 published measured terminal fall velocities of commonly occurring sands, to develop three equations relating a Reynolds number to a combination of solid and fluid properties called the Archimedes Buoyancy Index.

Gibbs, Matthews & Link (1971) presented empirical equations for the fall velocities of spheres in water, which have been modified by Komar (1981) for use in conditions other than quartz grains in water, grain densities ranging from foram shells (density 1.50) to magnetite (5.20). Baba & Komar (1981b) conducted experiments with natural quartz sand grains which showed that the measured fall velocity w could be converted to the settling velocity of a sphere ws using

$$w = 0.977\ ws^{0.913} \qquad (5.3)$$

and grain diameters were then obtained by using the equation of Gibbs et al (1971). These calculated diameters compare very well with sieve values adjusted for the fact that grains may pass diagonally through a square mesh sieve using

$$Db = 1.32\ Ds \qquad (5.4)$$

where Db is the mean intermediate grain diameter, and Ds is the sieve aperture size (Komar & Cui, 1984).

Slot (1984) also provided a formula for terminal grain fall velocity in terms of grain size.

5.5 Factors Other Than Size Which Control Grain Settling

When a particle is released into a fluid, six forces act upon it (Allen, 1984) :

1 Gravitational acceleration;

2 the resultant pressure;

3 fluid drag;

4 the inertia of the mass of fluid travelling with the particle;

5 the force due to the history of grain motion;

6 the particle immersed weight.

Grains first accelerate, but attain their terminal fall velocity within only a few grain diameters. The magnitude of the individual grain fall velocity is determined by a number of factors, grain size, density, shape and surface texture, and by fluid viscosity and turbulence intensity (Yalin, 1972; Raudkivi, 1976; Cliff, Grace & Weber, 1978).

5.5.1 Concentration

In this study, there are additional factors to those mentioned above, due to use of a bulk sample. These are the effects of grain-grain interactions, both in terms of grains being slowed (in the turbulence produced by other grains falling through the water column), and the high total mass of fluid entrained by the particles. This is a high factor immediately after sample release into the water, where the high concentration of grains may result in a density current or settling convection effect before each grain attains its terminal velocity (Kranenburg & Geldof, 1974).

Hulsey (1961) showed that fall velocities for a concentrated dispersion of grains can be up to 20% higher than for single particles, because of density current effects. However, the nature and effects of concentration effects upon measured settling velocity distributions is system-dependent, for

example, a long fall tower of large internal diameter will have relatively fewer concentration effects than a short small-bore tower. Also the nature of sample introduction at the top of the water column will affect concentration effects; the greater the initial spread of grains the smaller the initial settling convection effects.

Hulsey (1961) further showed that the velocity of a given particle falling as part of a sample apparently depends on the size limits and sorting of the sample. He concluded that settling methods could not give an accurate picture of size distribution, if grain settling creates fluid turbulence. However, he did recognise that the 2.2cm internal diameter of his settling tube was unsatisfactory, and that large tubes which allow grains to fall independently have considerable merits compared to his system. Large-bore tubes also reduce relative wall effects (see below), which may slow grain settling near the tube wall (Happel & Brenner, 1965).

5.5.2 Sample Weight

Hulsey (1961) concluded that sample size was a factor in determining fall velocity. With increasing sample weight, the faster-falling larger grains at the leading boundary of the sample fall faster, and the slower smaller grains at the trailing boundary fall slower. (He did not explain this effect). Thus, larger sample sizes affected fall velocity distributions by increasing the proportion of grains in both tails of the distribution, increasing the standard deviation. In his experiments, sample weight would have had to have been below 0.25g for the grains to settle with velocities independent of sample weight (his Fig. 6). In terms of the ratio of sample weight to the cross-sectional area of the fall tower, the 2-4g sample weight used in this study gives a ratio 12-25 times less than Hulsey, thus is well within a weight where grain-grain effects are likely to affect measured fall velocities.

Slot & Geldof (1986) state that sample weight used in an analysis is a compromise between the errors due to grain concentration effects, and the

signal to noise ratio, which depends on balance resolution. The resolution of the Oertling balance used is 0.01g, so the largest individual quartz grains (2mm sieve diameter) which weigh up to 0.013g underwater (calculated for a 2mm cube), are just capable of registering on the balance. Use of the School of Ocean Sciences fall tower, in many studies over a period of years, has shown that by taking suitable precautions whilst sampling, the noise level in the recorded data is negligible. This includes ensuring that all windows and doors in the laboratory are closed prior to and during sampling, and the computer program which records the time-weight data only allows sampling to begin if the balance has been registering zero weight constantly for 30 seconds.

For different grain sizes, Slot & Geldof (1986) measured errors due to concentration effects at different sample weights. From this, they calculated the range of sample weight which is both below maximum acceptable errors and above minimum acceptable signal to noise ratios. A grain size of 200-400um and sample weight of 2-4g produced errors due to concentration effects of <1-5%, added to which are systematic errors of 2% due to delay time between particle impact and balance movement. Rigler et al (1981) used samples usually 4-5g in weight in their tower of 19cm internal diameter. In all cases in this study, sample weights were 2-4g.

5.5.3 Grain Shape - Sphericity and Roundness

The settling of smooth spherical grains is well understood, empirically if not fundamentally (Komar & Reimers, 1978). Allen (1984) gives a review of theoretical and empirical work on the settling of spheres. Stokes (1851) theoretically deduced a relationship between fall velocity and sphere size (known as Stokes Law) ;

$$w = gD (ps - p) / 18 n \qquad (5.5)$$

where w = fall velocity, D = particle diameter, ps = particle density, p = fluid density, g = gravitational acceleration, n = fluid dynamic viscosity.

However, around fast-falling grains flow separation occurs, which greatly increases the fluid inertia, i.e. drag or retarding force of fluid on a sphere. Stokes Law ignores drag, and is only applicable at Reynolds numbers (Re) of below unity, where the Grain Reynolds number

$$Re = w D / n \qquad (5.6)$$

which is the dimensionless ratio of inertial to viscous forces. Yalin (1972) presents an empirically-based graph which shows that the fall velocity of a sphere can be related to sphere diameter by a grain Reynolds number, and the Archimedes Buoyancy Index (A), where

$$A = ((ps-p)/p) * (D^3 / n^2) \qquad (5.7).$$

This relationship is the one used as the basis for converting the measured fall velocities into grain sizes in this study, but with the important difference that the empirical relationship used is based on natural sand grains and not spheres.

The drag coefficient of non-spherical bodies is greater than the corresponding sphere because of their increased ratio of surface area to mass and presence of sharp edges and corners, and we can be fairly sure that the fall velocity of natural grains is less than that of spheres of the some equivalent size, such as sieve diameter (Komar & Reimers, 1978; Baba & Komar, 1981b; Komar, Baba & Cui, 1984). Irregularities on natural grains cause them to oscillate and spin as they fall. The larger the falling grain, the larger the scale of irregular motions, which possibly accounts for the progressive departure from the curve of settling of spheres with increasing grain size (Baba & Komar, 1981b).

Komar & Reimers (1978) studied fall velocities of smooth pebbles of different size and shape, falling in glycerine. They found that by using

empirical results, curves of fall velocity versus grain nominal diameter could be generated for different values of the Corey Shape Factor (CSF), where

$$CSF = Ds / (Di\ D1)^{0.5} \qquad (5.8)$$

where Ds = grain minor diameter, Di = grain intermediate diameter and D1 = grain major diameter (Albertson, 1953).

The above studies suggest that much of the reduction in fall velocity from that of spheres might be accounted for by grain sphericity effects, and in the study of Baba & Komar (1981b) using natural sand grains, grain roundness was found to have no measurable effect. Williams (1966) found that drag was increased by more than a few percent only if edges were sharp and so enhanced flow separation.

For samples of natural sand, measuring grain diameters individually to determine the CSF is a laborious process, and unwarranted unless the sample is known to contain many unusually non-spherical grains (Komar & Cui, 1984). It is considered that by using natural sand grains as the particles in the empirical fall velocity - grain size relationship, grain sphericity effects are negligible. The relative uniformity of sand grain roundness in the majority of the samples analysed means differences between samples are minimal, and the roundness effects are already included in the empirical relationship of fall velocity to grain size.

5.5.4 Grain Density

To measure the grain density of each sample would be extremely time consuming - especially considering that, to fully appreciate the influence of grain density upon the fall velocity distribution, one needs to know the distribution of density with grain size within each sample. One of the great advantages of fall tower methods of studying sediments is that, in falling, the grains become distributed without sole regard to their density or any other single physical property, but rather their hydrodynamic properties.

Rubey (1933) formulated the concept of 'hydraulic equivalence', which involves the simultaneous deposition of grains having the same fall velocity, regardless of differences in grain size, density, sphericity etc. In this way the measured fall velocity distribution is thought to reflect more fully the hydrodynamic regime in which the sediment was deposited, with less influence of provenance factors which may exert significant control over grain density, shape and texture (Taira & Scholle, 1979b; Komar & Cui, 1984).

Komar (1981) studied fall velocities of grains with densities varying between 1.5 and 4.2, and the applicability of the empirical Gibbs equation (Gibbs et al, 1971, which yields fall velocities of quartz spheres in water) to the fall velocities of those grains. He found that as grain density departs from that of quartz some systematic error was introduced. This error was relatively small and could be reduced further by using corrections for fall velocity and grain diameter with different grain density (his Figs.4 and 5).

Yalin (1977) demonstrated that a grain Reynolds number (Re) and the Archimedes Buoyancy Index (A) are able to directly relate grain size and fall velocity, Hallermeier (1981) used 115 fall velocities from 13 sources, including materials of different densities such as quartz, coal, pumice and plastic, to produce three equations relating Re and A.

In using the Gibbs equation, Komar & Cui (1984) found that for ordinary quartz-felspar sands, the use of 2.65 for a density gave satisfactory results, but a large content of heavy minerals would introduce some systematic error. However this could be partially corrected if the proportion of heavy minerals was known, using the correction factors of Komar (1981).

In this study, a density of 2.65 was used for all samples, as the sand fraction of all samples was dominated by quartz grains.

5.5.5 Fluid Temperature

The importance of knowing water temperature is that temperature variation causes change of fall velocity, through changing fluid viscosity. A measurement of the mid-depth temperature of the water in the fall tower was taken at the start of all sample runs, to +/-0.05 degrees. Other less significant factors changed by temperature are fluid density, grain density and the buoyancy of the weighing pan. There may also be an effect if there is a vertical temperature gradient in the tower.

The maximum temperature change that occurs over say, an 8 hour period is 2 degrees. Assuming a constant rate of change, the temperature will therefore vary by up to 0.04 degrees over a 10 minute sample run time, causing (at 18-20 degrees) a 0.2% change in absolute viscosity. At the same temperature, viscosity changes cause the fall velocity of 2mm diameter grains to change by 0.5% per degree and of 100um grains by 2% per degree (Slot & Geldof, 1986). So with the same assumed rate of temperature change, the fall velocity of 2mm grains is altered by 0.02%, and 100um grains by 0.08%, negligible under experimental conditions. Water density variation over such a 10 minute period is 1-2 orders of magnitude less. Slot & Geldof (1986) note the importance of maintaining as much as possible a uniform temperature throughout the fall tower. In their tower of height 1.65m, a one degree temperature difference between top and bottom gives rise to uncertainty of the order of 1% in the fall velocity, so in the 1.87m high tower used in this study a similar uncertainty would occur. However, thorough stirring of the water in the fall tower took place approximately every 1.5-2 hours during sampling, when the balance pan was cleared of sediment.

The computer program which records the time-weight data also requires the input of the mid-depth temperature, for use in later programs to calculate accurate values of water viscosity and density. These are important in the conversion of fall velocity to grain size (see below). In terms of variations in

temperature during each 10 minute sample run, it is concluded that its effects are negligible in this study.

5.5.6 Fluid Movement

Fall velocities are, of course, velocities of grains relative to the fluid through which they fall. In practice, this is measured as the time taken for a grain to travel between fixed points, within a stationary fluid. If the grains have a slow fall velocity, for example below 1cm/s (roughly, grains below 100um) slight currents in the fall tower could cause significant differences between actual and measured fall velocities. A number of actions were taken to reduce these possible effects :

1 - The fall tower was filled and kept out of direct sunlight for at least 48 hours before sampling was begun, and all the time during sampling;
2 - The computer program did not allow sampling to begin unless the balance had been reading zero for at least 30 seconds, ensuring no currents occurred towards the base of the water column;
3 - Mixing of the water in the fall tower occurred at intervals of 1.5-2 hours during sampling;
4 - A visual check for water movement was undertaken at intervals between sample runs.

At no time between sample runs were any convection currents seen in the water column; it is, therefore, thought that effects of convective fluid movement were negligible. However, at the triggering of the grain release mechanism, some samples caused a density current effect in the upper few centimetres of the water column. This tended to occur if the sample had not been distributed evenly enough in the ring-shaped sample hopper, or if in distributing the sample with water the water level was raised a few millimetres above the level in the tube itself. In the ideal situation the grains in the sample attain their terminal velocities immediately on release,

maintaining them throughout the whole water column. In reality, velocity variations occurred at the beginning of their fall, both acceleration to terminal velocity, and, when density currents happened as outlined above, acceleration to beyond terminal velocity relative to the fixed release and measurement positions followed by deceleration as the density current dispersed. As the density currents dispersed, some slight eddying was noted, with some relative upward motion maintained for up to five seconds.

The requirement is that such deviations from the ideal situation take place in a vertical distance very small compared to the total fall distance, or more precisely that the proportion of time each grain spends falling at a rate other than its terminal velocity is minimal compared to the total fall time. Sample runs which showed density current effects upon triggering did not see the continuation of the feature more than 10cm into the water column, or for more than 5 seconds. It is the fine sand grains that are most involved in the density current. For the above case of 5 seconds and 10cm penetration into the tower, measured settling velocities could be 4% in error for grains which normally take 400 seconds to fall 1.87m. It is unknown what effect the eddies had on the settling velocity of grains involved in the density current.

5.5.7 Wall Effects

Fall velocities of grains may be modified by the presence of boundaries to the fluid, such as settling tube walls (Allen, 1984). As particles approach the wall, or are near to the vessel in size their fall velocities are markedly reduced (Happel & Brenner, 1965). This is likely to be most significant in terms of measured fall velocity distributions with large grains that fall near to the wall for a large proportion of their fall time. Two features of the fall tower used minimise wall effects on the collected data :

1 - The internal diameter of the settling tube is large; at 28.5cm it is 1.5 times that of Rigler et al (1981), 1.6 times that of Slot & Geldof (1986), and 2.5 times that used by Baba & Komar (1981b), who stated that for their

tube, corrections for 'small grains' (they used 350um - 1.68mm) were negligible due to the large tube internal diameter. Thus for the tube used in this study, corrections for a large range of grain sizes are also negligible;

2 - It should be noted that wall effects on the data are decreasingly likely to be recorded with a decreasing ratio of balance pan to settling tube diameter. This is because those grains which have fallen close to the wall will miss the balance pan and not be recorded. In this system, the balance pan occupies 58% of the cross-sectional are of the water column, and so all grains which have been slowed by the presence of the wall will fall through the 4cm gap between the balance pan and tube wall. In this way wall effects on the recorded data are considered zero in this study.

The significance upon the representative nature of the recorded data of this relatively small balance pan in the fall tower will be discussed later in this chapter.

5.6 Data Manipulation - Conversion of Grain Fall Velocity to Sieve Diameter

5.6.1 The Program, FTOWER1

There follows a description of program FTOWER1, written to convert the settling velocity distribution obtained from the fall tower into a grain size distribution. The program may be seen as performing a number of steps :

1 Some data is discarded;

2 Data is corrected for sediment grains that did not land on the balance pan;

3 The cumulative percentage weight is calculated;

4 The fluid absolute viscosity, density, and kinematic viscosity are calculated;

5 Each time value is converted to a grain size.

These steps are each described below.

1 - The program discards the first 9.9secs of data, and takes the weight reading at this time to equal zero. This is done because, occasionally the operation of the sample release mechanism causes the balance reading to deviate from zero, by +/-0.01g. For a 1.87m fall distance a 2mm diameter grain will take 9.9secs to reach the balance pan (Hallermeier, 1981, his eqn. 13), so the discarded data will not contain settling velocity data. It is emphasised by Hallermeier (1981) that the ranges of test conditions in the data base presented by him (here used as the basis of the grain size derivation) should not be exceeded. Limiting values of the Archimedes Index A were 6 (very fine quartz grains in water), and 3×10^6 (very coarse sands). In this study, this means that the use of data collected more than 368sec after sample release, corresponding to a sieve diameter finer than 73.5um, is not justified. Therefore, this data is also discarded;

2 - Corrections are made to the data to correct for grains that missed the balance pan. Rigler et al (1981) assumed that statistically equivalent proportions of all size ranges within a sample are capable of passing between the pan and the tube wall during a sample run, and stated that good reproducibility of results supported such an assumption. To test this assumption for the fall tower used, natural sand from estuarine environments were sieved at 1/4 phi intervals, and accurately weighed. Fifteen sediment samples from a range of sieve intervals were then run through the fall tower, of which 13 were split and run as 3 subsamples.

This procedure allowed the construction of a correction curve; a graph of log. mean fall time (secs) against weight correction factor CF (Fig. 5.1), where

$$CF(t) = WA(t) / 1.60606\ WW(t) \qquad (5.9)$$

where

CF(t) = correction factor for grains which take t seconds to fall 1.87m

WA(t) = measured weight in air of whole sample WW(t) = measured weight in water of that part of sample recorded on the balance pan

1.60606 = ratio of sample weight in air to theoretical sample weight in water (for grain density of 2.65 and fluid density of 1.00).

The error bars on Fig. 5.1 represent 68% confidence limits on each data point, i.e. +/- 1 standard deviation. After removal of the apparently anomalous low data point at ~180seconds, a curve was fitted to this data. The style of curve, with upper and lower portions tending towards limits, is explained below in physical terms of grain settling processes within the tube. The curve's equation is

$$CF(t) = 1.06004 + \frac{0.60679}{(1 + EXP(-16.03199 * (t - 1.5909)))}$$

(eqn. 5.10).

Fig. 5.1 Fall tower calibration data - Correction curve for sediment weight collected on pan of Fall Tower, as a function of settling time. Error bars represent 68% confidence limits.

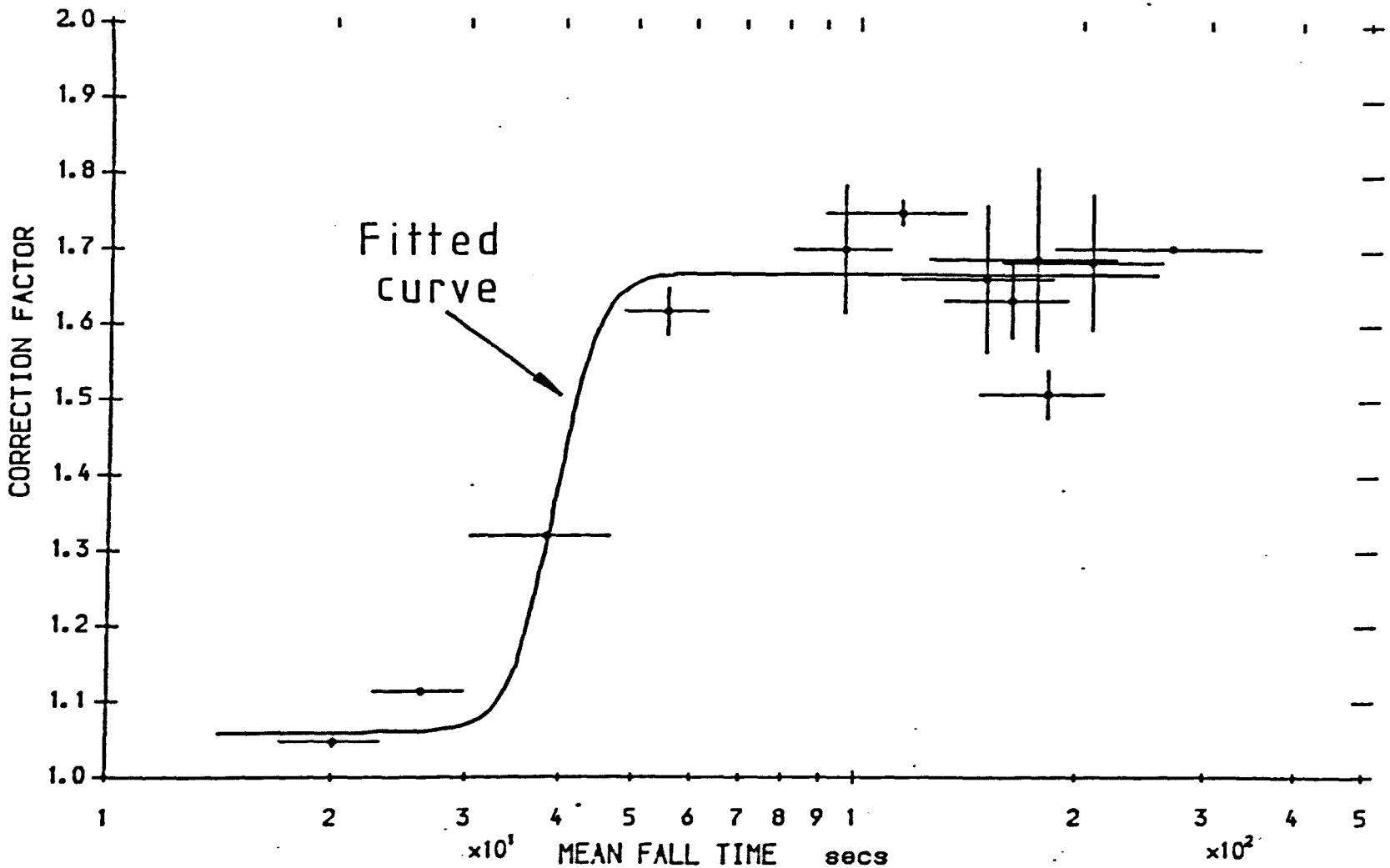

For small t, CF(t) tends towards 1.06004, and for large t, CF(t) tends towards 1.66683. This is good agreement with the theoretical limits deduced below.

With small t (<30 seconds), grains leaving the sample release mechanism accelerate nearly vertically downwards; a very high proportion of them fall onto the balance pan, hence the low correction factors in the left hand region of the curve. With increasing t (30- 100 seconds) lateral dispersion of the grains increases, due to grain-grain interactions and the increased expression of naturally variable grain fall paths due to increased fall time. Now significant amounts of sediment begin to miss the pan and fall between the pan edge and the tube wall. The bulk of grains within these estuarine sediment samples fall within these time limits.

With high values of t (>100 seconds) the dispersal of grains across the water column tends to become complete, and so the curve flattens out towards a limiting value. Assuming an even dispersion across the water column, the theoretical maximum correction factor is the ratio of the tube cross-sectional area to that of the pan, which is 1.72. The calculated limit from the curve fit to the test samples is only 3.3% different. For large grains, which would fall directly onto the pan, CF should tend towards unity; the curve fit gives a lower limit 6% above this.

Using the above relationship, measured cumulative weight at time t is corrected upwards to the weight which would have been recorded had the pan collected all grains reaching the pan at that time. So each increment of weight increase is multiplied by the corresponding correction factor, than added to the previous calculated cumulative weight.

It is clear from the above, that the assumption of Rigler et al (1981), that broadly equivalent proportions of each size range miss the collection pan, was not valid in this case, and probably not in their case either. Their quoted 'good reproducibility' merely reflects an effective splitting technique;

3 - Cumulative percentage weights are calculated using the final corrected cumulative weight value as 100%;

4 - Using the reading of water temperature, the water properties absolute viscosity, density and kinematic viscosity are calculated.

The absolute viscosity of fresh water is temperature dependent, and is given by Weast (1969) in two equations, each applicable over a different temperature range. For temperature T = 0-20 degrees centigrade, absolute viscosity ABV is given by

$$ABV = \log^{-1}\left(a/(b+(c+(t-20))+(d*((T-20)^2))-e\right) \quad \text{centipoises} \qquad (5.11)$$

where

a = 1302, b = 998.333, c = 8.1855, d = 0.00585, and e = 3.30233.

For T = 20 - 100 degrees centigrade

$$ABV = \log^{-1}\left(\left(\log(a)+(((b*(20-T)-(c*((T-20)^2)))/(T+D))\right)\right) \quad \text{centipoises} \qquad (5.12)$$

where

a = 0.01002, b = 1.3272, c = 0.001053, d = 105.

Water Density DEN is calculated by linear interpolation between the following density values given in Weast (1969),

Temperature Degrees C	Density g/cm^3
10	0.999728
15	0.999128
20	0.998234
25	0.997075
30	0.995678.

The kinematic viscosity KNV is then calculated using the relationship

$$KNV = ABV / DEN \ cm^2/s \qquad (5.13);$$

5 - Time values are converted to a grain size. The data base used for this empirical conversion is that presented by Hallermeier (1981) (his tables 1, 2 and 3). Yalin (1972) related the fall velocity of spheres to their diameter via a dimensionless empirical curve, of a grain Reynolds number Re to the Archimedes Index A, defined in equations 5.6 and 5.7 above. Hallermeier (1981) used this relationship for natural sand grains, and developed three equations which join into a single segmented curve when plotted on double logarithmic paper. The data used in shown in Fig. 5.2. A Chebyshev polynomial was fitted to the data between values of A of 5 and 2670000. The best fit line was given by a degree 3 equation, with coefficients of 7.215, 4.1134, -0.41564 and 0.048812, which gave a residual of 0.12664. This fit is shown superimposed upon the data.

5.6.1.1 The Conversion Process

Each time value in the data of each sample was converted into a settling velocity by division into the 1.87m fall distance. Both Re and A are functions of grain diameter D, so that to obtain D from each settling velocity value required iteration. The steps of the method followed by the computer program are as follows:

(i) Read time value t;

(ii) Calculate the known settling velocity wk using

$$wk = 187/t \quad cm/s \qquad (5.14);$$

(iii) Assume a value of A;

(iv) From A, calculate a value of R by using the Chebyshev polynomial equation (above);

Fall velocity data. Shows the relationship between Grain Reynolds Number and Archimedes Buoyancy Index. (Data from Hallermeier, 1981).

Fig. 5.2

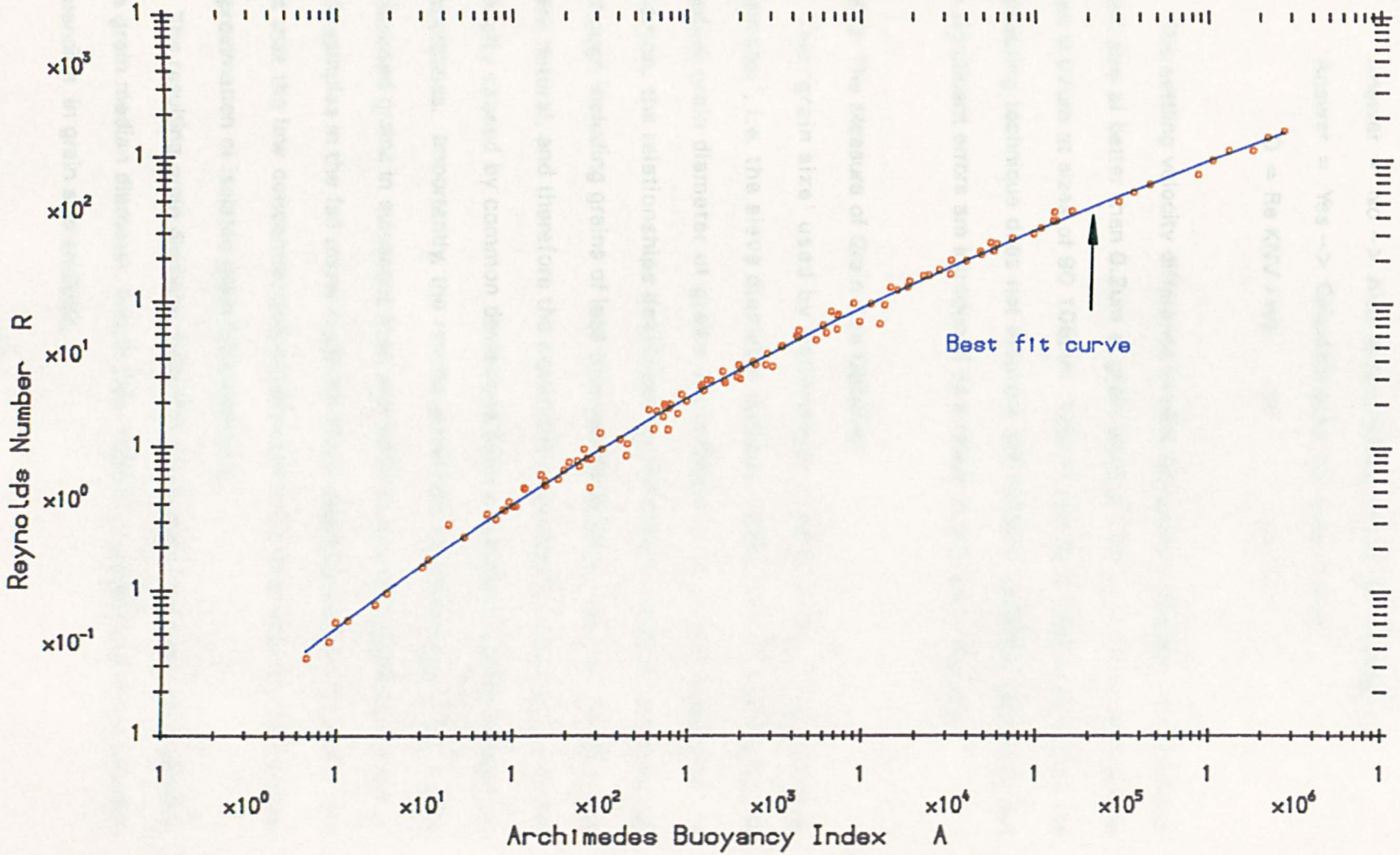

(v) Calculate the assumed settling velocity wa using

wa = function (R,A) (5.15);

(vi) Is (wk-ws) < 0.001cm/s ?

Answer = No --> Alter A accordingly and return to step (iv)

Answer = Yes --> Calculate grain diameter D from

D = Re KNV / wk cm (5.16).

The settling velocity difference in step (vi) gives a precision in calculated grain size of better than 0.2um at grain sizes of 700um to 2mm, and greater than 0.07um at sizes of 90 106um. This of course is false accuracy as the measuring technique does not measure fall velocity with that accuracy, but no significant errors are introduced as a result of the use of iteration.

5.6.2 The Measure of Grain Size Obtained

The 'grain size' used by Hallermeier (1981) is the 'median sieve diameter', i.e. the sieve diameter (Leeder, 1982), which measures the median grain diameter of grains approximating to triaxial ellipsoids. In addition, the relationships developed by him refer to natural sand grains, although including grains of less than quartz density. The sand grains used were natural, and therefore the equations presented include effects on fall velocity caused by common deviations from a spherical shape and perfect smoothness. Importantly, the results presented by Hallermeier (1981) refer to isolated grains in quiescent fluid, and while it is recognised that the use of bulk samples in the fall tower must introduce variations in fall velocities. It is felt that the low concentrations of particles used (see above) gives a good approximation of isolated grain fall conditions.

The resulting grain diameter from the above described analysis method is the grain median diameter, which Dyer (1986) considers the most valuable dimension in grain size analysis.

5.6.3 Precision of Grain Size Parameters

Replicate Sample Tests

Dyer (1986) makes the valuable point that in the literature there is a marked lack of data on replicate determinations of grain size distributions on several subsamples of the same sample. Great weight is sometimes placed on small differences between samples, but there is little assessment of whether these differences are larger than the error limits of the analysing technique. In this case, both the efficiency of the sample splitting method and the errors due to the fall tower are involved.

To determine the possible errors in the measures of grain size, four samples from Barmouth Bay and the Mawddach Estuary were selected, broadly on the basis of different mean grain size, and three replicate determinations of grain size made. Also used were data of ten sand fractions taken from a dynamic shelf environment in the English Channel, and run in triplicate on the U.C.N.W. fall tower by Shaghude (1989).

Using the descriptive scales of Table 5.1, the four samples from the Barmouth area are described thus:

A Fine-skewed, moderately-sorted coarse sand;

B Strongly coarse-skewed, moderately-sorted medium sand;

C Near-symmetrical, very well-sorted fine sand;

D Fine-skewed, very well-sorted very fine sand.

The samples from the English Channel ranged from well-sorted, very positively-skewed, medium sand, to well-sorted, very negatively-skewed, fine - very fine sand. Most were well-sorted, negatively-skewed, fine sands.

Results

The results of the repeated experiments are shown in Tables 5.2 and 5.3., and in Figs. 5.3 - 5.5, where each sample is presented as a cross centred at the position of the mean values, and the bars represent 95%

Table 5.1

DESCRIPTIVE SCALES OF GRAIN SIZE PARAMETERS (after Folk + Ward, 1957)

Sorting SD	Skewness SK	Kurtosis K
	-1.0	
Very well-sorted	Very negative	Very platykurtic
0.35	-0.3	0.67
Well-sorted	Negative	Platykurtic
0.50	-0.1	0.9
Moderately-sorted	Nearly symmetrical	Mesokurtic
1.0	0.1	1.11
Poorly-sorted	Positive	Leptokurtic
2.0	0.3	1.50
Very poorly-sorted	Very positive	Very leptokurtic
4.0	1.0	3.00
Extreaely poorly-sorted		Extreaely leptokurtic

TABLE 5.2

GRAIN SIZE PARAMETERS OF REPLICATE SAMPLES

Sample Identifiers	MOMENTS Mode	Mean	SD	SK	K	FOLK Mean	SD	SK	K
Sample A									
25-4-88 Barmouth Bay. Station 1, sample 01. 5 replicates									
Replicate mean	0.490	0.707	0.676	0.872	4.488	0.668	0.666	0.083	1.111
95% confidence limits	0.175	0 053	0.077	0.309	0.796	0.037	0.097	0.109	0.243
Sample B									
20-1-86 Mawddach Estuary. Borehole 41. 6 replicates									
Replicate mean	2.067	1.731	0.836	-0.686	2.926	1.685	0.858	-0.458	1.127
95% confidence limits	0.197	0.078	0.047	0.144	0.221	0.078	0.052	0.085	0.132
Sample C									
28-4-87 Mawddach Estuary. Transect 4, sample 02. 6 replicates.									
Replicate mean	2.633	2.261	0.268	0.468	3.527	2.644	0.264	0.033	1.353
95% confidence limits	0.080	0.097	0.029	0.900	0.553	0.021	0.025	0.131	0.069
Sample D									
28-4-87 Mawddach Estuary. Transect 1, sample 01. 6 replicates.									
Replicate mean	3.133	3.027	0.302	0.968	2.061	3.231	0.226	0.143	0.985
95% confidence limits	0.080	0.318	0.172	1.270	1.786	0.046	0.034	0.128	0.129

Table 5.3

Replicate fall tower data of Shagude (1989)

Grain sizes in phi (rounded up)

Sample	Mean	SD	Sorting	SD	Skew.	SD	Kurto.	SD
001	3.32	0.50	0.35	0.01	-0.94	1.04	3.7	0.2
002	2.79	0.29	0.53	0.05	-0.74	0.17	0.4	0.5
014	2.73	0.03	0.33	0.02	-0.23	0.11	2.4	0.2
017	2.66	0.03	0.37	0.04	-0.24	0.16	1.9	0.1
018	2.99	0.06	0.33	0.03	-1.14	0.17	2.9	1.7
031	1.98	0.04	0.44	0.04	-0.91	0.32	4.5	0.1
032	1.52	0.08	0.64	0.01	-0.30	0.20	0.2	0.2
033	2.43	0.01	0.20	0.01	0.88	0.33	4.1	1.0
034	1.72	0.03	0.64	0.01	0.18	0.11	0.1	0.1
040	1.44	0.05	0.47	0.01	2.61	0.18	8.5	0.6

confidence limits, i.e. +/- 2 standard deviations. Dots indicate the individual results from the English Channel data. Individual data from the Barmouth samples are not shown.

The significance of the analysing errors is outlined with reference to the Barmouth Bay grab samples, which are discussed in the following chapter. Folk & Ward graphic measures and modal data are only available for the Barmouth samples.

Mode phi - This data is available from the Barmouth samples only. A large factor is that the finer sediments are much better sorted, containing a low total range of grain sizes, and that compared to the 0.1phi interval to which the mode is expressed, the mode variation in the replicates is small. Another factor is the effect of putting each modal value into a division. If the true mode of the sample was close to a 0.1phi division, variation would tend to be reduced in the replicates, compared to if the true mode was close to a 0.05phi division, in which case the mode would more likely vary in the replicates. For the data in Barmouth Bay, where the mode varied between 1.7 and 2.8phi, relevant confidence limits are probably +/-0.08 - 0.19phi.

Mean phi (moments) - There is no clear trend of error with sediment size. Individual samples have very large errors, of up to +/- >1phi, seemingly resulting from the influence of one rogue result in each case. The high error associated with the very fine sand (3.1phi) may relate in part to the lower limit imposed on the fall tower data due to the calibration set used. Confidence limits relevant to most data in the bay are therefore ~ 0.1phi.

Mean phi (Folk & Ward) - The 95% error limits of this measure are smaller than the moments-derived data error. The confidence limits are between +/-0.021phi for fine sand and +/-0.078phi for the medium sand, and are not a function of grain size.

Standard deviation repeatability - v mean grain size

3 subsamples of each sample

Fig. 5.3

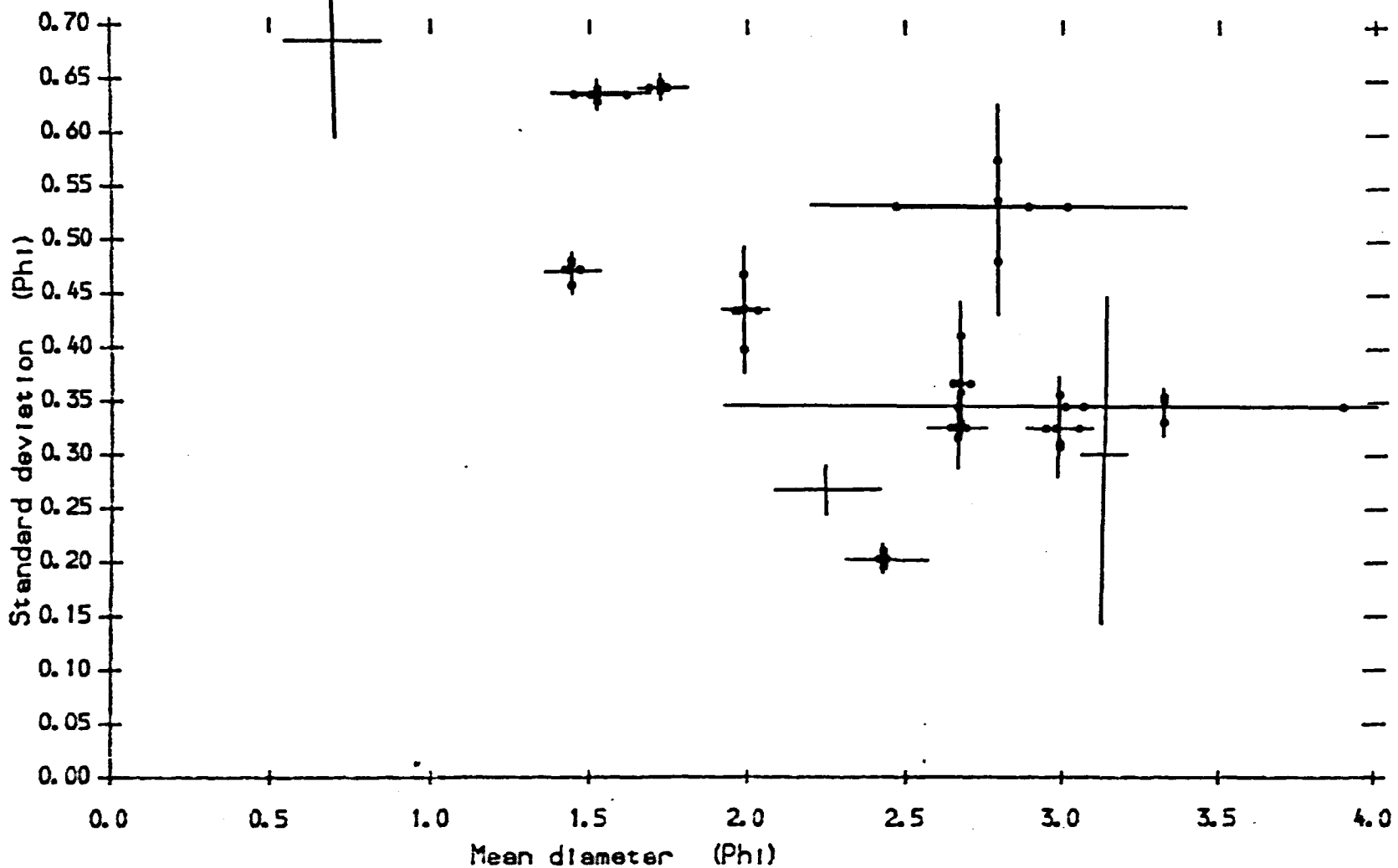

Skewness repeatability - v mean grain size

3 subsamples of each sample

Fig. 5.4

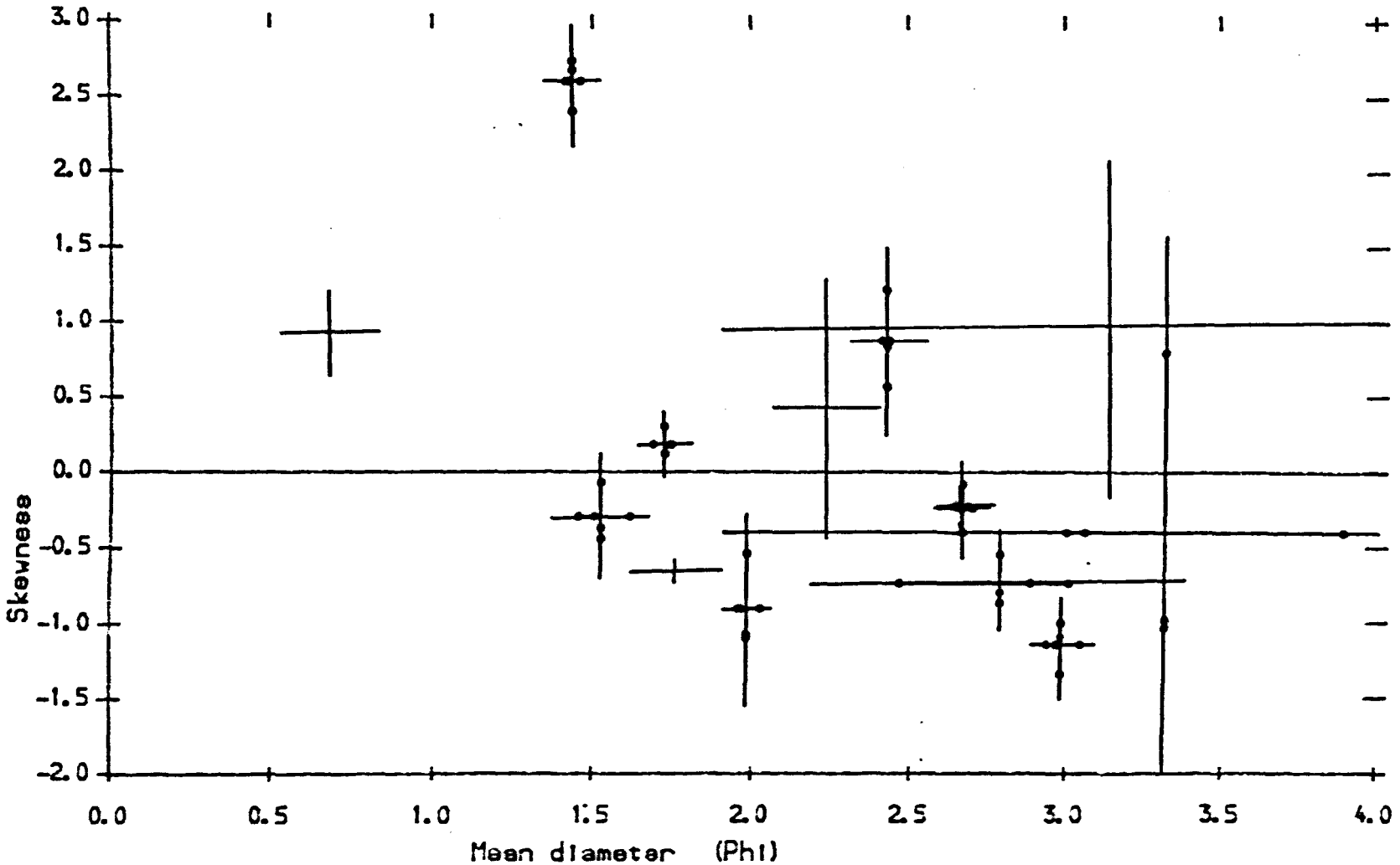

Kurtosis repeatability - v mean grain size

3 subsamples of each sample

Fig. 5.5

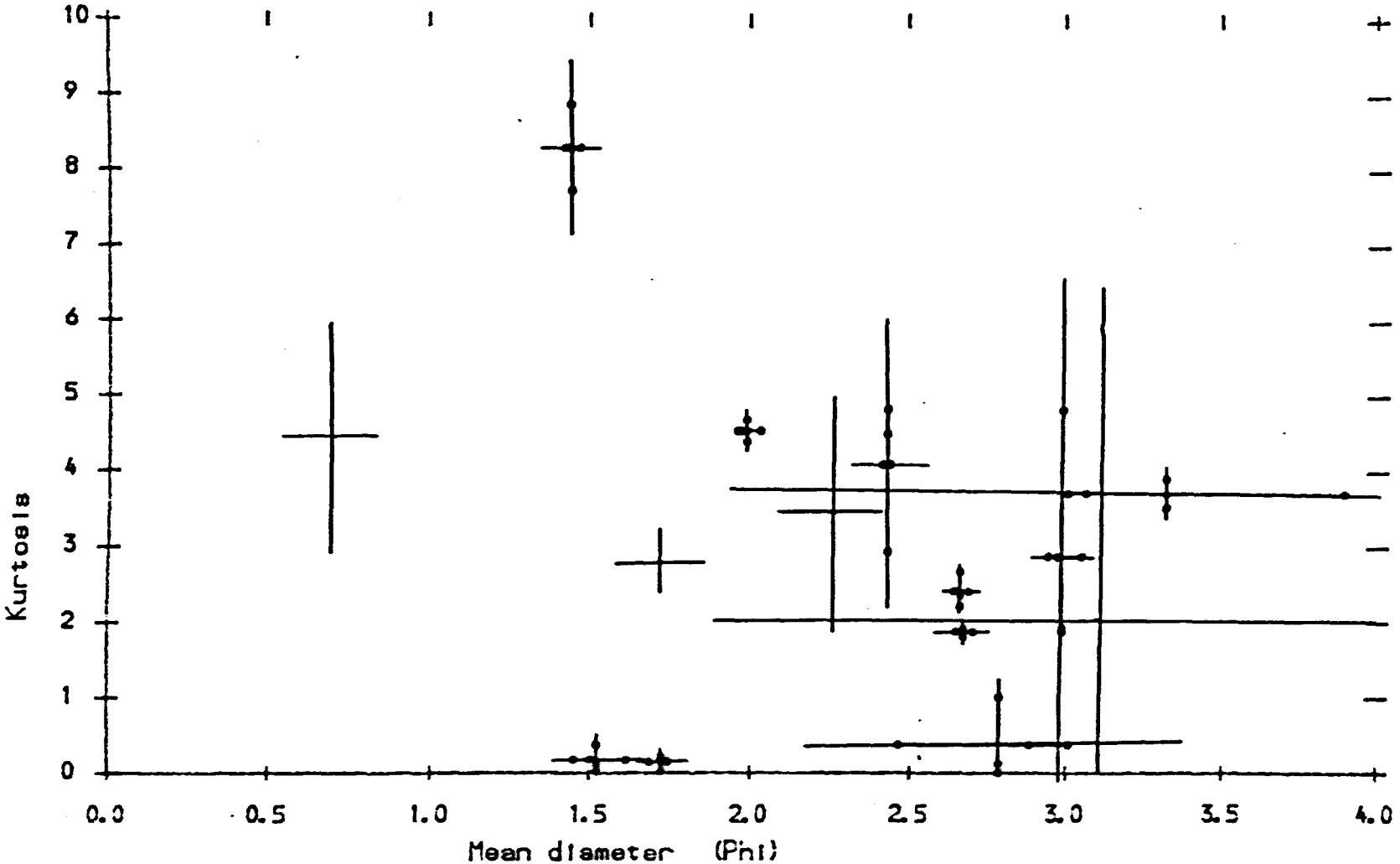

Sorting (moments) - there is no trend of SD error with sorting or mean grain size. For the contoured data in the bay the error limits are expected to be approximately +/- 0.08 - 0.1phi, so the 0.05phi contour interval in Fig. 6.9 (Chapter 6), the contour plot of sorting, is only justifiable in helping to show the contour trend.

Sorting (Folk & Ward) - Generally the error limits decrease with grain size, from +/-0.097phi for sample A to +/-0.025phi for sample C. Confidence limits for the bay samples are approximately +/-0.05phi, so the contours on Fig. 6.10 may have some errors associated with them.

Skewness (moments) - The variation in skewness is very high in the well-sorted fine sands. The skewness error bar seems strongly related to sorting; where sorting is very good, skewness values are more variable. Grab samples in the bay have sorting of 0.4 - 0.6phi and a mean size of 1.9 - 2.6phi. The estimated 95% confidence limits for those samples is +/- 0.5 - 1phi, so the skewness contour plot (Fig. 6.11) must be treated as containing significant analytical errors, and the conclusions therefrom seen with suspicion.

Skewness (Folk & Ward) - In terms of the contour plot (Fig. 6.12) the total variation of samples is - 0.42 to 0.13, and with confidence limits at +/- 0.1, the conclusions from the plot are drawn from a valid map.

Kurtosis (moments) - Kurtosis error has a relationship with sorting; with better sorting the kurtosis error increases. Kurtosis varied between 3 and 7 in the bay, and the 95% confidence limits are estimated at +/- 0.6. Kurtosis variation in Barmouth Bay is shown in Fig. 6.13.

Kurtosis (Folk & Ward) - The error limits vary between +/-0.069 for the fine sand sample C, and +/- 0.243 for the coarse sand A. The bay samples vary between 0.89 and 1.84, so the estimated confidence limits are +/- 0.13, thus the conclusions drawn from Fig. 6.14 are likely to have been drawn from a valid map.

5.7 Framework for Presentation and Discussion of Grain Size

The most common way of presenting grain size data is as either a frequency or a cumulative frequency distribution curve, with grain size expressed on the logarithmic phi scale. Frequency curves of natural sediments are often thought to approximate the symmetrical, bell-shaped curve of a normal (or Gaussian) distribution (Dyer, 1986); thus, plotting of weight percent cumulative curves on Gaussian paper may be undertaken. Most natural samples plot as a series of straight-lines by this method (eg Grace et al, 1978) and the common theory is that these straight-line segments represent a few log-normal sub-populations, either truncated or overlapping in form (Visher, 1969; Middleton, 1976; Sagoe & Visher, 1977). However, study of these hypotheses in natural systems has proved inconclusive (Viard & Breyer, 1979). There is a very large amount of literature (reviewed in Folk, 1966) on using the Gaussian distribution to characterise and compare samples, and deviations from it as environmentally sensitive measures.

An alternative to the assumption of log-normality, that is of the log-hyperbolic distribution, was proposed by Bagnold & Barndorff-Nielsen (1980). This was on the basis that when both frequency and size are plotted logarithmically, grain size curves approximate more closely to a hyperbola than the parabola which would be expected if a Gaussian distribution was present. This has been used by Christiansen, Blaesild & Dalsgaard (1984), who concluded that the traditional interpretation of segmented curves representing different modes of sediment transport is often unjustified. They showed that separate samples of sediment being actively transported in suspension, saltation and as bedload each gave a segmented shape when plotted on probability paper, yet all three transport modes each gave a hyperbolic distribution. The log-hyperbolic mode of presentation and description has not yet achieved wide usage.

5.7.1 Statistical Parameters

Both the Gaussian and log-hyperbolic systems of presentation are used to enable grain size distributions to be described and compared, by their reduction to a number of statistical parameters - a more simple task than to compare many different grain size curves by eye.

To accurately represent the Gaussian distribution the method of moments is used, determining the moment of each of the constant size increments. The distribution is reduced to four parameters: the mean, standard deviation (or sorting), skewness and kurtosis. A measure of the spread of grain sizes within the size distribution is given by the standard deviation, SD. For a Gaussian distribution, 68.3% of the distribution lies within +/- standard deviation of the mean, 95.5% within two standard deviations and 99.7% within three. A low value of sorting characterises a relatively uniform sediment, a sharp-peaked curve with few grains much smaller or larger than the mean.

A measure of the asymmetry of the distribution may be obtained from the third moment, skewness SK. The skewness is normalised by the cube of the sorting, making the skewness dimensionless and independent of the sorting. Grain size distributions which are symmetrical about the mean, have a skewness of zero, those with excess fine grains (i.e. the median and mode grain size coarser than the mean) have positive skewness, and those with excess coarse grains have negative skewness.

The fourth moment of the distribution, kurtosis (K), assesses the deviation from a Gaussian distribution at the tails of the distribution. A well-sorted sediment with zero skewness may have either an excess or deficit of grains at the extremes. Like skewness, kurtosis is normalised to become dimensionless and independent of sorting. A Gaussian curve has a kurtosis value of 3. A distribution with a frequency curve having a wide 'peak' (i.e. a deficit in extreme sizes) has kurtosis <3, and a curve with a sharp 'peak' (i.e. an excess of extreme sizes) has kurtosis >3.

Log-hyperbolic distributions, which are claimed to be a more appropriate and accurate assumption than a Gaussian shape, can be reduced to four parameters broadly equivalent to the four moments explained above (Christiansen et al, 1984; Barndorff-Nielsen & Blaesild, 1981), which can be used for environmental discrimination in the same way as the Gaussian moments, and the graphically-derived parameters of Inman (1952) or Folk & Ward (1957) (see below).

The actual process of calculating the moments of a distribution is a very laborious one, without the aid of a computer. Before their widespread use, parameters were derived from a few simple measurements direct from a cumulative frequency curve (Folk & Ward, 1957). Inclusive Graphic Skewness (SKI) is independent of sorting and has limiting values of -1 and +1. The Inclusive Graphic Kurtosis (KI), for a Gaussian curve equals one; it has limits of approximately 0.41 and 8. Folk & Ward (1957) presented descriptive scales of sorting, skewness and kurtosis (Table 5.1).

Grain size data from this study will be presented using both frequency and cumulative frequency curves, both are drawn using data points, at 0.1phi intervals. Both the method of moments and the graphical measures of Folk & Ward (1957) have been used to describe the distributions. The moment method posseses an extensive supporting literature; it is well-suited to the construction of bivariate plots and its computation is familiar to many geologists. Importantly, it is not tied to any particular physical theory of distribution, such as the normal, log-normal, or log-hyperbolic 'laws' (Leroy, 1981). The graphical measures have the advantage of wide use, and the descriptive scales associated with them. Compared to the moment measures, the graphical measures of mean and sorting are 88% and 79% efficient, respectively (McCammon, 1962).

Chapter 6

Grain Size Investigations - Review and Results

6.1 Introduction

Grain size distributions can reveal much about the sedimentary regime of a region. The surficial sediments of Barmouth Bay and the Mawddach Estuary have been sampled (sample positions given in Figs. 6.1 & 6.2), and in this chapter they are described in terms of their grain size distributions, and interpreted in terms of sediment mobility and sediment transport pathways.

This chapter first describes methods of interpreting grain size data, and the documented effects of transport upon grain size distributions. The grain size data is then analysed using the spatial distribution of it's grain size characteristics (and the mineralogy of some gravel fractions), to deduce the sources, transport paths, and sinks within the Bay- Estuary system. This data is complementary to the interpretation of the geophysical data presented in Chapter 1. Estuarine sediment samples are also interpreted in terms of local erosion-accumulation within the estuary.

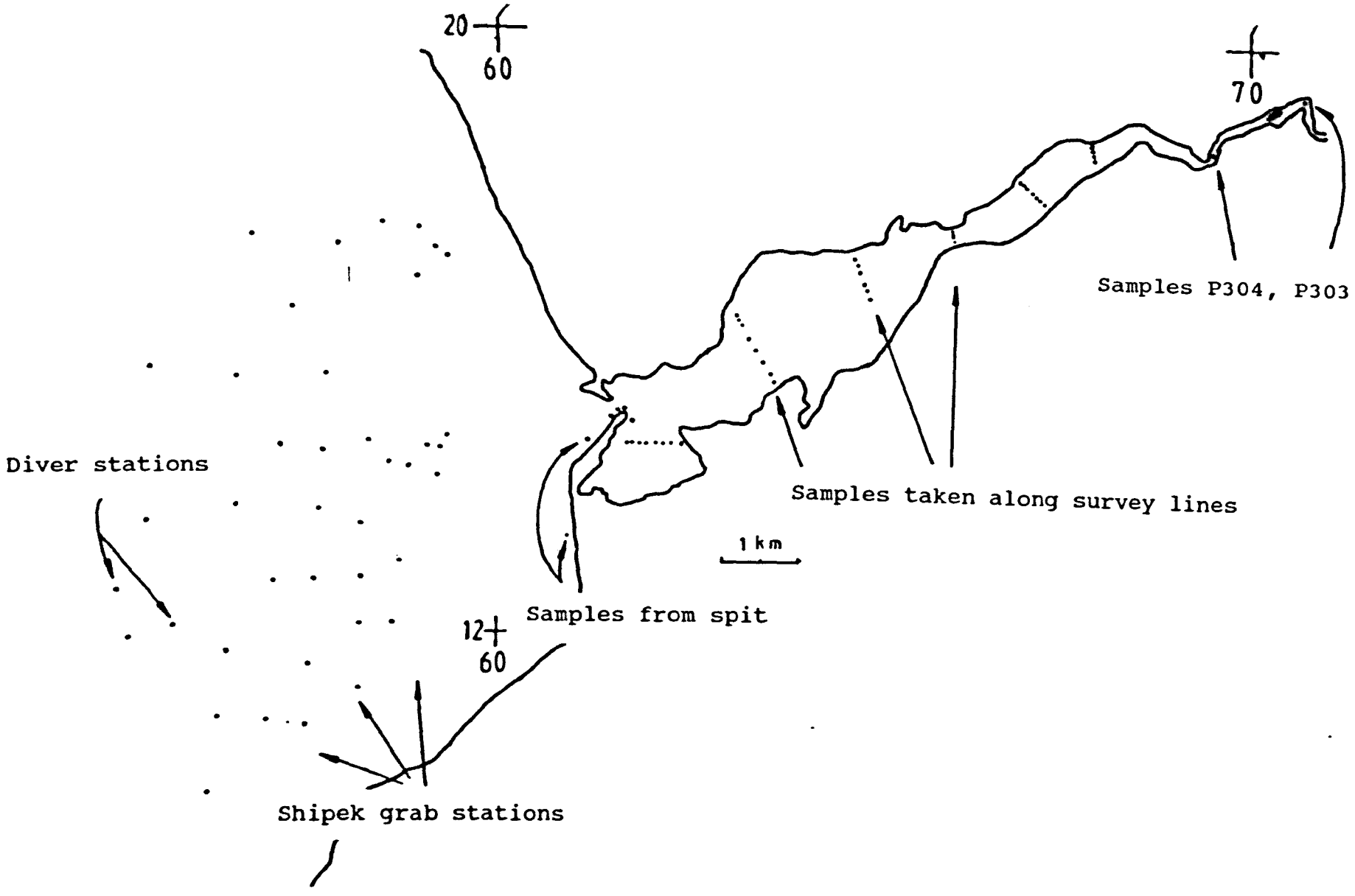

Fig. 6.1 Location map of bay and estuarine sample stations

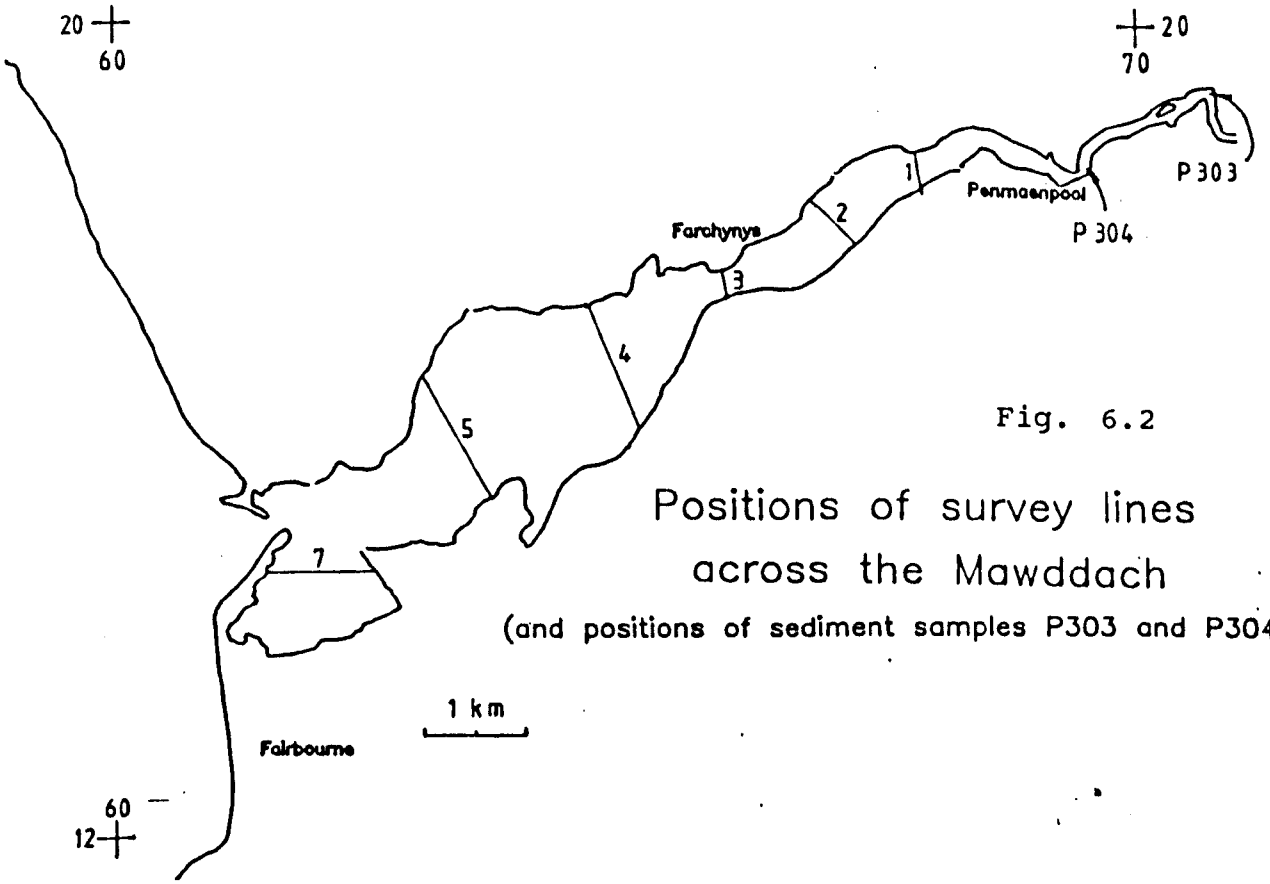

Fig. 6.2

Positions of survey lines across the Mawddach

(and positions of sediment samples P303 and P304)

Young (1961) and Schlee et al (1965) concluded that grain size parameters would not permit the distinguishing of beach from dune sands.

Friedman (1967) and Cronan (1972) have pointed out that polymodal sediments have unpredictable statistical parameters. Friedman (1967) also noted that the same sign of skewness may arise by different mechanisms, for example positive skewness of dune sands results from a truncated coarse tail. In river sands positive skew is produced by the presence of a fine tail. Analysis of samples from the Amazon-Solimoes River (Sedimentation Seminar, 1981) showed that cumulative frequency curves and bivariate textural plots were not environmentally sensitive. Successful indications of environment occurred in only 13% and 11% of cases respectively. It was pointed out that the grain size distribution is a function of three aspects :

1 the source distribution (i.e. provenance);

2 the transport processes (eg. water depth changes, shear stress, turbulence, flow velocity);

3 the processes operative at the site of deposition.

It was concluded that sieving alone is not a consistent and reliable technique to determine depositional environment, although some local positive results could be expected.

Recently, Sly at al (1983) studied the significance of sorting, skewness and kurtosis in different parts of the particle size distribution. Using a data base of nearly 1500 samples from Liverpool Bay and its beaches, the Mersey estuary, and the Great Lakes, they demonstrated that skewness-kurtosis plots could define separate fields for sediments apparently close to hydrodynamic equilibrium - but in separate hydraulic environments. They also made the point that sedimentologists have no proper means, by which to relate grain size distributions to the hydraulics of their sedimentary environments.

6.2.2 Other Statistical Work

Many sediments are not unimodal, so moment statistics alone are often ineffective for their description. In addition, relatively similar grain size distributions can be produced in different environments; a small number of numerical variables may not discriminate clearly between them. Some workers have tested a wide variety of variables of grain size distributions, to identify those parameters useful for environmental discrimination.

Multivariate discriminate function analysis has been used by Taira (1973), Reed et al (1975) and Taira & Scholle (1974, 1979b). The latter authors found that the useful variables were those related to the tails of the distribution, especially the fine tail. River, beach and dune sediments were well discriminated. They noted that discriminant analysis should be used only as one of many lines of evidence, when used for ancient sediments.

Fieller et al (1984) used just four parameters derived from a log-hyperbolic curve (Bagnold & Barndorff-Nielsen, 1980) and three from a skew-Laplace distribution, fitted to sediments from coastal environments. Their bivariate plots had some success in environmental discrimination. Bagnold (1954) suggested that the gradients of the two fitted limbs of the log-hyperbolic distribution are related to the grain transport modes; the significance of saltation and of coarse 'grain creep'.

6.2.3 Simpler Measures

An alternative to calculating moments, which reflects the entire grain size distribution, is to measure a small number of individual properties of the curve. Passega (1957, 1964) made use of only three measures: the one percentile size (C), to measure the coarsest grains; the median (M); and the percentage finer than 31um (L) to measure the fine tail. He took the CM or LM relationship as a measure of the 'competency' of the current, i.e. whether or not it can move the available size grains. Plotting these parameters against each other, for suites of samples showed different environments plotted in different areas. However, it is often difficult to

measure C and L accurately.

A simple and common method of distinguishing different sedimentary environments is the diagram presented by Shepard (1954), in which sediment types are placed according to the proportions of sand, silt and clay. Recently, Pejrup (1988) proposed an amended ternary diagram of ratios of fine sediments, which he argued was based upon hydrodynamic principles.

6.2.4 Transport Effects on Grain Size

Krumbein (1938) suggested the importance of progressive or continuous changes in grain size distributions, from source to final deposit. A number of workers have recognised progressive changes with distance (McCave, 1978; Haner, 1984), and time (Rana et al 1973). Dyer (1986) summarised the sequence of effects on grain size with increasing transport from source :

1 - Near the source the fine fraction would be transported in suspension, but the coarser fraction is transported on or near the bed. Thus a sample of the mobile fraction of the bed surface would be relatively coarse, poorly sorted and positively skewed, i.e with a a skew towards the fine fraction. On the bed a coarse lag deposit may be left, a few grains thick which protects the material beneath. (In flume experiments, Rana at al (1973) showed that mean bed diameter increases and sorting improves with time);

2 - Downstream, current velocities are lower and most coarse grains have been left behind. The bed is negatively skewed and better sorted;

3 - With further transport, the coarse material is absent. Intermediate sizes are transported by saltation and the fine fraction by suspension. Mean grain size is decreased, sorting has improved and skewness moved towards zero;

4 - Eventually, the low velocities can only transport the intermediate sizes occasionally as surface creep, and much more of the fine material is on the bed. Sorting will have worsened and the grain size distribution will be positively skewed;

5 - At the extreme end of a transport path, only the fine material will be present, in a well sorted and symmetrical distribution.

Some quantitative studies have also considered the transport effects upon grain size. McLaren (1981, 1982) suggested that the mean, sorting and skewness of distributions need not reflect either transport processes or depositional environment. Rather, they reflect the source distribution and the processes of winnowing, selective deposition and total deposition. His model assumed that light grains have a greater probability of erosion and transport than heavy grains. He predicted :

1 - If a source sediment undergoes erosion, and the resultant sediment in transport is deposited completely, than the deposit must be finer, better sorted and more negatively skewed than the source sediment (Case I);

2 - The lag remaining must therefore be coarser, better sorted and more positively skewed (Case II);

3 - If sediment in transport undergoes selective deposition, the resultant deposit may either be finer (Case IIIA), or coarser (Case IIIB) than the source, but the sorting will be better and the skew more positive.

McLaren & Bowles (1985) analysed this model and applied it to both flume experiments and field data. They modified the model in two ways :

- Successive deposits may be more poorly-sorted than their source, although thought uncommon in reality;

- When sediments become finer, their skew must become more negative, i.e. Case IIIA is rejected.

These trends can be used to infer probable sources and deposits; therefore, to identify the net sediment transport paths between deposits.

6.2.5 Hydrodynamic Interpretation and Modes of Transport

Several workers have advanced the idea that different grain populations within a grain size distribution are related to a different sediment transport mechanism (Visher, 1969; Middleton, 1976; Sagoe & Visher, 1977). Leeder (1982) defines three sediment transport modes :

1 - Bedload (or traction load) includes rolling, saltating and collision-interrupted 'saltating' grains. All bedload grains transfer momentum to the stationary bed surface by grain-grain contacts;

2 - Suspended load includes all grains kept aloft by fluid turbulence, so that the upward momentum transfer from fluid eddies, namely the turbulent bursting process (Jackson, R.G., 1976) balance the weight force of the grains;

3 - Washload is defined broadly as the more-or- less permanently suspended clay size grains present in water flows.

As discussed above, some authors have proposed that cumulative curves may be composed of two or more log-normal grain populations, and that each population may be related to a different transport mechanism. The transport mechanisms recognised by Visher (1969) were bedload 'surface creep', saltation and suspension, in order of decreasing grain size, whose populations were truncated against each other. Middleton (1976, and see references therein) assumed overlapping log-normal populations, but considered the transport modes represented to be 'traction' (rolling, sliding and saltation, i.e. bedload), intermittent suspension and suspension.

The significance of Middleton's work was that he interpreted the 'break' of slope in the cumulative curve in hydraulic terms, considering that a criterion for suspension is approximately

$$Ws / U^* = 1 \qquad (6.1)$$

where Ws = settling velocity and U^* = shear velocity.

However this uses the mean shear velocity rather than the maximum fluctuating shear velocity. Noting the effect of taking a mean value, Bridge (1981b) calculated

$$Ws / U^* = 0.64 \qquad (6.2)$$

where U^* = mean shear velocity.

Leeder (1982) considers that for full suspension

$$Ws / U^* < 0.8 \qquad (6.3).$$

Bridge (1981a) considers the recognition of three overlapping populations as unnecessary, pointing out that 'intermittent suspension' is the zone of overlap between bedload and suspension populations rather than a population in itself. He also noted little work on the distinction between transport mode and the mechanics of deposition on the bed, except that of Moss (1962, 1963, 1972), who based his grain populations on the mechanism of bed construction. The finest population was termed 'interstitial' as these grains occur in the spaces between the larger 'framework' grains, which constitute the majority of the bed.

The framework grains were equated to the saltation load, and the interstitial population to part of the suspension load. The coarse-tail population represents transport by surface creep. He elegantly related grain shape to these populations, demonstrating :

1 - the coarse fraction showed relatively low elongation factors (<0.7) and were therefore relatively easy grains to roll along the bed;

2 - the framework population is of relatively uniform hydraulic size, containing longer elongate grains and smaller more equant ones;

3 - the interstitial population contained small spherical grains and larger more elongate ones capable of penetrating between grains on the bed.

Moss contended that these three populations could be recognised in the cumulative frequency curve.

Noteable in the hydraulic interpretation of grain size distributions is the modelling work of Bridge (1981). By considering a frequency distribution of instantaneous bed shear stresses as the sum of many small divisions, for each division he calculated the rate of bedload transport (using the theoretical equation of Bagnold, 1966) for grain sizes transportable as bedload at each range of shear stress. The relative weight of sediment in transport, determined for all the shear stress values, constitutes the grain size distribution obtained from sampling on the bed. All the calculated grain size curves showed a 'break' in slope representing the maximum suspendable grain size at maximum fluctuating shear stresses. He obtained close agreement with natural bedload distributions. By mixing different flow-related bedload distributions, he obtained typical grain size distributions of deposited sediments; he concluded that flow unsteadiness plays a part in controlling grain size of deposited material.

6.3 Barmouth Bay - a Heterogeneous Sea Bed

Conclusions and interpretations, based upon the contour maps of grain size parameters, and interpreted side scan sonar data, are much enhanced if there is knowledge of the possible heterogeneity of the sea bed sediments. Grab samples, taken up to 1km apart, cannot reflect other than broad trends in the bay. As part of the study of surface sediment distribution, two stations in the bay were sampled by divers :

Station 1 at G.R. 5584012026 at high water spring tide;
Station 2 at G.R. 5509012456 at high water neap tide.

At each station three sea bed samples were taken.

Station 1 - The echo sounder showed a strong reflection, indicating a hard substrate; this was confirmed by the samples. These were a sandy gravel (01), a gravelly sand (02), and a sandy mud (03). Details of these samples are shown in Table 6.1.

Sample 01 was taken directly beneath a 2m cube scaffolding frame, sample 02 taken 5m away from the frame, and 03 from the immediate subsurface. Divers reported that visibility in the lower 1m of the water column was zero, indicating high near-bed concentrations of suspended material. The interpretation of these observations is that in this area currents transport fine sand over a lag gravel surface. This gravel overlies, armours, and is possibly derived from, a diamicton which contains gravel, sand and fines (this chapter).

Station 2 - The echo sounder indicated an acoustically soft sea bed. The samples collected are all well- sorted fine sands. Divers reported the presence of near-symmetrical ripples, with broadly shore-parallel crestlines,

TABLE 6.1

DETAILS OF BED SEDIMENT SAMPLES TAKEN BY DIVERS

Sample Identifiers	MOMENTS Mode	Mean	SD	SK	K	FOLK Mean	SD	SK	K
25-4-88 Barmouth Bay									
Station 1 sample 01	0.55	0.800	0.709	0.794	3.75	0.757	0.696	0.134	1.101
02	2.55	2.351	0.468	-0.607	4.345	2.352	0.443	-0.247	1.168
03	2.355	2.198	0.72	-0.841	4.665	2.327	0.718	-0.107	1.55
Station 2 sample 05	2.35	2.063	0.514	-0.494	3.73	2.091	0.494	-0.299	1.23
06	2.35	2.29	0.359	0.132	3.748	2.309	0.355	-0.137	1.31
07	2.45	2,268	0.406	-0.248	3.819	2.271	0.395	-0.216	1.281

continued	%fines	%gravel
Station 1 sample 01	0.64	64.64
02	2.03	13.36
03	66.76	2.97
Station 2 sample 05	1.14	0.49
06	1.59	0.28
07	1.92	0.23

wavelengths of approximately 0.25 - 0.3m, and heights of 0.05 - 0.1m. Visibility was limited to below 2m. Sample 05 was taken directly beneath a 2m scaffolding cube (into which was fixed an Interocean S4 current meter, which unfortunately produced no data after a 2 week deployment), and samples 06 and 07 taken 15 and 30m respectively away from the cube on a bearing of 200degrees.

Deposition rates

Data were taken also concerning deposition rates and depth of disturbance in this area, by the use of six bed-level indicators. Each consists of an aluminium rod 1m long and 1cm in diameter, which were pushed into the bed to a depth of approximately 0.4m. The relative level of sediment was then recorded by placing an aluminium disc (diameter ~6cm) over the pole to sit flat on the bed, and above the disc a clip was attached to stop the disc moving vertically upwards.

The six rods were placed in a line (aligned 020 - 200degrees) at horizontal displacements of 0, 5, 10, 15, 20 and 30m. With net deposition over time the disc will be buried, and with net erosion over time the disc will fall relative to the fixed clip, hence examination of these indicators after a period of time can reveal the time-averaged net rate of deposition or erosion that occurred. Similar rods have been successfully used by Hunter et al (1988) in their studies of nearshore ripple bands.

After deployment for a week the changes in bed level were :

at 10m - the disc was 2cm beneath the clip, i.e. 2cm of erosion had occurred;

at 15m - the clip was at bed level but the disc was lying below 2cm of sediment, i.e. over one week bed levels had decreased by 2cm and then increased again to the original level.

What these results demonstrate is that sediment of this size (~2.3phi) is mobile during normal current conditions, i.e. that sediment transport thresholds are exceeded. The near-symmetrical bedforms are interpreted as either wave- or combined-flow ripples, due to their symmetry and their alignment parallel to the prevailing wave crests (see Chapter 1). In this environment, it is likely that spot samples of the surface sediments will sometimes recover the mobile sediment cover, and sometimes the relatively immobile coarse lag material, or a mixture of the two. The large difference between for example, samples 01 and 02, provides a gauge of sample variation over a short distance, with a full 2phi difference in their mode and mean grain size, and completely opposite sense of skewness.

6.4 Barmouth Bay - Grain Size Analysis

Methods

There is no method of measuring grain size which will measure the whole range of sizes, from muds, to silts, sands and gravels. There are also great problems in integrating grain size data from different size fractions, particularly in the stability of the statistics used to describe the whole distribution. Thus, effort was concentrated upon the sand fraction, which dominates the surficial sediments of both Barmouth Bay and the Mawddach Estuary; in this study there is no size analysis of the fine sediment. However, the spatial distribution of concentration of the mud and gravel fractions has been analysed, and contributes greatly to the interpretation of the data.

After initial wet sieving, through 63um sieves, the coarse fraction of each sample was dried and dry- sieved through a 2mm (-1phi) sieve. Thus the first distinction made between samples was the weight proportion of grains <63um, >63um and <2mm, and >2mm; here, respectively referred to as fines, sand and gravel. Only the sand fraction in this study corresponds to a term in the Udden-Wentworth scale; 'fines' includes both silt and clay divisions, and 'gravel' used here includes granule and pebble divisions. No sediment of cobble or boulder size (i.e. >64mm) was present in any collected samples. The weight percentage of the fine, sand and gravel fractions have been plotted as contoured maps of the sea-floor. Sample stations are marked by a cross (Fig. 6.3). It is important here to note that the division of grain size fractions (63um and 2mm), are directly measured intermediate sieve diameters, not derived from fall velocity data.

6.4.1 Gravel Fraction (Fig. 6.4)

Weight percentages of grains >2mm in each sample varied between 0% and 58%. Notably high were samples 402 and 406 at 57.7% and 49.6%

Fig. 6.3 Barmouth Bay - Sediment Grab Sample Stations

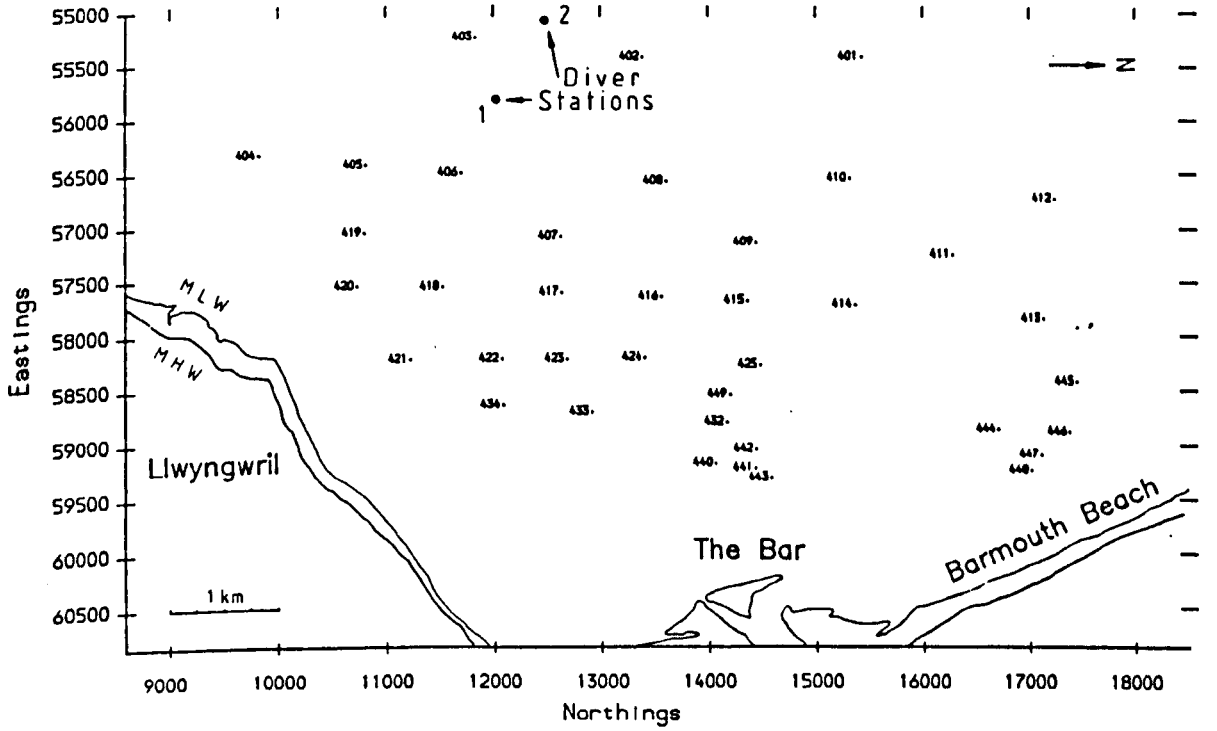

Fig. 6.4 Barmouth Bay - Sediment % wt > 2.0mm (gravel)

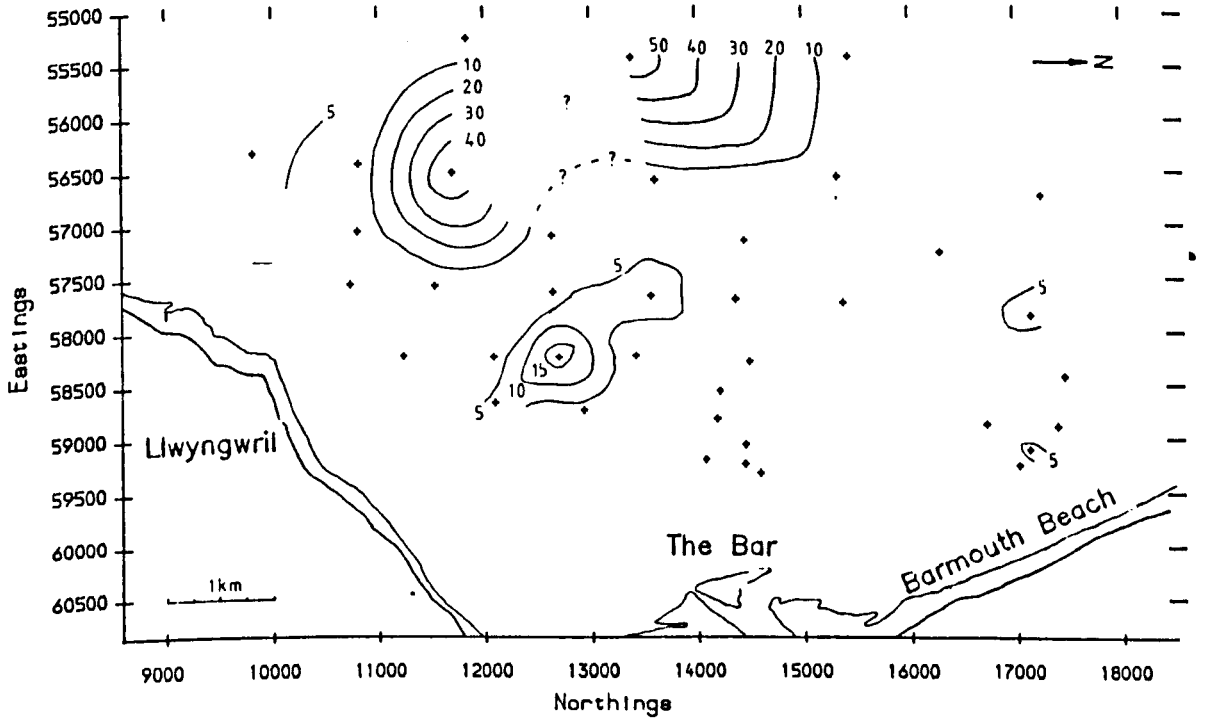

respectively, and a sample taken at 55840 12026 by divers (Station 1, sample 01) contained 64.6% gravel, so the area 5km SW of the bar has high concentrations of the gravel fraction. Another sample (No. 423), 2.5km SW of the bar had 16.5% gravel. Most of the samples contained less than 1% gravel, this often being shell debris.

An area 3.5km W of the bar of approximately 2km^2 has very low concentrations of gravel, below 0.2%, as do samples 420 and 421 off Llwyngwril. There is an overall trend of decreasing gravel percentages landwards, but the distribution pattern is very much one of restricted peaks above a base level of below 1%.

6.4.2 Sand Fraction (Fig. 6.5)

Virtually all the samples contained 80% - 99% sand-sized grains, except samples 402 and 406, with 41.1% and 49.3% sand respectively. An area 2.5km SW of the bar has relatively low proportions of sand, down to 80.6% in sample 423. The base level of percentage sand in the bay is above 95%, with a majority containing 97- 98%. The diver sample from Station 1, sample 01 contained just 34.7% sand.

6.4.3 Fine Fraction (Fig. 6.6)

All the data is very low, between 1 and 3%. Between 2 and 3km offshore there is a N-S trending area >3lm long, where the fine fraction consists of up to 3% of each sample. Seaward of this is an area approximately 3km by 2km where all the data is between 1 and 1.5%. There is more variation (i.e. more contours) in the shoreward part of the sampling area.

6.4.4 The Sand Fraction - Detailed Grain Size Analysis

Below are presented the results of detailed grain size analysis, using the fall tower, of the sand fraction of each sample. They are presented as a

Fig. 6.5 Barmouth Bay - Sediment % wt 0.063 - 2.0mm (sand)

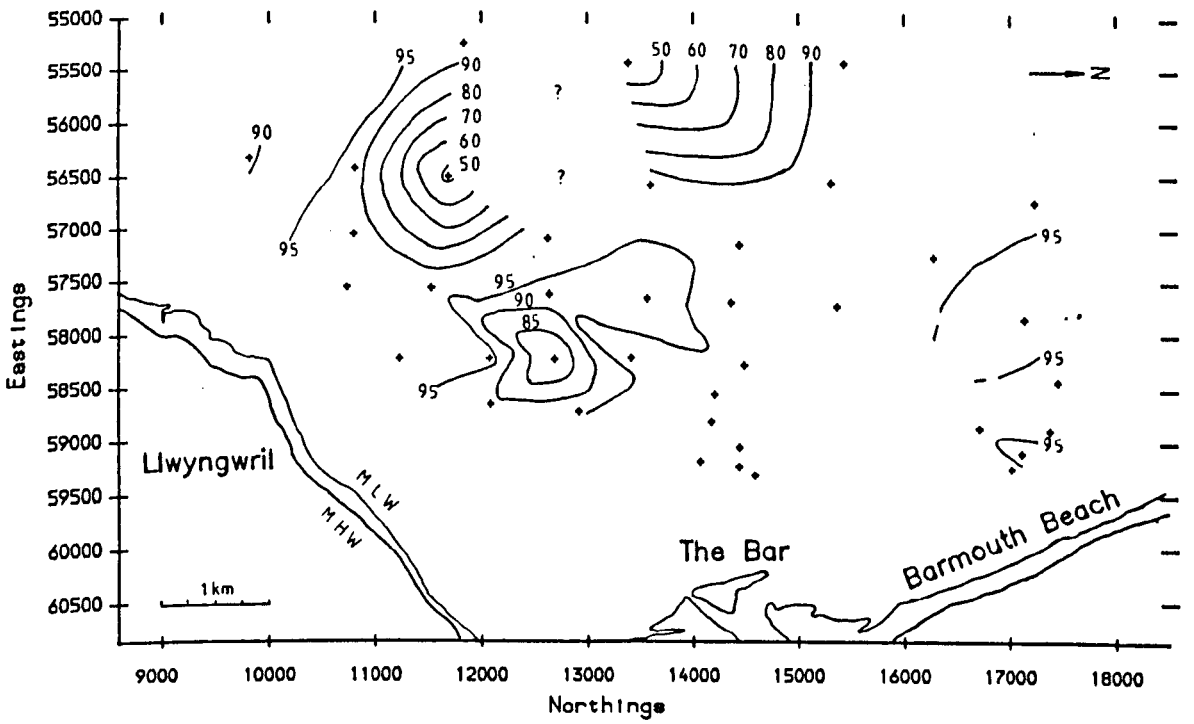

Fig. 6.6 Barmouth Bay - Sediment % wt < 0.063mm (silt, mud)

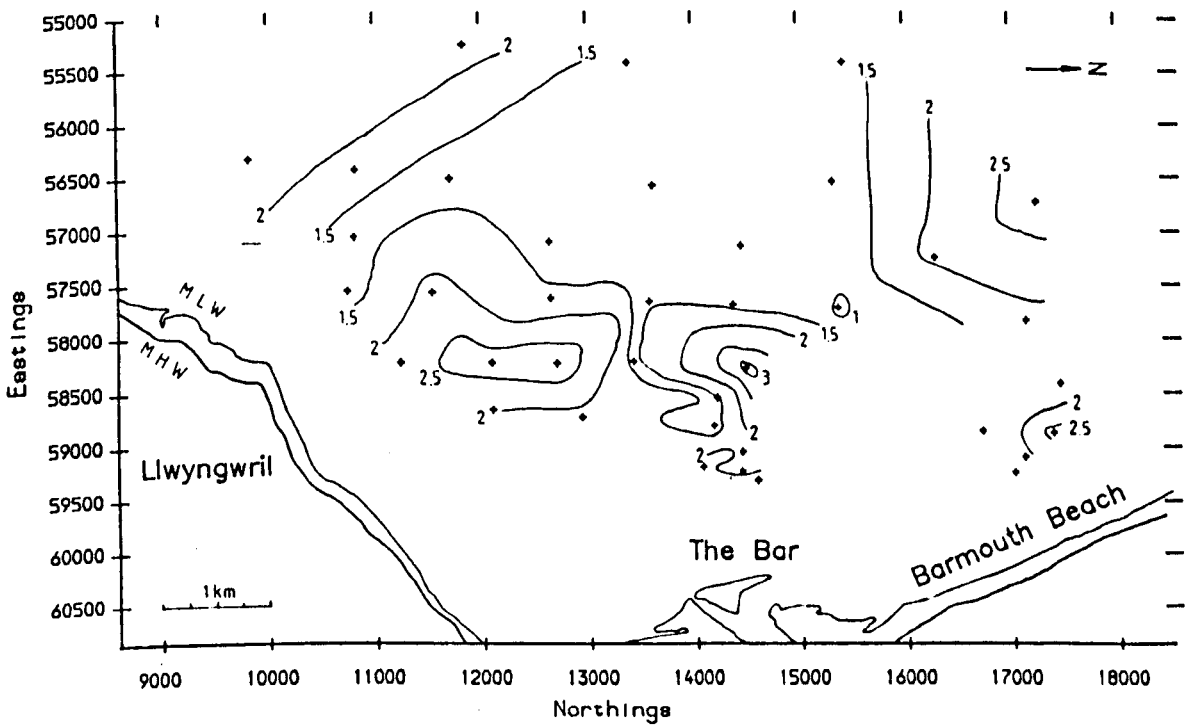

series of contoured maps. The maps show spatial variations in grain size parameters, but it should be remembered that the the grain size distribution has been derived from a distribution of fall velocity, and so reflects hydrodynamic size rather than the physical size. Numbers in brackets indicate sample numbers.

6.4.4.1 Mode Distribution (Fig. 6.7)

The peak mode of the samples varies between 1.65 and 2.85phi, being coarsest at medium sand size 4km W of the bar (sample 408) at 1.65phi, and 1.95phi 1km off the coast at Llwyngwril. The finest mode occurs off Barmouth Beach, at 2.85phi and 1km to the W of the bar at 2.75phi. Broad trends shown in the data are that the shoreward side of the sampled grid has modes fining northwards. In the central and north of the area, there is a shoreward fining tendency. There is a 0.5- 1km wide belt of relatively constant mode running between the SW edge of the area for 4km NE towards the bar.

6.4.4.2 Mean Distribution (Fig. 6.8)

Data varies between 1.8 and 2.67phi and, like the mode, is coarsest at 4km to the W of the bar (408) and off Llwyngwril (420, 419) at 1.80 and 1.86phi respectively. It is finest at 2.67phi (fine sand) 1km off the bar (440). There is an overall shoreward fining trend in th central and north of the area, and a weak fining SW to NE from Llwynwril to the bar.

6.4.4.3 Sorting Distribution (Figs. 6.9, 6.10)

(a) Moments - all samples in the bay have sorting between 0.35 and 0.62phi i.e. very well-sorted to moderately sorted. Sorting is best in the northern central part of the area, 5.5km WsW of the bar (403) and off Llwyngwril, both at <0.4phi. the sorting is worst 1km W of the Bar at 0.61phi (442) and 1.5km SW of the bar (422) at 0.62. There appears an ill-defined (bearing in mind the 95% confidence limit on the data of

Sand Fraction

Fig. 6.7 Barmouth Bay - Mode grain size (phi)

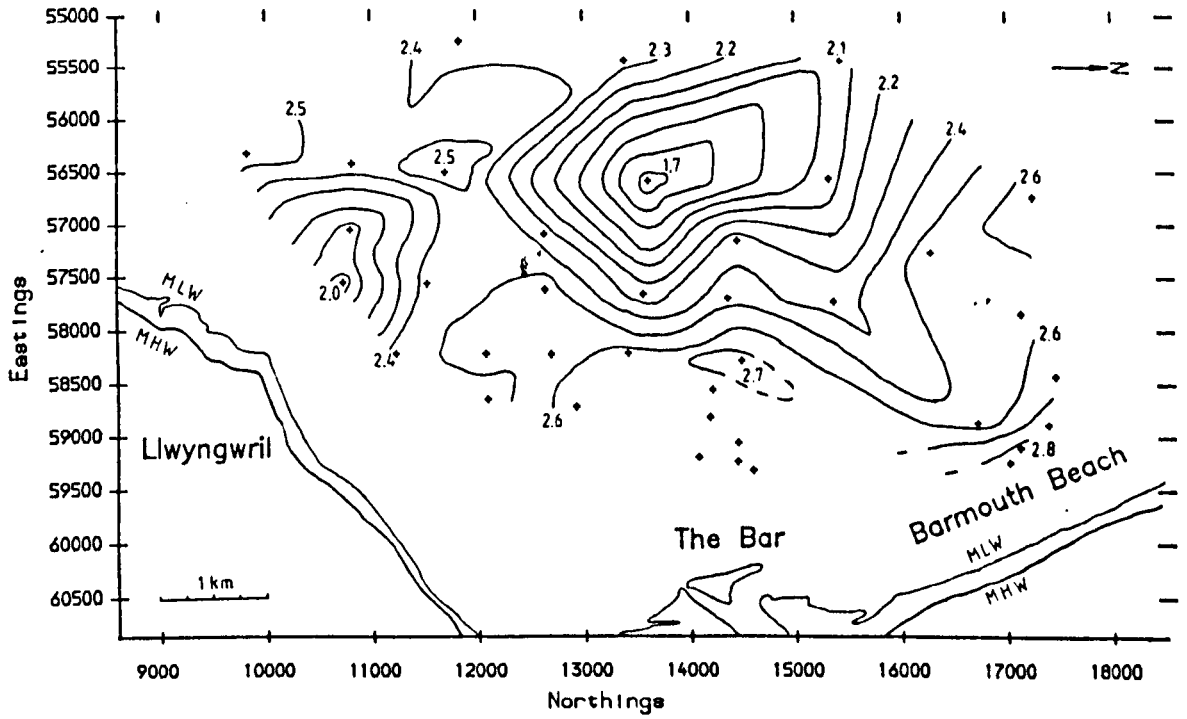

Sand Fraction

Fig. 6.8 Barmouth Bay - Mean grain size (phi)

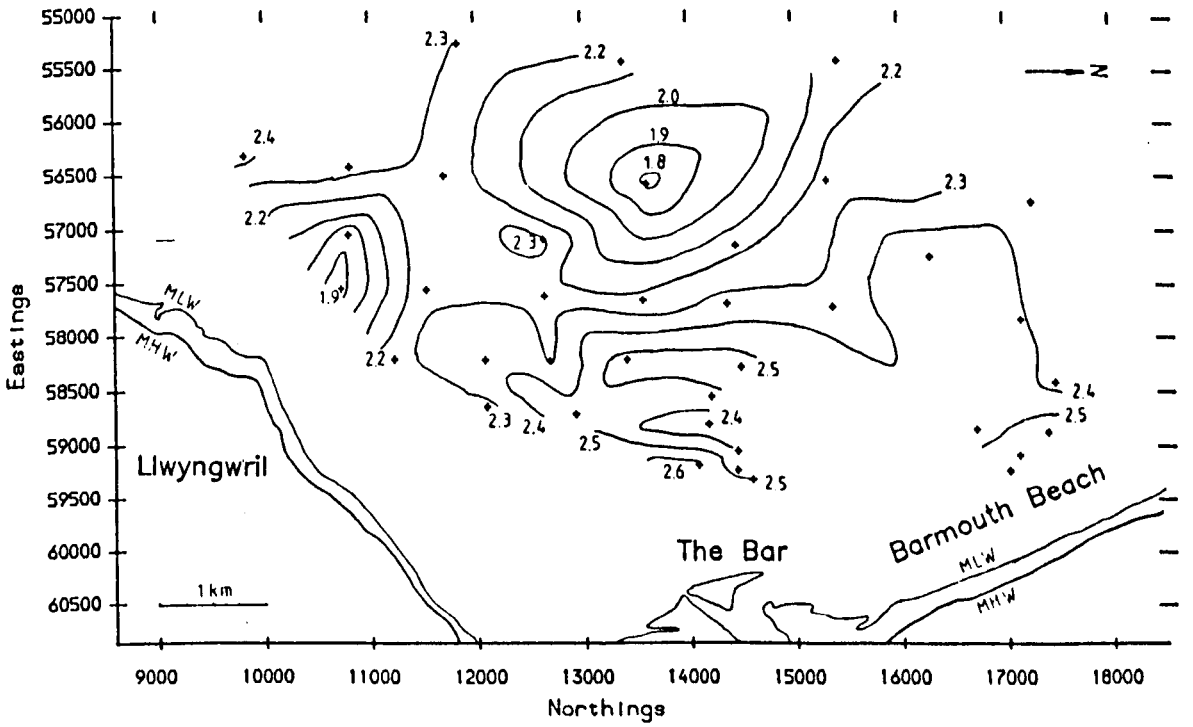

Sand Fraction

Fig. 6.9 Barmouth Bay - Sediment sorting (phi) - (moments)

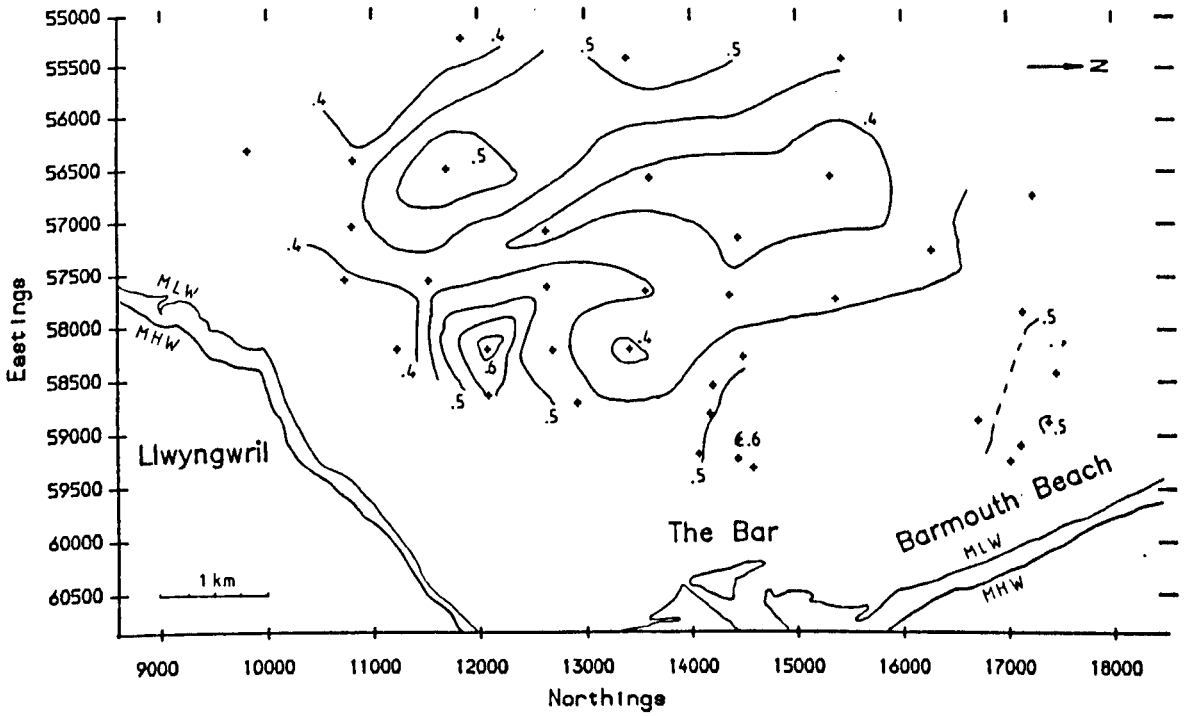

Sand Fraction

Fig. 6.10 Barmouth Bay - Sediment sorting (phi) - (Folk)

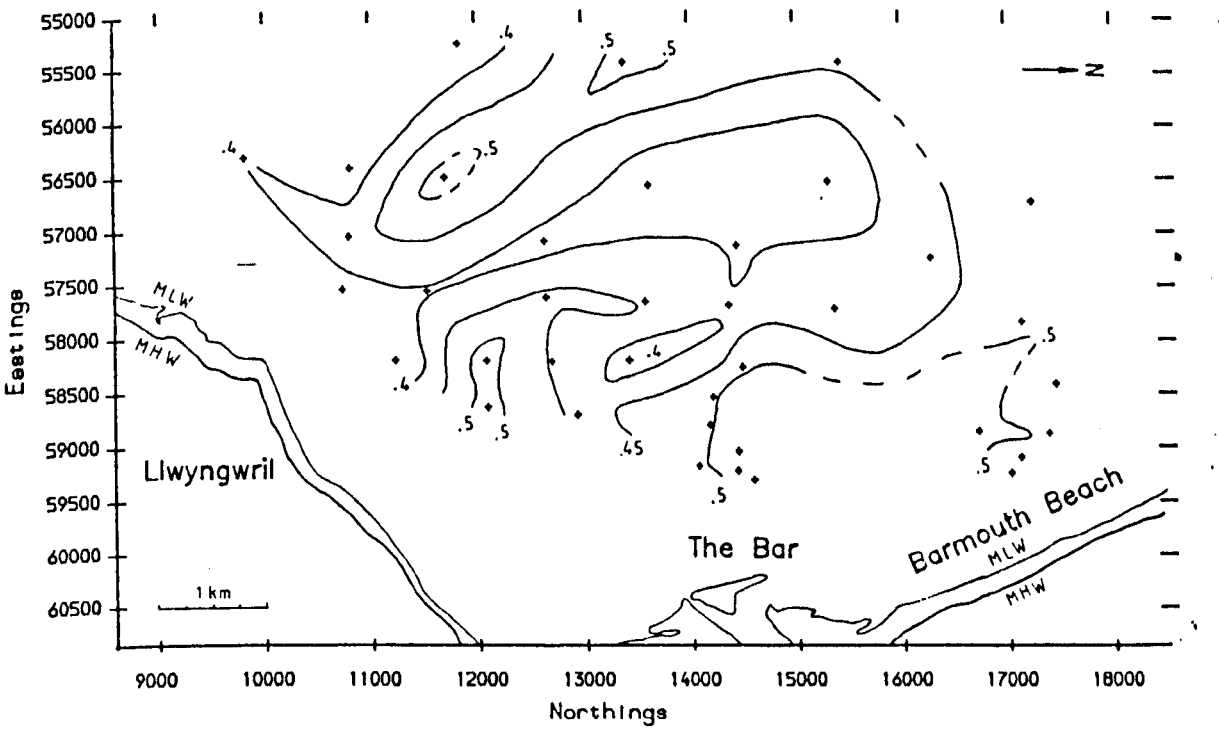

approximately +/-0.08phi) N-S elongate belt af well- sorted sand, which may extend SW to include sample 402 (there is insufficient data to determine this).

(b) Folk & Ward - the map is very similar to the moments sorting map, both in contour positions and contour shape.

6.4.4.4 Skewness Distribution (Figs. 6.11, 6.12)

(a) Moments - the sand fraction skewness varies between -1.64 and +0.47, i.e. very negatively-skewed to very positively-skewed. Skewness is most negative at 1.5km SW of the bar and in a belt extending from the bar SW to the edge of the grid. Skewness is negative over the majority of the bay, with the only positively- skewed area in the NW of the area, >2km W of the bar (408, 410). One sample (403) in the extreme west also has a positive skew.

It is particularly important, in this case, to recall the above described data replication results. The estimated 95% confidence limits of +/-1phi mean that this plot must be treated with suspicion. Broad trends shown in the data are tendencies, for increasing negative skewness southwards and shorewards. Individual samples which show markedly different skewness values may represent reality, an effect of the heterogeneous nature of the bed, or size measurement errors.

(b) Folk & Ward - Skewness values calculated by this method are of lower magnitude than calculated by the moments method (Dyer (1986) states it is 0.23 times as much) and vary between -0.44 and +0.13. A very similar contour pattern is shown, with areas of +ve and -ve skew broadly in the same areas as the moments map. the confidence limits are approximately +/-0.1, so the similarities between the two maps suggest that the true skewness distribution is as shown, certainly in terms of broad trends.

Sand Fraction

Fig. 6.11 Barmouth Bay - Sediment skewness (phi) - (moments)

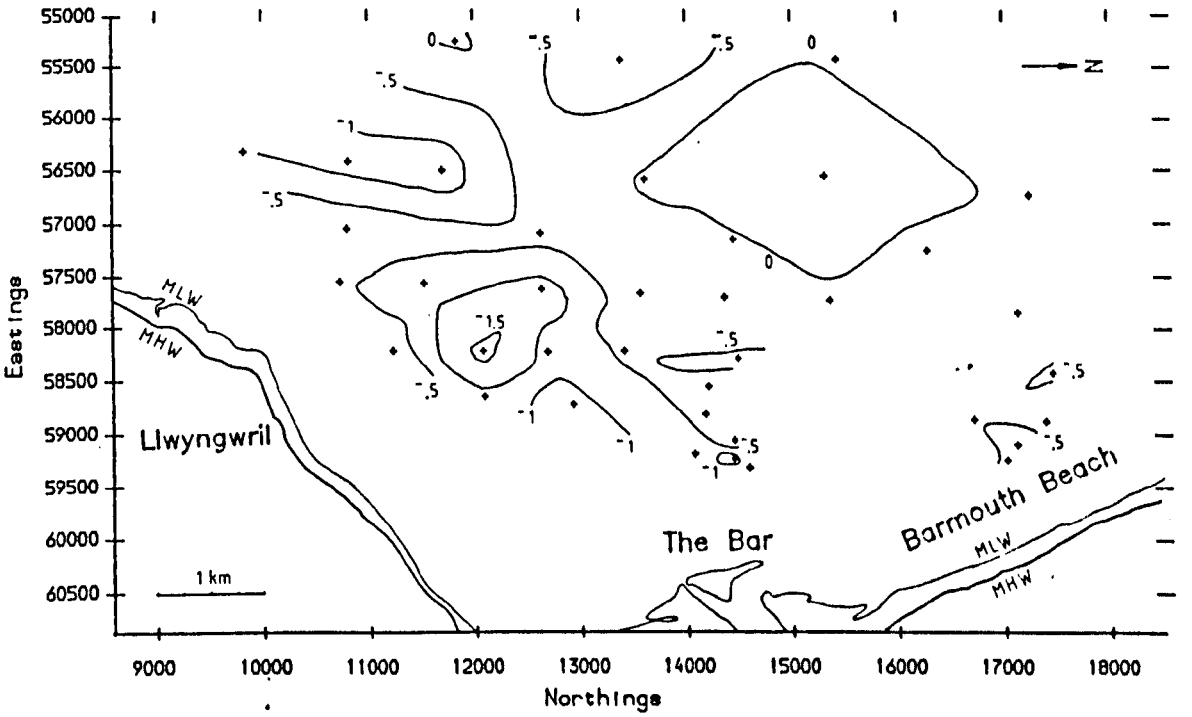

Sand Fraction

Fig. 6.12 Barmouth Bay - Sediment skewness (phi) - (Folk)

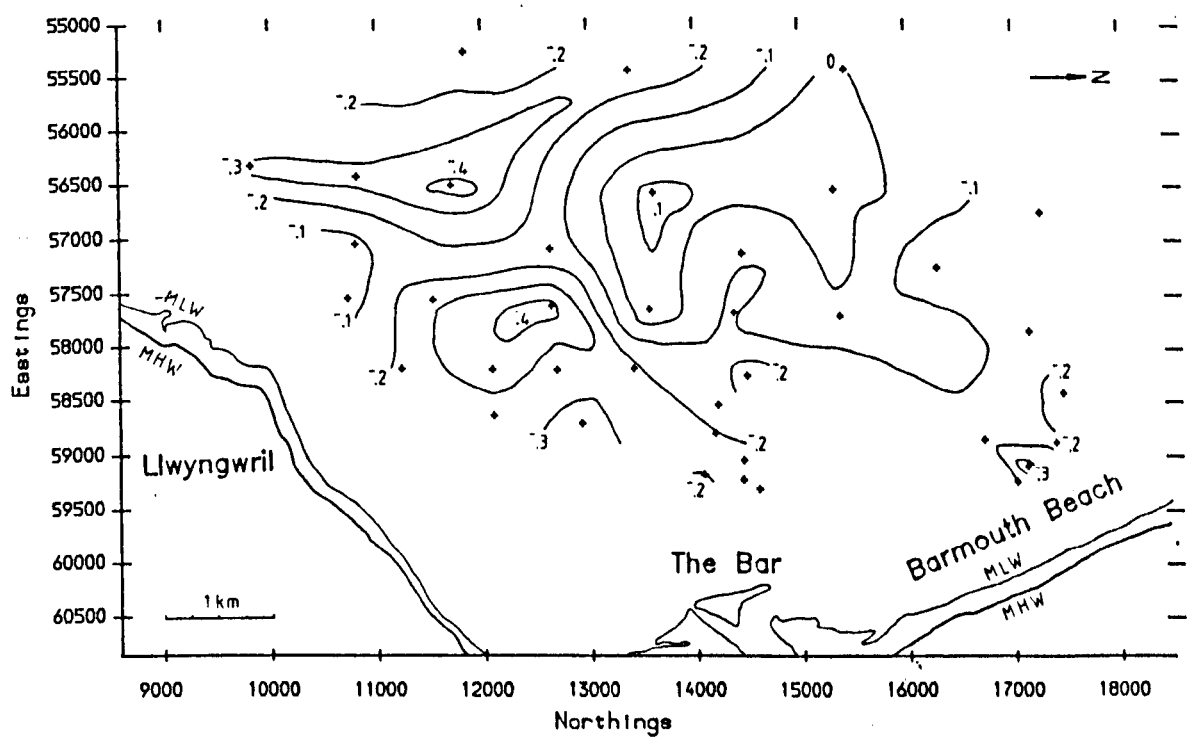

6.4.4.5 Kurtosis Distribution (Figs. 6.13, 6.14)

(a) Moments - Kurtosis varies between 2.52 and 7.59 (a Gaussian distribution will have a value of 3). It is highest, (i.e there are a surplus of extreme sizes) in the far SW of the area (405) at 7.59 and at one point (422) 1.5km SW of the bar at 6.17. Low values of kurtosis (i.e. a deficit of extreme sizes) occur in the NW of the area at below 3, and at 0.5km W of the Bar (442, 432) at 2.52 and 2.61.

The vast majority of kurtosis values are above 3, and in the west of the area there is a southward trend of increasing kurtosis. The error bars are +/- 0.6 so the trend is a true one. Extending from the SW extreme of the area 3.4km towards the bar there is a weakly- shown strip of sea bed where the sand fraction kurtosis is above 4.5.

(b) Folk & Ward - These values vary between 0.884 and 1.842. The general contour pattern is similar, but also shows a high kurtosis area 1.25km W of the bar.

6.4.4.6 Initial Interpretation

One of the aspects most strongly shown in the data is the low concentrations (<3%) of grains below 63um. This implies that any fine-grained sediment transported into the bay may not be subject to currents weak enough to allow deposition to take place. There is no evidence that there is a lack of available fine-grained sediment in Cardigan Bay and its estuaries, as samples taken on the extensive saltmarshes near Penmaenpool in the Mawddach Estuary contain up to 95% sediment finer than 63um (Transect 1, sample 01, 26-4-86). Such saltmarshes are extensive in the estuaries of the Mawddach, Dwyryd (Mahamod, 1989) and Dovey (Haynes & Dobson, 1969). In Tremadoc Bay, the central bathymetric depression of approximately 10 by 5km has surficial sediments finer than medium silt (Marine Science Laboratories, 1976). This is a reflection of the low tidal and wave energy levels in central Tremadoc Bay.

Sand Fraction

Fig. 6.13 Barmouth Bay - Sediment kurtosis (phi) - (moments)

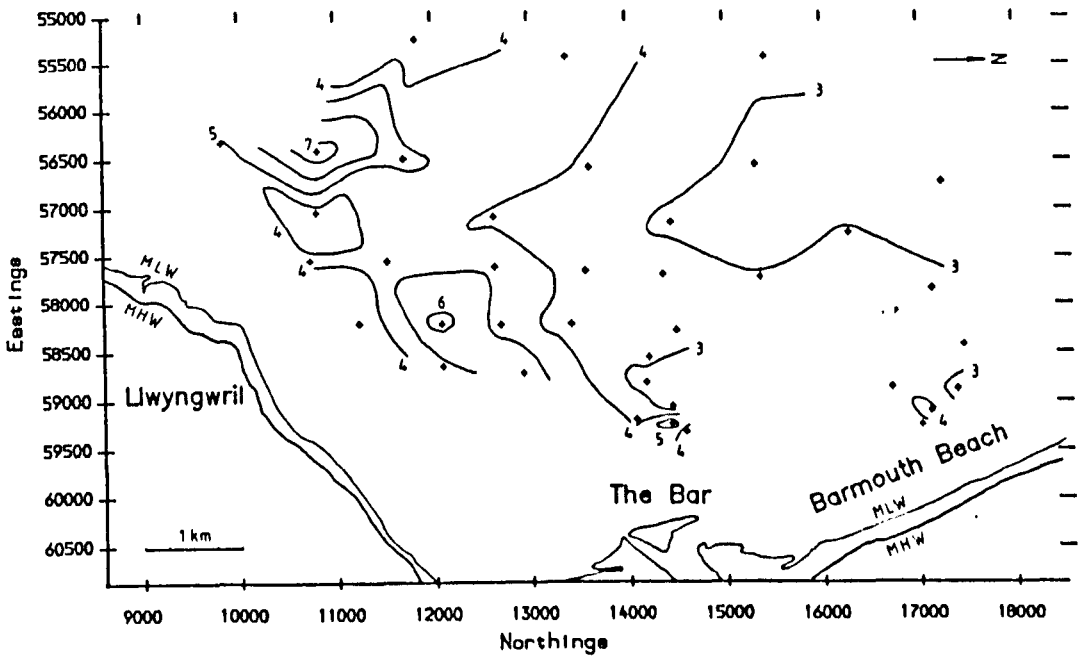

Sand Fraction

Fig. 6.14 Barmouth Bay - Sediment kurtosis (phi) - (Folk)

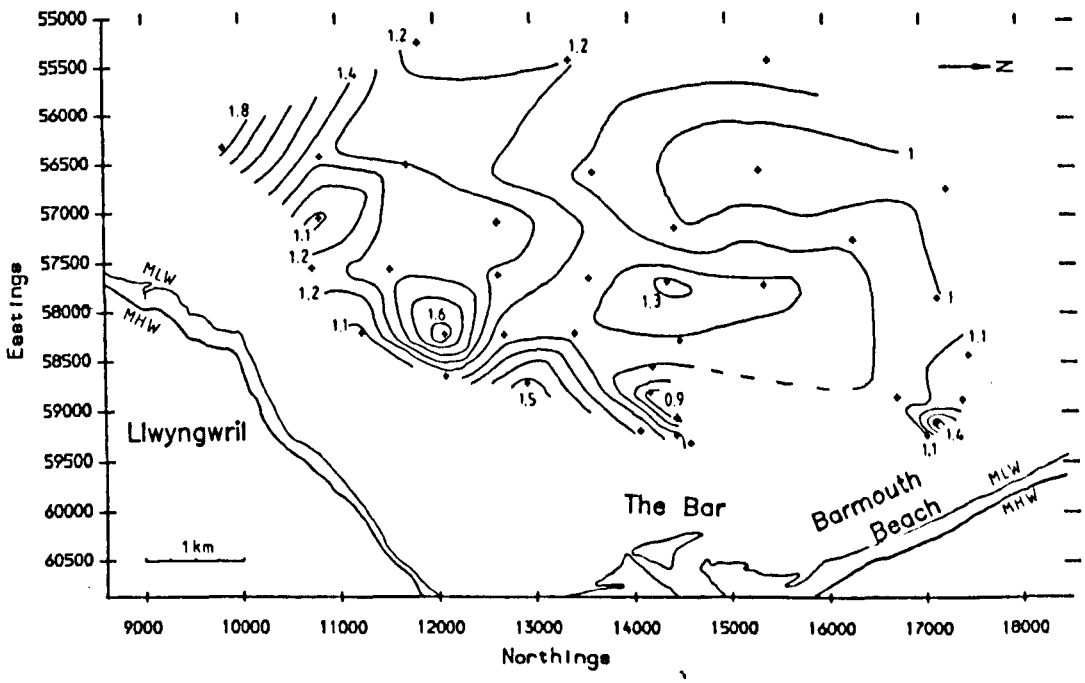

The proportions of sand in the sediments of Barmouth Bay are very high, implying sand-sized material is most in equilibrium with the energy regime of the bay. The three main estuaries of Cardigan Bay contain much sand, as do the beaches fringing the bay, and the dune systems of Morfa Harlech and Morfa Dyffryn in northern Cardigan Bay. The sea bed sediment survey of Moore (1968) showed that much of inner Cardigan Bay, between Aberystwyth and Harlech, has mobile sand at the surface. Gravel concentrations are generally low, and grains coarser than 2mm are either fragments derived from pre-existing rocks, or biogenic material comprising disarticulated or broken shells.

This would suggest that hydrodynamic conditions in Barmouth Bay are 'in equilibrium' with the fine sand sized bed. However, tidal and wave energy are high enough to transport fine sand at all stages of the spring-neap cycle. Certainly the very fast tidal currents in the Mawddach Estuary are capable of transporting medium and coarse sand, and locally gravel, and are not representative of the fine sand which dominates the estuarine sediments. Thus, energy levels are inconsistent with both muddy or gravelly sedimentation, neither fully consistent with fine sand accumulation, so the supply of fine sand to the coastline must be partly source controlled.

6.5 Sediment Petrology

One method of examining the provenance of the sediments in the area and, hence, aiding interpretation of the grain size data, is by relating their petrology to the possible source areas and sediments. There are two main possible sources for the sediment, a local (Welsh) source and reworking of material transported into Cardigan Bay by the Irish Sea ice sheets. The petrological characteristics of Welsh and Irish Sea deposits were described in Chapter 1. Here, it is relevant that Welsh deposits are texturally relatively immature; they have a sand fraction dominated by lithic fragments. The geology of the Mawddach area (Chapter 1) suggests that grey-green metamorphics, quartzose schists and recrystallised sandstones would indicate sediments of a local origin. Irish Sea deposits contain marine sands, shell fragments and distinctive erratics, such as red sandstones, various limestones and flints.

6.5.1 Gravel Fractions

Eight sediment samples were analysed for the petrology of their gravel fraction. These were chosen mainly by position, to cover from the estuary head to the west of the samples in the bay. Sample positions can be seen on Figure 6.1. Each sample was viewed under a binocular microscope and its mineralogical and grain characteristics noted. At Penmaenpool, the sediment on the estuary bed consisted of an incomplete fine sand cover above a gravelly substrate. The data from both these sediment types are presented (A = gravelly substrate, B = fine sand). Results are tabulated in Table 6.2.

Table 6.2

Petrological characteristics of the gravel fraction of sediments from the Mawddach Estuary and Barmouth Bay.

Petrological characteristic	Sample: Llanelltyd Bridge	Maes-y-Garnedd P303	Penmaenpool A	Penmaenpool B
Clear Quartz	trace	5-10%	5-10%	70%
Fe-stained Quartz	15-20%	trace	-	10-15%
Vein Quartz	-	trace	-	-
Lithic fragments	>80%	>90%	>80%	<20%
Bioclastic "	-	-	-	trace
Grain size	<90mm	most >10mm	<0.5-0.7mm	<0.5mm
Sorting	poor	med-poor	poor	good
Roundness	rounded-v.angular	subrounded-v.angular	subrounded-v.angular	subrounded-subangular
Sphericity	med.-v.low	med.-low	(med.-)low	med.-high

Petrological characteristic	Sample: S401	S402	Spit04	Borehole 4 Depth 0.5m	Borehole 4 Depth 4.0m
Clear Quartz	trace	trace	-	trace	-
Fe-stained Quartz	15-20%	trace	trace	-	trace
Vein Quartz	-	-	<10%	<5%	-
Lithic fragments	>60%	-	~90%	-	~90%
Bioclastic "	10-20%	~20%	trace	trace	<10%
Grain size	<	<25mm	<30mm	most <6mm	<7mm
Sorting	poor	poor	poor	poor	med.-poor
Roundness	v.rounded-angular	v.rounded-subangular	v.rounded-v.angular	v.angular	subangular-v.angular
Sphericity	high-low (lithics)	high-low	med.(-low)	med.-low	med.-low

6.5.2 Grain Types

The grain types found in each gravel fraction are listed below, with a brief conclusion of their likely origin :

Llanelltyd Bridge - Vein Quartz, Fe-stained quartz, mica schists, slate, sandstone. Locally derived;

Maes-y-Garnedd (P303) - Acidic vein fills, micaceous and phyllitic schists, slate, quartz schists, very white granite, Fe-rich basic igneous rock, basic igneous rock with vesicles and amygdales. Sediment sample has an overall grey colour, with a very few red grains. Conclusion : locally derived;

Penmaenpool (mixture of A and B) - Vein quartz, mica schists, slate, acidic igneous rock. Conclusion : sample is mixture of quartz sand (marine) and locally derived gravel;

Spit04 - Quartz sandstones, vein quartz, acid igneous, green texturally immature Quartz sandstone, mica schist, red granite. Grey green schists predominate, very few red grains occur. Conclusion : sample is dominantly local material, but perhaps with some exotic material added (eg. red granite);

Borehole 4, depth 0.5m - slate, mica schists, meta- Quartz sandstone, basic igneous, Fe-oxide lumps (presumed weathered ferromagnesian minerals), one grain of fine-grained red felspathic sandstone. All grains look very freshly broken. Conclusion : most is local material; there is the possibility that some grains derive from building foundations on the end of Ro Wen. Thus, there may be anthropogenic influences upon sediment type within the estuary;

Borehole 4, depth 4.0m - Schists, quartz sandstone, and one grain each of white granite, pink granite, basalt and concrete ! Conclusion : as above for depth 0.5m;

Station 01 - Bioclastic grains (bored gastropod and bivalve fragments), vein quartz, red granite, quartz sandstone, red sandstone, immature red conglomerate (Felspar rich), gabbro-dolerite-basalt, and very few schistose grains. Red grains constitute >60%. Conclusion : not locally derived, very different to the estuarine gravel because of high concentrations of igneous rocks, red sedimentary rocks and bored bioclastic grains, and lack of metamorphic grains. Appears to be a mixture of local and Irish Sea ice derived material, but dominated by sediment of Irish Sea origin;

Station 02 - Vein quartz, red granite, acidic igneous, red sandstones, basalt, and a few mica schists. Red grains constitute >40%. Conclusion : as for S401.

6.5.3 Conclusion

The basic and important conclusion from these data is that the gravel fraction of sediment in the Mawddach Estuary has been derived from offshore areas, probably from reworking of sediments deposited by the Irish Sea ice sheet and associated post-glacial deposits. Given that the gravel is far less transportable than the dominant sand, it may be reasonable to assume that the sand has possibly have been derived from offshore. The reworked sediment has been moved landward within the estuary up to a limit between Penmaenpool and Maes-y- Garnedd, in agreement with the flow data (Chapter 2) and the calculated sediment transport data (Chapter 1).

6.6 Modal Behaviour

The spatial variation of the percentage frequency of the sand fraction modal classes is shown in Fig. 6.15. (Each modal class is 0.1phi wide). In the north of Barmouth Bay, the modal frequency is 10-12; these are marked contrast to the high and variable values in the south, which reach 20% (sample 405). There is a well-defined SW-NE trend of the high frequencies, with a decrease to the NE. This suggests two things :

1 - the sand in the south of the area (of the Patchy Sand Facies) is more mobile than in the north (Outer Sand Facies);

2 - the sand in the extreme SW is more 'in equilibrium' with the hydrodynamic regime than further N or NE.

The first suggestion broadly agrees with the conclusions drawn from the side-scan data presented in Chapter 1. The second is a far more tentative statement, because it is a continuation of the first and of the large task of defining what 'hydrodynamic regime' the sediments may be subjected to.

In the sediment samples collected from Barmouth Bay and the Mawddach Estuary, many showed more than one grain size mode in the sand fraction, i.e. more than one peak on the frequency curve. In Barmouth Bay the majority of samples were bimodal, with only 8 samples clearly unimodal (401, 403, 407, 409, 415, 418, 419 and 421). The unimodal samples occupy an area which is N-S elongate at an easting of 57000, and extends north from 10500 for 4.5km. The area is approximately 1km wide E- W, and has at its south end an easterly extension of at least 2km.

The above unimodal sand fractions all occur where there are < 2.5% fines present in the sample, < 1% gravel and > 97% sand. Hence where > 1% gravel occurs in the sediment the sand fraction is polymodal, so there may be a common source of gravel and polymodal sand. In addition, where there are > 2.5% fines the sand is also polymodal. So it may be implied

Fig. 6.15 Barmouth Bay - % frequency of peak modal class

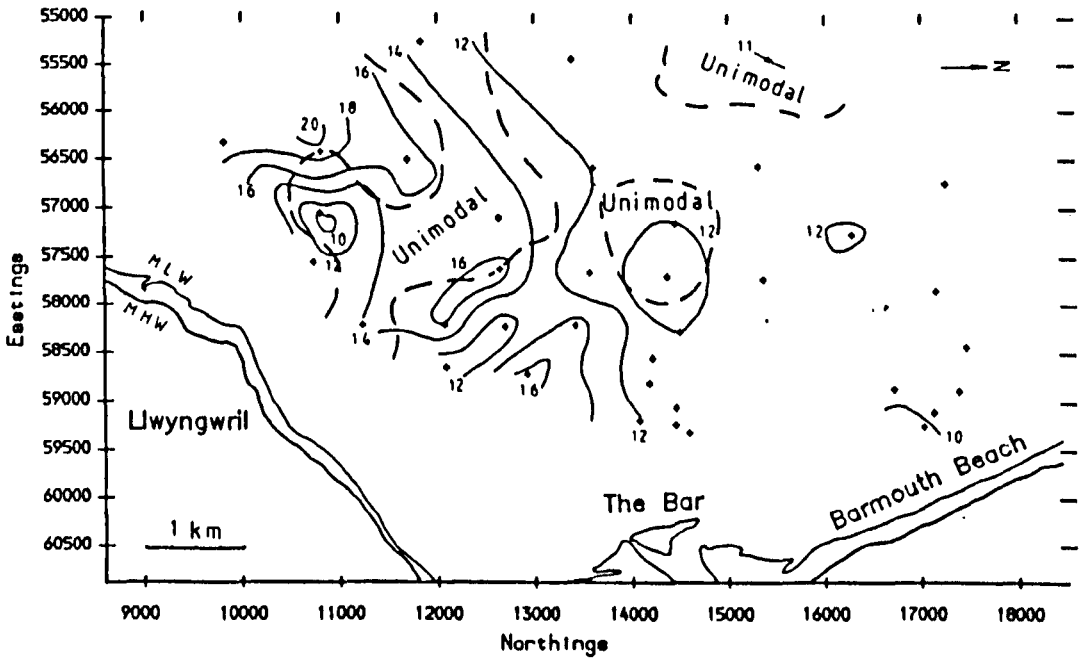

Fig. 6.16
Modal frequencies of the sand fraction

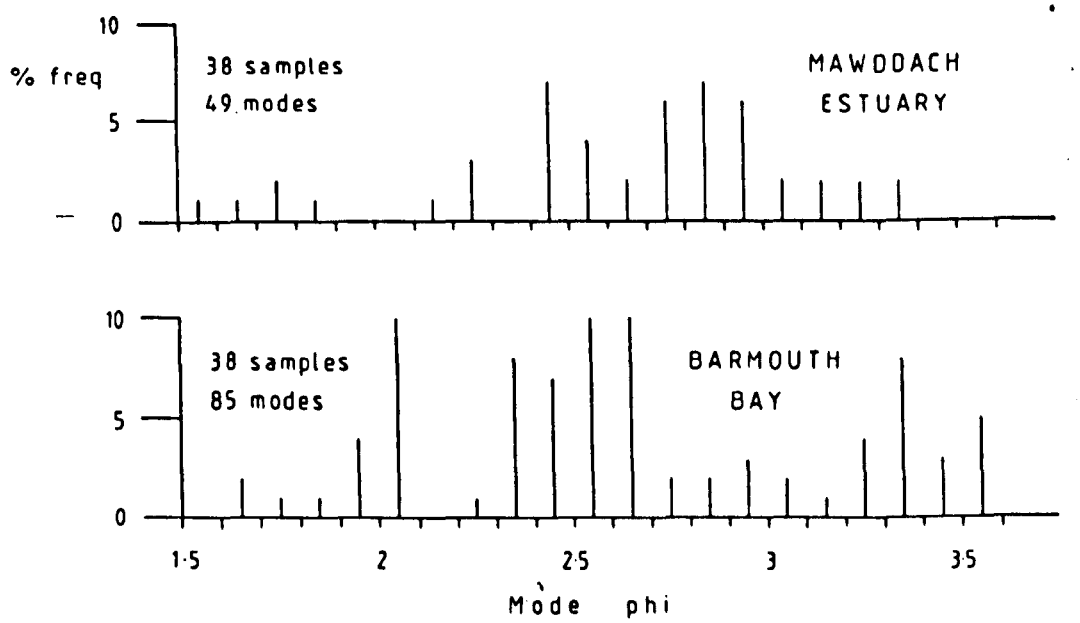

that there is a spatially common source of gravel, polymodal sand, and fines. Either there are closely associated separate sources of these grain sizes, or one very poorly-sorted sediment source supplying grains to the bay. (This implication inherently assumes that it is not the present-day hydrodynamic, i.e. transport factors which are dominant in producing the relationship of common occurence of these grain sizes. It is reasonable to suppose that such a characteristic of a sediment is highly unlikely to have been produced by the dominance of shelf hydrodynamic processes over other factors such as grain provenance. Hydrodynamic processes which cause sediment erosion, transport and deposition do not operate equally on all grain sizes. A current allowing incipient deposition of gravel would be too strong to allow deposition of fine sand or mud. Thus the implication of a source control is not an unfavourable one).

The distribution of modes present in the sand fraction of estuarine and bay sediments is shown in Fig. 6.16. (Estuarine sampling strategy and results are presented in Section 6.8). All the modes present are plotted, both primary and subordinate modes of each frequency curve. An initial indication of the common polymodality of the sand fraction in the bay in contrast to the estuary is the high ratio of total number of modes to samples in the bay.

The graphs show two marked differences, at 2phi, and between 2.75 and 2.95phi. The 2phi mode forms the modal class in 10% of samples in the bay, but is absent in the estuary. A possible explanation is that the hydrodynamic regime of the bay is insufficiently strong to mobilise this material, so it does not get transported into the ultimate coastline sink, the estuary. That the 2.75-2.95phi fine sand is dominant in the estuary, but is absent in the bay, may also possibly be explained in terms of the bay to estuary transport path. Hydrodynamic processes in the bay may have preferentially removed these sizes of sand from the bay, and transported it down the sediment transport path into the estuary. Once in, it is slowly

transported landward, but, until this sand is accumulated in less dynamic conditions, either in the uppermost estuary, or on sandflats bordering the main estuarine channel, it does not reflect the overall high current regime of the estuary.

From the modal data the three most common modes in the bay, 2.05, 2.55, and 3.35phi, were chosen for consideration of their distribution in Barmouth Bay. The percentage fraction of these modes are shown as contoured maps, discussed below.

6.6.1 2.05phi Mode (Fig. 6.17)

This mode is of fine-medium sand, and the percentage of this fraction varies between 2 and 11%. It is most prevalent 5.2km SW of the bar (419), for over 2km E-W at northing 15500 on the seaward edge of the area (401, 410), and 1.25km WSW of the bar (416). In broad terms the central, NW and extreme SE of the area have the highest proportions of this mode. Lowest concentrations are near Barmouth Beach (447) and at the SW extreme of the area (404). There is also a belt of low percentages extending from the SW towards the bar.

There appears more variation in the proportion of this mode in the SE, but this may in part be caused by the variable sample interval. If real, it might imply a more spatially uniform hydrodynamic regime in the NW, and/or deposition or transport in the NW in contrast to localised erosion in the SE. The contoured map suggests that the isolated samples with high percentages of this mode may be sources of this mode to the bay.

6.6.2 2.55phi Mode (Fig. 6.18)

These grains are of fine sand size, and their percentage varies between 1.5% and 18.5%. High proportions are found in the extreme SW (404), and from there NE towards the bar. Low proportions are present 4.5km SW of the bar (419, 420) and between 2.4 and 4km W of the bar (408, 416). the distribution suggests a fairly widespread mode with, low proportions

Fig. 6.17 Barmouth Bay - distribution of 2.05 phi mode (%)

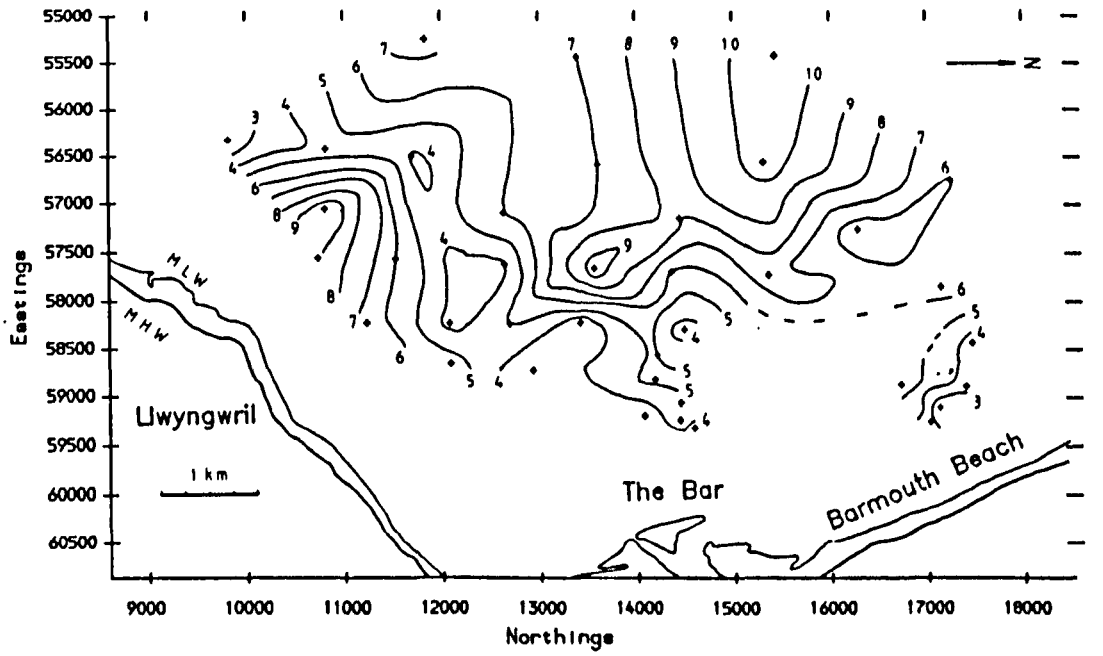

Fig. 6.18 Barmouth Bay - distribution of 2.55 phi mode (%)

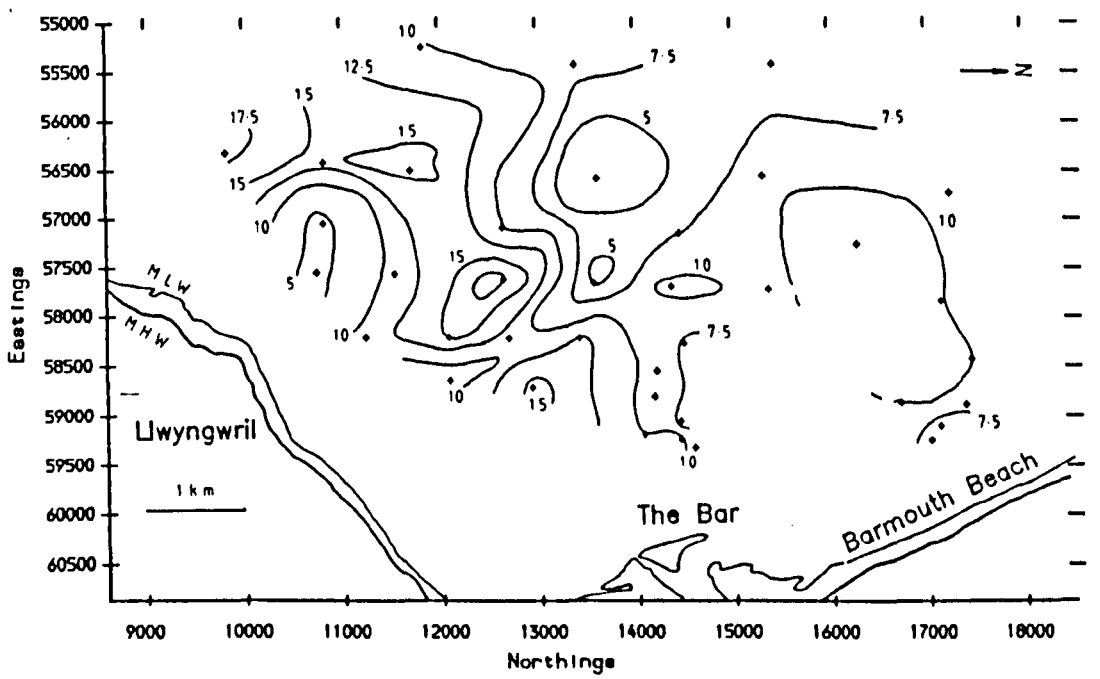

only local features. If the above hypothesis regarding local points of sediment supply is correct, it may suggest that the source contains little of this grain size.

6.6.3 3.35phi Mode (Fig. 6.19)

The percentage of this very fine sand mode varies between 0 and 10%, however the 10% value was found in only one sample (410) 4km WNW of the bar, and all other values are below 4%. Locations with high percentages (i.e.approaching 4%) are 2km W of the bar (425) and towards Barmouth Beach (448). The SW quadrant of the sampled area has only 0 - 0.5% of this mode, and this area is bounded in its southern part by the -11m ODN contour.

The pattern of variation of this mode is very similar to that of the percentage of fines in the total sample (Fig. 6.6), so that fine sand and finer grains are most common within 3km of the shoreline. This is surprising considering that the effect of waves on the bed increases shorewards (Chapter 1) and is likely to maintain fine grains in suspension rather than allow their deposition, so another factor may be involved in the control of distribution of fine sediment. The N-S aligned group of samples with < 3% fines corresponds to the position of a similar feature in the 3.35phi mode map, perhaps suggesting an eroding source of fine sediment there. Correspondence of this feature in these diagrams is a qualitative indication of the reliability of the grain size data derived from the fall tower.

6.7 Dowling Plots (Figs. 6.20 - 6.25)

A series of plots of the type presented by Dowling (1977) have been drawn for a number of transects in Barmouth Bay; four shore-perpendicular, three shore- parallel and one between the bar and the SW extreme of the surveyed area. Dowling (1977) noted that comparison of grain size distributions by analysis of derived statistical parameters can sometimes mask subtle variations within the data. By presenting data as a contour map of the space - frequency size domain along profiles of interest, he suggested that a qualitative comparison can be made of the complete distributions, enabling variations to be observed more easily than by viewing numerous size frequency diagrams. These plots represent the grain size distribution as a function of spatial displacement.

6.7.1 Results

The shore-perpendicular plots (Figs. 6.20 & 6.21) all show an overall seaward coarsening of the sand fraction in both 3% contours and modal size, but with some scatter. Some modal behaviour occurs in the samples nearest the coast but the modal sizes involved are different. They do, however, tend to occur in the finer fractions of each sample, and the N-S transect 1km west of the bar (Fig. 6.22) shows a consistent modal fraction at 3.4phi, although the frequency of this mode is below the 3% level in some samples and so is not shown on the diagram.

Modal percentages are generally low, but reach >15% at 13000N, where there is also a lack of 1.5 - 2.0 phi sediment in the coarse tail. The next seaward N-S transect (Fig. 6.23) shows these features at the 12000N region, and still further seaward the same is shown south of 11000N, where modal percentages reach >18%.

The N-S transect plots show a trend of southwards increasing modal frequency. In the bay, there appears to be a continuum of grain sizes over

Fig. 6.20 Dowling plots showing change in grain size distribution;

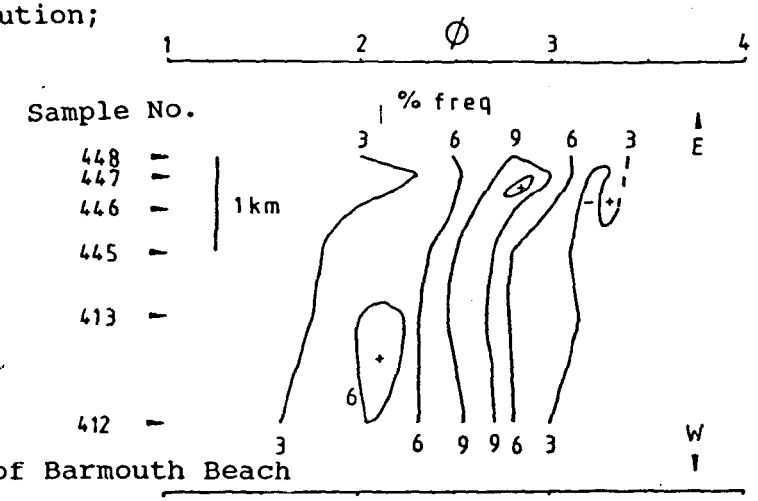

a) W of Barmouth Beach

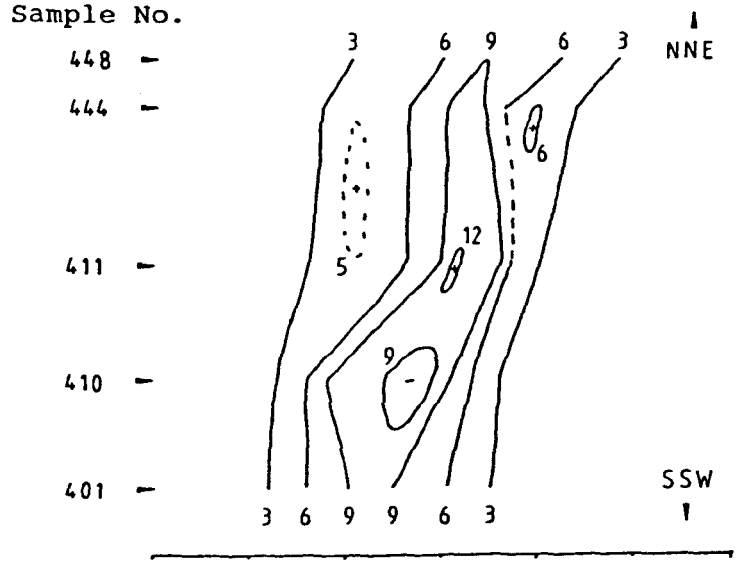

b) SSW from Barmouth Beach

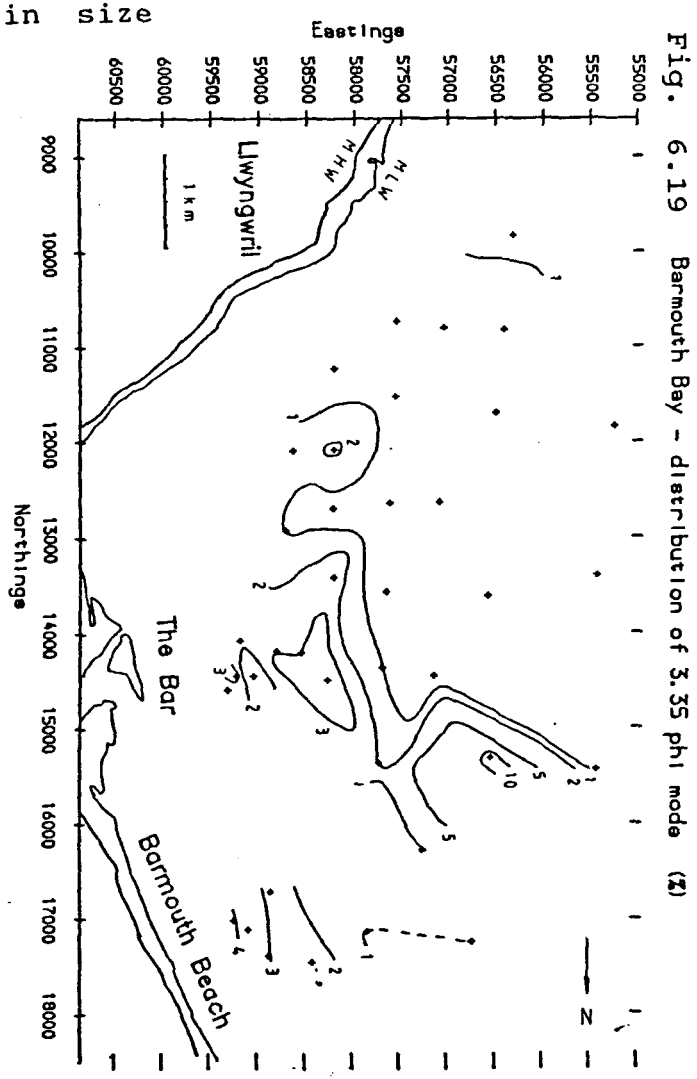

Fig. 6.19 Barmouth Bay - distribution of 3.35 phi mode (%)

Fig. 6.21 Dowling plots showing change in grain size distribution;

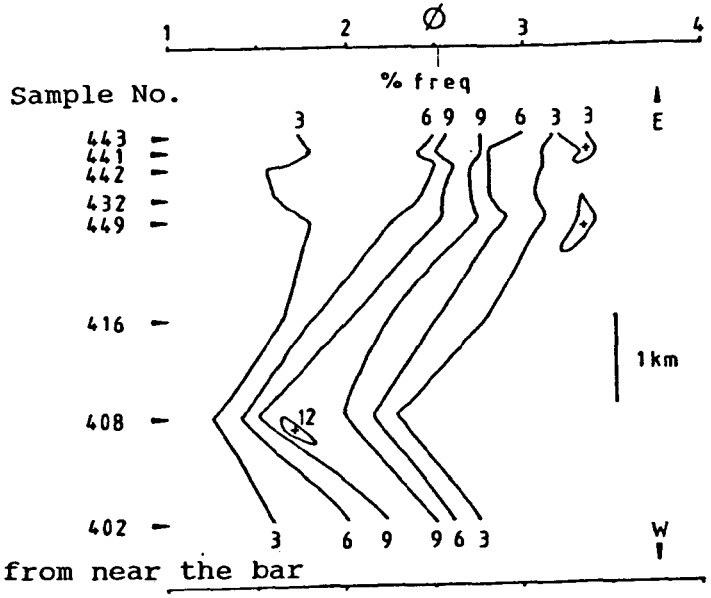

a) W from near the bar

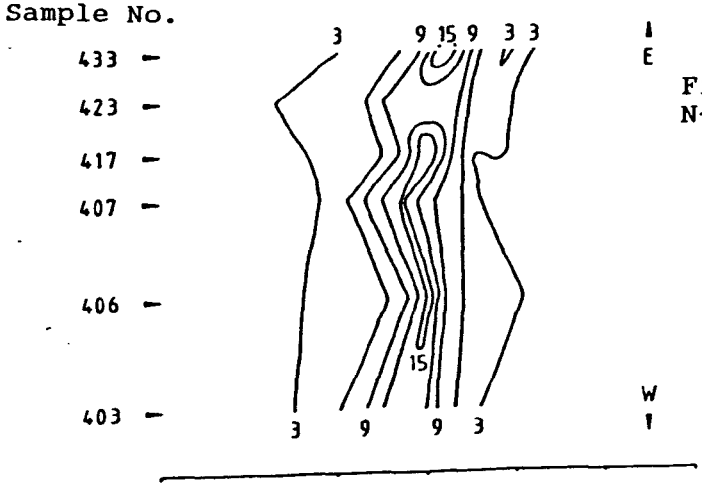

b) ~W from 2km W if the middle of Ro Wen

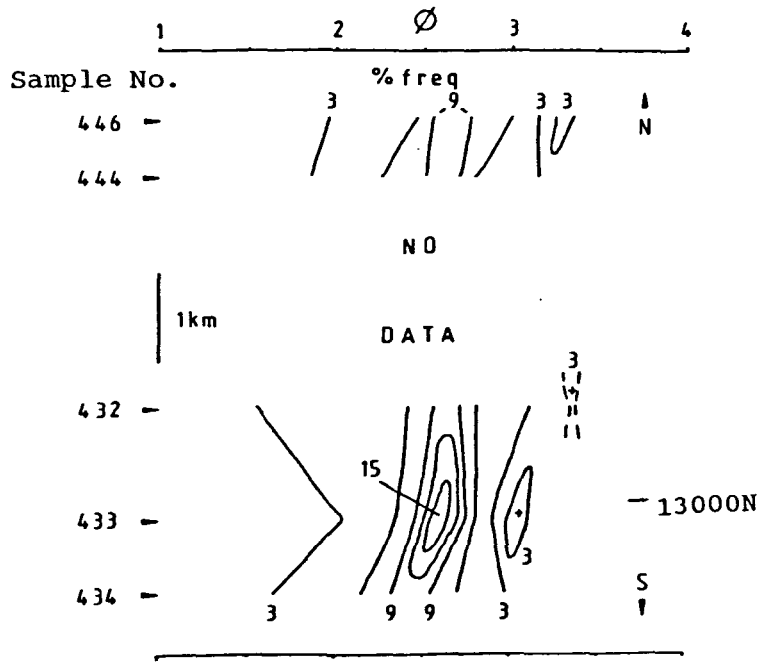

Fig. 6.22 Dowling plot showing change in grain size distribution N-S in inner Barmouth Bay

Fig. 6.23 Dowling plot showing change in grain size distribution N-S in central Barmouth Bay

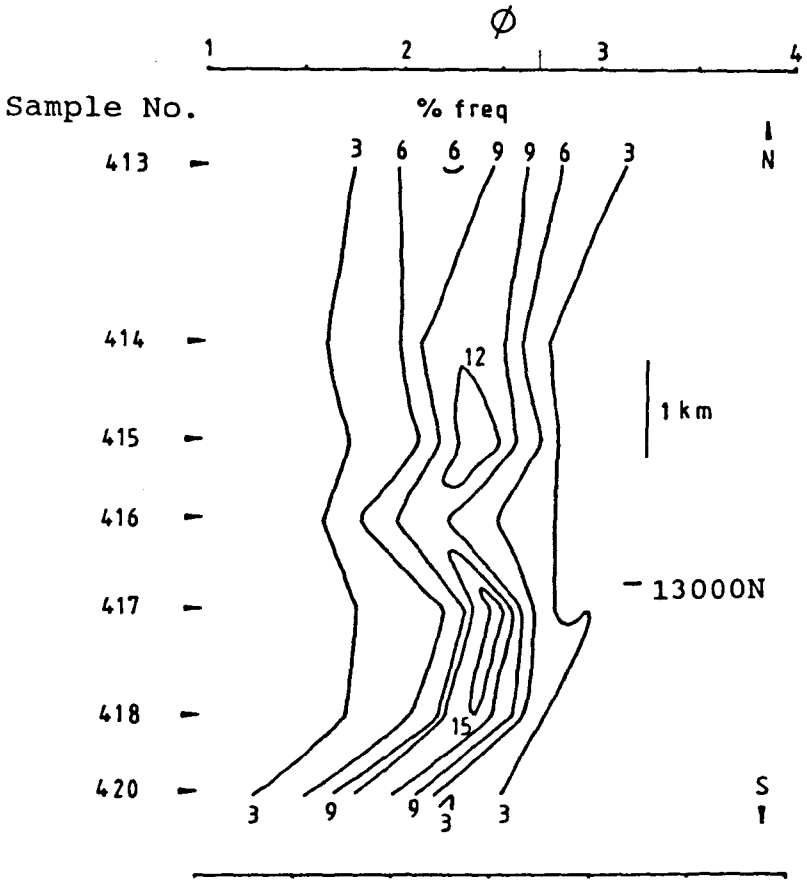

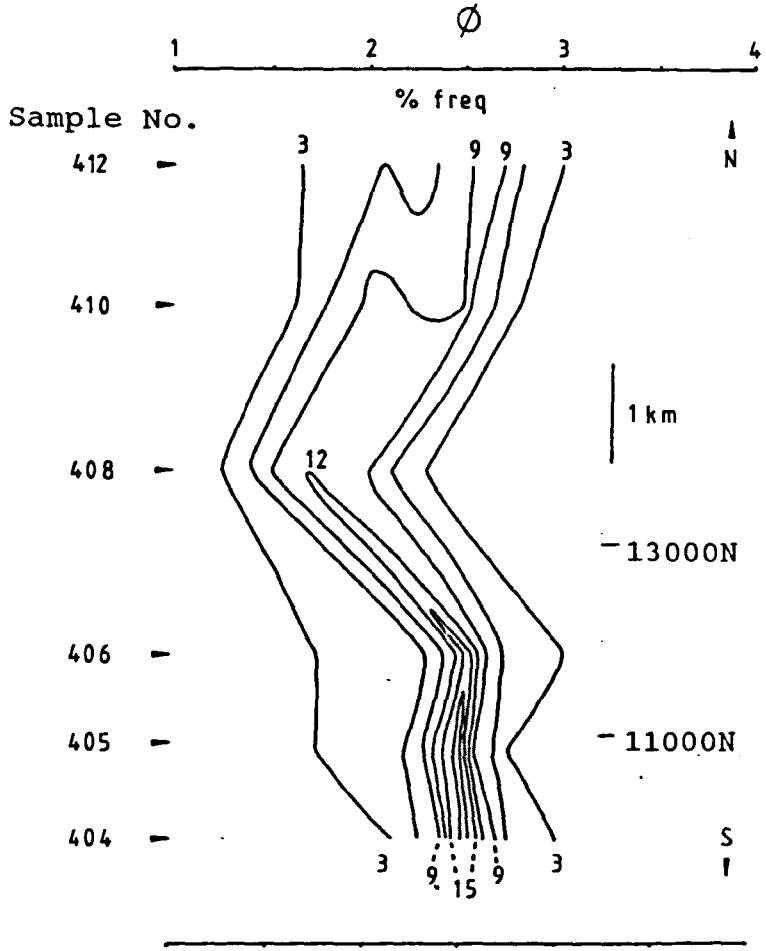

Fig. 6.24 Dowling plot showing change in grain size distributio N-S in outer Barmouth Bay

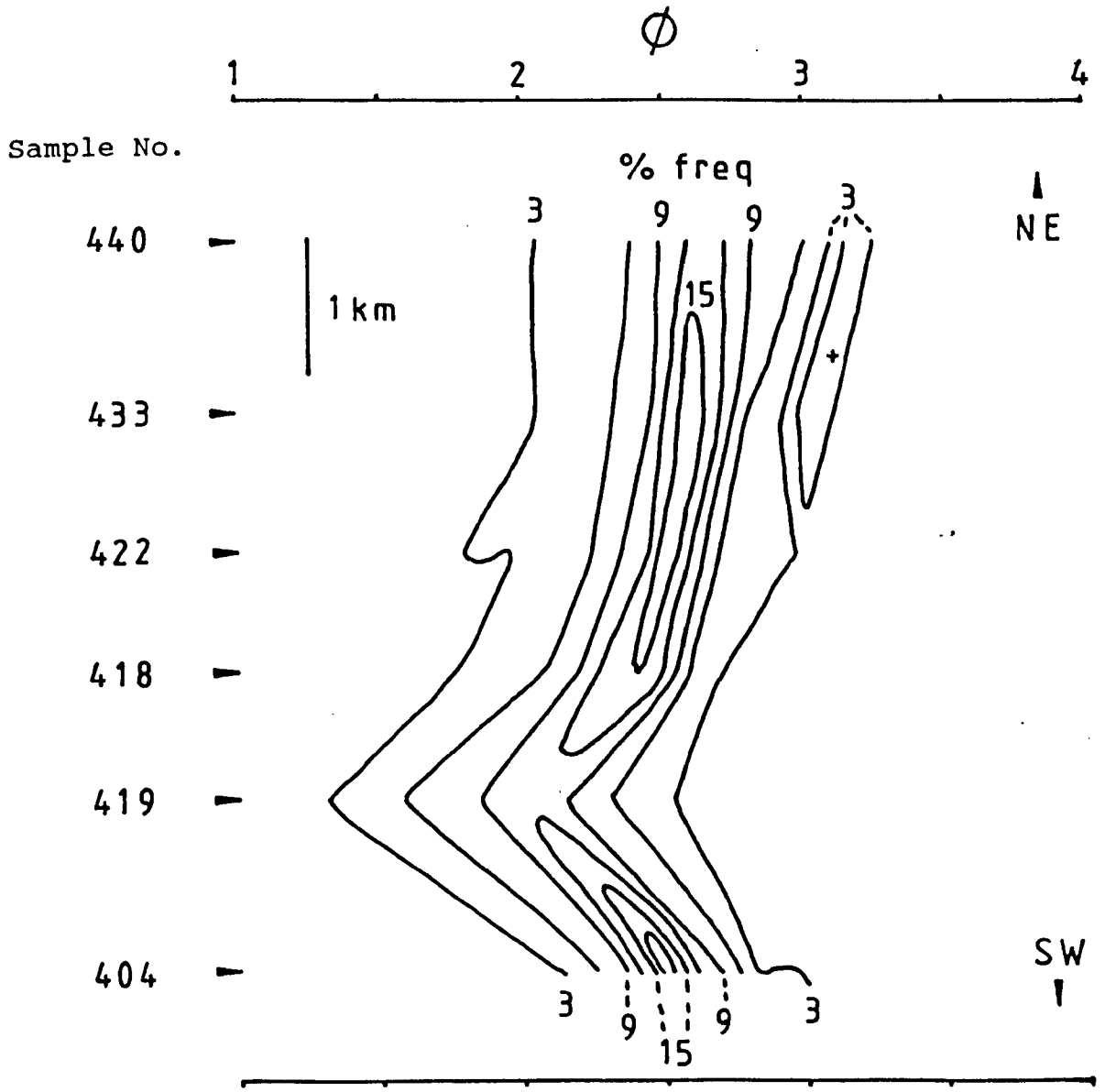

Fig. 6.25 Dowling plot showing change in grain size distribution SW from 1km W of the bar

most of the sand fraction grain size range, implying that this fraction is near equilibrium with the hydrodynamic regime. On the basis of these diagrams, and the maps of the various grain size parameters in the bay, a Dowling plot was drawn for the data between samples 404 and 440 (the SW extreme of the area to 1km SW of the bar), to show variation along that line (Fig. 6.25). This shows a well-developed fining trend shorewards from sample 419, and when viewed in conjunction with the other grain size data further suggests a NE-directed sand transport path. Sample 404 may thus represent part of a parallel transport path, perhaps more related to wave-caused longshore drift. However, side-scan data (Chapter 1) suggests it is more likely that sample 419 represents a gap in the incomplete cover of mobile sand, through which the underlying material was recovered by the grab; it is likely therefore, that sample 404 forms part of a continuum with the other surficial fine sands.

6.7.2 Fairbourne Spit and Barmouth Beach

A small number of sediment samples were taken from the intertidal zones of the seaward side of Fairbourne Spit (or Ro Wen), and from Barmouth Beach. Results of their analysis are shown in Table 6.3.

Most of the samples taken at the shoreline have sand fractions which are coarse-skewed or near- symmetrical very well-sorted fine sands. Only one sample contains >0.2% of gravel (21.5% at P305), and all samples contain approximately 1% fines, except at the northern tip of the spit where only 0.05% was present. The samples taken at the northern tip of Fairbourne Spit (sample P305 and those with the prefix SPIT) demonstrate grain size characteristics consistent with those which may be expected at such a location. Here the sediments on the more exposed seaward side are coarser, more negatively skewed and less well-sorted than those on the landward side. This is consistent with a high energy erosional seaward side and a lower energy (?depositional) side to a barrier in a strongly wave-influenced environment.

Dowling-type maps has been plotted for the sand fraction of Fairbourne Spit (Fig. 6.26) using a size interval of 0.1phi and a contour (i.e. size frequency) interval of 3%. It shows well the coarsening of the entire distribution around the tip of the spit, and the similarity of the sediments on the seaward flank of the spit and the immediate landward side. No overall coarsening or fining of the sand fraction is detectable along the spit length, which may be because of one or more of :

1 - insufficient samples;

2 - no account having been taken of shore-perpendicular grain size changes;

3 - hydrodynamic conditions being relatively invariable along the spit length;

4 - there is a limited supply of sand sizes.

The three samples taken on the Barmouth shoreline show the sand fraction has a northerly fining of its fine end, of up to 0.75phi over 1km. Sorting, although sediments remained well-sorted, also decreased in this direction.

TABLE 6.3

DETAILS OF BED SEDIMENT SAMPLES TAKEN FROM FAIRBOURNE SPIT AND BARMOUTH BEACH

Sample Identifiers		Mode	MOMENTS Mean	SD	SK	K	FOLK Mean	SD	SK	K
24-2-88 Barmouth Beach										
G.R.60301725 Sample	P300	2.45	2.371	0.431	-0.379	3.658	2.370	0.417	-0.104	1.100
G.R.60501600 "	P301	2.25	2.088	0.384	-0.051	4.199	2.105	0.366	-0.258	1.087
G.R.60701565 "	P302	2.25	2.196	0.311	-0.262	3.728	2.184	0.287	-0.222	1.189
18-7-86 Fairbourne Spit										
Sample	SPIT06	2.45	0.374	0.264	0.873	3.629	2.413	0.271	0.006	1.198
"	SPIT02	2.45	2.372	0.327	0.154	3.11	2.381	0.331	-0.069	1.121
"	SPIT05	2.25	2.152	0.3	0.363	3.919	2.1 7	0.3	-0.179	1.105
"	SPIT04	2.15	1.999	0.451	?	?	2.016	0.380	-0.221	1.148
24-2-86										
G.R.61301470 Sample	P305	2.45	2.402	0.271	-0.054	3.925	2.426	0.261	-0.073	1.316
G.R.61051305 "	P306	2.45	2.387	0.257	0.279	3.623	2.412	0.255	-0.184	1.289

continued		%fines	%gravel
Sample	P300	0.92	0.05
"	P301	0.91	0
"	P302	0.72	0.17
"	SPIT06	1.03	0
"	SPIT02	0.32	0.06
"	SPIT05	0.05	0
"	SPIT04	1.03	0
"	P305	0.98	21.52
"	P306	1.19	0

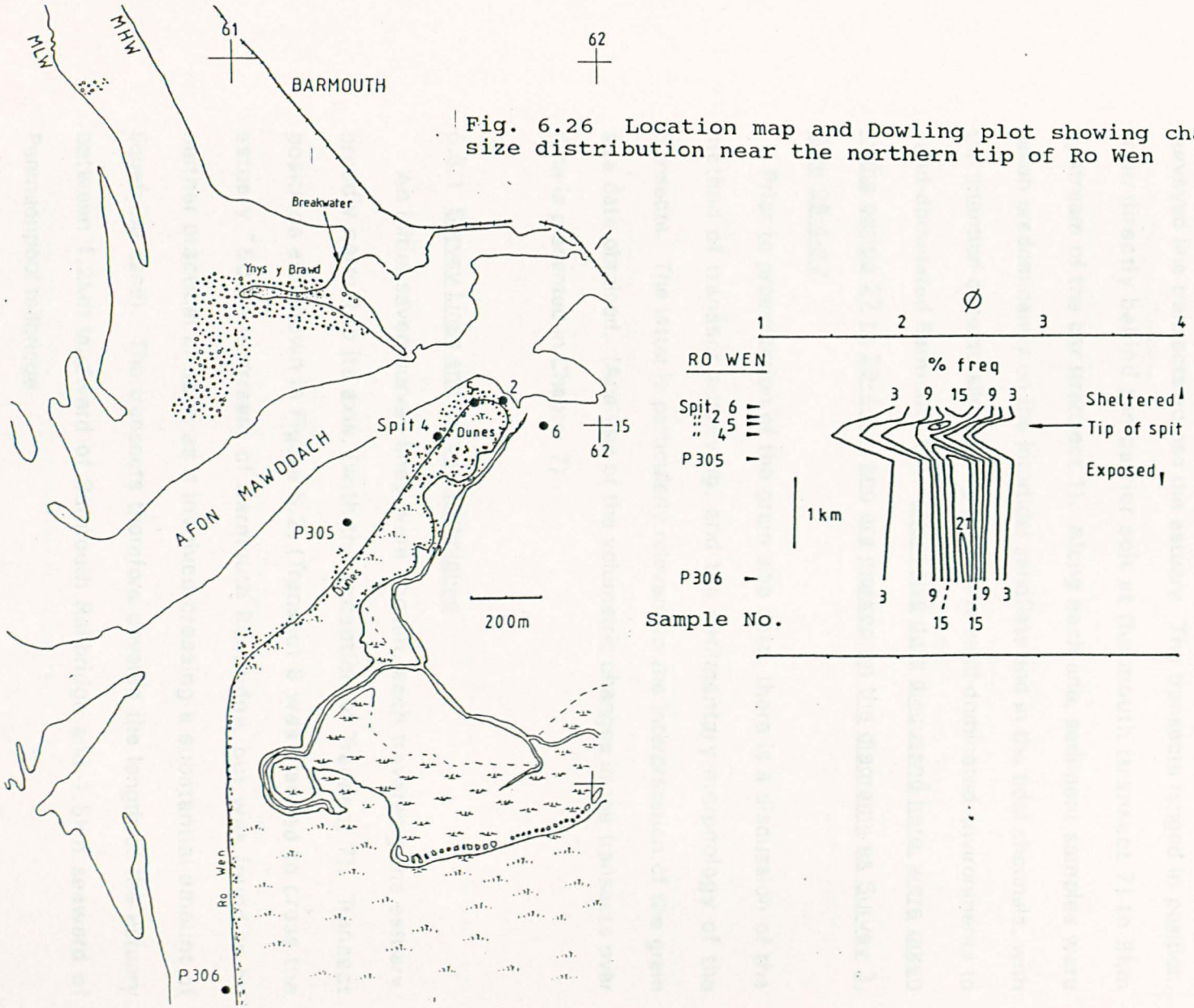

Fig. 6.26 Location map and Dowling plot showing change in grain size distribution near the northern tip of Ro Wen

6.8 Estuarine Sediment Samples

Introduction

In order to study grain size within the estuary itself and, particularly, of the sandflats, many surface samples were taken over the study period along surveyed line transects across the estuary. The transects ranged in position, from directly behind the barrier spit at the mouth (transect 7) to 9km upstream of the bar (transect 1). Along each line, sediment samples were taken predominantly on the intertidal sandflats and in the tidal channels, with the intention of texturally relating these fine sand-dominated environments to sand-dominated Barmouth Bay. Grain size data discussed here, were taken in the period 27 to 29-4-87, and are marked on the diagrams as Survey 3, date 28-4-87.

Prior to presentation of the grain size data, there is a discussion of the method of transect surveying, and the sedimentary morphology of the transects. The latter is particularly relevant to the interpretation of the grain size data obtained. (Analysis of the volumetric changes in the transects over time is presented in Chapter 7).

6.8.1 Survey Lines and Survey Techniques

An initial seven survey lines were chosen, each traversing the estuary broadly normal to its axis, (with the exception of Transect 7). Transect positions are shown in Figure 6.2, (Transect 6 was planned to cross the estuary ~500m upstream of Barmouth Railbridge, but was found to be neither practical or safe, as it involved crossing a substantial amount of liquefying sand). The transects therefore covered the length of the estuary between 1.2km landward of Barmouth Railbridge and 1.5km seaward of Penmaenpool tollbridge.

Each line was marked at each end by pre-existing fixed points or by immovable posts cemented into the ground specifically for the purpose, and

were surveyed in to O.D.N.. The only problem encountered was with Transect 2, where it was evident that the poles had moved vertically between surveys. Only the first survey of this transect could therefore be reduced to O.D.N., hence no volumetric comparisons are possible between successive surveys of Transect 2, and only morphological comparisons have been made. Thick fog during the first survey of Transect 2 resulted in the loss of the northernmost 100m of data.

The equipment used for the surveying procedure was a Wild theodolite, with an attached Citation Electronic Distance Measurer (E.D.M.), and a staff pole with a prism reflector on top. The basic method of operation of the system is that the operator sights onto the reflector and obtains the vertical angle between the theodolite and reflector. The E.D.M., which is aligned precisely parallel with the theodolite, transmits a series of infra-red signals forwards to the reflecting prism, and calculates the average time taken for the pulses to travel twice the distance between transmitter and reflector, i.e. out and back. The travel time is internally converted into a slant range, which, when combined with the vertical angle, allows calculation by the E.D.M. of both horizontal range and vertical displacement of the reflector from the E.D.M..

Prior to surveying, it was ensured that the centre of the reflector was exactly the same height above ground as the centre of the E.D.M. transmitting lens, thus removing any need for a correction constant. The first and last surveyed points on the lines were onto the fixed points of known elevation, thus each survey was reduced to elevations with respect to O.D.N..

Survey Dates

Table 6.4 lists the dates of survey of each transect.

Table 6.4

Dates of Survey of Estuarine Transects (dd-mm-yy)

Transect number	Survey Number 1	2	3	4	5
1	26-04-86	14-04-87	28-04-87	--	--
2	26-04-86	14-04-87	28-04-87	--	20-07-88
3	26-04-86	14-04-87	28-04-87	13-07-87	--
4	26-04-86	14-04-87	28-04-87	13-07-87	--
5	26-04-86	14-04-87	28-04-87	--	--
7	--	14-04-87	28-04-87	--	--

6.8.2 Morphology of Estuarine Transects

Brief descriptions of the sedimentary geomorphology of each transect are given below, with a description of the changes found between surveys. Transect morphologies are shown in Figs. 6.27 - 6.32, with elevations reduced to O.D.N.. To aid comparisons of the transects, dotted lines indicate the morphology of the previous survey.

Transect 1

This transect is approximately 370m long, crosses the upper estuary at a gentle channel bend, and includes on the southern bank two marsh levels, at +2.5 and +2.0m O.D.. The marsh is dissected by a few creeks up to 1.5m deep. The main estuarine channel is shallow, with the lowest bed elevation ~-0.3m O.D.. Towards the north side of the channel, a low amplitude bar had developed prior to the survey of 28-04-87. Overall, the transect displays a morphology expected at a channel bend, with a steeper slope on the outer bank.

The surveyed morphology of the channel area is probably less variable than is suggested by the data. There are practical problems with surveying

Bed profiles of Transect 1

Fig. 6.27

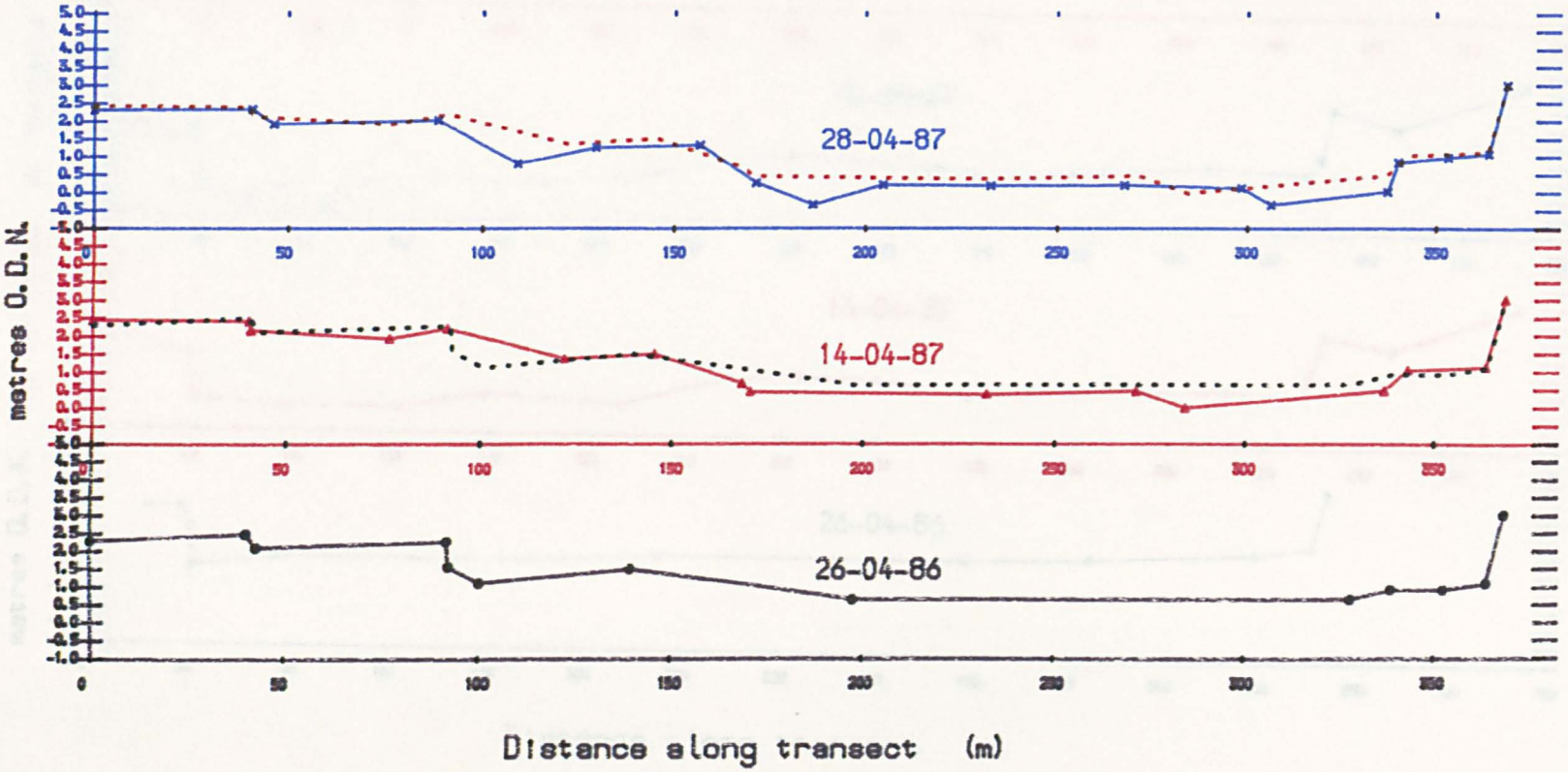

Bed profiles of Transect 2

Fig.6.28

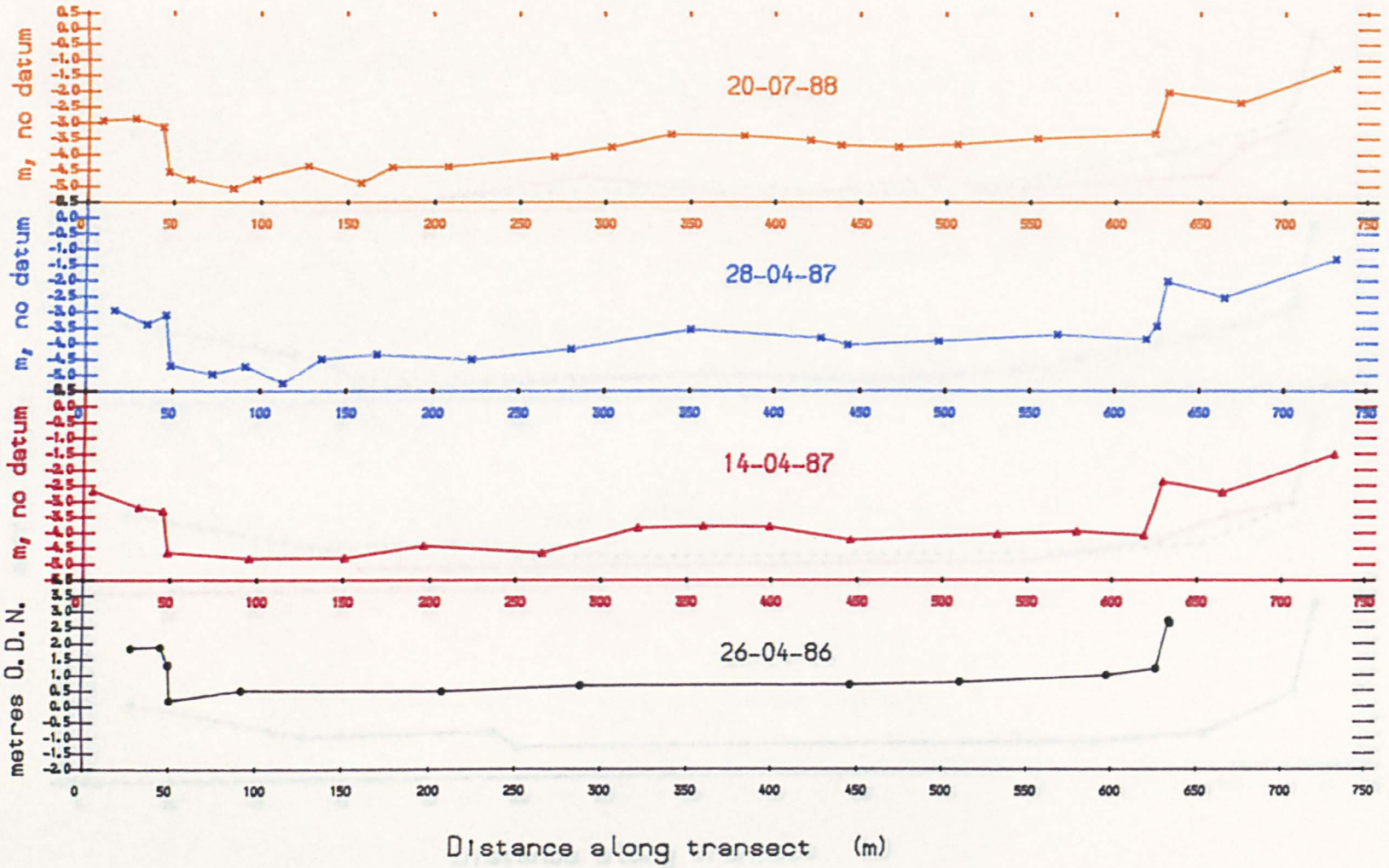

Bed profiles of Transect 3

Fig. 6.29

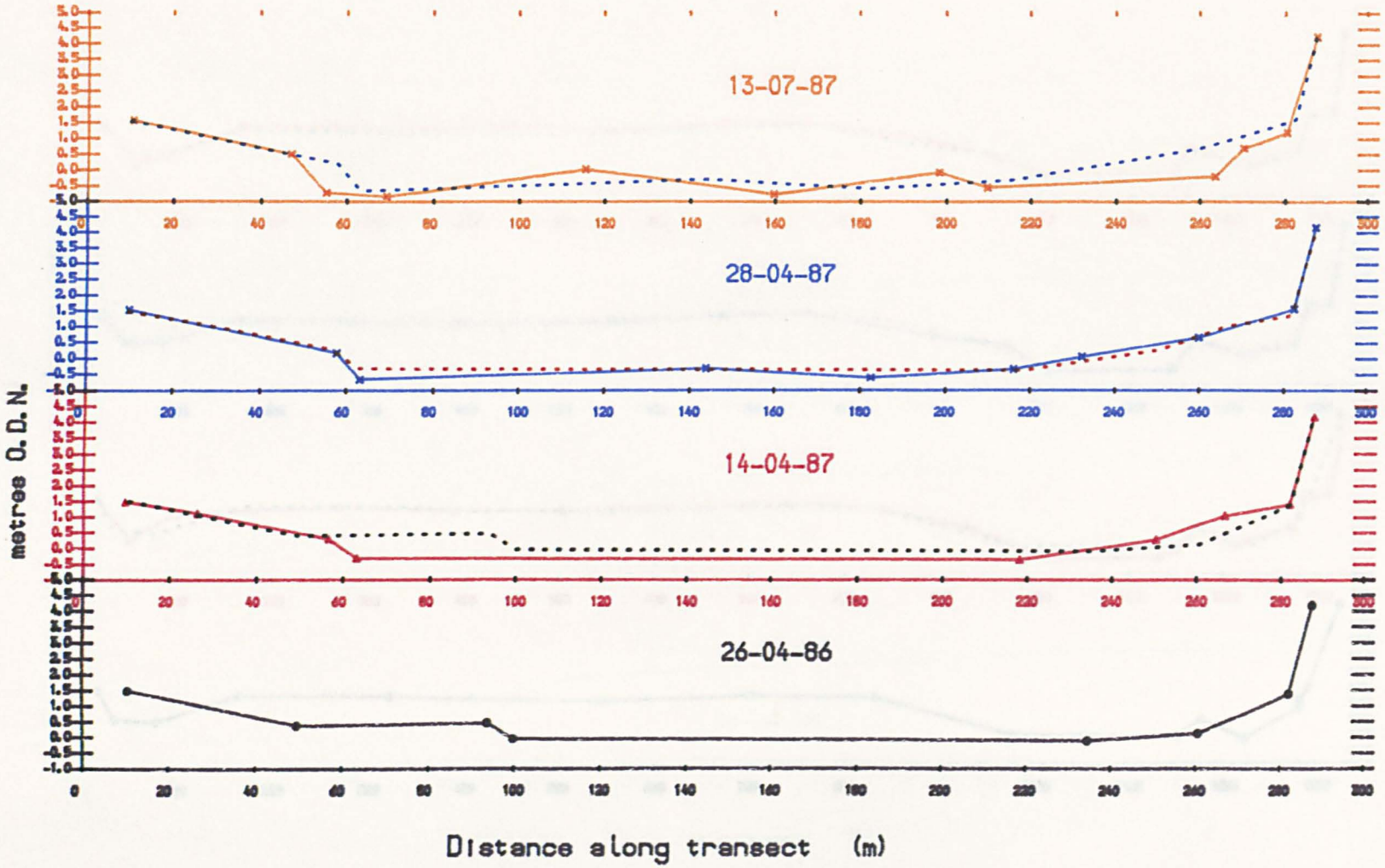

Bed profiles of Transect 4

Fig. 6.30

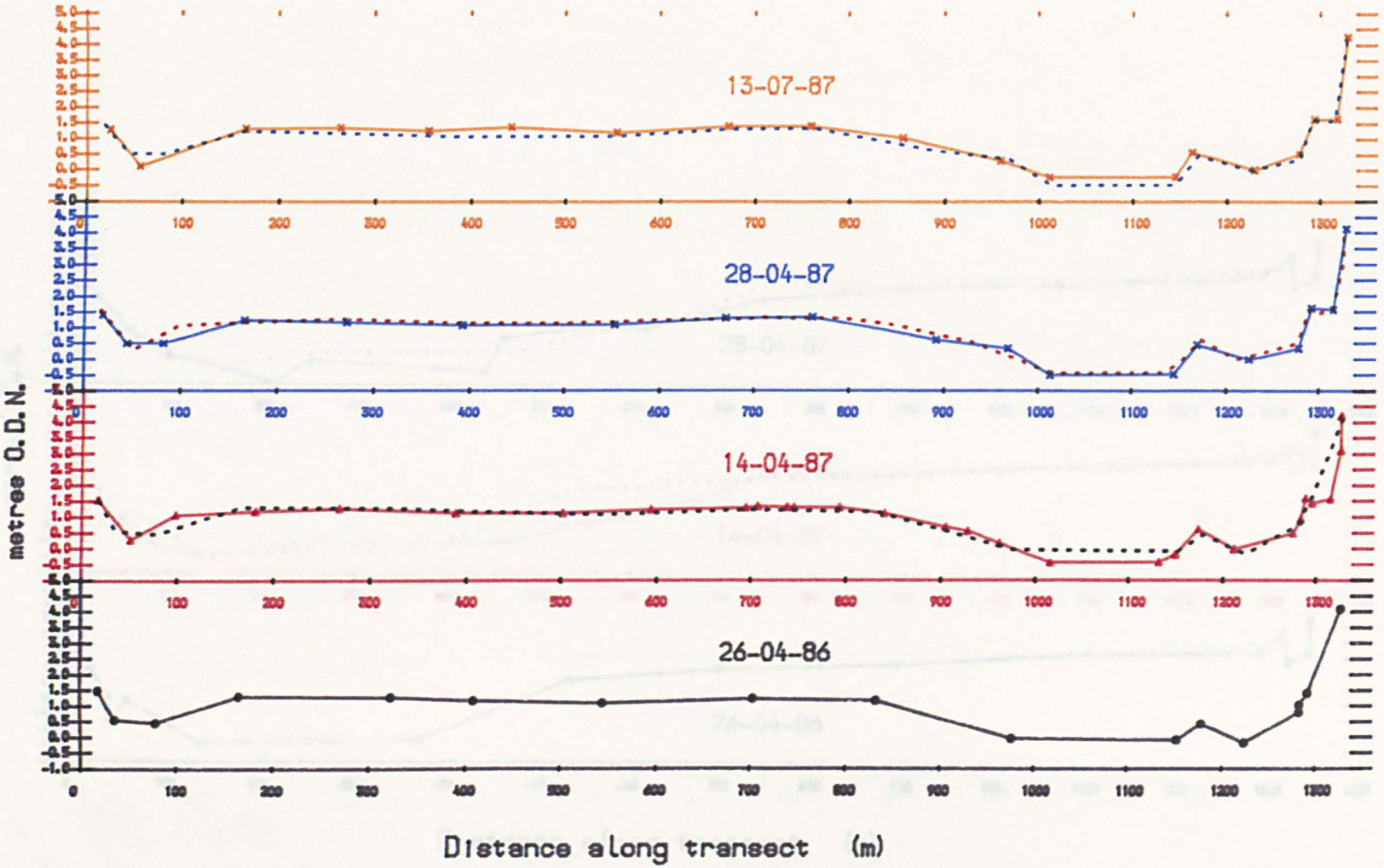

Bed profiles of Transect 5

Fig. 6.31

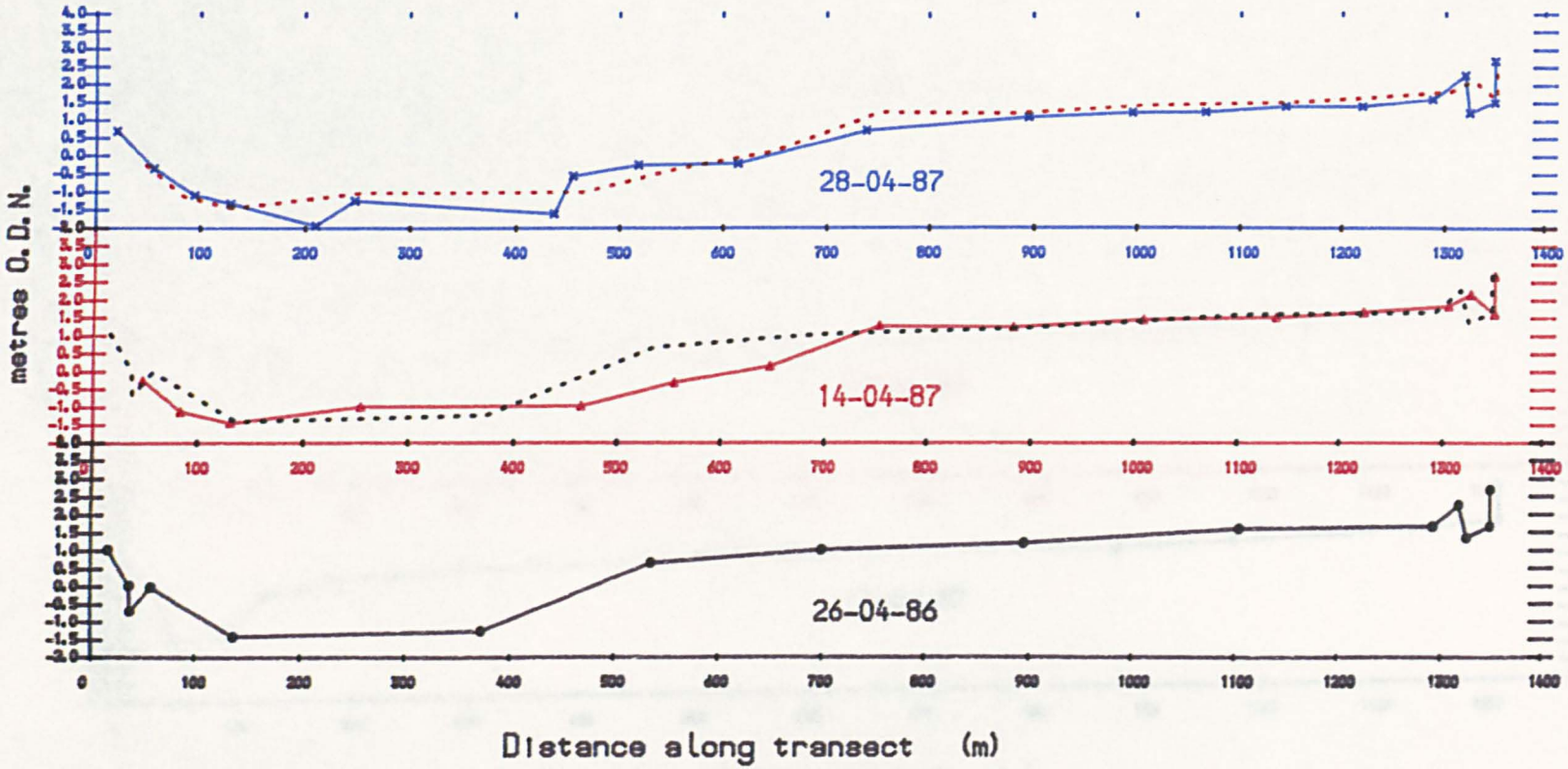

Bed profiles of Transect 7

Fig. 6.32

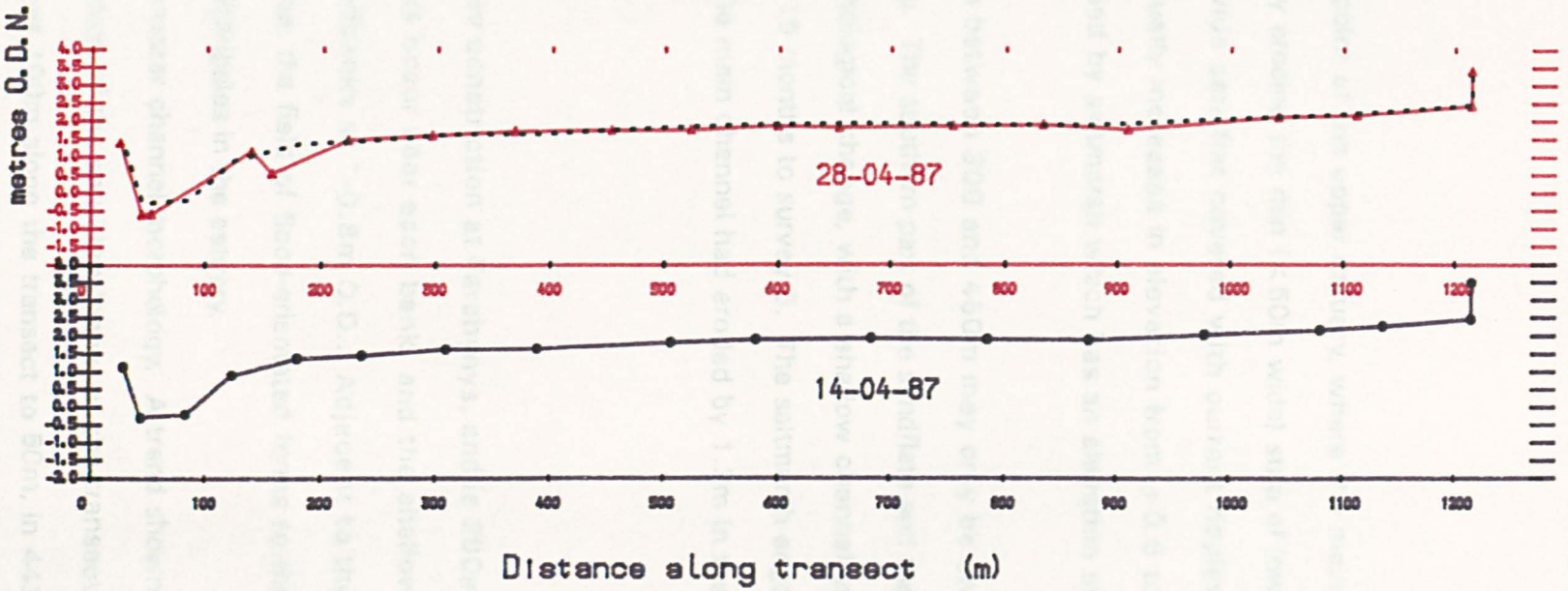

the morphology of the channel. Water level was relatively high during the survey of 26-04-86, and it did not prove possible to survey the channel base. The final survey showed active erosion of a laminated silt/fine sand sequence on the north bank, and some erosive change of the channel itself. This suggests that there may be considerable short-term (periods of days) change in the bed levels.

Transect 2

This crosses at the widest point of the upper estuary, where the main channel is near to and is actively eroding the thin (<50m wide) strip of low saltmarsh (+1.8m O.D.). A wide sandflat covered with current ripples extends northwards, and gradually increases in elevation from +0.5 to +1.2m O.D.; it is then succeeded by saltmarsh which has an elevation of +2.7m O.D..

The apparent accumulation between 300 and 450m may only be an artefact of the surveying process. The southern part of the sandflats and the main channel show most morphological change, with a shallow channel at ~160m having developed in the 15 months to survey 5. The saltmarsh edge forming the southern edge of the main channel had eroded by 1.2m in the same period.

Transect 3

This crosses the mid-estuary constriction at Farchynys, and is 290m long. Small intertidal sandflats occur near each bank, and the shallow channel contains shifting sandbanks at ~-0.8m O.D.. Adjacent to the transect are intertidal megaripples; the field of flood-orientated forms to the NE are the furthest landward megaripples in the estuary.

Detail is lacking on the underwater channel morphology. A trend shown well by the transects is the erosion of the southern 'bank' of the transect, which retreated from a position at 100m along the transect to 50m, in 443 days, i.e. at an average of ~0.1m/day. The bed level behind this feature

apparently remained virtually unchanged throughout. From the first to the third survey, the N end of the transect accreted sediment, and then had up to 1m of sand eroded, some of which may have contributed to the formation of prominent intra-channel bars.

Transect 4

This traverses the lower estuary ~1km seaward of Transect 3, and is over 1300m in length. At the southern end there is 150m of low ground related to a blind flood channel, i.e. closed at its landward end. The channel had previously been a more major feature, suggested by the now derelict jetty adjacent to the survey line. Beyond this channel is over 800m of laminated mudflats, containing Spartina townsendii in varying concentrations, and which is present up to 550m along the survey line. The majority of the mudflat lies at an elevation of +1 - +1.2m O.D. Beyond is the wide main estuarine channel, containing (at elevations below -0.5m O.D.) flood-orientated megaripples 8-10m in wavelength. This observation further suggests net flood sediment transport in the estuary. A channel parallel sandbank occurs near the northern bank, which is a saltmarsh scarp.

The apparent large changes in channel morphology in the south (0-180m), and in the elevation of the channel base in the north (1020-1140m) are surveying artefacts. More useful in terms of gauging the variation of bed levels is the data across the laminated mudflats. Due to the flatter topography of this area, differences of bed level are better defined by the data. There is an overall increase in elevation of this area, though exhibiting a little erosion in the fortnight between the second and third survey.

Transect 5

This extends 1350m northeast from Fegla Fach, and crosses the main channel in its southern 500m. The main channel and sandflats (up to the 970m mark) are both megarippled. The megaripples are ebb-orientated and

have a wavelength of 7-8m up to the 500m point, are near-symmetrical for 200m, and in the northern part of the field are flood orientated. Rippled sands then pass into a ridge of vegetated cavity sand (+2m O.D.) at ~1320m, beyond which is soft waterlogged saltmarsh at +1.6m O.D..

Large amounts of erosion occurred at the northern edge of the main channel in the year to the second survey, and there was a related development of an intra-channel bar, with its crest at -1m O.D.. There was also substantial modification in just 14 days prior to the third survey. The channel base and sand flats in the north were both eroded, with the only net deposition being a bench on the inside of the channel bend at the 500m point.

Transect 7

This transect lies E-W across the sandflats east of the spit Ro Wen. At its western end it traverses the back-barrier channel which runs parallel with Ro Wen. The sandflats increase in elevation to the east, from +1.6m O.D. at 300m to +2.4m O.D. at 1215m. Current, wave, and combined-flow ripples decrease in quantity eastwards, becoming absent at about the 600m mark, beyond which flat beds occur.

The second survey showed little gross morphological change from the first, except for the development of a small channel at 160m. The sandflats had apparently eroded slightly since the first survey.

6.8.3 Grain Size Results

There follows a discussion of the grain size data. A brief overview of the proportions of fines (grains <63um) and gravel (>2mm) in the estuary, is followed by details of the variation of grain size parameters, of the sand fraction, along each transect.

6.8.3.1 Proportion of Fines and Gravel

The percentage of sediment below 63um (4phi) varies between 0.47% (sample 103) and 13.2% (101), although much higher values (up to 95%) occur in samples taken from saltmarshes in the upper estuary. The proportion of fines in sediment depends on the physiographic subenvironment (channel, sandflat, mudflat, saltmarsh) from which the sample was taken. Most samples have less than 2% fines. Proportions of gravel range between 0 and 10% (except for P303 which contained 88.75%). Along most transects, values were below 2%, but Transect 7 samples typically contained 4 - 5% gravel.

6.8.3.2 Sand Fraction

Grain size parameters (calculated by the moments method) derived from the sand fraction of the estuarine sediment samples are plotted against distance along transect in Figs. 6.33 - 6.37. The graphic grain size parameters show almost identical trends and are not presented here. The error bars upon each data point are approximate 95% confidence limits, however as it was not possible to identify relationships of variable error with any of the grain size parameters (Chapter 5, Section 5.6.3), the error bars represent likely errors for the sediment type found in the estuary. i.e. well-sorted fine sands. Therefore, they are only a guide, and are constant along each transect.

—

Transect 1

The mode and mean grain size of the sand fraction are coarser in the channel centre than at the channel edges or on the saltmarsh. Sorting is very good (~0.22phi) all across the channel, with no measurable variation. Skewness is positive, except sample 3, which was taken from a rippled intertidal bar, whose negative skew is due to a smaller proportion of 3.2-3.3phi grains. There is no evidence of modal behaviour in these samples,

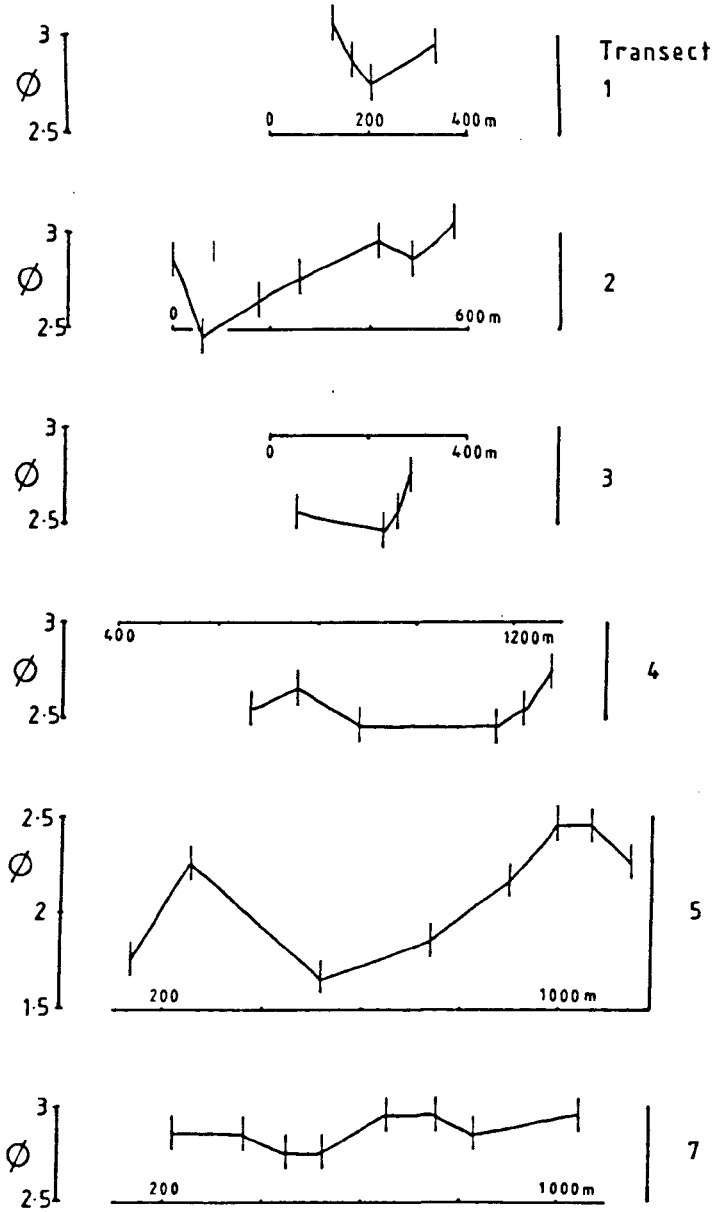

Fig. 6.33 Sand fraction - Mode size along the estuarine transects

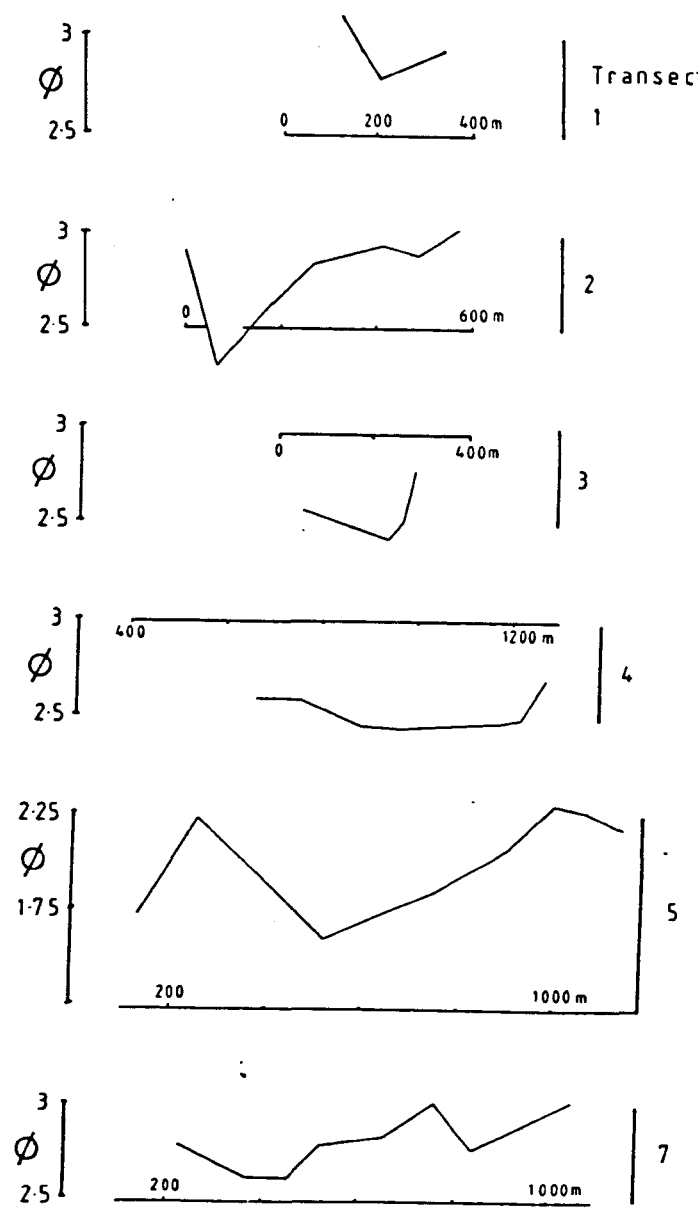

Fig. 6.34 Sand fraction - Mean size along the estuarine transects

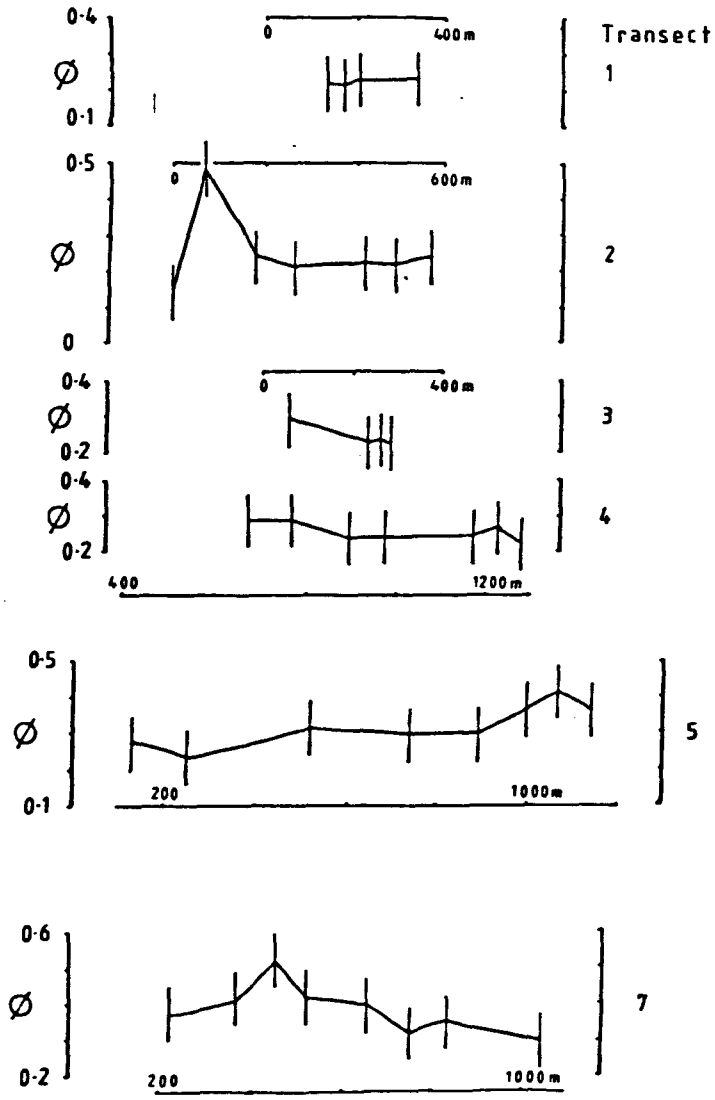

Fig. 6.35 Sand fraction - Sorting along the estuarine transects

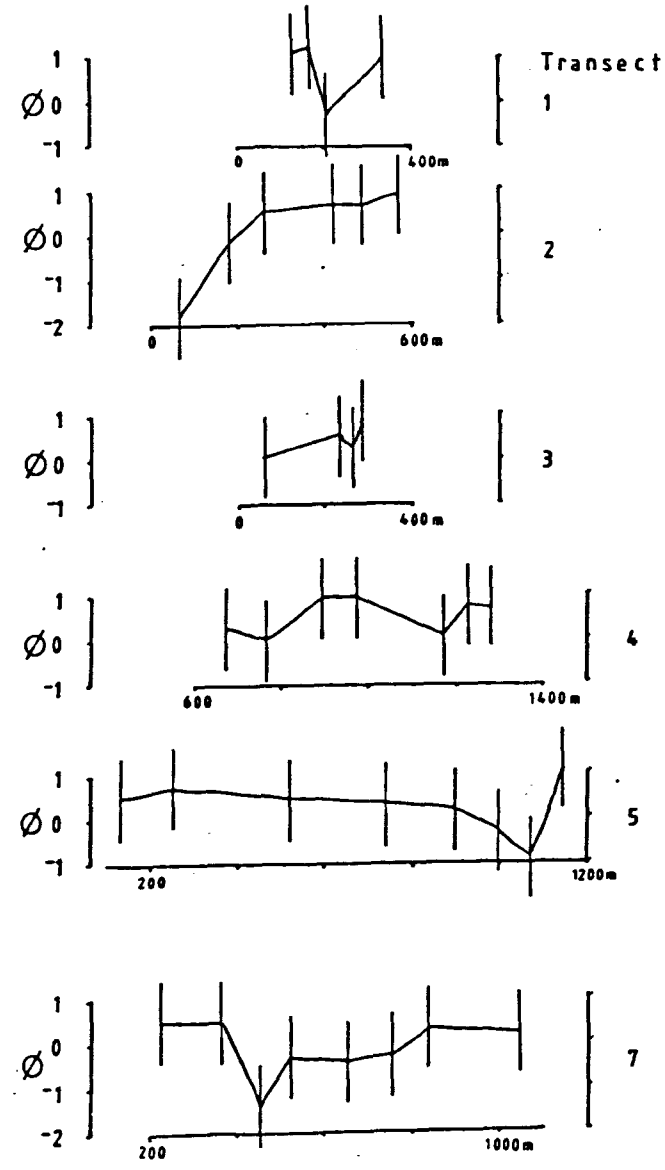

Fig. 6.36 Sand fraction - Skewness along the estuarine transects

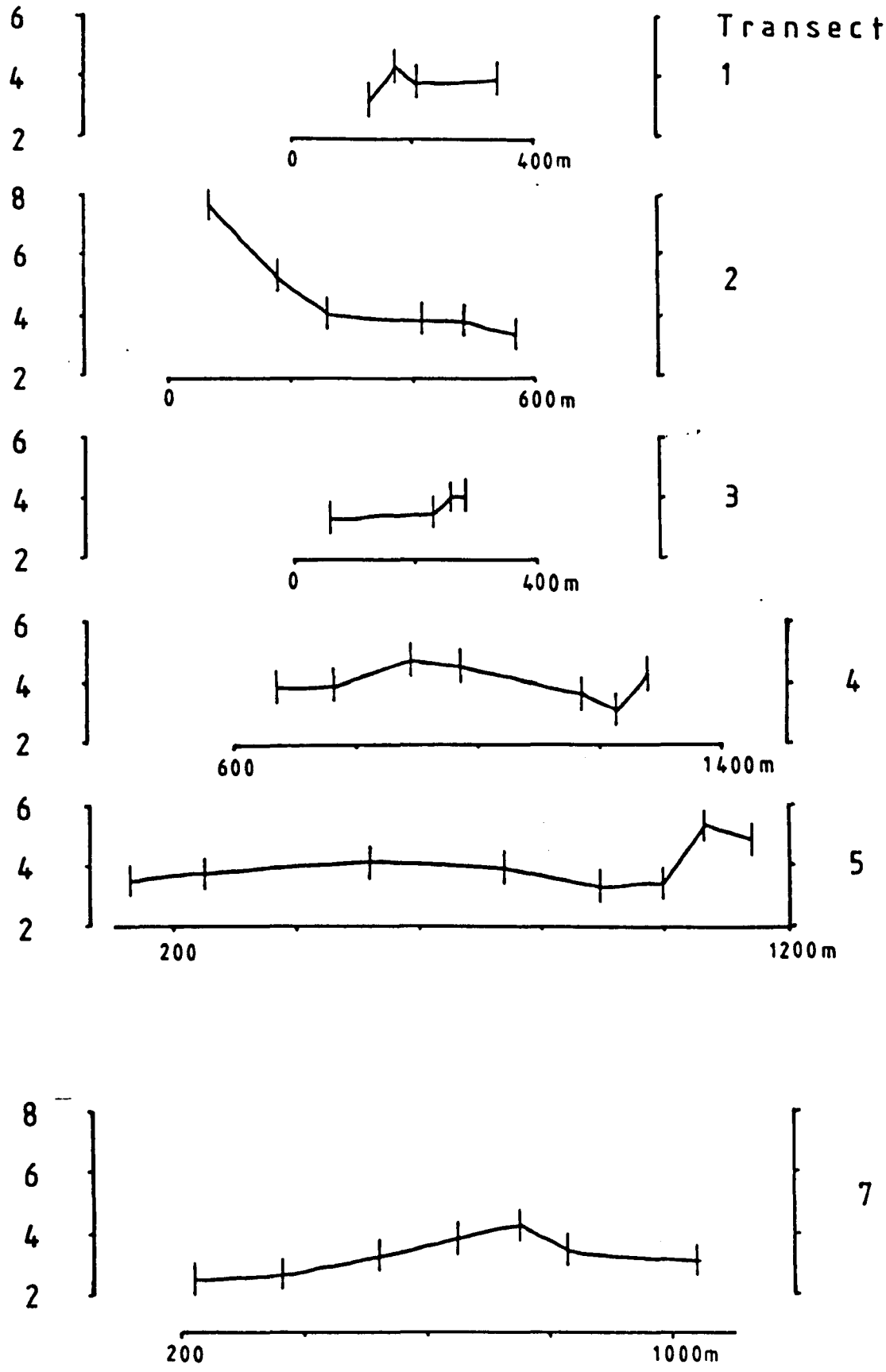

Fig. 6.37 Sand fraction - Kurtosis along the estuarine transects

and it appears that the sand size distribution along this transect is predominantly controlled by flow hydrodynamics than by a source control.

Transect 2

The mode size is very variable, coarsest at 2.45phi on the outside of the channel bend, fining northwards to 3.05phi on the sandflats. The variation of mean grain size (not shown) is identical in pattern to the mode, suggesting the relative unimportance of modal behaviour in controlling the mean size in these samples. Sorting is constant at 0.1-0.24phi, except samples 1 and 2 which are respectively significantly better and worse sorted. Skewness is negative in the main channel and positive further north on the sandflats. Sample 2 has 10% of grains coarser than 1.8%, compared to sample 3 with only 2% in this range. There is a clear trend of decreasing kurtosis along the transect, from 7.7 to only 3.4.

Sample 2 was taken in the main channel bend, on the outside of which there is active erosion of the saltmarsh platform, and compared to the remainder of the transect is coarse, poorly sorted, strongly negatively skewed and leptokurtic. It also has more gravel, though only 1.38%. The conclusion from this is that sample 2 (and less so sample 3) has these attributes due to the combined effects of high fluid power, and having a sediment 'source' in the saltmarsh sequence that is both nearby and heterogeneous in terms of grain size. The eroding succession contains both relatively coarse and fine sediment, which contribute to the poorer sorting and high kurtosis. The fast tides are able to carry away much of the fine grains, resulting in a negatively skewed sediment, and are also responsible for the overall coarseness of the sediment in the channel.

Transect 3

The mode and mean have identical trends, relatively coarse in the channel and fining either side. The sorting is slightly better on the north bank than the south, though like skewness, variation is small compared to

the size of the error bars. Kurtosis variation along the line is also near negligible. It was noted that there is erosion of the south sandflat, with a decimetre high cliff present. Over repeated surveys, this was seen to be a long term process (>3yrs) with the channel progressively migrating southwards. Relative deposition on the north bank is hinted at by the finer, more positively skewed sediment found there.

Transect 4

This transect also shows fining away from the main estuarine channel. Sorting is best in the channels, but there is little variation along the line. Skewness is positive on the south side of the main channel, and on the northern sandflats, which implies that these regions are depositional. Kurtosis is markedly higher on the southern edge of the main channel, lowest on the northern sandflats, and when taken with the skewness variation supports the idea of deposition in these areas. Observations along the line show that the coloniser Spartina is abundant on the southern sandflats, becoming absent at 550m from the southern estuary margin.

Transect 5

The mean and mode is very variable along this transect, the mean having extreme values of 1.61 and 2.27phi. From the main channel northwards there is a well-defined fining to the 1000m mark. At 250m the bed is as fine as on the northern sandflats. This sample was taken from the crest of an intertidal megaripple on an interchannel bar, suggesting the bar may have been depositional in nature. Sorting generally worsens and skewness lessens northwards. Skewness is strongly negative at 1100m, and with poor sorting and high kurtosis this implies an erosional regime. Between 120 and 970m the transect contains megaripples, which for their first 500m are ebb-orientated, and the last 250m are flood-orientated, and between there is a transition zone. The conclusion from the grain size data is that the south

of this transect is potentially depositional, and that for 300m near the north end it is probably erosional with a net flood-directed bed transport. A comparison of transect morphology confirms this erosional tendency for the north part of the sandflats (Fig. 6.31).

Transect Z

The mode and mean curves show similar trends, with coarse samples at 400-500m and at 800m. Sorting is worst at 450m and increases eastwards. Skewness is significantly negative at 450m and generally low up to 800m. The samples taken between 200m and 400m are the only ones in the estuary with kurtosis of below 3, i.e. with fewer extreme grain sizes (in the sand range) than for a Gaussian distribution.

6.8.4. Dowling Plots along the Estuary

To indicate along-estuary variation of grain size, two Dowling plots have been constructed: one for samples taken from the main estuarine channel; and one for samples taken from the centre of the sandflats at each transect (Figs. 6.38 and 6.39). Channel samples shows well that samples are unimodal; the strong modal frequency has up to 27% (by weight) of the sand fraction, occurring within classes of 0.1phi width. There is also a very well-defined landward fining, of ~0.1phi / km. The limit of occurrence of fine sand is between Penmaenpool (P304) and Borthwnog (P303). These two points tend to suggest one or both of :

- the estuarine sediment has been derived from the sea;
- the estuarine sediment is in equilibrium with a hydrodynamic regime which decreases in energy landward.

As with the sediment in Barmouth Bay, the fine sand in the estuary shows gradual spatial changes in mean size and other grain size parameters. This infers that the sediments are in some sort of equilibrium with the hydrodynamic regime, rather than being controlled by the availability of only fine sand-sized material. Taken with the geological and sediment transport

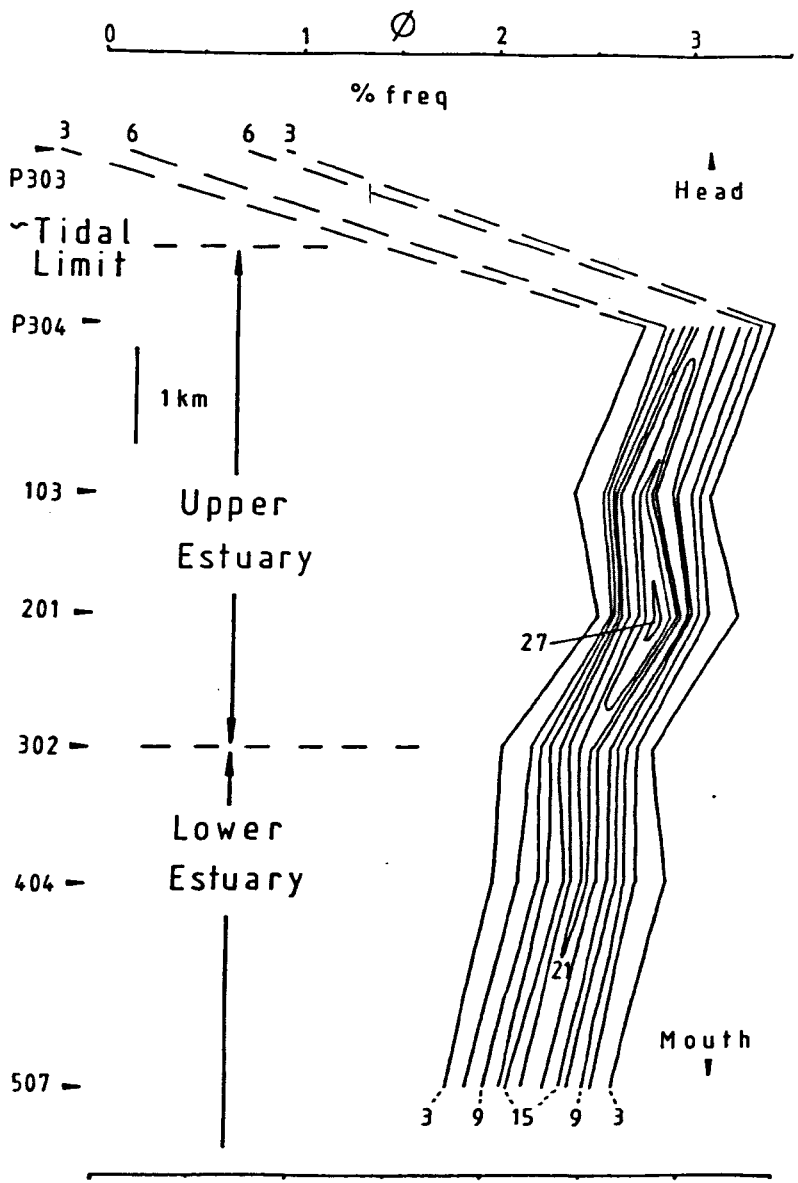

Fig. 6.38 Dowling plots of channel samples along the estuary

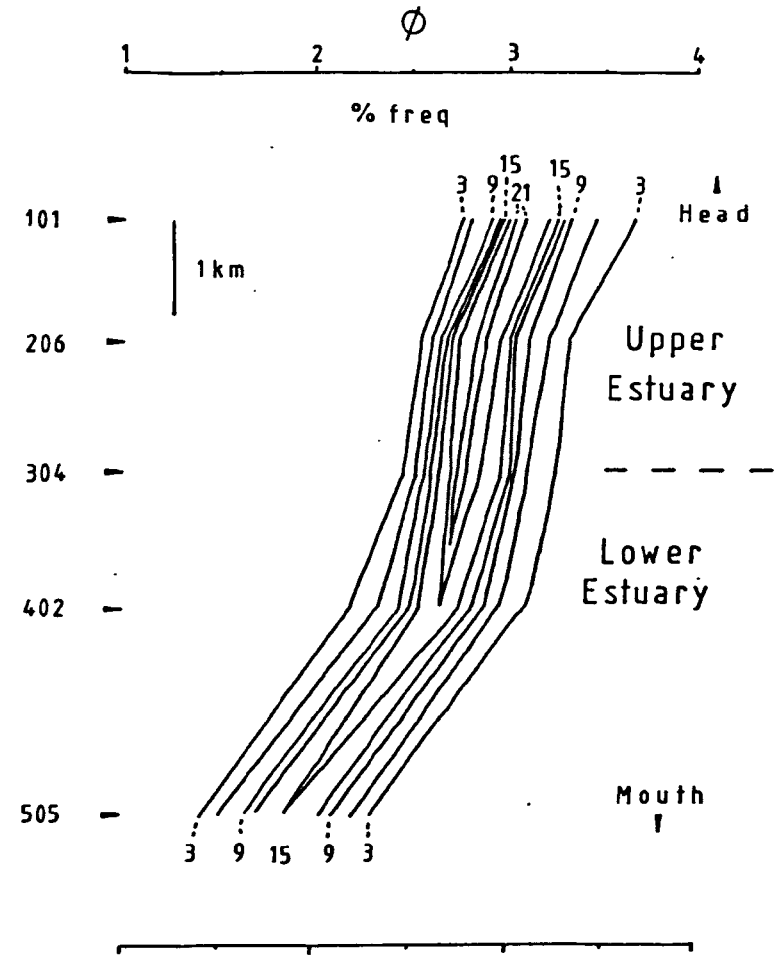

Fig. 6.39 Dowling plots of sandflat samples along the estuary

evidence of Chapter 1, and the petrological data above, both these statements are favoured.

The sandflat samples (Fig. 6.39 and Table 6.5) show similar trends to the channel samples. Sorting increases landward, skewness becomes more positive, and there is a landward increase of % fines. Sample 505 from Transect 5 is much coarser than the others because it was taken from a megaripple crest in a flood- orientated megaripple field, thus is possibly derived from coarse material at the north end of the railbridge.

Table 6.5

Grain Size Parameters from Sandflat Sediment Samples

Transect	Sample	Mean phi	S.D. phi	Skew.	Kurt.	%fines
Head						
1	101	3.10	0.22	1.02	3.21	13.2
2	206	2.88	2.85	0.64	3.79	1.43
3	304	2.75	0.22	0.87	3.97	1.13
4	402	2.60	0.28	0.01	3.89	1.30
5	505	1.85	0.29	0.33	3.97	0.93
Mouth						

6.8.5 Estuarine Samples - General Points

1 - most strikingly, estuarine sands are overwhelmingly positively skewed whereas all samples in the bay, except those in the NW, are negatively skewed. On the evidence of Duane (1964) (see Section 6.2.1), this would suggest the estuary is an area of net sediment accumulation. This agrees with conclusions from petrological (this chapter) and sediment flux (Chapter 1) considerations;

2 - the estuarine sediments are better sorted than those in the bay, possibly because of the relatively constant range of hydrodynamic conditions (i.e. limited wave and wind effects) and there is a weak trend of better sorting landward in channel sediments. This also suggests sediment derivation from the bay;

3 - modal grain sizes are coarser in estuarine channels than on sandflats, and the modal size fines landward in channels, particularly in the upper estuary. This is interpreted as a result of hydrodynamic gradients. The sandflats have a grain size change of up to 0.8phi across them;

4 - both the mean and mode is noteably finer along transect 7 than the main part of the lower estuary, probably as a result of being sheltered from waves, and being removed from the influence of the main tidal currents in the estuary;

5 - all estuarine samples except two have kurtosis greater than 3, i.e. greater than that for a Gaussian distribution. Despite the errors involved in its measurement, kurtosis values appear to be high where sedimentary regimes are either actively erosional or depositional.

6.9 Conclusions

There is a great volume of literature on the measurement, description and interpretation of grain size distributions, much of it stemming from the work of Folk and fellow workers in the late 1950's. However, as yet there is no proved grain size description scheme to replace the graphic or moments schemes, which have drawbacks in the assumptions inherent in their use. There are some reasonably well- accepted systematic changes in grain size distributions along a sediment transport path, which when applied to field measurements can provide much information on sediment transport.

Conclusions regarding possible erosional or depositional regimes in the bay and estuary are limited by the errors inherent in the sampling and measurement processes. However, large-scale spatial trends do allow a useful amount of environmental interpretation, especially when suggested by a number of different parameters. For example; there is a consistency in the interpretation of both mean grain size and skewness in the estuary.

The sediment on the bed of Barmouth Bay is heterogeneous in nature, with well-sorted fine sand forming a mobile layer over a coarse sand substrate. The fine sand is between 2.2 and 2.5phi in mean size; it is well-sorted, with most sorting values lying between 0.4 and 0.5phi. The sediment in the bay is negatively skewed, except for a few samples in the northwest of the sampled area. Maps of both skewness and kurtosis show a broad SW - NE gradients, with skewness becoming more positive and kurtosis decreasing to the northeast.

Estuarine sediments are better sorted than those in the Bay; there is a weak trend of better sorting, to landward in the estuarine channel sediments. In marked contrast to the sediments in the Bay, estuarine sands are overwhelmingly positively skewed. Modal grain sizes are coarser in estuarine channels than on sandflats; the modal size fines landward in channels, particularly in the upper estuary. The sandflats have a grain size

change, of up to 0.8phi across them. Both the mean and mode are noteably finer behind the spit Ro Wen, than the main part of the lower estuary. In the estuary, high kurtosis values tend to occur where sedimentary regimes are either actively erosional or depositional.

The dominant control in determining grain size gradients in the bay and estuary appears a hydrodynamic one, evidenced by gentle and continuous spatial gradients of these parameters. Within the fine-sand samples, the only modal behaviour found is in the nearshore zone, within 1km of the shore, where a weak 3.4phi mode is present in concentrations of ~3%.

The petrology of the gravel fractions of the sediments suggests that below the tidal limit, the estuarine sediment is very similar to that in the bay, and is possibly derived from reworking of sedimentary material related to the Irish Sea ice sheet. Near to and inland of the tidal limit the sediment in the Mawddach is local in origin, derived from erosion of the high metamorphic terrain to the north and east.

There is some evidence for the active supply of sediment to Barmouth Bay from erosion of the bed. This evidence is the interpreted common spatial source of fines, polymodal sand and gravel, which lies at sea bed exposures of sub-bottom reflectors interpreted as glacial in origin (Chapter 1). However, the main sediment source to the bay is implied to be offshore to the southwest (see Chapter 1).

Chapter 7

Sediment Transport Paths, and Estuarine Morphological Change

7.1 Introduction

Previous chapters have investigated the geological, hydrodynamic and sedimentological characteristics of the area. This chapter addresses some aspects of sediment transport and morphological change.

Firstly, this chapter considers the sediment transport paths of Barmouth Bay, attempting to identify sediment sources, conduits and sinks. This has been approached in a number of ways:

1 - by analysing the distribution of different bedform types within the Bay, and the implied gradients of mean spring peak surface currents;

2 - by using grain size data, and the concepts of McLaren & Bowles (1985) regarding systematic changes in grain size distributions along sediment transport paths

3 - by using the conclusions of Duane (1964) regarding the depositional implications of sediment skewness;

4 - by considering distribution patterns of various grain size statistics.

Secondly, this chapter analyses a time series of 6 estuarine cross-sectional profiles to study the short and longer-term physical responses of the estuary, in terms of net erosion or accumulation of sediment, to it's hydrodynamic environment.

Finally, data is presented on the variation of estuarine cross-section along the estuary, and whether the pattern of cross-section variation can help indicate areas of sediment accumulation or erosion.

7.2 Sediment Transport Pathways in Barmouth Bay

7.2.1 Use of Surficial Bedform Arrays

Travelling down a longitudinal velocity gradient may also represents distance along a potential sediment transport path, from source towards sink. On this basis, the model of a series of bedform zones related to particular velocity ranges (Fig. 7.1) (Belderson, Johnson & Kenyon, 1982), and further published evidence on bedform stability (described in Chapter 1, Sections 1.14.3 and 1.14.4), can be used to imply net sediment transport directions. From side scan sonograms, identification of bedforms and bedform arrays can allow designation of velocity ranges to areas of sea floor; hence, identification of directions along which velocities are inferred to constantly increase or decrease.

However, there is no simple relationship of a decrease in peak velocity, to an increased tendency towards sediment deposition. For instance, if the subordinate tidal current is of near equal velocity but of much greater duration that the dominant tide, the net sediment transport direction may be up the gradient of spring tide velocity of the dominant tide. It is also possible that during the spring-neap lunar cycle the tide direction with the peak velocity may change from flood to ebb, or vice-versa, so that the designation of 'dominant' tide may not be obvious or meaningful.

Another variable in the process of relating sets of co-existing bedforms to velocities is that the bedforms produced are related to sand supply (Belderson et al, 1982; Smith, 1988).

Other field based evidence of net sand transport directions relevant to this geophysical study are :

- megaripple and sandwave movements and asymmetry (eg McCave & Langhorne, 1982; Smith, 1988);
- obstacle mark polarity (Caston, 1979);

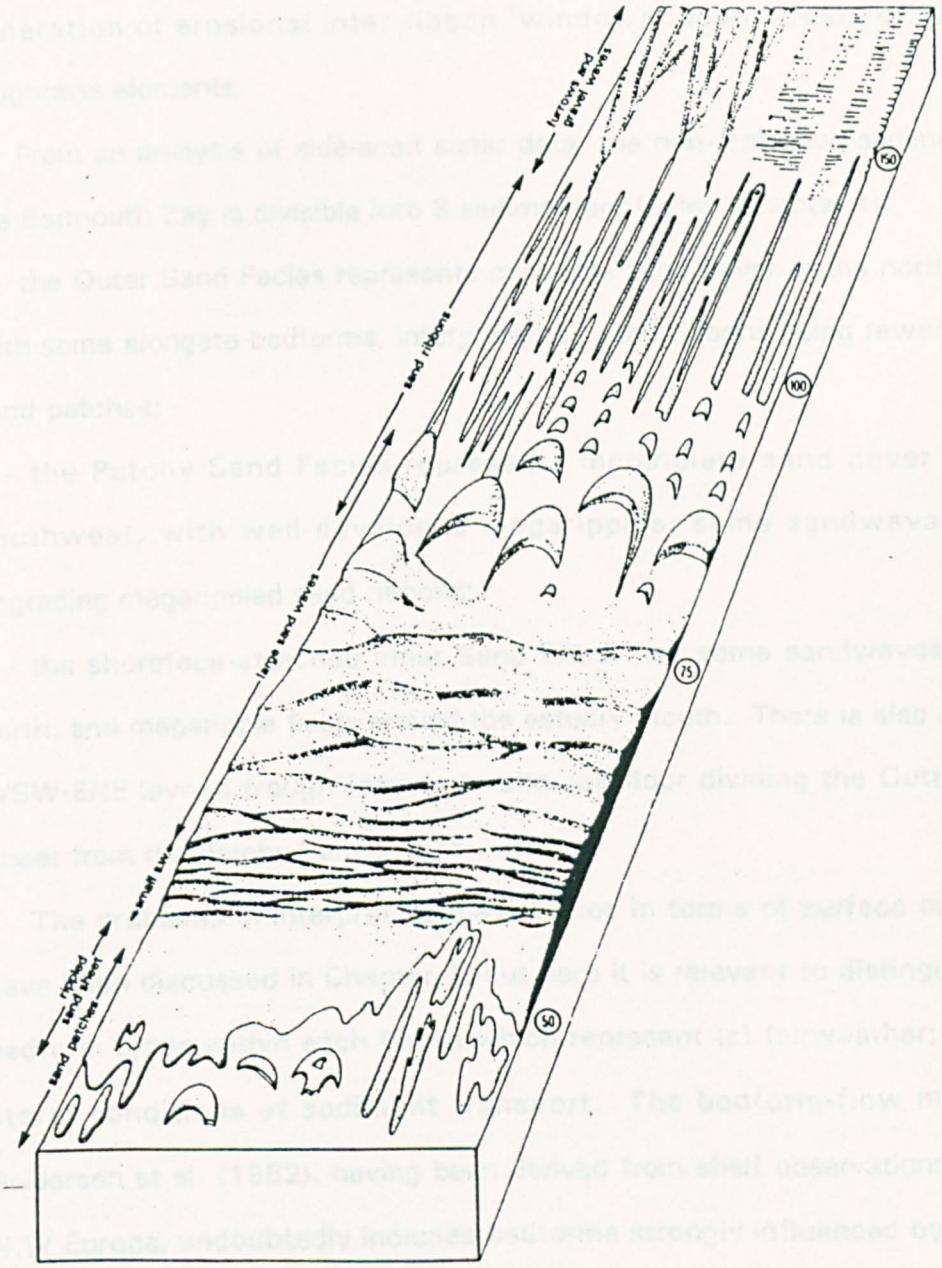

Block diagram of the main lower flow regime bedforms made by tidal currents on the continental shelf, with the corresponding mean spring peak near-surface tidal currents in cm/s.

After Belderson, Johnson + Kenyon (1982)

Fig. 7.1

Implied net sediment transport is towards the upper right

- sand ribbon polarity. Kenyon (1970) noted that individual sand ribbons tend to broaden and merge together in the direction of weakening peak tidal currents. However, this is not always seen (e.g Amos & King, 1984), and McLean (1981) described bifurcations opening downcurrent due to generation of erosional inter-ribbon 'windows' downstream of seabed roughness elements.

From an analysis of side-scan sonar data, the non- cohesive sediment in the Barmouth Bay is divisible into 3 sedimentary facies (Chapter 1):

1 - the Outer Sand Facies represents complete sand cover in the northwest, with some elongate bedforms, interpreted as sand ribbons being reworked to sand patches;

2 - the Patchy Sand Facies represents incomplete sand cover in the southwest, with well-developed megaripples, some sandwaves, and degrading megarippled sand ribbons;

3 - the shoreface-attached Inner Sand Sheet has some sandwaves in the north, and megaripple fields around the estuary mouth. There is also a major WSW-ENE leveed trough feature on the sea floor dividing the Outer Sand Sheet from the Patchy Sand Facies.

The problems in interpreting these facies in terms of surface currents have been discussed in Chapter 1, but here it is relevant to distinguish the bedform types within each facies which represent (a) fairweather; and (b) storm conditions of sediment transport. The bedform-flow model of Belderson et al (1982), having been derived from shelf observations around N.W Europe, undoubtedly includes bedforms strongly influenced by waves, but the shallow nature of Barmouth Bay means that the use of the relationships for inferring relative storm current strengths, is extremely unwise. Thus, despite the fact that substantial sediment transport occurs during storms, this particular discussion is limited to fairweather tidal conditions.

The bedform types interpreted as being produced under normal tide-dominated conditions, and their implied peak surface flow velocities for mean spring tides, in cm/s, are as follows:

OSF - elongate sand patches, <50,
sandwaves in south, and megaripples, 60-75;

PSF - sandwaves 65-75, megaripples 60-70,
sand patches <50;

ISS - sandwaves 65-75, local megaripples 60-70,
sand ribbons >90;

Leveed trough - sandribbons >90,
megarippled sandribbons 90.

From this, a general implication is that the highest tidal velocities, and thus the start of potential sediment transport paths, occur within the leveed-trough feature in the central bay, and locally on the front of the Bar near the estuary mouth. In terms of the facies defined here, the northern parts of the Outer Sand Facies would be most likely to represent the end of a sediment transport path i.e. a potential sediment sink. Thus, the main sediment transport pathway is implied to be away from the leveed-trough feature, northwards to the Outer Sand Sheet. Sediment is also inferred to be transported shorewards to the southern and northern parts of the Inner Sand Sheet, and then northwestwards into the outer bay. The presence of sandribbons on the seaward-facing slope of the Bar suggests that sediment would be transported away from this region. Presumably sediment would be moved either longshore or into the estuary.

These implications are broadly consistent with those of Moore (1968) (discussed in Chapter 1, section 1.4, Fig. 7.2), and the limited tidal current data available (Chapter 1, section 1.7), except that current data west of the estuary mouth suggests that ebb currents are strongest, thus flood-directed sediment transport may be less likely. The complex coastline morphology, and influence of the estuary, has created a complex pattern of bedform

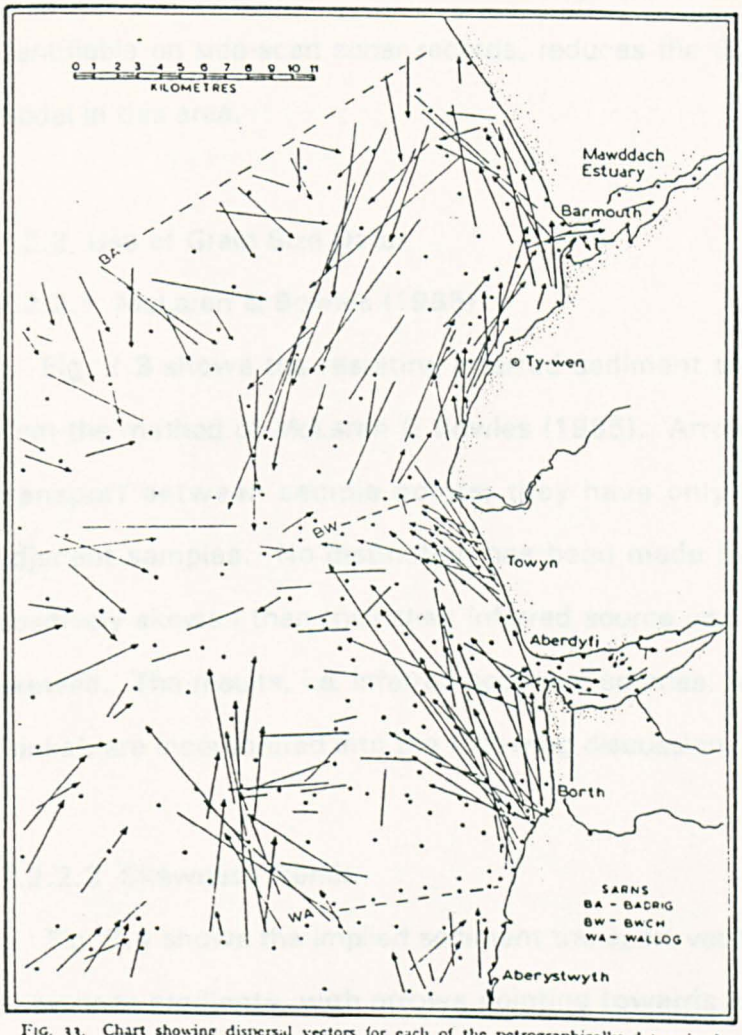

FIG. 33. Chart showing dispersal vectors for each of the petrographically determined grain types.

Fig 7.2 Chart showing dispersal vectors for each of the petrologically determined grain types (After Moore, 1968).

arrays in Barmouth Bay. This, and the large areas where few bedforms are identifiable on side-scan sonar records, reduces the use of the bedform-flow model in this area.

7.2.2 Use of Grain Size Data

7.2.2.1 McLaren & Bowles (1985)

Fig. 7.3 shows the resulting inferred sediment transport paths derived from the method of McLaren & Bowles (1985). Arrows indicate direction of transport between sample points; they have only been drawn between adjacent samples. No distinction has been made between deposits more positively skewed than their their inferred source and those more negatively skewed. The results, i.e. inferred sediment sources, transport pathways and 'sinks', are incorporated into the following discussion.

7.2.2.2 Skewness Trends

Fig. 7.4 shows the implied sediment transport vectors using sand fraction skewness gradients, with arrows pointing towards areas of relatively more positive skewness. Duane (1964) showed that positive skewness indicated areas of net sediment accumulation.

7.2.3 Discussion

The following discussion should be read with an appreciation of the variation inherent in the grain size samples, caused by the fact that the grab may have sampled the fine sand cover and/or the coarser substrate at each station.

Moore (1968) stated there were four contemporary coastal sources of sediment to Barmouth Bay, named above. The analysis of Figs. 7.3 and 7.4 suggests the following sources <u>within</u> the bay (in no particular order) :

Fig. 7.3 Implied sediment transport vectors in Barmouth Bay
- using the method of McLaren + Bowles (1985)

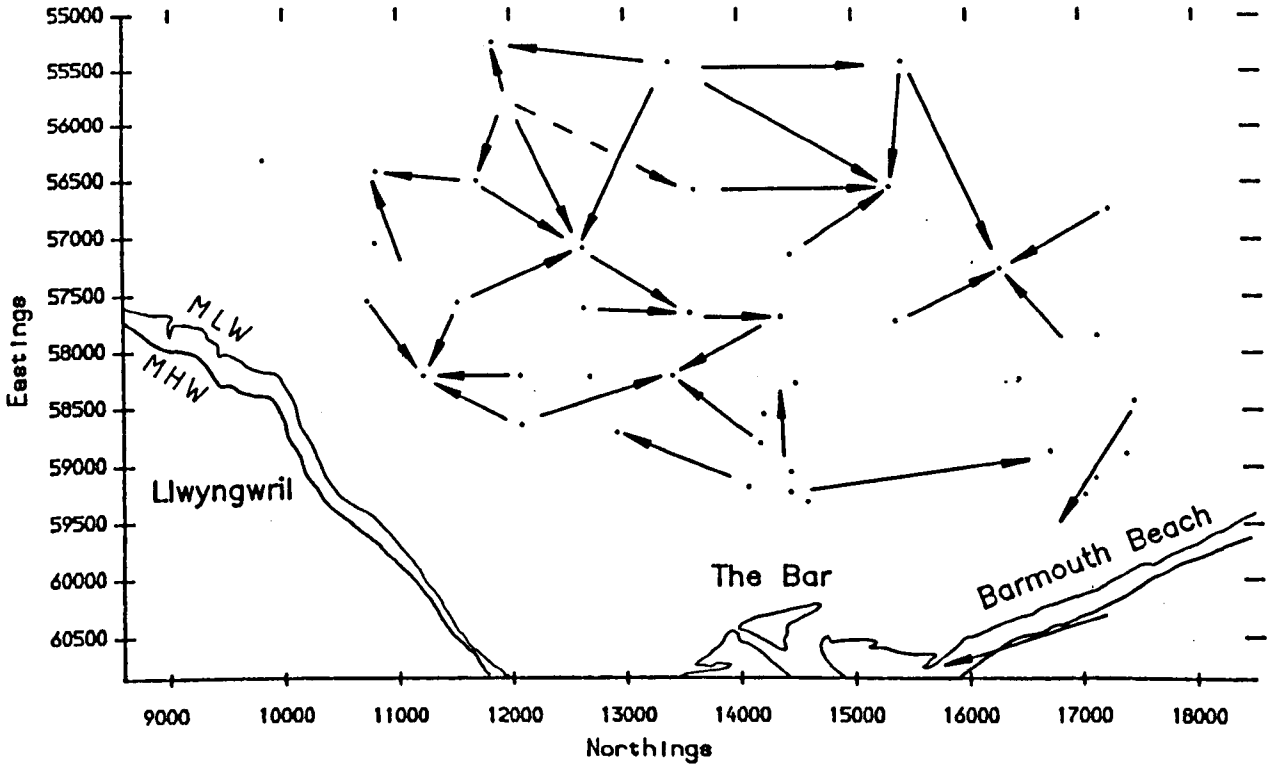

Fig. 7.4 Implied sediment transport vectors in Barmouth Bay
- using sand fraction skewness gradients

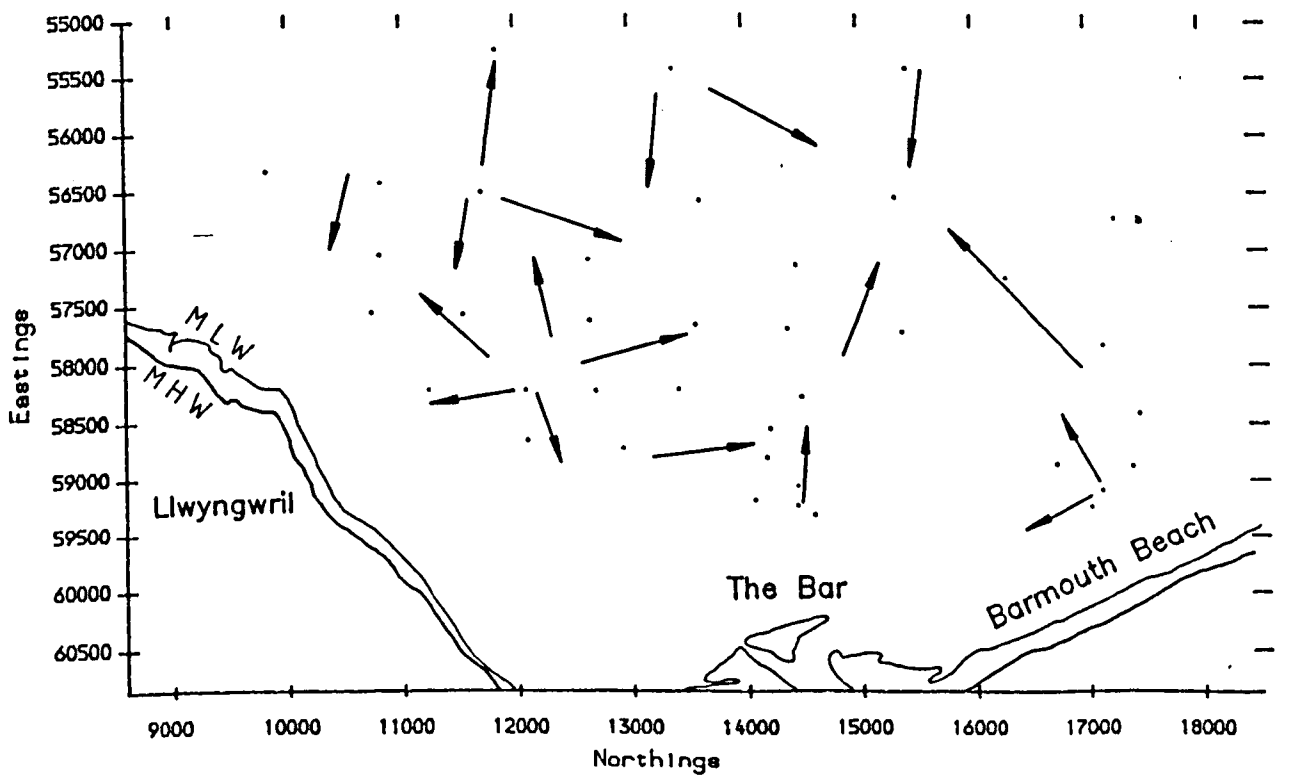

SEDIMENT SOURCES

1 - the extreme SW of the survey area (samples 404/5/6). Evidence : skewness, kurtosis;

2 - off Llwyngwril (samples 419/20). Evidence : mean, 2.05 phi mode, McLaren method;

3 - 2.7km SW of the bar (sample 422). Evidence : sorting, kurtosis;

4 - 2.5km W of the bar (sample 416). Evidence : 2.05 phi mode;

5 - 1km W of the bar (samples 440/1/2/3). Evidence : sorting, McLaren method;

6 - the central western part of the area (samples 401/2/8/and diver samples from stations 1 and 2). Evidence : mean, skewness; McLaren method.

Depositional zones in the Bay are unlikely to all be permanent sites of deposition. Storms are capable of mobilising the bed throughout the bay, so a concept of sediment 'stores' may be more useful. These may be depositional in nature under normal hydrodynamic conditions; during times of severe wave action, they may act as marine sediment supplies, allowing sediment redistribution and redeposition. The following sites are implied to be sediment 'stores' within the bay :

SEDIMENT STORES

1 - the NW of the area (samples 408/9/10/11/12). Evidence : McLaren method, sorting, skewness, 3.35 phi mode;

2 - 2.5km SW of the bar (samples 424/33). Evidence : McLaren method;

3 - 2km W of the bar (sample 425). Evidence : McLaren method, 3.35 phi mode, and weaker evidence from the %fines distribution map;

4 - 1km W of the bar (sample 440/1/2/3). Evidence : mean. N.B. This is contradicted by the map of sorting, and by the McLaren method, which suggest it is a source;

5 - 3.5km SW of the bar (sample 421). Evidence : McLaren method;

6 - 3km NNW of the bar (samples 444/6/7/8). Evidence : McLaren method,

mode, 3.35 phi mode;

7 - 3km N of the bar, on Barmouth beach (sample P300). evidence : McLaren method, sorting.

The concentrations of fines in the sediment samples is consistently very low; this tends to confirm the conclusion of Moore (1968), that the present hydrodynamic regime of the bay is too energetic to allow fine sediment to be deposited. This is in contrast to Tremadog Bay.

Within the Bay, sediment transport pathways can be inferred using grain size data, in a number of ways. Regions of near-constant size distributions and/or a continuous trend in, for example, mean size, sorting or skewness, have been used to delineate transport pathways (Dyer, 1986; McLaren & Bowles, 1985).

Transport pathway A - The major pathway identified in this study lies from the SW edge of the area, ~4-5km northeastwards towards the bar. In terms of sediment characteristics, the evidence for this pathway is sevenfold:

1 - the sand fraction mode distribution (Fig. 6.7) shows a 0.5-1.0km wide belt of constant mode;

2 - the sand skewness is strongly negative, but tends to become less negative northeastwards (Figs. 6.11, 6.12, 7.4);

3 - the sand kurtosis (moments) is above 4 (Fig. 6.13);

4 - there are consistently high proportions of the 2.55 phi mode in the sand fraction (Fig. 6.18);

5 - there are even contours of the 2.05 phi mode (Fig. 6.17) at the 3.5-4.5 % level;

6 - the sand fraction shows a well-developed fining trend northeastwards (Fig. 6.8);

7 - there are high and northeasterly-decreasing sand modal frequencies (Fig. 6.15).

(There is also indirect evidence for this pathway; local fishermen state that during southwesterly storms their lobster pots are moved substantial distances, >2km, to the NE from the area off Llyngwril (pers. comm. Tony Page, 1987)).

Transport pathway B - There is also a pathway from the SW of the area towards the the NNE, to the central north of the area. Evidence : McLaren method, mode, skewness, and possibly also kurtosis.

Transport pathway C - Dispersion occurs from G.R. 570108 (sample 419). Evidence : McLaren method, mode, and (less strongly) the 2.05 phi mode.

Transport pathway D - Overall there is northward and shoreward transport within the sampled area. Evidence : McLaren method, mean, mode, and the sorting data of Moore, (1968).

Pathways A and B are not resolvable into separate systems, as different lines of evidence give slightly different implied positions and directions. Their combined transport pattern may be envisaged as a northward and eastward dispersal fan. Figure 7.5 shows implied bed sediment transport directions derived from asymmetry of megaripples and sandwaves, imaged using echo-sounder and side-scan. Firm evidence is sparcely distributed, and conclusions are limited by the possibility that bedform symmetry reverses over a tidal cycle. However, it does suggest net shoreward transport from the southwest of the bay, and southward shore-parallel transport along Barmouth Beach.

Overall then, from the available evidence, the dominant transport path in the Bay is fed from the southwestern Bay, in the Patchy Sand Facies. Material is derived from erosion of glacial and peri-glacial sediments beneath the mobile sand, and presumably from further south and west of the surveyed area. Sediment within the leveed trough in the central bay is very

Fig. 7.5 Implied sediment transport pathways in Barmouth Bay, using bedform orientation suggested by side-scan sonar and echo-sounder data.

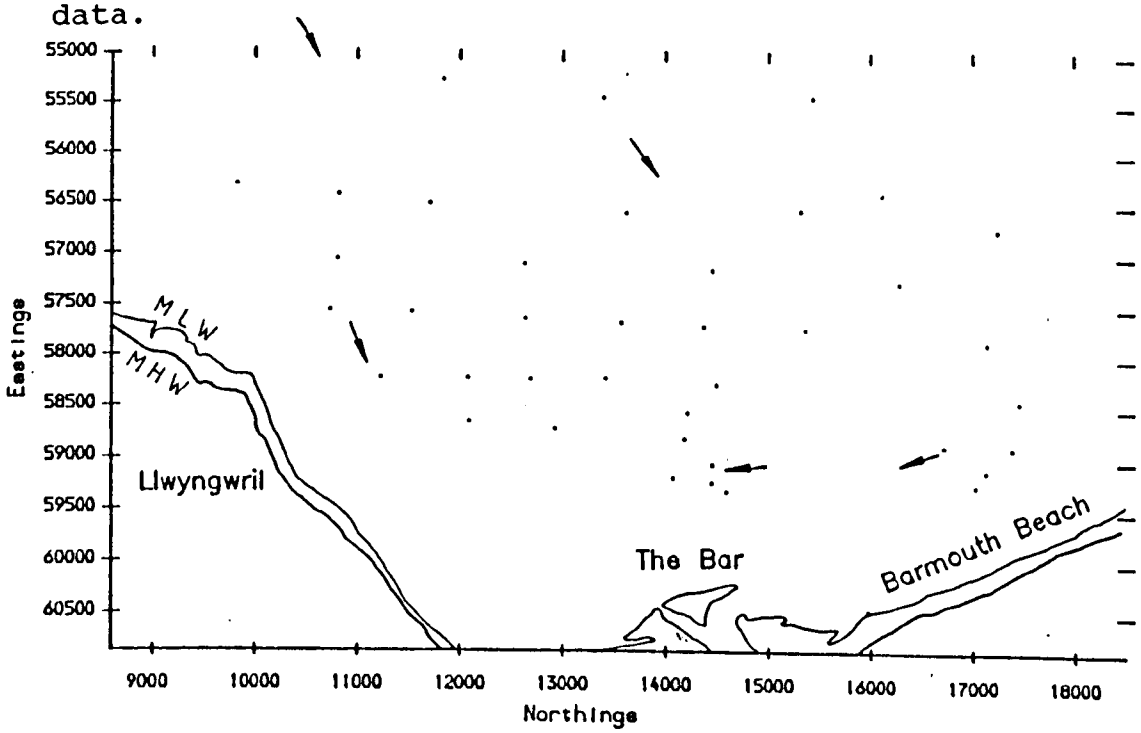

mobile, even under normal tide-dominated conditions. Bed material moved northwards into the Outer Sand Facies presumably would bypass the leveed trough most near it's seaward end where it's relief is least. The clarity of the transport paths is disrupted by the incomplete nature of the sand cover over much of the Bay.

7.3 Estuarine Accumulation and Erosion

Many modern estuaries are often considered as simple 'sediment sinks' of material supplied from either shelf or hinterland; they are, however, complex hydrographic, chemical, biological and sedimentological systems in their own right. The following sections analyse a time series of 6 cross-estuary profiles to quantify temporal and spatial changes in the volume of sediment beneath them. The sections were surveyed with the view to calculating modern net rates of sediment accumulation or erosion, as done in 2 similar Welsh estuaries, the Taf (in southwest Wales) and the Dwyryd (in Tremadog Bay), by Jago (1974) and Mahamod (1989) respectively. Both these workers had discovered high long-term sediment accumulation rates, and it was hoped to compare the Mawddach with these estuaries.

Survey line positions and morphology were shown in Chapter 6, in relation to the grain size survey of the sandy portions of the estuary. Table 7.1 gives the survey dates of the transects.

Table 7.1

Dates of Survey of Estuarine Transects (dd-mm-yy)

	Survey Number				
Transect number	1	2	3	4	5
1	26-04-86	14-04-87	28-04-87	--	--
2	26-04-86	14-04-87	28-04-87	--	20-07-88
3	26-04-86	14-04-87	28-04-87	13-07-87	--
4	26-04-86	14-04-87	28-04-87	13-07-87	--
5	26-04-86	14-04-87	28-04-87	--	--
7	--	14-04-87	28-04-87	--	--

7.3.1 Implications for Estuarine Sediment Transport and Deposition

Bed-level Changes

From the surveyed cross-estuary transects, total areas of erosion E and accumulation A along the transects, between times of survey periods, have been calculated, i.e. the area difference between plots of successive bed profiles. From these a number of parameters have been derived:

B = mean bed elevation over the transect (m O.D.N.);

Tot = mean of total areas of erosion and accumulation, i.e. 'total volume transported' over the survey line (m^2);

E = mean area of erosion per metre of transect (m^2/m);

A = mean area of accumulation (m^2/m);

T = mean of E and A, i.e. 'volume transported' per metre of survey line (m^2/m);

Ch = (A-E)/2, mean change in bed level per metre of the transect (m^2/m); (where +ve = net accumulation, and -ve = net erosion);

Chrate = mean rate of change of Ch since the last survey ($m^2/m/day$).

These parameters were calculated along the transects, between points near each end of the transect, which were covered by all the surveys of that line (Table 7.2). In practical terms these limits were :

Transect 1 between 2 and 368m;

Transect 3 between 13 and 287m;

Transect 4 between 25 and 1326m;

Transect 5 between 48 and 1348m;

Transect 7 between 30 and 1215m.

(The zero positions of each transect do not mark the 'edge of the estuary', but represent the position of the marker posts to which each survey

Table 7.2

Some parameters derived from the whole survey lines

Transect	Survey	Parameter B mODN	Tot m2	E m2/m	A m2/m	T m2/m	Ch m2/m	Chrate m2/m/day
1	1	1.237	-	-	-	-	-	-
	2	1.124	45.74	0.1827	0.0675	0.1251	-0.1153	-3.26E-4
	3	0.894	45.83	0.2399	0.0106	0.1252	-0.2293	-1.64E-2
Net erosion of 0.93mm/day								
3	1	0.271	-	-	-	-	-	-
	2	0.114	40.04	0.2251	0.0672	0.1461	-0.1579	-4.47E-4
	3	0.045	16.67	0.0954	0.0262	0.0608	-0.0692	-4.94E-3
	4	-0.078	39.67	0.2069	0.0827	0.1448	-0.1242	-1.63E-3
Net erosion of 0.79mm/day								
4	1	0.851	-	-	-	-	-	-
	2	0.834	95.54	0.0189	0.0649	0.0734	-0.0171	-4.84E-5
	3	0.768	62.30	0.0806	0.0151	0.0479	-0.0655	-4.68E-3
	4	0.891	97.70	0.0133	0.1368	0.0751	+0.1235	+1.63E-3
Net deposition of 0.09mm/day								
5	1	0.484	-	-	-	-	-	-
	2	0.352	190.53	0.2125	0.0806	0.1466	-0.1318	-3.74E-4
	3	0.162	177.10	0.2312	0.0413	0.1362	-0.1899	-1.36E-2
Net erosion of 0.88mm/day								
7	2	1.708	-	-	-	-	-	-
	3	1.656	48.51	0.0677	0.0142	0.0409	-0.0535	-3.83E-3
Net erosion of 3.7mm/day								

Table 7.3

Some parameters derived from portions of the survey lines

Transect	Survey	Parameter B mODN	Tot m2	E m2/m	A m2/m	T m2/m	Ch m2/m	Chrate m2/m/day
4	1	1.047	-	-	-	-	-	-
	2	1.085	30.86	0.0182	0.0570	0.0376	+0.0194	+5.50E-5
	3	1.029	33.24	0.0689	0.0122	0.0405	-0.0283	-2.02E-2
	4	1.168	59.89	0.0035	0.1426	0.0730	+0.0695	+9.14E-4
Net deposition of 0.28mm/day								
5	1	1.395	-	-	-	-	-	-
	2	1.438	18.18	0.0125	0.0561	0.0343	0.0218	+6.18E-5
	3	1.210	60.47	0.2282	0.0000	0.1141	-0.1141	-8.15E-3
Net erosion of 0.5mm/day								
7	2	1.911	-	-	-	-	-	-
	3	1.876	25.21	0.0441	0.0090	0.0265	-0.0175	-1.25E-3
Net erosion of 2.5mm/day								

Notes : Transect — Portion of Transect used

Transect	Portion of Transect used
4	180 - 1000m
5	750 - 1280m
7	250 - 1200m

was horizontally reduced). However, a limitation on the calculated data is that each transect was defined by relatively few points, so that any changes in the mean level of the area may have been obscured by the inaccuracies in the repeatability of the surveying process, particularly in areas of topographic change or when survey results were affected by different low water levels (see above, Transect 4). The above parameters were therefore recalculated on portions of certain transects, where similar numbers and positions of survey points had been taken, and where topographical effects were likely to be minimal. Effectively, the recalculated data covers the mudflat or sandflat sections of those transects which crossed large portions of this estuarine sub-environment. Results are tabulated in Table 7.3.

Overall sedimentation rates are dominantly erosional, between erosion of 3.7mm/day and accumulation of 0.09mm/day over the whole estuary. The net sedimentation rates of Transects 4,5 and 7 calculated from the whole transect, and the sandflat parts are comparable, but give consistently more depositional results. This may indicate that the sandflats in the estuary are relatively more depositional than channels. However, they do tend to confirm that the surveying process does not introduce large errors to the results.

The most clear result from these analyses is apparently one of dominant net erosion over each transect. However, it is important to note a number of factors which limit this conclusion :

1 - these data cover a relatively short period of time with few repeated surveys;

2 - it must be considered whether the transects chosen are representative (in bed level terms) of change in the estuary, or parts of it. This is an inevitable unknown, as 'representative' itself is only definable in qualitative terms in such a physically, spatially and temporally variable environment. Where it is clear that local geomorphological effects, such as channel meandering or collapse of a saltmarsh scarp are of importance to the result, they may be

removed from the overall picture, but where this is not the case it is necessary to assume that the data is of a representative nature;

3 - also important is the time variability of cross- sectional area, and the validity of comparisons between data measured on different dates. The data here suggest that the highest net rates of erosion occurred along each transect in the fortnight between surveys 2 and 3, with up to 1.36E-2 m^2/m/day eroded from the whole of Transect 5, and 8.15E-2 m^2/m/day from the sandflats between 750 and 1280m. This change in bed level in just 2 weeks is substantially higher than the changes measured between other surveys or over the full survey period of 443 days, thus conclusions are grossly limited by the fact that the short-term variation in the measurements are probably greater than any trends present in the system over a period of 15 months.

Despite the above reservations regarding the data, there is a suggestion in the data that the estuary changes in a systematic fashion in terms of bed level. Highest calculated net rates of erosion (Chrate) occurred on all transects between surveys 2 and 3, with all values between 4.94E-3 and 1.64E-2 m^2/m/day. There is also a consistency in the value of Chrate between survey 1 and 2, with values between 4.85E-5 and 3.26E-3 m^2/m/day. (It is here emphasised that each individual transect survey is entirely independent of every other one, so there is no possibility of a common surveying factor causing these apparent relationships).

Together, these similarities suggest that in terms of periods of months, there may be systematic changes in bed-levels throughout the length of the estuary, with common periods and similar rates of change in sediment levels. That there is apparent similarity of this measure of sediment transport, i.e. bed level change normalised by transect length, also suggests that there may be a relationship between estuarine width, (i.e. transect length) and the net sediment transport rates. The data also has implications in terms of the 'reaction rate' of estuarine sediment levels, i.e. the potential for rapid

morphological change over the whole estuary. Clearly great changes can occur in periods of days to weeks.

As an average of Transects 1,3,4,5 and 7, a drop in estuarine bed level of 0.12m occurred in 14 days prior to survey 3. Calculated total load transport rates for the strongest ebb flow through the channel at Penrhyn Point are 0.0038m^3/m/tide (this chapter), and by multiplying by channel width (~200m) a rough estimate of total ebb sediment flux can be deduced as 0.76m^3/m/tide, i.e. 2 tonnes moved 1m seawards. If the erosion of 0.12m did occur throughout the estuary, and was all transported out through the estuary mouth into Barmouth Bay, this is equivalent to a total volume of 1140000m^3, or ~40000m^3/tide (taking the area of the estuary to be ~9.5km^2, Chapter 1). This is 50000 times greater than the above, and clearly is not a feasible situation.

A number of conclusions are possible, first that the estuarine survey was too limited in extent, and liable to extreme bias, possibly with all transects showing one end of a set of sediment level changes in the estuary. Clearly if large amounts of sediment had been eroded from the surveyed parts of the estuary, and the majority of it remained in the estuary, then some estuarine areas must have experienced similar rates of net deposition. Some inherent bias in the choice of sites to survey may have been to choose transects where large areas of sediment exposed at low water, i.e. lines of high elevation. These higher intertidal areas may be more susceptible to short-lived high energy conditions liable to cause their erosion.

Transect 4 is the only one to show sediment net accumulation over the 4 survey period, with a net accumulation rate of 0.09mm/day. The main site of net deposition are the flats south of the main estuarine channel, which are accumulated at a mean 0.28mm/day. The Spartina colonisation may be a factor in this tendency; the stems slow the tidal currents over the mudflats, and enhance the rate at which sediment settles out of suspension, thus

increasing sediment accumulation. Comparisons of Ordnance Survey maps show that the southern mudflats have been advancing northwards for at least the last 15 years. According to local evidence, Spartina concentration on these sandflats has been increasing over a similar period.

Conclusion

The long-term (15 months) tendency shown by this data, over complete estuarine transects, is for net erosion over time; variation is between 0.9mm/day (0.3m/yr) of erosion and 0.1mm/day (0.036m/yr) of accumulation. The sandflats also show no clear pattern; the data suggest either erosion at 0.5mm/day (0.18m/yr) or accumulation at 0.28mm/day (0.1m/yr). These compare with quoted long-term accumulation rates of 0.155m/yr in the Taf (Jago, 1974), and 0.049m/yr in the Dwyryd (Mahamod, 1989), and when viewed in the absence of other data, indicate the the Mawddach Estuary is eroding. However, the representative nature of the surveyed transects is in doubt.

7.4 Estuarine Cross-Sectional Areas

7.4.1 Introduction

It has earlier been demonstrated (Chapter 2) that the Mawddach Estuary shows characteristics intimately related to it's physical form, in particular the hydrographic consequences of the mid-estuary constriction at Farchynys. The following sections investigate:

1 - whether a relationship exists between a physical measure of estuarine size, the cross-sectional area, and the distance from the estuary head;

2 - whether deviations from such a relationship can provide information on the nature of sedimentation along the estuary, and hence on potential morphological changes within the estuary.

Many macrotidal and mesotidal estuaries assumed to be in 'long-term equilibrium' tend to show a logarithmic increase in their cross-sectional area towards their mouths (Dyer, 1973, page 4). This is a rather general statement on the subject, but it is a useful concept upon which some observations and speculations about the sediment transport regime of the estuary can be based. Prandle & Rahman (1980) proposed a general theory of the tidal response in estuaries, using a power law variation of estuary width and depth, i.e. cross section. They examined 10 estuaries and found good fits to a power law approximation for 4 of them, and somewhat poorer fits for 4 others. However, their work implied some validity for the model.

In meso- and macro-tidal estuaries, tidal ranges are by definition high (up to 5m in the Mawddach). Given that this means that the estuarine cross-section is greater at high water than at low water, a pertinent question is: if an 'equilibrium' exists, at which particular tidal height does the estuary most exhibit this 'equilibrium'? Clearly the estuarine cross- section measured at high water springs is considerably greater than that at low water springs, and there is much intermediate variation.

A second problem is that the relationship of cross-sectional area to variation in tidal height is not a constant one along the length of the estuary. This is because of two factors:

1 - estuarine bed level cross-sections do not have constant shape along the estuary length;

2 - estuarine bed-level cross-sections do not slope logarithmically towards a central channel base.

Both of these factors would need to be satisfied if the cross-sectional area of the estuary increased seaward logarithmically at all stages of the tidal cycle.

An important point is that the idea of an 'equilibrium' implies that change will occur (i.e net sediment transport) if a state of disequilibrium is reached. It must be recognised that this requires processes of change, which will be related to the energy available in the estuarine regime. Hence the system is inherently more likely to be near equilibrium to spring tidal conditions rather than neaps, because the processes of change are more powerful, i.e. sediment transport is greater on spring tides than on neaps.

The following section will use the hypothesis 'macro- and meso-tidal estuaries (or sections within them) which are in long-term sedimentary equilibrium with their hydrodynamic regime, display a logarithmic increase in their cross-sectional area towards the mouth'.

_ This hypothesis will be examined using the Mawddach Estuary as an example, and also considered will be the roles of the above two aspects, tidal height change and cross-sectional morphology.

7.4.2 Cross-Sections in the Mawddach

When considering the Mawddach Estuary in this context, there are two important physical areas to consider, the mouth and the region of Transect 3, in mid-estuary.

At the estuary mouth, there has been considerable morphological change caused by man. The Admiralty Chart 1484 dated 1890, but probably updated to 1923 (it quotes magnetic variation for that year), shows the existence of Trwyn-y-Gwaith, the breakwater SE of Ynys- y-Brawd. Therefore, this feature has been an influence on the Mawddach Estuary for at least 66 years.

A barrage exists linking the mainland with Ynys-y- Brawd, built in 1972/3. This closed the northern channel and has resulted in the tidal prism entering the estuary solely through the southern channel between Ynys-y-Brawd and Penrhyn Point. This has undoubtedly lead to a decreased total estuarine cross-sectional area at the mouth. Also significant is that, unlike the rest of the estuary, and in addition to tidally- caused sediment transport, the mouth is also under considerable influence from waves. Longshore drift is likely to be a long-term process acting to decrease the size of the mouth. Smaller estuarine systems in Cardigan Bay, eg. at Harlech and Tywyn, have been virtually completely closed by northerly advance of a spit across their mouths. It should, therefore, not be unexpected that the estuary mouth is smaller than would be predicted by a logarithmic relationship.

The second factor of importance is the rock constriction in mid-estuary, at Farchynys, which as shown in Chapter 2 is a major control upon estuarine circulation. It was suggested that because of its limited size, discharge through it is constrained, and so it controls estuarine circulation landward.

Table 7.4 shows cross-sectional areas for six sections across the Mawddach, from the estuary mouth to the tollbridge at Penmaenpool. These data are plotted in Fig. 7.6.

7.4.3 Discussion

The first aspect of the data to note is that the transects used for the calculations may not be representative of the estuary. It is an inherent, but untested assumption in the discussion below that the data are a fair representation of estuarine morphology; also that between each pair of

Fig. 7.6

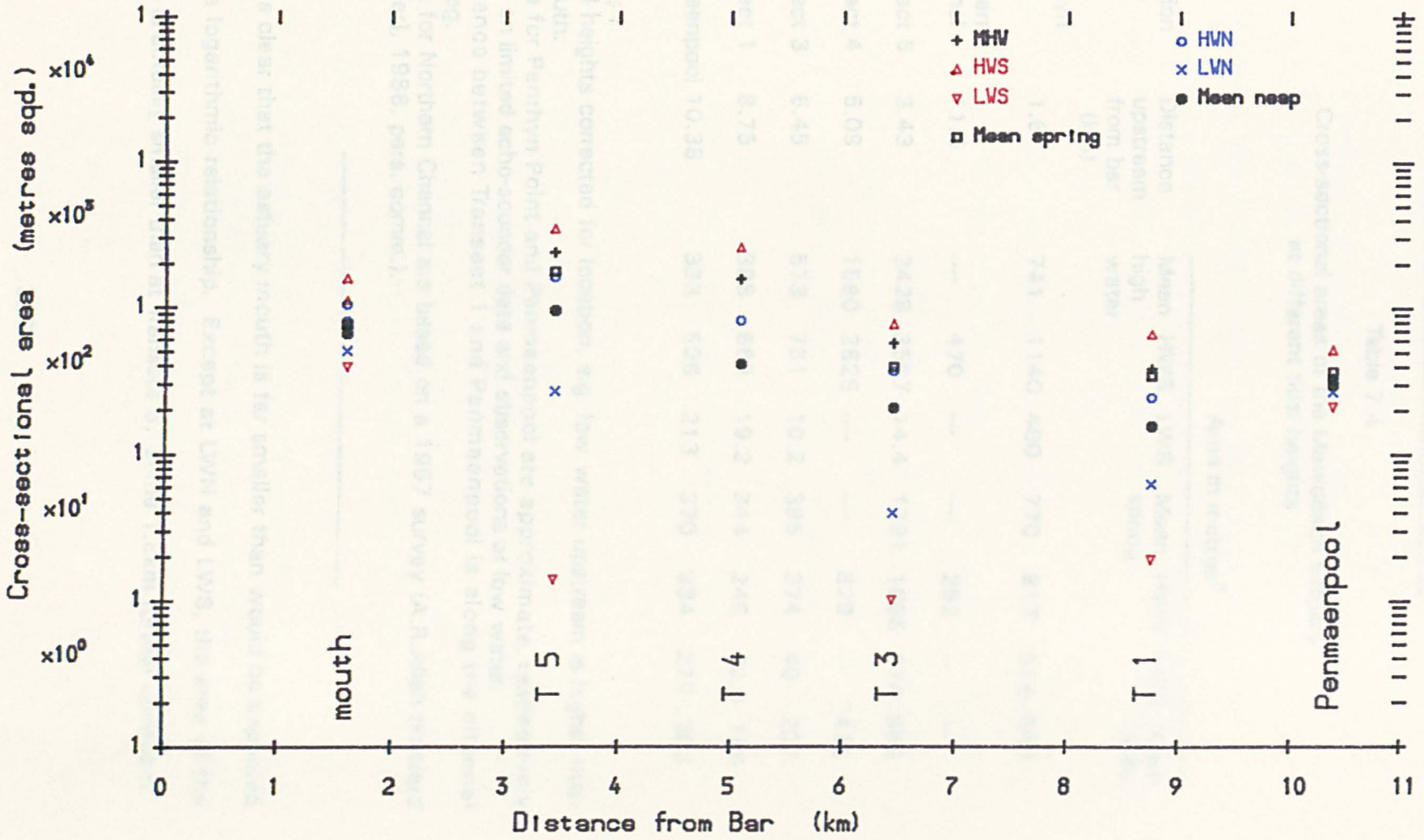
Estuarine x-sectional areas at various tidal heights
+ MHW
o HWN
△ HWS
× LWN
▽ LWS
● Mean neap
□ Mean spring
Cross-sectional area (metres sqd.)
x10⁴
x10³
x10²
x10¹
x10⁰
mouth
T 5
T 4
T 3
T 1
Penmaenpool
0
1
2
3
4
5
6
7
8
9
10
11
Distance from Bar (km)

transects the estuary displays characteristics intermediate in nature to each pair. Another unknown is the time-variability of cross-sectional area, and how valid it is to compare data measured on different dates. Thus, any conclusions made are inevitably limited.

Table 7.4

Cross-sectional areas of the Mawddach Estuary at different tidal heights

Location	Distance upstream from bar (km)	Area in metres^2						
		Mean high water	HWS	LWS	Mean spring	HWN	LWN	Mean neap
Penrhyn Point	1.6	741	1140	400	770	817	514	666
Northern Channel	~1.6	----	470	---	----	252	---	---
Transect 5	3.43	2429	3567	14.4	1791	1658	274	966
Transect 4	5.08	1580	2625	----	----	829	---	~415
Transect 3	6.45	573	781	10.2	396	374	40	207
Transect 1	8.75	386	669	19.2	344	246	62.9	155
Penmaenpool	10.38	333	526	213	370	334	272	303

Notes:
- Tidal heights corrected for location, e.g. low water upstream is higher than at mouth.
- Data for Penrhyn Point and Penmaenpool are approximate, respectively based on limited echo-sounder data and observations at low water.
- Distance between Transect 1 and Penmaenpool is along the channel thalweg.
- Data for Northern Channel are based on a 1967 survey (A.R.Allan [Posford Duvivier], 1988, pers. comm.).

It is clear that the estuary mouth is far smaller than would be expected from a logarithmic relationship. Except at LWN and LWS, the area of the mouth is actually smaller than at Transect 5, some 1.8km further upstream.

It is also apparent that Farchynys (Transect 3) is small in cross-section. The cross-sectional area here at each tidal height cannot be increased, as the north bank is made of rock outcrop, and the south bank is a man-made slate wall. Thus in terms of adaptation of estuarine cross-sections upstream of this constriction, the 'logarithmic equilibrium' of the upper estuary may be controlled by this section. As tidal energy is the major energy input in the estuary, and is derived from seaward of the constriction, the upper estuary cross- sections need have no continuous trend with the lower estuary. In the data plotted, this is apparent as a decrease of slope in the lines, and this adds to the tidal wave evidence (Chapter 2) that the Mawddach estuary can be considered as a two-part dynamic sedimentary system, one either side of the Farchynys constriction.

There is a convergence of points towards the head of the estuary, which is interpreted as reflecting decreasing tidal influence, especially upstream of Transect 1. More evidence of tidal control of estuarine cross-sections is the fact that the data suggests the estuary is nearer to an 'equilibrium form' (i.e. closer to a logarithmic form) under conditions of tidal inundation rather than at LW.

When the area of the (now blocked) northern channel of the estuary mouth is added to todays data for Penrhyn Point, there is only a small increase in size. Although the survey for the northern channel was conducted in 1967, and the other data ~20 years later, Admiralty Charts show there has been little discernible change in the channel at Penrhyn Point, and it is concluded that the cross-sectional area of the mouth 20 years ago was little nearer to a size consistent with the logarithmic 'ideal'. This would imply that the influence of man upon the system will have added to, rather than 'caused' the apparent recent tendency for sediment accumulation in the present-day estuary. The influence of the spit is a greater factor in controlling the area of the mouth, and so presumably affecting sedimentation.

It is speculated that because the mouth and Farchynys are now relatively fixed in their cross- sectional area, the entire lower estuary is likely to be undergoing change to (re)form a near logarithmic cross-sectional increase between them. This would mean that the whole lower estuary will accumulate sediment, something in accord with local observation over the last few years. All lines marking cross-sectional areas along the estuary at high tides suggest this.

In the upper estuary, a logarithmic area relationship is shown for MHW and HWS tides. The calculation of sediment transport fluxes through the estuary at Penrhyn Point, Farchynys and Penmaenpool (this chapter) show that very little sediment transport occurs in the upper estuary on neap tides. Ten times more sediment transport occurs on spring tides than on neaps, i.e. only spring tides provide sufficient energy to create significant change in the estuarine morphology. At present the upper-estuarine system appears near 'equilibrium', with relatively low inferred sediment accumulation rates (3.9E-3 mm/yr), 25 times lower than in the lower estuary. This interpretation is also in line with evidence from local people, who have seen neither significant erosion or deposition in the recent past in the upper estuary.

If continued seawards, the straight line representing areas at HWS in the upper estuary meets the present point for the estuary mouth. Whether this is significant or merely chance is unknown, however it may indicate that (if anywhere) it is the lower estuary which is implied to be most likely to be affected by the construction of the barrage across the northern channel.

These rather speculative interpretations nevertheless appear to agree with other qualitative lines of evidence regarding areas and rates of sedimentation in the estuary. It would be interesting to survey the tidal heights, currents, and cross- sections of an estuary (or part of one) in great detail, in order to ascertain how valid the 'logarithmic equilibrium' model is, and to determine to which current or transport parameter the system is most closely 'adjusted' to. As the process of morphological change requires sediment erosion,

transport and deposition, it is likely that the parameter concerned, if one exists, would be related to sediment transport. One possibility is that the cross-sectional pattern of the estuary is most 'in equilibrium' with the mean tidal height in the estuary at the time of peak total estuarine sediment flux. This of course is a very simplified idea, as many other factors are involved in estuarine circulation and sediment transport. For instance, times of peak transport flux may vary within the Mawddach because of the progressive nature of the tide. The limited data collected in this study do not allow an investigation of these ideas.

7.5 Summary and Conclusions

There is a pattern of sediment transport pathways within Barmouth Bay, identified by grain size and side- scan evidence. The major transport path begins at the southwest extreme of the survey area and continue for 4-5km northeastwards, becoming indistinct near the ebb tide delta. This is related to the flood tide, and is probably enhanced during southwesterly storms. Bed sediment is moved along this pathway as sand ribbons and megaripples. Related to this pathway is more northward sediment dispersal into the central northern region of Barmouth Bay. There is overall northward and shoreward sediment transport within Barmouth Bay, but with offshore components west of the bar, and southward transport along Barmouth Beach.

The study of the temporal and spatial variability of estuarine bed levels has given an unclear picture of estuarine sediment transport. Six transects across the estuary were repeatedly surveyed over a period of 15 months. The representative nature of the transects chosen is in question, and only tentative conclusions are possible regarding estuary-wide trends. The conclusions are :

1 - the Mawddach Estuary shows long-term variation in deposition rates between 300mm/yr of erosion and 36mm/yr of accumulation

2 - the sandflats are relatively depositional compared to the whole range of estuarine sub-environments, showing long-term deposition rates between erosion at 180mm/yr and accumulation at 280mm/yr

3 - the measured drop in bed-level of 0.12m along the transects in the fortnight between surveys 2 and 3 could not have taken place over the whole estuary, thus there are major short-term shifts of sediment within the estuary. These may take the form of erosion of sandflats and accumulation in tidal channels as intra- channel bars.

The hypothesis 'macro- and meso-tidal estuaries which are in long-term sedimentary equilibrium with their hydrodynamic regime will show a logarithmic increase in cross-sectional area seaward', has elucidated controls on estuarine sedimentation :

1 - measurements demonstrate that the estuary is nearer to a logarithmic shape on spring tides than on neaps; this is explained by the fact that the necessary process of morphological change, i.e. sediment transport, is more active with higher tidal range. It is implied that spring tides may cause strong net accumulation in the lower estuary, but that the upper estuary is subject to little change. These tentative conclusions agree well with those derived from calculations of net sediment transport fluxes;

2 - man's major influence on the cross-section of the Mawddach, namely the blocking of one of the two tidal channels at the mouth, has probably merely added to, rather than initiated, any trends of accumulation in the estuary;

3 - the principle controls on long-term estuarine sedimentation are the presence of the shingle spit Ro Wen, which limits channel size at the mouth, and the rock bounded mid-estuary constriction at Farchynys. This has created a two-component estuarine system, with different long-term sedimentary responses in each;

4 - it is speculated that the parameter to which the estuarine sedimentary system would be most closely 'adjusted' to, is one related to flow conditions at the time of peak sediment transport rates along the estuary.

Chapter 8

Concluding Remarks

This concluding chapter briefly discusses this research, integrating geological data with conclusions drawn from sedimentological and oceanographic data. The discussion is centred around a series of summary diagrams. Lack of radiocarbon dates forces the discussion to consider loosely defined time periods, the 'early' and 'late' Holocene, rather than more specific time intervals.

The Mawddach Estuary and Barmouth Bay are today very active regions of sediment transport, dominated by tidal and wave-induced currents. The Bay and Estuary are subject to strong tidal currents, created by a tidal wave skewed by bed friction as it passes over the shallow waters of the area. This creates a flood-dominated inner shelf and estuarine environment, which, combined with the dominant southwesterly wave regime, results in net flood-directed sediment transport. An exception is northern Barmouth Bay, where 'overflow' water from Tremadoc Bay passes southwards through the Mochras Channel (Caston, 1965), and contributes to net accumulation of sediment south of Sarn Badrig in northern Barmouth Bay (Fig. 8.1).

The Estuarine Fill

Analysis of pre-existing borehole data has shown that the estuary is infilled with a marine transgressive sequence 30-75m thick; the surficial estuarine sands are up to 5m in thickness, and form a landward-thinning sand wedge ~11km in length (Fig. 8.1). Following process studies of megaripple migration characteristics and surveys of the estuary, it can be stated that within the estuary, the seaward end of the sand body is dominated by megaripple cross- bedding, preserved in infilled tidal channels. Behind the spit Ro Wen, current- and wave- rippled lamination will dominate,

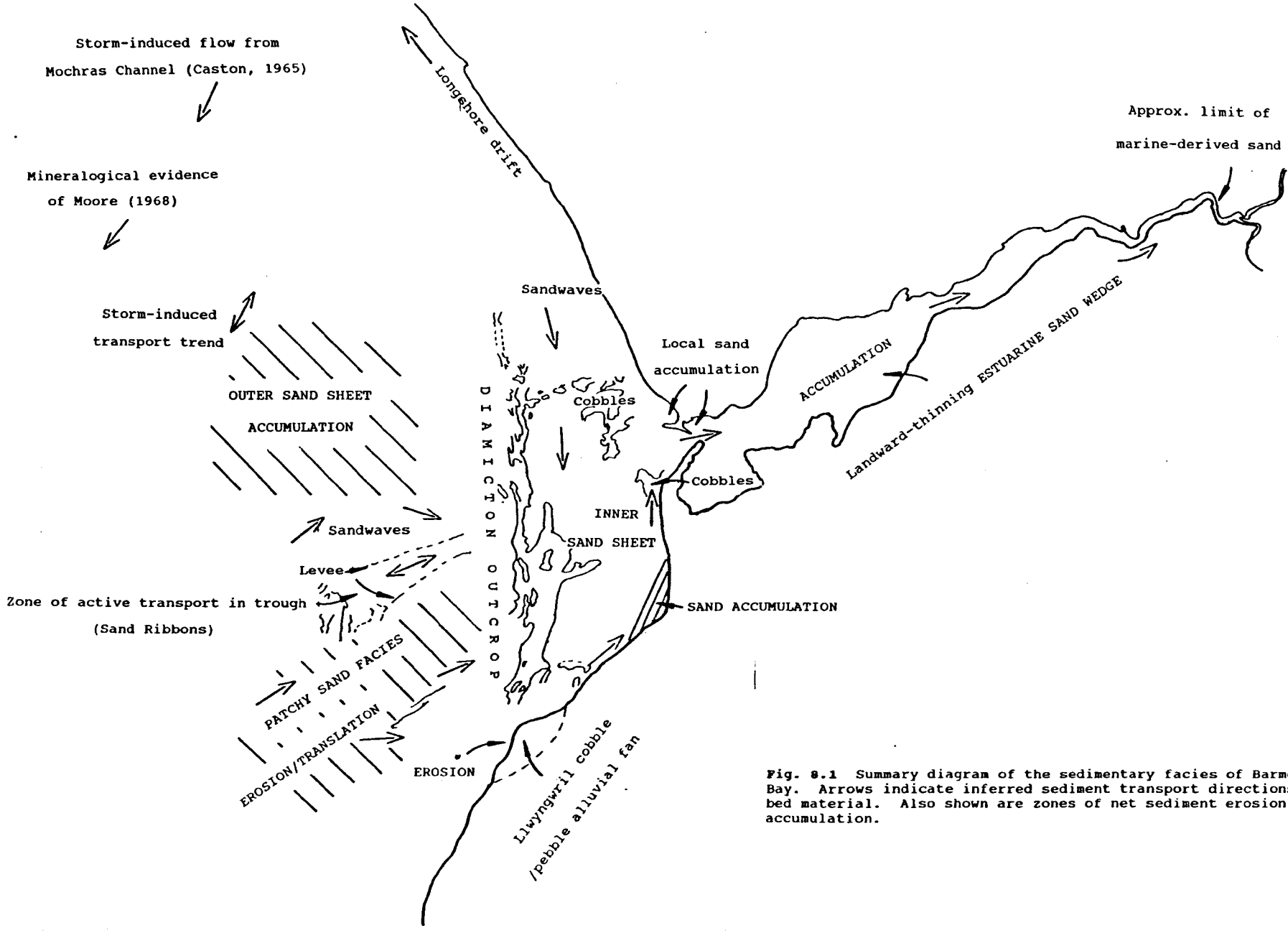

Fig. 8.1 Summary diagram of the sedimentary facies of Barmouth Bay. Arrows indicate inferred sediment transport directions of bed material. Also shown are zones of net sediment erosion and accumulation.

whereas towards the estuary head, large- scale trough cross-bedding and ripple cross-lamination is likely to dominate preserved sediments. Grain size analyses have revealed, that, landward, the upper surface of the sand body decreases in grain size, improves in sorting, and shows increasing positive skewness; these trends are consistent with petrological evidence that the fine sand is derived from erosion of Holocene glacial and post-glacial sediments, in Barmouth Bay and areas further offshore. It is unknown what vertical textural trends, if any, occur within the sand body.

The recognition of inshore silici-clastic tidal deposits in the geological record relies upon a number of criteria (Terwindt, 1988), which, in association, may be used to identify a tidal deposit. These criteria include :

* autochthonous fauna and flora, and ichnofossils;
* consistent lateral sequences of tidal bundles in cross-bedded sets;
* lateral spring-neap tide sequences, sometimes with oppositely-directed cross-lamination, and mud-drapes;
* bi-directional cross-bedding;
* rapid, often abrupt, facies changes, and frequent planes of discontinuity;
* various types of dm-m scale vertical sequences.

Variations in details in these and other features may be used to distinguish between subtidal, intertidal and supratidal deposits, and to infer tidal flow strengths. However, to infer tidal range, or relative changes in sea-level, the type and vertical distribution of facies is considered. Within an estuarine fill, a particular vertical facies sequence may represent the product of an overall relative sea- level trend. Under conditions of falling sea-level, facies would represent an upwards change from estuarine to fluvial conditions, with sediment supplied dominantly from the land mass. Under a rising sea level, the facies would change upwards from fluvial, through estuarine, and, ultimately, to marine conditions of deposition, with sediment

supplied dominantly from marine sources. However, despite rising or falling sea-levels, sediment supply to an estuary may still be mixed, from both marine and land sources. Land sources may contribute to the estuarine fill near the head or local minor freshwater inputs, especially during river floods.

In the case of the Mawddach, the glacially-related sediments at the base of the valley fill are derived from inland, and the surface estuarine sediments have been shown to be derived from offshore. Intermediate sediments have been interpreted as recording the transition from fluvial to estuarine conditions, and would contain an upwards-increasing proportion of marine-derived sediment. It is unknown at what level in the sequence landward-directed sediment transport started or became dominant, although by the time that estuarine conditions became established, sediment transport would have been predominantly landward. In boreholes off Aberporth (Haynes, et al, 1977) and in Tremadoc Bay (Spencer, 1976), the transition from brackish to marine conditions occured ca. -40m and -30m respectively. Therefore, it is possible that most of the Mawddach valley fill above the -35m glacially-scoured Palaeozoic surface, is estuarine in origin.

Evolution of the Coastal System

In terms of the origin and evolution of the sedimentary facies, the 'estuarine system' extends beyond the mouth of the modern estuary. For example; seismic evidence has revealed the likely presence of a early post-Glacial barrier in northern Barmouth Bay allowed the deposition of the sediments of the Early Holocene Lacustrine/Lagoonal seismic facies (Fig. 8.2). Deposition landward of this barrier was probably in a marine-influenced sedimentary environment, which, at that time, was almost certainly a northern extension of the mouth of the fluvially-dominated Mawddach valley river (Fig. 8.3). (A possible modern analogue is the fine sediment now accumulating on the southern margins of the sheltered tidal areas behind the spit Ro Wen). This sheltered environment may have extended southwards behind the end morainic complex of tills, sands and gravels.

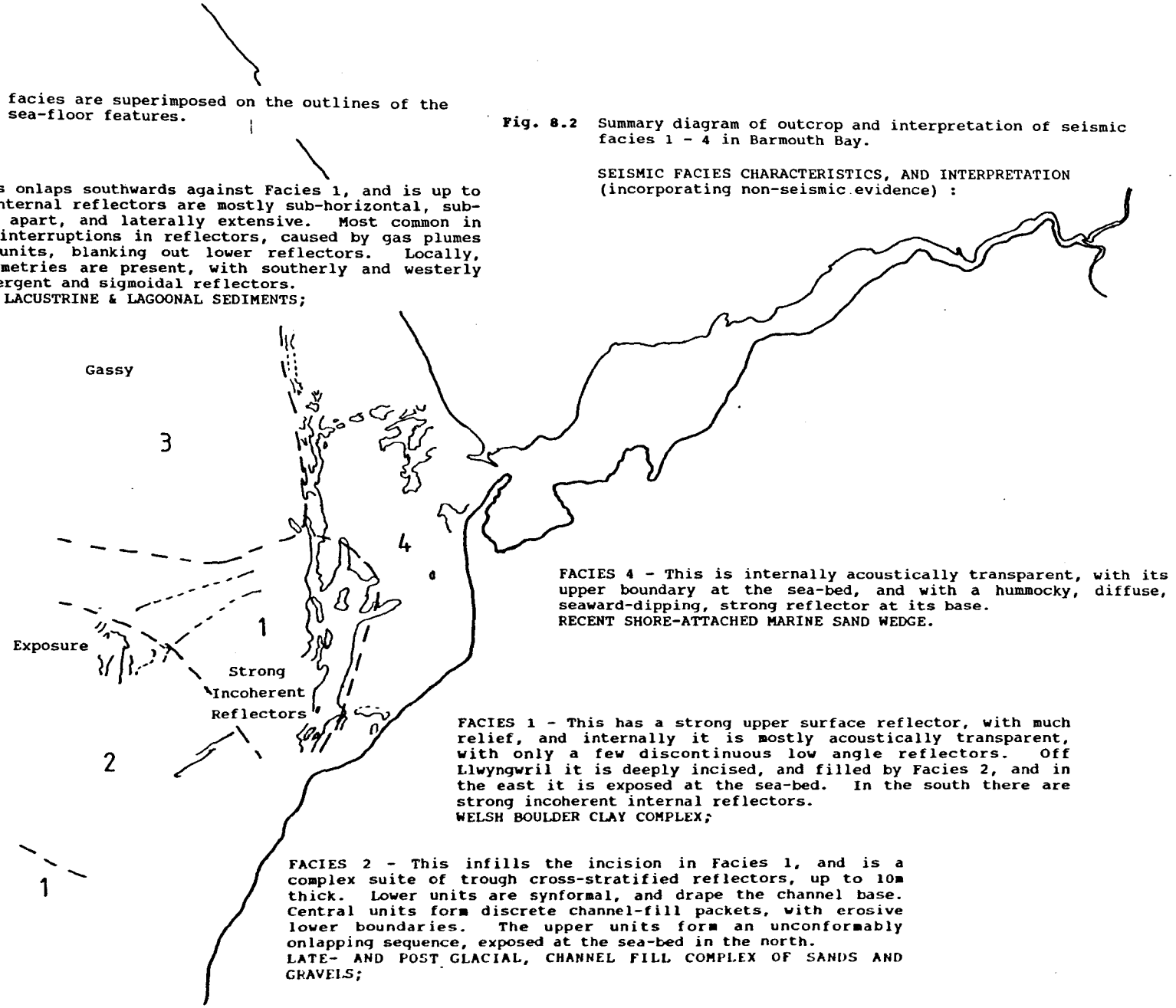

Fig. 8.2 Summary diagram of outcrop and interpretation of seismic facies 1 - 4 in Barmouth Bay.

SEISMIC FACIES CHARACTERISTICS, AND INTERPRETATION (incorporating non-seismic evidence) :

The seismic facies are superimposed on the outlines of the present-day sea-floor features.

FACIES 3 - This onlaps southwards against Facies 1, and is up to >10m thick. Internal reflectors are mostly sub-horizontal, sub-parallel, 1-3m apart, and laterally extensive. Most common in the north are interruptions in reflectors, caused by gas plumes in the upper units, blanking out lower reflectors. Locally, basin edge geometries are present, with southerly and westerly onlap, and divergent and sigmoidal reflectors.
EARLY HOLOCENE LACUSTRINE & LAGOONAL SEDIMENTS;

FACIES 4 - This is internally acoustically transparent, with its upper boundary at the sea-bed, and with a hummocky, diffuse, seaward-dipping, strong reflector at its base.
RECENT SHORE-ATTACHED MARINE SAND WEDGE.

FACIES 1 - This has a strong upper surface reflector, with much relief, and internally it is mostly acoustically transparent, with only a few discontinuous low angle reflectors. Off Llwyngwril it is deeply incised, and filled by Facies 2, and in the east it is exposed at the sea-bed. In the south there are strong incoherent internal reflectors.
WELSH BOULDER CLAY COMPLEX;

FACIES 2 - This infills the incision in Facies 1, and is a complex suite of trough cross-stratified reflectors, up to 10m thick. Lower units are synformal, and drape the channel base. Central units form discrete channel-fill packets, with erosive lower boundaries. The upper units form an unconformably onlapping sequence, exposed at the sea-bed in the north.
LATE- AND POST GLACIAL, CHANNEL FILL COMPLEX OF SANDS AND GRAVELS;

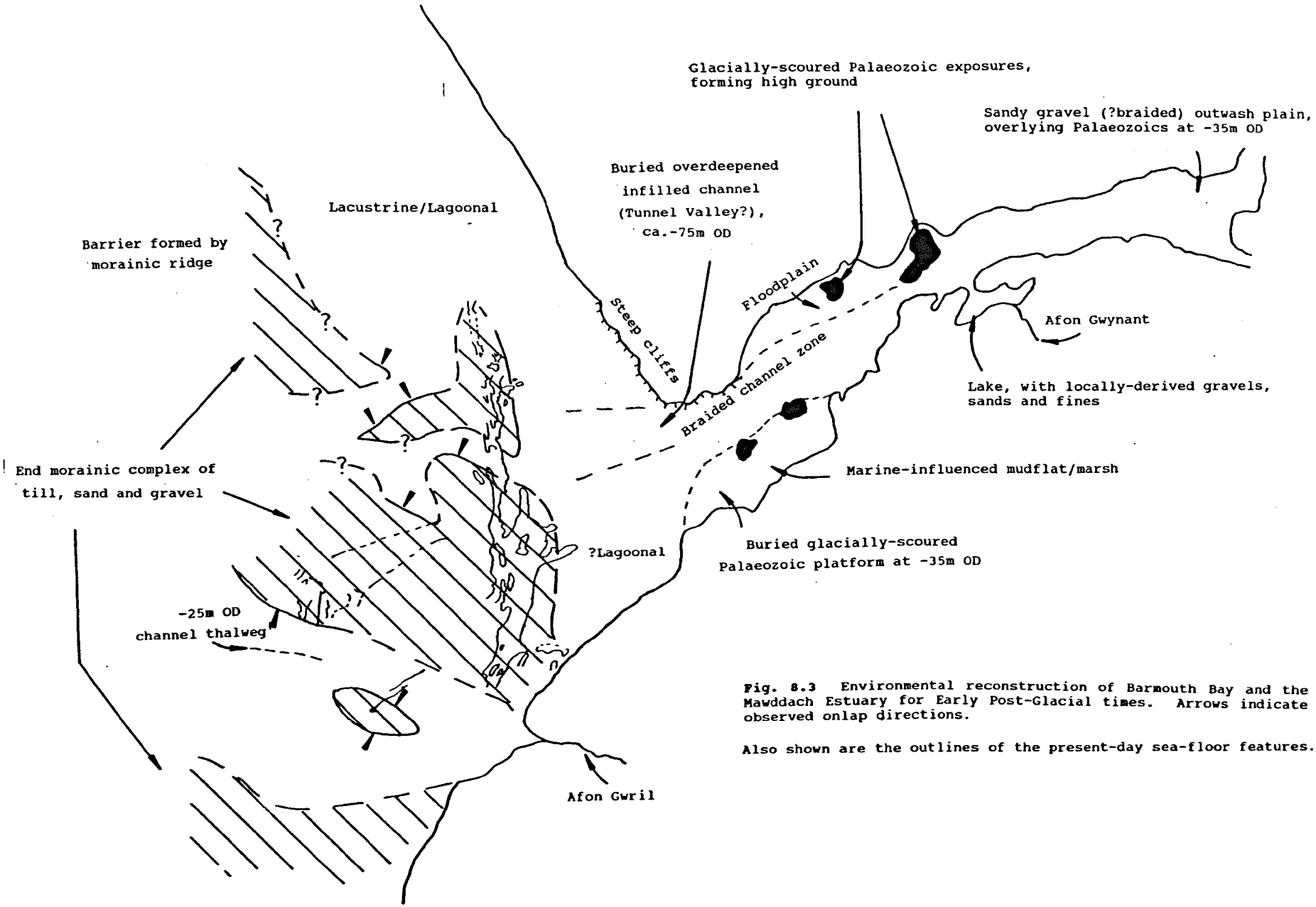

Fig. 8.3 Environmental reconstruction of Barmouth Bay and the Mawddach Estuary for Early Post-Glacial times. Arrows indicate observed onlap directions.

Also shown are the outlines of the present-day sea-floor features.

Further south, the Afon Gwril flowed into Barmouth Bay, incising the morainic complex to beneath -30m O.D.N., and depositing a complex suite of cross- stratified channel units, comprised of sands and gravels. There is insufficient data to determine whether there was a confluence of the Mawddach and Gwril rivers, limiting the geomorphological reconstruction shown in Fig. 8.3..

This study has found a modern coincidence in position of the N-S aligned break in the bathymetric slope, with the outcrop of what is interpreted as glacial diamict, at ca. -10m. This allows the speculative conclusion that this constitutes a drowned palaeo-shoreline, presumably forming low morainic cliffs. Once inundated by the rising sea-level, erosion by the advancing surf zone would have enhanced supply of sandy and muddy sediment to the estuary. It would also allow wave-induced longshore transport along the coast from Llwyngwril to Fairbourne, where it may have supplied sediment to commences building of the spit Ro Wen (Fig. 8.4). Sediment would also have been supplied for coastal accretion at Barmouth, and north of Llanaber.

There is no data on the timing of formation of the gravel spit Ro Wen at the estuary mouth, however, it is speculated that it formed broadly contemporaneously with the spit across the Dyfi Estuary to the south, thought by Wilks (1977,79) to have formed ca. 5000 yr. B.P..

Spit formation is likely to have had major effects upon sedimentation within the estuarine system. Behind the spit, shelter from strong tidal currents and waves would have allowed relatively fine-grained sediments to begin to accumulate, followed by progressive vegetational colonisation (Fig. 8.4). With northwards spit growth, there would have been corresponding progradation of intertidal flats and supratidal marsh, and restriction of the tidal channels towards the northern side of the estuary mouth, as today. Landward of the spit, there is likely to have been increasing asymmetry of the tidal wave with time, due to at least two factors:

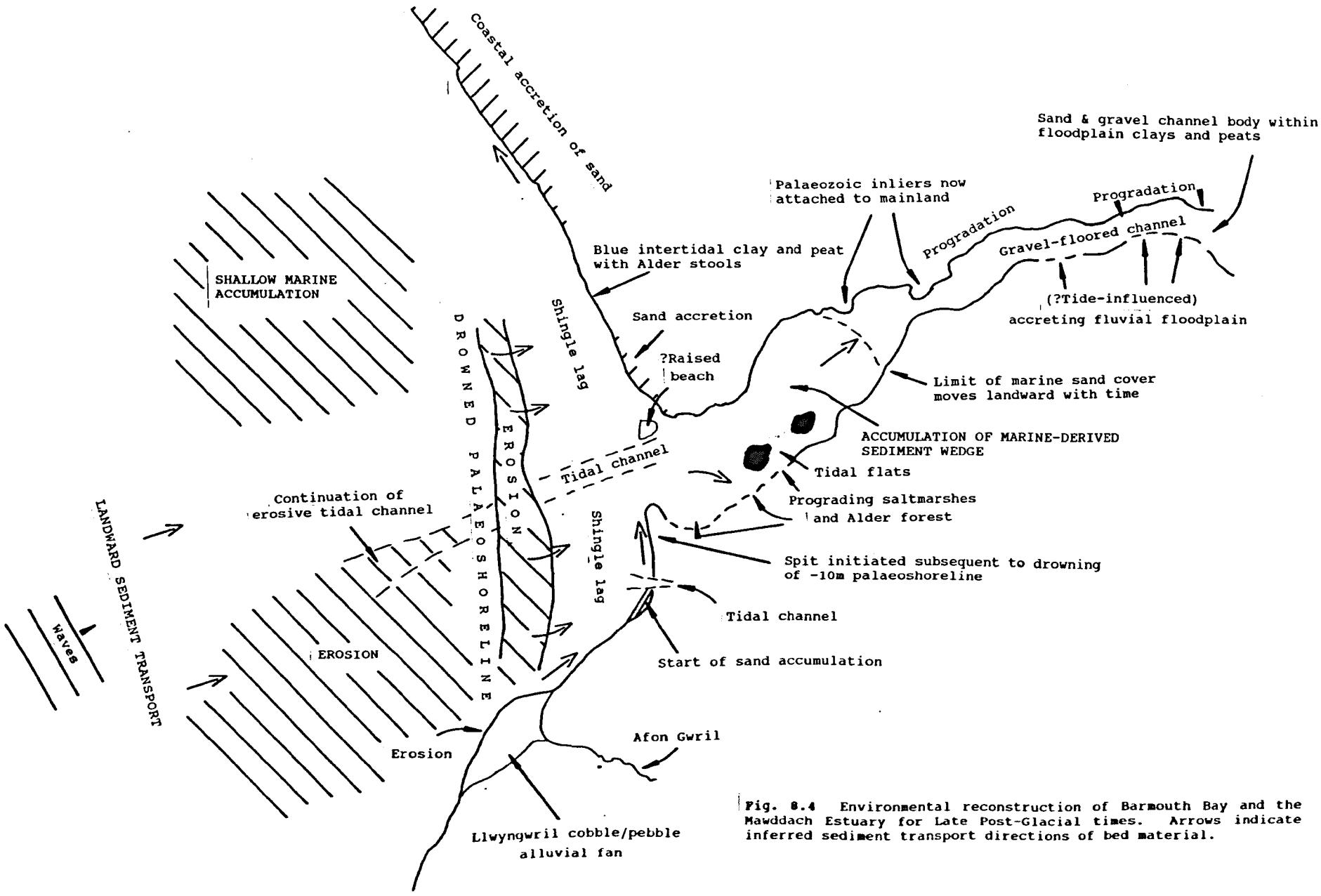

Fig. 8.4 Environmental reconstruction of Barmouth Bay and the Mawddach Estuary for Late Post-Glacial times. Arrows indicate inferred sediment transport directions of bed material.

1) gradual steepening of the tidal wave as it was forced to enter the estuary through a smaller entrance;

2) a progressively shallowing estuary.

These factors may have enhanced flood sediment transport within the estuary.

A similar effect may have occurred in mid-estuary. The saltmarshes north of the rocky mound of Farchynys, are inundated by the sea on the largest spring tides. They are probably relatively recent deposits, and it is likely that Farchynys was previously surrounded by tidal flats or channels. As sediment accumulated on these flats, the island became joined to the northern bank of the estuary, and the tide was forced to pass throught the narrow constriction on the southeastern side of the island, as it does today. Thus net landward sediment transport would have been enhanced.

These changes in estuarine morphology may also have been related; the formation of the spit would have increased marine sediment input into the estuary, encouraging potential sediment accumulation on sandflats and saltmarshes, such as those at Farchynys. Both these morphological changes are likely to have also affected the hydrographic properties of the estuary; they would have decreased the distance of penetration of saline water up the estuary, and increased the mean elevation of low water. Additionally, waves effects within the estuary will have been diminished, leading to, weaker surface mixing, and greater potential for flow stratification. These changes may have had consequences in terms of the type and distribution of estuarine flora and fauna.

Processes and Sediments - Ancient v Modern

Such major morphological changes will have also undoubtedly created change in the estuarine sediments and preserved sedimentary structures, so that, for example, within the modern estuarine sand wedge, there may be

upwards-increasing expression of flood-directed sediment transport. In the case of tidal megaripples, it is probable that through time, there will have been an overall increase in the proportion of flood- orientated tidal bundles preserved, as sediment accumulation continued within a regime of increasing flood-directed sediment transport. Theoretically, there will also be a tendency for an upwards-increasing occurence of flood-orientated tidal bundles towards the northern side of the estuary mouth, and towards the axis of the estuary, further inland. This is of course a simplification, because superimposed upon this trend will be the effects of channel avulsion, and channel migration, so that no such pattern may actually have been preserved. Additionally, this research has shown that even with near-complete preservation, the sedimentary structures produced by tidal megaripples may not easily be interpreted as products of a mesotidal flood-dominated tidal regime.

Mineralogically (and broadly texturally), the estuarine sand body will be very similar to those now present in Barmouth Bay; their preservation potentials and morphology are, however, very different. The estuarine sand has a high preservation potential, with little potential for removal until the next glaciation of Snowdonia, when it would probably be removed by a Mawddach valley glacier and related outwash. In contrast, the shelf sands are thin, mobile, and likely to be continuously reworked, as at present. In particular, the sand ribbons and megaripples of the patchy sand facies, occuring in an erosive or translational sedimentary environment, have very low preservation potential. The outer sand facies, possibly depositional, and the shoreface-attached inner sand sheet, are slightly more likely to be preserved, but are liable to large erosive episodes, such as during storms.

Estuarine sedimentation will have occurred within fluvial channels flooded by rising sea-levels, in, for example, the units comprising the channel fill sequence of the palaeo-Gwril. Channel filling is continuing today, within the Mawddach Estuary, with gradual landward movement of the limit of marine-

derived sediment. As in the present estuary, the landward and basal portions of the channels will represent fluvially- dominated sedimentation, with increasing tidal signatures in a seaward direction, and upwards in the sequence.

Thus, in many ways, sedimentation within the modern Mawddach estuary may be very similar to sedimentation in Barmouth Bay during the Holocene sea- level rise. However, there are also important differences between them :

1 - The present estuary is laterally constrained by the bedrock valley sides; in the Early Holocene, beyond the valley mouth there was increased potential for lateral sediment dispersal and estuarine facies development. This is reflected in the complex nature of the seismic facies found in Barmouth Bay;

2 - The modern coincidence in position of the N-S trending cliffs of Palaeozoic rocks, and the Mawddach Estuary mouth, is likely to have resulted in a different regime of sediment supply into the area by longshore drift, and the supply of fine sediment will have diminished during the Holocene, as coastal erosion of glacial deposits at, and south of Llwyngwril moved landwards towards the cliffline of highly resistant Palaeozoic rocks;

3 - In Early Holocene times, seismic evidence shows that, in addition to the Mawddach River, Barmouth Bay had a coastal sediment source at Llwyngwril, evidenced by a buried channel system; this system is now represented by a large coastal shingle fan;

4 - At some stage in the evolution of the spit Ro Wen, prior to the deposition of the southern part of the Inner Sand Sheet, there was a further shallow channel connecting the Mawddach Valley to Barmouth Bay, situated at the southern margin of the valley mouth; this is suggested by a depression in the base of the Inner Sand Sheet. The timing and nature of this connection is unknown, but it seems likely that it was tidally-influenced at some stage, and it may be filled with estuarine sediment.

There are other ways in which understanding of the modern hydrodynamic and sedimentary regime of the Bay and Estuary, presented here, can contribute to the understanding and interpretation of preserved facies, and to speculation about their nature and extent. For example; prior to the formation of the Mochras Channel, northern Barmouth Bay probably contained little surface sediment derived from Tremadoc Bay and the Llyn Peninsular area. In the late-Holocene and Recent, the storm-induced 'overflow' of water through this channel has probably contributed significantly to the sediment budget of Barmouth Bay. Prior to channel formation, there was also probably no large anticlockwise circulation of sediment within Barmouth Bay, rather a progressive accretion of sediment along the southern fringes of Sarn Badrig (Wingfield, pers. comm.) and local accumulation along the Barmouth-Harlech coast. Now, it is likely that both patterns occur.

Another example of the complementary nature of the hydrodynamic and geological data in this thesis, is in the interpretation of the wide 'trough and levee' feature in central Barmouth Bay. Its occurrence has been shown to be probably related to both underlying geology and modern sediment dynamics, but explanation of its origin or maintainance would be incomplete without considering a combination of geological, sedimentological and oceanographic data.

ACKERS, P. & WHITE, W.R. (1973) Sediment transport: new approach and analysis. Proc. Am. Soc. civ. Eng., Jour. Hydraul. Div., HY11, 2041-2060.

ADAMS, C.E. & WEATHERLY, G.L. (1981) Some effects of suspended sediment stratification on an oceanic bottom boundary layer. J. Geoph. Res., 86, 4161-4172.

ALBERTSON, M. (1953) Effects of shape on the fall velocity of gravel particles. Proc. 5th Iowa Hydraulics Conf., Iowa City, Iowa, 243-261.

ALLEN, J.R.L. (1968a) Current Ripples. North Holland, Amsterdam, 433pp.

ALLEN, J.R.L. (1968b) The nature and origin of bed-form hierachies. Sedimentology, 10, 161-182.

ALLEN, J.R.L. (1976a) Computational models for dune time-lag: general ideas, difficulties and early results. Sed. Geol., 15, 1-53.

ALLEN, J.R.L. (1976b) Computational models for dune time-lag: population structures and the effects of discharge patterns and coefficient of change. Sed. Geol., 16, 99-130.

ALLEN, J.R.L. (1976c) Time-lag of dunes in unsteady flows: an analysis of Nasner's data from the R. Weser, Germany. Sed. Geol., 15, 309-321.

ALLEN, J.R.L. (1976d) Computational models for dune time-lag: an alternative boundary condition. Sed. Geol., 16, 255-279.

ALLEN, J.R.L. (1978) Polymodal dune assemblages: an interpretation in terms of dune creation-destruction in periodic flows. Sed. Geol, 20, 17-28.

ALLEN, J.R.L. (1980a) Sandwave immobility and the internal master bedding of sandwave deposits. Geol. Mag., 117, 437- 446.

ALLEN, J.R.L. (1980b) Sand waves: a model of origin and internal structure. Sed. Geol., 26, 281-328.

ALLEN, J.R.L. (1981a) Lower Cretaceous tides revealed by cross- bedding with mud drapes. Nature, 289, 579- 581.

ALLEN, J.R.L. (1981b) Palaeotidal speeds and ranges estimated from cross-bedding sets with mud drapes. Nature, 293, 394- 396.

ALLEN, J.R.L. (1984a) Sedimentary Structures, their character and physical basis. Elsevier, Amsterdam.

ALLEN, J.R.L. (1984b) Experiments on the terminal fall of bivalve molluscs loaded with sand trapped from a dispersion. Sed. Geol., 39, 197-210.

ALLEN, J.R.L. (1984c) Experiments on the settling, overturning and entrainment of bivalve shells and related models. Sedimentology, 31, 227-250.

ALLEN, J.R.L. & COLLINSON, J.D. (1974) The superimposition and classification of dunes formed by unidirectional aqueous flows. Sed. Geol., 12, 169-178.

ALLEN, J.R.L. & FRIEND, P.F. (1976a) Changes in intertidal dunes during two spring-neap cycles, Lifeboat Station Bank, Wells-next-the Sea, Norfolk (England). Sedimentology, 23, 329-346.

ALLEN, J.R.L. & FRIEND, P.F. (1976b) Relaxation times of dunes in decelerating aqueous flows. J. geol. Soc. London, 132, 17-26.

ALLEN, P.A. & HOMEWOOD, P. (1984) Evolution and mechanics of a Miocene tidal sandwave. Sedimentology, 31, 63-81.

ALLEN, P.M., COOPER, D.C. & SMITH, I.F. (1979) Mineral exploitation of the Harlech Dome, North Wales. Mineral Reconnaisance Programme Rep. Inst. Geol. Sci., No. 29.

ALLEN, P.M. & JACKSON, A.A. (1985) Geology of the country around Harlech. H.M.S.O., London.

AMOS, C.L. & KING, E.L. (1984) Bedforms of the Canadian eastern seaboard : a comparison with global occurences. Mar. Geol., 57, 167-208.

BABA, J. & KOMAR, P.D. (1981b) Measurements and analysis of settling velocities of natural quartz sand grains. J. Sed. Petrol., 51, 631-640.

BAGNOLD, R.A. (1954) The physics of blown sand desert dunes. Methuen, London.

BAGNOLD, R.A. (1963) Mechanics of marine sedimentation. In : Hill, M.N. (ed.) The Sea, 3, 507-582. Wiley Interscience.

BAGNOLD, R.A. (1966) An approach to the sediment transport problems from general physics. U.S. Geological Survey Prof. Paper, 422-I, p1-37.

BAGNOLD, R.A. & BARNDORFF-NIELSEN, O. (1980) The pattern of natural size distributions. Sedimentology, 27, 199-207.

BARNDORFF-NIELSEN, O. & BLAESILD, P. (1981) Hyperbolic distributions and ramifications: contribution to theory and application. in: Tallie, C, Patil, G.P. & Baldessari, B.A. (eds), Statistical distributions in scientific work, 4, p1944. Reidel Publishing Company.

BELDERSON, R.H., JOHNSON, M.A. & KENYON, N.H. (1982) Bedforms. in: Stride, A.H. (ed.) Offshore Tidal Sands. Chapman & Hall.

BELDERSON, R.H., KENYON, N.H., STRIDE, A.H. & STUBBS, A.R. (1972) Sonographs of the sea floor. Elsevier.

BERBEN, F.M.L. ET AL (1978) Ribblevormen, waterbeweging en hun onderlinge samenhang in een getijdengebied (Plaat van Ossenisse, Westerschelde). Geografisch Instituut, Rijksuniversiteit Utrecht.

BIJKER, E.W. (1967) Some considerations about scales for coastal models with moveable beds. Delft Hydraul. Lab. Rep. No. 50, :142pp.

BLACK, K.P. & HEALY, T.R. (1986) The sediment threshold over tidally induced megaripples. Mar. Geol., 69, 219- 234.

BLACK, K.P. & HEALY, T.R. (1988) Formation of ripple bands in a wave-convergence zone. Jour. Sed. Petrol., 58, 195-207.

BLATT, H., MIDDLETON, G.V. & MURRAY, R. (1980) Origin of Sedimentary Rocks. Prentice-Hall, Englewood Cliffs, New Jersey, 782pp.

BLUNDELL, D.J., DAVEY, F.J. & GRAVES, L.J. (1971) Geophysical surveys over the South Irish Sea and Nymphe Bank. Jour. Geol. Soc. London., 127, 339-375.

BLUNDELL, D.J., KING, R.F. & WILSON, C.D.V. (1964) Seismic investigations of the rock beneath the northern part of Cardigan Bay, Wales. Quart. Jour. Geol. Soc. London, 120, 35-51.

BLUNDELL, J., GRIFFITHS, D.H. & KING, R.F. (1969) Geophysical investigations of buried river valleys around Cardigan Bay. Geol. Jour., 6, 161-180.

BOERSMA,J.R. & TERWINDT, J.H.J. (1981) Neap-spring tide sequences of internal shoal deposits in a mesotidal estuary. Sedimentology, 28, 151-170.

BOERSMA, J.R., VAN DE-MEENE, E.A. & TJALSMA, R.C. (1968) Intricated cross-stratification due to interaction of a mega ripple with its lee-side system of backflow ripples (Upper-pointbar deposits, Lower Rhine). Sedimentology, 11, 147-162.

BOOTHROYD, J.D. & HUBBARD, D.K. (1974) Bedform development distribution pattern, Parker and Essex Estuaries, Massuchusetts. U.S. Army Corps Engineers Coastal Eng. Res. Center Misc. Paper 1-74.

BOOTHROYD, J.D. & HUBBARD, D.K. (1975) Genesis of bedforms in mesotidal estuaries. in: Cronin, L.E. (ed.) Estuarine Research, Vol. II, Geology and Engineering, 217-234. Academic Press, New York.

BOULTON, G.S. (1986) Push-moraines and glacier-contact fans in marine and terrestrial environments. Sedimentology, 33, 677-698.

BOWDEN, K.F. & GILLIGAN, R.M. (1971) Characteristic features of estuarine circulation as represented in the Mersey Estuary. Limnology Oceanography, 16, 490-502.

BOWEN, D.Q. (1977) The coast of Wales. In : Kidson, C. & Tooley, M.J. (Eds.) The Quaternary history of the Irish Sea. Seel House Press, Liverpool.

BRIDGE, J.S. (1981a) Hydraulic interpretation for grain- size distributions using a physical model for bedload transport. Jour. Sed. Petrol., 51, 1109-1124.

BRIDGE, J.S. (1981b) A discussion of Bagnold's (1956) bedload theory in relation to recent developments in bedload modelling. Earth Surf. Processes, 6, 187-190.

BRITISH GEOLOGICAL SURVEY (1988) Cardigan Bay. Sheet 52degs.N - 6 degs.W. 1:250000 Series. Sea Bed Sediments.

BRITISH GEOLOGICAL SURVEY (1990) Cardigan Bay, 1:250,000, Quaternary Geology.

BRITISH RAILWAYS BOARD, SOIL MECHANICS SECTION (1980) Seismic refraction survey, Barmouth Viaduct. London.

BRITISH RAILWAYS BOARD, SOIL MECHANICS SECTION (1982) Report on Barmouth, proposed reconstruction of estuary viaduct. London.

BUCKLES, J., HANRATTY, T.J. & ADRIAN, R.J. (1984) Turbulent flow over large-amplitude wavy surfaces. J. Fluid Mech., 140, 27-44.

CACCHIONE, D.A. & DRAKE, D.E. (1982) Measurements of storm-generated stresses on the continental shelf. Jour. Geophy. Res., 87, 1952-1961.

CAMERON, W.M. & PRITCHARD, D.W. (1963) Estuaries. In : Hill, M.N. (ed.) The Sea, Vol.II. Wiley, New York.

CARLING, P.A. (1981) Sediment transport by tidal currents and waves; observations from a sandy intertidal zone (Burry Inlet, South Wales). in: Nio, S.-D. et al (eds.) Holocene Marine Sedimentation in the North Sea Basin. Spec. Publs. int. Ass. Sediment. 5, 65-80. Blackwell Scientific Publications, Oxford.

CASTON, G.F. (1979) Wreck marks : indicators of net sand transport. Mar. Geol., 33, 193-204.

CASTON, V.N.D (1965) Localised sediment transport and submarine erosion in Tremadoc Bay, northern Wales. Mar. Geol., 3, 401-410.

CHALLINOR, J. & BATES, D.E.B. (1973) Geology explained in North Wales. David & Charles, Newton Abbott.

CHETTLEBURGH, M.J. (1986) Report of soils and foundation conditions : feasibility study, Mawddach Marina, Barmouth. Report No. LS1881, Soils and Materials Testing Ltd. Llanddulas, N. Wales.

CHRISTIANSEN, C., BLAESILD, P. & DALSGAARD, K. (1984) Reinterpreting 'segmented' grain size curves. Geol. Mag., 121, 47-51.

CLAYPOOL, G.E. & KAPLAN, I.R. (1974) The origin and distribution of methane in marine sediments. In : Kaplan, I.R., Natural gases in marine sediments. Plenum Press, New York.

CLIFF, R., GRACE, J.R. & WEBER, M.E. (1978) Bubbles, drops and particles. Academic Press, New York.

COLEMAN, N.L. (1981) Velocity profiles with suspended sediment. Jour. Hydraul. Res., 19, 211-229.

COLLINS, M.B.C., AMOS, C.L. & EVANS, G. (1981) Observations of some sediment transport processes over intertidal flats, The Wash, U.K. in: Nio, S.-D. et al (eds.) Holocene Marine Sedimentation in the North Sea Basin. Spec. Publs. int. Ass. Sediment. 5, 81-98. Blackwell Scientific Publications, Oxford.

COLLINSON, J.D. (1970) Bedforms of the Tana River, Norway. Geogr. Ann., A52, 31-36.

CONYBEARE, H. (1870) Description of viaducts across the estuaries on the line of the Cambrian Railway. Proc. Inst. civ. Engnrs., 32, 137-145.

COOK, D.O. (1982) Discussion : nearshore bedform patterns along Rhode Island from side-scan sonar surveys. Jour. Sed. Petrol., 52, 677-678.

COPESTAKE, P. (1978) Forminifera from the Lower and Middle Lias of Mochras Borehole. PhD Thesis, University of Wales, Aberystwyth.

COSTELLO, W.R. & SOUTHARD, J.B. (1981) Flume experiments on lower flow regime bed forms in coarse sand. J. Sed. Petrol., 51, 849-864.

CRONAN, D.S. (1972) Skewness and kurtosis in polymodal sediments from the Irish Sea. J. Sed. Petrol., 42, 102- 106.

DALRYMPLE, R.W. (1984) Morphology and internal structure of sandwaves in the Bay of Fundy. Sedimentology, 31, 365- 382.

DALRYMPLE, R.W., KNIGHT, R.J. & LAMBIASE, J.J. (1978) Bedforms and their hydraulic stability relationships in a tidal environment, Bay of Fundy, Canada. Nature, 275, 100-104.

DAVIES, T.R.H. (1980) Bedform spacing and flow resistance. J. Hydraul. Engng., Am. Soc. civ. Engrs., 106, HY3, 423-433.

DE BOER, P.L. (1981) Mechanical effects of micro- organisms on intertidal bedform migration. Sedimentology, 28, 129-132.

DE MOWBRAY, T. & VISSER, M. (1984) Reactivation surfaces in subtidal channel deposits, Oosterschelde, Southwest Netherlands. J. Sed. Petrol., 54, 811-824.

DEVOY, R.J.N. (1977) Flandrian sea-level changes in the Thames Estuary and the implications for land subsidence in England and Wales. Nature, 220, 712-715.

DOBSON, M.R., EVANS, W.E. & JAMES, K.H. (1971) The sediment on the floor of the southern Irish Sea. Mar. Geol., 11, 27-69.

DOBSON, M.R., EVANS, W.E. & WHITTINGTON, R.J. (1973) The geology of the South Irish Sea. Inst. Geol. Sci., Rep. No. 73/11, 35pp. H.M.S.O., London.

DOWLING, J.J. (1977) A grain size spectra map. J. Sed. Petrol., 47, 281-284.

DRAKE, D.A. & CACCHIONE, D.A. (1989) Estimates of the reference concentration (Ca) and resuspension coefficient (Xo) from near bottom observations on the California shelf. Cont. Shelf Res., 9, 51-64

DRAPER, L. (1967) Wave activity at the sea bed around N.W. Europe. Mar. Geol., 5, 133-140.

DUANE, D.B. (1964) Significance of skewness in recent sediments, Western Pamlico Sound, North Carolina. J. Sed. Petrol., 34, 864-874.

DYER, K.R. (1970) Current velocity profiles in a tidal channel. Geoph. J. Royal Astron. Soc., 22, 153-161.

DYER, K.R. (1973) Estuaries: a physical introduction. Wiley, London.

DYER, K.R. (1980) Velocity profiles over a rippled bed and the threshold of sand. Est., Coast. Shelf Sci., 10, 181-199.

DYER, K.R. (1986) Coastal and estuarine sediment dynamics. Wiley Interscience, New York.

ELLIOTT, T. & GARDINER, A.R. (1981) Ripple, megaripple and sandwave bedforms in the macrotidal Loughor Estuary, South Wales, U.K. in: Nio, S.-D. et al (eds.) Holocene Marine Sedimentation in the North Sea Basin. Spec. Publs. int. Ass. Sediment. 5, 51-64. Blackwell Scientific Publications, Oxford.

ENGELUND, F. & HANSEN, E. (1967) A monograph on sediment transport in alluvial streams. Technisk Vorlag, Copenhagen, 62pp.

EYLES, N. & MCCABE, A.M. (1989a) Glaciomarine facies within subglacial tunnel valleys : the sedimentary record of glaciomarine downwarping in the Irish Sea Basin. Sedimentology, 36, 431-448.

EYLES, N. & MCCABE, A.M. (1989b) Glacio-marine deposits of the Irish Sea Basin : the role of glacioisostatic disequilibrium. In : Ehlers, J., Gibbard, P & Rose, J. (eds.) Glacial deposits of the British Isles. A.A. Balkema, Rotterdam. (In press).

FAIRBRIDGE, R.W. (1961) Eustatic changes of sea level. Phys. Chem. of the Earth, 5, 99-185.

FENEMORE, P.R. (1976) Reflection and refraction seismics in Tremadoc Bay. MSc Thesis, University College of North Wales, Bangor.

FIELLER, N.R.J., GILBERTSON, D.D. & OLBRICHT, W. (1984) A new method for environmental analysis of particle size distribution data from shoreline sediments. Nature, 311, 648-651.

FLEMMING, B.W (1976) Side scan sonar : a practical guide. The International Hydrographic Review, 53.

FLOOD, R.D. (1983) Classification of sedimentary furrows and a model for furrow initiation and evolution. Geol. Soc. Am. Bull., 94, 630-639.

FOLK, R.L. (1966) A review of grain size parameters. Sedimentology, 6, 73-93.

FOLK, R.L. (1974) Petrology of sedimentary rocks. Hemphills, Austin, Texas.

FOLK, R.L. & WARD, W.C. (1957) Brazos River bar, a study in the significance of grain size parameters. J. Sed. Petrol., 27, 3-27.

FREDSOE, J. (1975) The friction factor and height- length relationships in flow over a dune covered bed. Inst. Hydrodyn. and Hydraul. Engrg., Prog. Rep. 37, 31- 36. Tech. Univ. Denmark.

FRIEDMAN, G.M. (1961) Distinction between dune, beach and river sands from their textural characteristics. J. Sed. Petrol., 31, 514-529.

FRIEDMAN, G.M. (1967) Dynamic processes and statistical parameters compared for size frequency distributions of beach and river sands. J. Sed. Petrol., 37, 327-354.

FROSTICK, L.E. & MCCAVE, I.N. (1979) Seasonal shifts of sediment within an estuary mediated by algal growth. Est. Coastal. Mar. Sci., 9, 569-576.

GADD, P.E, LAVELLE, J.W. & SWIFT, D.J.P. (1978) Estimates of sand transport on the New York Shelf using near- bottom current-meter observations. Jour. Sed. Petrol., 48, 239-252.

GARRARD, R.A. (1977) The sediments of the South Irish Sea and Nymphe Bank area of the Celtic Sea. In : Kidson, C. & Tooley, M.J. (Eds.) The Quaternary history of the Irish Sea. Seel House Press, Liverpool.

GARRARD, R.A. & DOBSON, M.R. (1974) The nature and maximum extent of glacial sediments off the west coast of Wales. Mar. Geol., 16, 31-44.

GEORGE, T.N. (1933) The submerged forest series near Barmouth, with notes on the distribution of Scrobicularia. Proc. Swansea Sci. & Field Nat. Soc., 1, 187-191.

GIBBS, R.J. (1972) The accuracy of particle size analysis utilising settling tubes. J. Sed. Petrol., 42, 141-145.

GIBBS, R.J., MATTHEWS, M.D. & LINK, D.A. (1971) The relationship between grain size and settling velocity. J. Sed. Petrol., 41, 7-18.

GORNITZ, V., LEBEDEFF, S. & HANSEN, J. (1982) Global sea level trend in the past century. Science, 215, 1611-1614.

GRACE, J.T., GROTHAUS, B.T. & ELRICH, R. (1978) Size frequency distributions taken from within sand laminae. J. Sed. Petrol., 48, 1193-1202.

GRAF, W.H. (1971) Hydraulics of Sediment Transport. McGraw-Hill, New York, 513pp.

GRANT, J. (1988) Intertidal bedforms, sediment transport, and stabilization by benthic microalgae. in: de Boer, P.L., van Gelder, A. & Nio, S.-D. (eds.) Tide Influenced Sedimentary Environments and Facies, 499- 510. D. Reidel, Dordrecht, Holland.

GRANT, W.D. & MASDEN, O.S. (1979) Combined wave and current interaction with a rough bottom. Jour. Geoph. Res., 84, 1797-1808.

GRANT, W.D. & MASDEN, O.S. (1986) The continental shelf bottom boundary layer. Ann. Rev. Fluid Mech., 18, 265- 305.

GREENLY, E. (1919) The geology of Anglesey. Mem. Geol. Surv., 2 vols.

GREENLY, E. (1928) Some recent work on the submerged forest in Anglesey. Proc. Liverpool Geol. Soc., 15, 56- 62.

GRIFFITHS, R.H., KING, R.F. & WILSON, C.D.V. (1961) Geophysical investigations in Tremadoc Bay, North Wales. Quart. Jour. Geol. Soc. London, 117, 171-191.

GROSS, T.F. & NOWELL, A.R.M. (1983) Mean flow and turbulence scaling in a tidal boundary layer. Cont. Shelf. Res., 2, 109-126.

GUY, H.P., SIMONS, D.B. & RICHARDSON, E.V. (1966) Summary of alluvial channel data from flume experiments 1956-61. U.S. Geol. Surv. Prof. Paper 462-I, 1-96.

HALLERMEIER, R.J. (1981) Terminal settling velocity of commonly occurring sand grains. Sedimentology, 28, 859- 865.

HAMILTON, E.L. & BACHMAN, R.T. (1982) Sound velocity and related properties of marine sediments. Jour. Acoust. Soc. Am., 72, 1891-1904.

HANER, B.E. (1984) Santa Ana River: An example of a sandy braided floodplain system showing sediment source area imprintation and selective sediment modification. Sed. Geol., 38, 247-261.

HANSEN, D.V. & RATTRAY, M. (1966) New dimensions in estuary classification. Limnology Oceanography, 11, 319-326.

HAPPEL, J. & BRENNER, H. (1965) Low Reynolds number hydrodynamics. Prentice Hall, Englewood Cliffs, New Jersey.

HARDISTY, J. (1983) An assesment and calibration of formulations for Bagnolds bedload equation. Jour. Sed. Petrol., 53, 1007-1010.

HARRELL, J.A. & ERIKSSON, K.A. (1979) Empirical conversion equations for thin-section and sieve derived size distribution parameters. J. Sed. Petrol., 49, 273- 280.

HARRIS, P.T. (1988) Large-scale bedforms as indicators of mutually evasive sand transport and the sequential infilling of wide-mouthed estuaries. Sed. Geol., 57, 273-298.

HARVEY, J.G. & VINCENT, C.E. (1977) Observations of shear in near-bed currents in the Southern North Sea. Est. Coast. Mar. Sci., 5, 715-731.

HAYNES, J.R. & DOBSON, M.R. (1969) Physiology, Foraminifera and sedimentation in the Dovey Estuary (Wales). Geol. J., 6, 217-256.

HAYNES, J.R., KITELEY, R.J., WHATLEY, R.C. & WILKS, P.J. (1977) Microfaunas, microfloras and the environmental stratigraphy of the Late Glacial and Holocene in Cardigan Bay. Geol. J., 12, 129-158.

HEATHERSHAW, A.D. (1979) The turbulent structure of the bottom boundary layer in a tidal current. Geophy. Jour. Roy. Astron. Soc., 58, 395-430.

HEATHERSHAW, A.D. (1981) Comparisons of measured and predicted sediment transport rates in tidal currents. Mar. Geol., 42, 75-104.

HEATHERSHAW, A.D. & HAMMOND, F.D.C. (1979) Offshore sediment movement and its relation to observed tidal current and wave data. Swansea Bay (SKER) Project Topic Report 6. Institute of Oceanographic Sciences, Report No. 93, Surrey, U.K.

HEATHERSHAW, A.D. & LANGHORNE, D.N. (1988) Observations of near-bed velocity profiles and seabed roughness in tidal currents flowing over sandy gravels. Est., Coast. Shelf Sci., 26, 459-482.

HERBERT-SMITH, M. (1971) The palynolgy of the Mochras Borehole. PhD Thesis, University of Wales, Aberystwyth.

HERBERT-SMITH, M. (1979) The age of the Tertiary deposits of the Llanbedr (Mochras Farm) Borehole as determined from palynological studies. Rep. Inst. Geol. Sci., No. 78/24, 15-29.

HESSION, M.A. (1989) The Quaternary Geology of the South Irish Sea. PhD thesis, University of Wales, Aberystwyth.

HESSION M.A. & WHITTINGTON, R.J. (1987) Aspects of the Quaternary sediments of the Anglesey Sheet. Proc. Geol. Assoc., 98, 398-400.

HOWARTH, M.J. (1982) Tidal currents of the continental shelf. in: Stride, A.H. (ed.) Offshore Tidal Sands. Chapman & Hall, 10-26.

HUBBARD, D.K., OERTEL, G. & NUMMEDAL, D. (1979) The role of waves and tidal currents in the development of tidal-inlet sedimentary structures and sand body geometry : examples from North Carolina, South Carolina, and Georgia. J. Sed. Petrol., 49, 1073-1092.

HULSEY, J.D. (1961) Relations of settling velocity of sand- sized spheres and sample weight. J. Sed. Petrol., 31, 101- 112.

HUNTER, R.E., DINGLER, J.R., ANIMA, R.J. & RICHMOND, B.M. (1988) Coarse-sediment bands on the inner shelf of southern Monterey Bay, California. Mar. Geol., 80, 81- 98.

HUNTER, R.E. & KOCUREK, G. (1985) An experimental study of subaqueous slipface deposition. J. Sed. Petrol., 56, 387- 394.

INMAN, D.L. (1952) Measures for describing the size distribution of sediments. J. Sed. Petrol., 22, 125- 145.

JACKSON, P.S. (1981) On the displacement height in the logarithmic velocity profile. J. Fluid Mech., 111, 15- 26.

JACKSON, R.G.II. (1976a) Large scale ripples of the lower Wabash River. Sedimentology, 23, 593-623.

JACKSON, R.G. (1976b) Sedimentological and fluid- dynamic implications of the turbulent bursting phenomenon in geophysical flows. J. Fluid Mech., 77, 531-560.

JAGO, C.F. (1974) The sedimentology of estuarine and coastal plain deposits between Pendine and Wharley Point, Carmarthen Bay. PhD Thesis, Imperial College, London.

JAGO, C.F. (1980) Contemporary accumulation of marine sand in a macrotidal estuary, southwest Wales. Sed. Geol., 26, 21-49.

JAIN, S.C. & KENNEDY, J.F. (1974) The spectral evolution of sedimentary bed forms. J. Fluid Mech., 63, 301-314.

JELGERSMA, S. (1966) Sea level changes in the last 10000 years. In : International Symposium on World Climate from 8000-0B.C., Roy. Met. Soc., pp54-69.

JENKINS, A. (1976) Circulation and salinity in the Conwy Estuary. MSc Thesis, U.C.N.W. Bangor, North Wales.

JOHNSON, B. (1975) Upper Domerian and Toarcian forminifera from the Llanbedr (Mochras Farm) Borehole, North Wales. PhD Thesis, University of Wales, Aberystwyth.

JONAS, P.C.J. (1977) The recent sedimentology of the Towy Estuary, Dyfed, South Wales. PhD Thesis, Imperial College, London.

JONES, A.S.G. (1971) A textural study of marine sediments in a portion of Cardigan Bay (Wales). Jour. Sed. Petrol., 41, 505.

JONES, B. (1933) The geology of the Fairbourne - Llwynwril district, Merioneth. Quart. Jour. Geol. Soc. London, 89, 145-170.

JONES, G.B., FLOODGATE, G.D. & BENNELL, J.D. (1986) Chemical and microbiological aspects of acoustically turbid sediments : preliminary investigations. Mar. Geotechnology, 6, 315-332.

JONES, M.E. (1984) Megaripple stability in the S.W. Menai Strait. MSc Thesis, U.C.N.W. Bangor, North Wales.

JONES, R.E.H. (1981) The source, transport and metal concentrations of suspended sediments in the Conwy Estuary. PhD Thesis, U.C.N.W. Bangor, North Wales.

JOPLING, A.V. (1966) Some principles and techniques used in recontructing the hydraulic parameters of a paleo- flow regime. J. Sed. Petrol., 36, 5-49.

KACHEL, N.B. & STERNBERG, R.W. (1971) Transport of bedload as ripples during an ebb current. Mar. Geol., 10, 229-244.

KEMP, P.H. & SIMONS, R.R. (1982) The interaction between waves and a turbulent current : waves propogating with the current. Jour. Fluid. Mech., 116, 227-250.

KENNEDY, S.K., MELOY, T.P. & DURNEY, T.E. (1985) Sieve data - size and shape information. J. Sed. Petrol., 55, 356-360.

KENYON, N.H. (1970) Sand ribbons of European tidal seas. Mar. Geol., 9, 25-39.

KIDSON, C. (1977) Some problems of the Quaternary of the Irish Sea. In : Kidson, C. & Tooley, M.J. (Eds.) The Quaternary history of the Irish Sea. Seel House Press, Liverpool.

KLEIN, G. DE V. (1970) Depositional and dispersal dynamics on intertidal sand bars. J. Sed. Petrol., 40, 1095-1127.

KNIGHT, R.J. (1980) Linear sand bar development and tidal current flow in Cobequid Bay (Bay of Fundy), Nova Scotia, Canada. In; McCann, S.B. (ed) The Coastline of Canada. Geol. surv. Can., Pap. 80-10, 153-180.

KOHSIEK, L.H.M., BUIST, H.J., BLOKS, P., MISDORP, R., VAN DEN BERG, J.H. & VISSER, J. (1988) Sedimentary processes on a sandy shoal in a mesotidal estuary (Oosterschelde, The Netherlands). in: de Boer, P.L., van Gelder, A. & Nio, S.-D. (eds.) Tide Influenced Sedimentary Environments and Facies, pp201-214. D. Reidel, Dordrecht, Holland.

KOHSIEK, L.H.M. & TERWINDT, J.H.J. (1981) Characteristics of foreset and topset bedding in megaripples related to hydrodynamic conditions on an intertidal shoal. in: Nio, S.-D., Schuttenhelm, R.T.E, & van Weering, Tj.C.E. (eds.) Holocene Marine Sedimentation in the North Sea Basin. Spec. Publs int. Ass. Sediment., 5, 27-37. Blackwell Scientific Publications, Oxford.

KOMAR, P.D. (1981) The applicability of the Gibbs equation for grain settling velocities to conditions other than quartz grains in water. J. Sed. Petrol., 51, 1125-1132.

KOMAR, P.D., BABA, J. & CUI, B (1984) Grain size analyses of mica within sediments and the hydraulic equivalence of mica and quartz. J. Sed. Petrol., 54, 1379-1391.

KOMAR, P.D. & CUI, B. (1984) The analysis of grain-size measurements by sieving and settling-tube techniques. J. Sed. Petrol., 54, 603-614.

KOMAR, P.D. & REIMERS, C.E. (1978) Grain shape effects on settling rates. J. Geol., 86, 193-209.

KRANENBURG, C. & GELDOF, H.J. (1974) Concentration effects on settling tube analysis. Jour. Hydraul. Res., 12, 337-355.

KRUGERMEYER, L. & GRUNWALD, M. (1978) The influence of sea waves on the wind profile. Boundary-Layer Meteorology, 10, 403- 414.

KRUMBEIN, W.C. (1938) Size-frequency distributions of sediments and the normal phi curve. J. Sed. Petrol., 8, 84-90.

LAILEY, R.S. (1980) Tidal convergence in the Conwy Estuary. MSc Thesis, U.C.N.W. Bangor, North Wales.

LANE, E.W. & KALINSKE, A.A. (1939) The relation of suspended to bed material in rivers. Trans. Am. Geophys. Union, 20, 637-641.

LANGHORNE, D.N. (1973) A sandwave field in the Outer Thames Estuary, Great Britain. Mar. Geol., 14, 125-143.

LANGHORNE, D.N. (1982) A study of the dynamics of a marine sandwave. Sedimentology, 29, 571-594.

LANGHORNE, D.N. ET AL (1985) Observations of the changes of intertidal bedforms over a spring-neap cycle. Report No. 203. Institute of Oceanographic Sciences.

LANGHORNE, D.N. & READ, A.A. (1986) The evolution and mechanics of modern intertidal and subtidal bedforms: their relevance to geological structures. J. geol. Soc. London, 143, 957-962.

LARCOMBE, P. (1986) Megaripple evolution and sediment transport over a spring-spring cycle on an intertidal shoal in the macrotidal Conwy Estuary, North Wales. MSc Thesis, U.C.N.W. Bangor, North Wales.

LECKIE, D. (1988) Wave-formed, coarse-grained ripples and their relationship to hummocky cross- stratification. Jour. Sed. Petrol., 58, 607-622.

LEEDER, M.R. (1982) Sedimentology : process and product. Allen & Unwin.

LEES, B.J. (1983) The relationship of sediment transport rates and paths to sandbanks in a tidally dominated area off the coast of East Anglia, U.K.. Sedimentology, 30, 461- 483.

LEROY, S.D. (1981) Grain size and moment measures: a new look at Karl Pearson's ideas on distributions. J. Sed. Petrol., 51, 625-630.

LETTAU, H. (1969) Note on aerodynamic roughness- parameter estimate on the basis of roughness element description. Jour. Appl. Meteorol., 8, 828-832.

LEVEY, R.A., KJERFE, B. & GETSEN, R.T. (1980) Comparison of bedform variance spectra within a meander bend during flood and average discharge. J. Sed. Petrol., 50, 149-155.

LLOYD, L. (1974) The town and port of Barmouth. L. Lloyd.

LOWE, J.J. & WALKER, M.J.C. (1984) Reconstructing Quaternary Environments. LOngman, New York,, 390pp.

LUDWICK, J.C. & HENDERSON, P. (1968) Particle shape and interference of size from sieving. Sedimentology, 11, 197- 235.

MAHAMOD, Y.B. (1989) Sedimentary processes in the Dwyryd Estuary. PhD Thesis, U.C.N.W. Bangor, North Wales.

MARINE SCIENCE LABORATORIES (1976) Geotechnical mapping of the sea-bed. Final report, Part 1 - The experimental area. NERC contract no. F60/4/22. U.C.N.W. Menai Bridge, Gwynedd.

MASON, C.C. & FOLK, R.L. (1958) Differentiation of beach, dune and eolian flat environments by size analysis - Mustang Island, Texas. J. Sed. Petrol., 28, 211-226.

MAZEL, C. (1985) Side scan sonar record interpretation. Klein Associates, Inc,. New Hampshire.

MCCAMMON, R.B. (1962) Efficiences of percentiles for describing the mean size and sorting of sedimentary particles. J. Geol., 70, 453-465.

MCCAVE, I.N. (1973) Some boundary-layer characteristics of tidal currents bearing sand in suspension. Mem. Soc. R. des Sciences de Liege, 6, 187-206.

MCCAVE, I.N. (1978) Grain size trends and transport along beaches: example from eastern England. Mar. Geol., 28, M43- M51.

MCCAVE, I.N. & GEISLER, A.C. (1979) Megaripples, ridges and runnels on intertidal flats of the Wash, England. Sedimentology, 26, 353-371.

MCCAVE, I.N. & LANGHORNE, D.N. (1982) Sand waves and sediment transport around the end of a tidal sand bank. Sedimentology, 29, 95-110.

MCKINNEY, T.F., STUBBLEFIELD, W.L. & SWIFT, D.J.P. (1974) Large-scale current lineations on the central New Jersey shelf : investigations by side-scan sonar. Mar. Geol., 17, 79-102.

MCLAREN, P. (1981) An interpretation of trends in grain size measures. J. Sed. Petrol., 51, 611-624.

MCLAREN, P. (1982) Discussion - Hydraulic control of grain size distributions in a macrotidal estuary. Sedimentology, 29, 437-439.

MCLAREN, P. & BOWLES, D. (1985) The effects of sediment transport on grain size distributions. J. Sed. Petrol., 55, 457-470.

MCLEAN, S.R. (1981) The role of non-uniform roughness in the formation of sand ribbons. Mar. Geol., 42, 49- 74.

MCMILLAN, N.F. (1949) Notes on the Postglacial clays in Anglesey. Proc. Liverpool Geol. Soc., 20, 106-110.

MCMULLEN, R.M. (1964) Modern sedimentation in the Mawddach Estuary, Barmouth, North Wales. PhD Thesis, Univ. of Reading, 260pp.

MCWHIRTER, N. & MCWHIRTER, R. (1975) Guinness Book of Records. Redwood, Enfield.

MIDDLETON, G.V. (1976) Hydraulic interpretation of sand size distributions. Jour. Geol., 84, 405-426.

MIGNIOT, C. (1977) Action des courants, de la houle et du vent sur les sediments. Houille Blanche, 1, 9-47. (In French).

MILLER, A.A. (1946) Some physical features related to the river development in the Dolgelly district. Proc. Geol. Assoc., 57, 174-203.

MILLER, M.C., MCCAVE, I.N. & KOMAR, P.D. (1977) Threshold of sediment motion under unidirectional currents. Sedimentology, 24, 507-528.

MOORE, J.R. (1968) Recent sedimentation in Northern Cardigan Bay, Wales. Bull. Br. Mus. Nat. Hist., 2, No. 2.

MOORE, N.H. (1976) Physical oceanographic and hydrological observations in the Loughor Estuary (Burry Inlet). In: Nelson-Smith, A. & Bridges, E.M. (Eds.) Problems of a Small Estuary. Quadrant Press, Swansea, pp. 1:3/1-1:3/15.

MORANG, A. & MCMASTER, R.L. (1980) Nearshore bedform patterns along Rhode Island from side-scan sonar surveys. Jour. Sed. Petrol., 50, 831-840.

MORGAN, D.W. (1948) Brief Glory - the story of a quest. Brython Press, Liverpool.

MOSS, A. (1962) The physical nature of common sandy and pebbly deposits, Part 1. Am. J. Sci., 260, 337-373.

MOSS, A. (1963) The physical nature of common sandy and pebbly deposits, Part 2. Am. J. Sci., 261, 297-343.

MOSS, A.J. (1972) Bed-load sediments. Sedimentology, 18, 159-219.

MULLINS, H.T. & NAGEL, D.K. (1982) Evidence for shallow hydrocarbons offshore Santa Cruz County, California. Am. Assoc. Petrol. Geol. Bull., 66, 1130-1140.

NASH, L.A. (1987) Settling velocity and threshold characteristics of biogenic sediments. PhD Thesis, University College, Swansea, Wales.

NASNER, H. (1974) Uber das Verhalten von Transportkorpen im Tidegebiet. Mitt. Franzius Inst., 40, 1- 149.

NELSON, J.M. & SMITH, J.D. (1989) Mechanics of flow over ripples and dunes. Jour. Geoph. Res., 94, 8146- 8162.

NIO, S.-D., SIEGENTHALER, C. & YANG, C.-S. (1983) Megaripple cross bedding as a tool for the reconstruction of the palaeo-hydraulics in a Holocene subtidal environment, S.W Netherlands. Geol. Mijnbouw, 62, 499-510.

NUMERICAL ALGORITHMS GROUP LTD. (1986) NAG Fortran Library Manual - Mark 11. Oxford.

NUNES, R.A. (1982) Dynamics of small-scale fronts in estuaries. PhD Thesis, U.C.N.W. Bangor, North Wales.

NUNES, R.A. & SIMPSON, J.H. (1985) Axial convergence in a well- mixed estuary. Est. Coastal Shelf Sci., 20, 637-649.

O'FARRELL, S.P. (1983) The axial convergence in the Conwy and Mawddach Estuaries, Gwynedd. MSc Thesis, U.C.N.W. Bangor, North Wales.

O'SULLIVAN, K.N. (1979) The sedimentology, geochemistry and conditions of deposition of the Tertiary rocks of the Llanbedr (Mochras Farm) Borehole. Rep. Inst. Geol. Sci., No. 78/24, pp1-13.

OWEN, M.W. & THORN, M.F.C. (1978) Effect of waves on sand transport by currents. Proc. 16th Coastal Eng. Conf., 1675- 1687.

PAOLA, C. (1985) A method for spatially averaging small- scale bottom roughness. Mar. Geol., 66, 291-301.

PASSEGA, R. (1957) Texture as characteristic of clastic deposition. Am. Ass. Petro. Geol. Bull., 41, 1952-1984.

PASSEGA, R. (1964) Grain size representation by C.M. patterns as a geological tool. J. Sed. Petrol., 34, 830-847.

PATTINSON, C. (1979) The distribution and behaviour of some nutrient and trace metal species in three Welsh estuaries. PhD Thesis, Univ. of Liverpool.

PEJRUP, M. (1988) The triangular diagram used for classification of estuarine sediments: a new approach. in: de Boer, P.L., van Gelder, A. & Nio, S.-D. (eds.) Tide Influenced Sedimentary Environments and Facies, 289-300. D. Reidel, Dordrecht, Holland.

PHILLIPS, W.E.A., STILLMAN, C.J. & MURPHY, T. (1976) A Caledonian plate tectonic model. Jour. Geol. Soc. London, 132, 579-609.

PICKRILL, R.A. (1986) Sediment pathways and transport rates through a tide-dominated entrance, Rangannu Harbour, New Zealand. Sedimentology, 33, 887-898.

POWELL, D.W. (1956) Gravity and magnetic anomalies in North Wales. Quart. Jour. Geol. Soc. London, 111, 375- 397.

PRANDLE, D. & RAHMAN, M. (1980) Tidal response in estuaries. Jour. Phys. Oceanog., 10, 1552-1573.

PRITCHARD, D.W. (1955) Estuarine circulation patterns. Proc. Amer. Soc. Civil. Eng., 81, No. 717.

PRITCHARD, D.W. (1967) Observations of circulation in coastal plain estuaries. in: Lauff, G.H. (ed.) Estuaries. Am. Ass. Adv. Sci., 83, 37-44. Washington.

RANA, S.A., SIMONS, D.B. & MAHAMOOD, K. (1973) Analysis of sediment sorting in alluvial channels. Proc. Am. Soc. civil Engng, 99, HY11, 1967-1980.

RAUDKIVI, A.J. (1966) Bedforms in alluvial channels. J. Fluid Mech., 26, 507-514.

RAUDKIVI, A.J. (1976) Loose boundary hydraulics. Pergamon, Oxford.

REED, W.E., LE FEVER, R. & MOIR, G.J. (1975) Depositional environment from settling velocity (psi) distributions. Geol. Soc. Am. Bull., 86, 1305-1315.

RIGLER, J.K., COLLINS, M.B. & WILLIAMS, S.J. (1981) A high precision digital recording sedimentation tower for sands. J. Sed. Petrol., 51, 642-644

ROUSE, H. (1937) Modern conceptions of the mechanics of fluid turbulence. Trans. Am. Soc. civ. Engnrs., 102, 436-505.

RUBEY, W.W. (1933) The size distribution of heavy minerals within a water-laid sandstone. J. Sed. Petrol., 3, 3-29.

SAGOE, K.M.O. & VISHER, G.S. (1977) Population breaks in grain size distributions of sand - a theoretical model. J. Sed. Petrol., 47, 285-310.

SCHLEE, J., UCHUPI, E. & TRUMBULL, J.V.A. (1965) Statistical parameters of Cape Cod beach and eolian sands. U.S. Geol. Surv. Prof. Paper 501-D, 118-122.

SCHWAB, W.C. & MOLNIA, B.F. (1987) Unusual bed forms on the North Aleutian Shelf, Bristol Bay, Alaska. Geo- Marine Letters, 7, 207-215.

SEDIMENTATION SEMINAR (1981) Comparison of methods for size analysis of sands of the Amazon-Solimoes Rivers, Brazil and Peru. Sedimentology, 28, 123-128.

SHAGHUDE, Y. (1989) Title unknown. MSc. thesis, Department of Oceanography, University of Southampton

SHEPARD, F.P. (1954) Nomenclature based on sand-silt- clay ratios. J. Sed. Petrol., 24, 151-158.

SHEPARD, F.P. & YOUNG, F. (1961) Distinguishing between beach and dune sands. J. Sed. Petrol., 31, 196-214.

SHI, N.C., LARSEN, L.H. & DOWNING, J.P. (1985) Predicting suspended sediment concentration on continental shelves. Mar. Geol., 62, 255-276.

SIEGENTHALER, C. (1982) Tidal cross-strata and the sediment transport rate problem: a geologists approach. Mar. Geol., 45, 227-240.

SIMPSON, J.H. & NUNES, R.A. (1981) The tidal intrusion front: an estuarine convergence zone. Est. Coastal Shelf Sci., 13, 257-266.

SIMPSON, J.H. & TURRELL, W.R. (1986) Convergent fronts in the circulation of tidal estuaries. in: Wolfe, D.A. (ed.) Estuarine Variability, 139-152. Estuarine Research Federation.

SLOT, R.E. (1984) Terminal velocity formula for objects in a viscous fluid. Jour. Hydraul. Res., 22, 235-243.

SLOT, R.E. & GELDOF, H.J. (1986) An improved settling tube system for sand. Delft University of Technology, Department of Civil Engineering, Report no. 86-4, The Netherlands.

SMITH, B. & GEORGE, T.N. (1961) British Regional Geology, North Wales. H.M.S.O., London.

SMITH, D.B. (1988) Bypassing of sand over sand waves and through a sand wave field in the central region of the southern North Sea. In : de Boer, P.L. et al (eds.) Tide-influenced sedimentary environments and facies. pp 39-50. D. Reidel Publishing Company.

SMITH, J.D. & HOPKINS, T.S. (1972) Sediment transport on the continental shelf off Washington and Oregon in the light of recent current measurements. In : Swift, D.J.P. (Ed.) Shelf sediment transport : process and pattern. Dowden, Hutchinson & Ross, Stroudsberg, pp 143-180.

SMITH, J.D. & MCLEAN, S.R. (1977a) Spatially averaged flow over a wavy surface. J. Geoph. Res., 82, 1735- 1746.

SMITH, J.D. & MCLEAN, S.R. (1977b) Boundary layer adjustments to bottom topography and suspended sediment. in : Nihoul, J.C.J. (ed.) Bottom Turbulence 123- 151. Elsevier, New York.

SOMMERVILLE, J.H. (1973) A continuous seismic profiling survey of Tremadog Bay. MSc Thesis, U.C.N.W. Bangor, North Wales.

SOULSBY, R.L. (1980) Selecting record length and digitisation rate for near-bed turbulence measurements. J. Phys. Oceanog., 10, 208-219.

SOULSBY, R.L. (1983) The bottom boundary layer of shelf seas. In : Johns, B. (ed.) Physical oceanography of coastal and shelf seas. Elsevier, Amsterdam, pp189-266.

SOULSBY, R.L. & DYER, K.R. (1981) The form of the near- bed velocity profile in a tidally accelerating flow. J. Geoph. Res., 86, 8067-8074.

SPENCER, C.H. (1976) A palaeoecological study of foraminifera and ostracoda from a borehole in Post- Glacial sediments of Tremadoc Bay, North Wales. MSc Thesis, University College of Wales, Aberystwyth.

STEERS, J.A. (1948) The coastline of England and Wales. Cambridge University Press.

STEERS, J.A. (1969) The sea coast. Collins.

STERNBERG, R.W. (1972) Predicting initial motion and bedload transport of sediment particles in the shallow marine environment. In : Swift, D.J.P. (Ed.) Shelf sediment transport : process and pattern. Dowden, Hutchinson & Ross, Stroudsberg, pp 61-79.

STERNBERG, R.W., KRANK, K., CACCHIONE, D.A. & DRAKE, D.E (1988) Suspended sediment transport under estuarine tidal channel conditions. Sed. Geol., 57, 257-272.

STOKES, G.G. (1851) - (quoted in Allen, J.R.L., 1984) Trans. Cambridge Philos. Soc., Math. Phys. Sci., 9, 8- 27.

STRIDE, A.H., BELDERSON, R.H. & KENYON, N.H. (1972) Longitudinal furrows and depositional sand bodies of the English Channel. Mem. Bur. Rech. Geol. Min., Fr. 79, 233- 244.

STUCKRATH, T. (1969) Die Bewegung von Grossrippein an der Sohle Rio Parana. Mitt. Franzius Inst., 32, 267- 293.

SWIFT, D.J.P. (1976) Coastal sedimentation. In : Stanley, D.J. & Swift, D.J.P. (Eds.) Marine sediment transport and environmental management. Wiley, New York.

SWIFT, D.J.P. & FREELAND, G.L. (1978) Current lineations and sand waves on the inner shelf, Middle Atlantic Bight of North America. Jour. Sed. Petrol., 48, 1257-1266.

TAIRA, A. (1973) A new method for the recognition of sedimentary environments using photo-electric settling tube and stepwise discriminant analysis of sediments. Geol. Soc. Am. Abs., with Programs, 5, 833-834.

TAIRA. A. & SCHOLLE, P.A. (1974) Recognition of depositional environments in sediments using settling tube data. Am. Assoc. Petroleum Geologists, Soc. Econ. Palaeo. Miner. Ann. Mtg. Abs., 1, p88.

TAIRA, A. & SCHOLLE, P.A. (1979b) Discrimination of depositional environments using settling tube data. J. Sed. Petrol., 49, 787-800.

TAYLOR, P.A. & DYER. K.R. (1977) Theoretical models of flow near the bed and their implications for sediment transport. in : Goldberg, E.D. et al (eds.) the Sea, Vol. 6, 579- 601. Wiley Interscience, New York.

TAYLOR SMITH, D. (1987) Geotechnical studies in Tremadog Bay. Proc. Geol. Assoc., 98, 385-96.

TERWINDT, J.H.J. (1971) Sand waves in the southern bight of the North Sea. Mar. Geol. 10, 51-67.

TERWINDT, J.H.J. (1981) Origin and sequences of sedimentary structures in inshore mesotidal deposits of the North Sea. in: Nio, S.-D., Shuttenhelm, R.T.E. & van Weering, Tj.C.E. (eds.) Holocene Marine Sedimentation in the North Sea Basin. Spec. Publs. int. Ass. Sediment. 5, 4-26. Blackwell Scientific Publications, Oxford.

TERWINDT, J.H.J. (1988) Palaeo-tidal reconstructions of inshore tidal depositional environments. In: be Boer, P.L., van Gelder, A. & Nio, S.-D. (eds.) Tide influenced sedimentary environments and facies, pp233- 263. D.Reidel Publishing Company.

TERWINDT, J.H.J. & BROUWER, M.J.N. (1986) The behaviour of intertidal sandwaves during neap-spring tide cycles and the relevance for palaeoflow reconstructions. Sedimentology, 33, 1-31.

TEYSSEN, T. (1984) Physical model and FORTRAN IV program to estimate palaeotidal flow velocities from features of sand waves. Computers & Geosciences, 10, 237-244.

THORNE, P.D., HEATHERSHAW, A.D. & TROIANO, L. (1984/5) Acoustic detection of seabed gravel movement in turbulent tidal currents. Mar. Geol., 54, M43-M48.

UNCLES, R.J. ET AL (1985) Observed fluxes of water, salt and suspended sediment in a partly-mixed estuary. Est. Coastal Shelf Sci., 20, 147-167.

VAN DEN BERG, J.H.J. (1982) Migration of large-scale bedforms and preservation of crossbedded sets in highly accretional parts of tidal channels in the Oosterschelde, SW Netherlands. Geol. Mijnbouw, 61, 253- 263.

VAN DEN BERG, J.H.J. (1987) Bedform migration and bedload transport in some rivers and tidal environments. Sedimentology, 34, 681-698.

VAN RIJN, L.C. (1984a) Sediment transport, part I : bedload transport. J. Hydraul. Engng., Am. Soc. civ. Engrs., 110, 1431-1456.

VAN RIJN, L.C. (1984b) Sediment transport, part III : bed forms and alluvial roughness. J. Hydraul. Engng., Am. Soc. civ. Engrs., 110, 1733-1754.

VANONI, V.A. (1974) Factors determining bed forms of Alluvial Streams. J. Hydraul. Div. Am. Soc. civ. Engrs., 100, HY3, 363-377.

VIARD, J.P. & BREYER, J.A. (1979) Description and hydraulic interpretation of grain size cumulative curves from the Platte River system. Sedimentology, 26, 427-439.

VINCENT, C.E., YOUNG, R.A. & SWIFT, D.J.P. (1981) Bedload transport under waves and currents. Mar. Geol., 39, M71-M80.

VISHER, G.S. (1969) Grain size distributions and depositional processes. J. Sed. Petrol., 39, 1074-1106.

VISSER, M.J. (1980) Neap-spring cycles reflected in Holocene subtidal large-scale bedform deposits: a preliminary note. Geology, 8, 543-546.

VOS, P.C., DE BOER, P.L. & MISDORP, R. (1988) Sediment stabilization by benthic diatoms in intertidal sandy shoals: qualitative and quantitative observations. in: de Boer, P.L., van Gelder, A. & Nio, S.-D. (eds.) Tide Influenced Sedimentary Environments and Facies, 511- 526. D. Reidel, Dordrecht, Holland.

WEAST, R.C. (1969) Handbook of chemistry and physics. The Chemical Rubber Company, Cleveland, Ohio.

WELSH WATER AUTHORITY (1978) Results of hydrographic surveying and recomendations for Barmouth sewage disposal. Tidal Waters Report TW78/5.

WELSH WATER AUTHORITY (1980) Barmouth sewage disposal : a long sea outfall alternative. Tidal Waters Report TW80/2.

WENTWORTH, C.K. (1919) A scale of grade and class terms for clastic sediments. Jour. Geol., 30, 377-392.

WERNER, F. (1982) Discussion : nearshore bedform patterns along Rhode Island from side-scan sonar surveys. Jour. Sed. Petrol., 52, 674-677.

WERNER, F. & NEWTON, R.S. (1975) The pattern of large- scale bedforms in the Langeland Belt (Baltic Sea). Mar. Geol., 19, 29-59.

WEST, J.R. & COTTON, A.P. (1981) The measurement of diffusion coefficients in the Conwy Estuary. Est. Coastal Shelf Sci., 12, 232-336.

WIBERG, P. & SMITH, J.D. (1988) A comparison of field data and theoretical models for wave-current interactions on the bed on the continental shelf. Cont. Shelf Res., 2, 147- 162.

WIJBENGA, J.A.H. & KLAASEN, G.J. (1983) Changes in bedform dimensions under unsteady flow conditions in a straight flume. in: Collinson, J.D. & Lewin, J. (eds.) Modern and Ancient Fluvial Systems. Spec. Publs. int. Ass. Sediment. 6, 35-48. Blackwell Scientific Publications, Oxford.

WILKINSON, R. H. (1984) A method for evaluating statistical errors associated with logarithmic velocity profiles. Geo- Marine Letters, 3, 49-52.

WILKS, P.J. (1977) Flandrian sea-level change in the Cardigan Bay area. PhD Thesis, University of Wales.

WILKS, P.J. (1979) Mid-Holocene sea-level and sedimenation interactions in the Dovey Estuary area, Wales. Palaeogeog, Palaeoclimatol, Palaeoecol,. 27, 17- 36.

WILLIAMS, G.P. (1966) Particle roundness and surface texture effects on fall velocity. J. Sed. Petrol., 36, 255-259.

WILLIAMS, G.P. (1967) Flume experiments on the transport of a coarse sand. U.S. Geol. Surv. Prof. Paper 562-B.

WINGFIELD, R.T.R., HESSION, M.A. & WHITTINGTON, R.J. (1989) Anglesey, 1:250,000, Quaternary Geology. British Geological Survey.

WOODING, R.A., BRADLEY, E.F. & MARSHALL, J.K. (1973) Drag due to regular arrays of roughness elements of varying geometry. Boundary Layer Meteor., 5, 285-308.

WOODLAND, A.W. (1971) (Ed.) The Llanbedr (Mochras Farm) Borehole. Rep. Inst. Geol. Sci., No 71/18, 155pp.

WRIGHT, L.D. ET AL (1975) Sediment transport and deposition in a macrotidal river channel: Ord River, Australia. In: Cronin, L.E. (Ed.) Estuarine Research, Vol. 2. Academic Press, New York, pp309-321.

YALIN, M.S. (1963) An expression for bedload transportion. Proc. Am. Soc. civ. Engnrs., Jour. Hydraul. Div., HY3, 221-250.

YALIN, M.S. (1972) Mechanics of sediment transport. Pergamon, Oxford.

YALIN, M.S. (1977) Mechanics of sediment transport. Pergamon, Oxford.

YALIN, M.S. & KARAHAN, E. (1979) Steepness of sedimentary dunes. J. Hydraul. Div. Am. Soc. civ. Engrs., 105, HY4, 381-392.

YANG, C.S. (1986a) Estimates of sand transport in the Oosterschelde tidal basin using current meter measurements. Mar. Geol., 72, 143-170.

YANG, C.S. (1986b) On Bagnolds sediment transport equation in tidal marine environments and the practical definition of bedload. Sedimentology, 33, 465-486.

YANG, C.S. & NIO, S.D. (1985) The estimation of palaeohydrodynamic processes from subtidal deposits using time series analysis methods. Sedimentology, 32, 41-57.

YATES, J. (1832) A notice of a submerged forest in Cardigan Bay. Proc. Geol. Soc., 1, 407.

ZARILLO, G.A. (1982) Stability of bedforms in a tidal environment. Mar. Geol., 48, 337-351.

Appendix 2.1

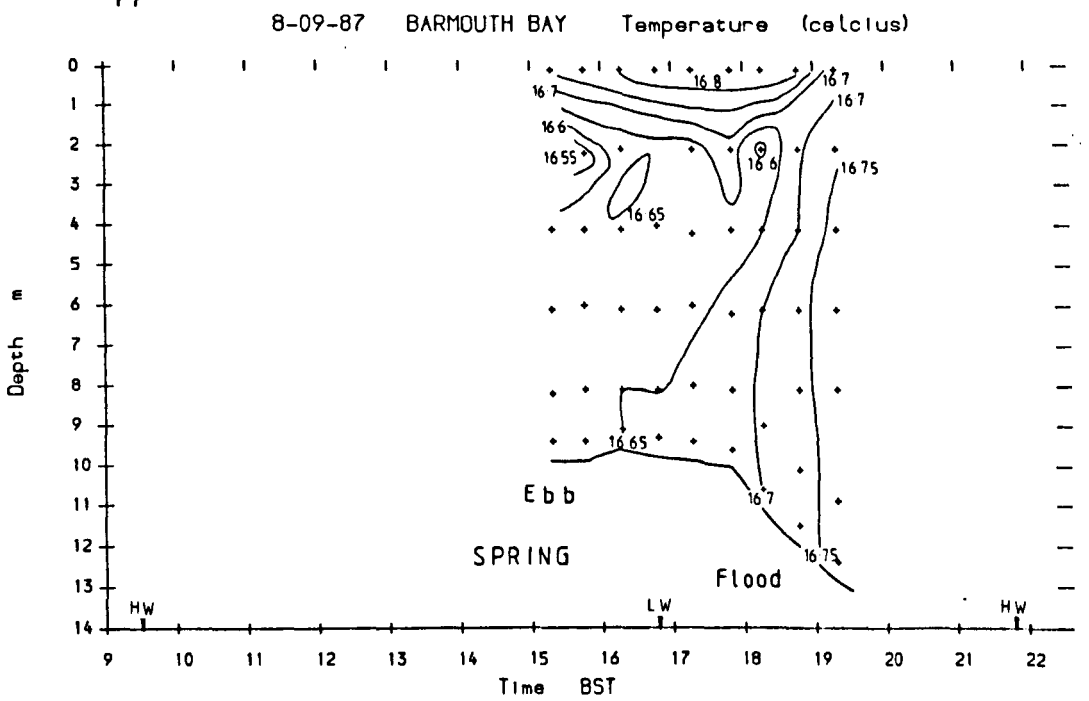
8-09-87 BARMOUTH BAY Temperature (celcius)
Depth m
Time BST
HW
LW
HW
Ebb
Flood
SPRING
16.8
16.7
16.7
16.6
16.55
16.6
16.75
16.65
16.65
16.7
16.75

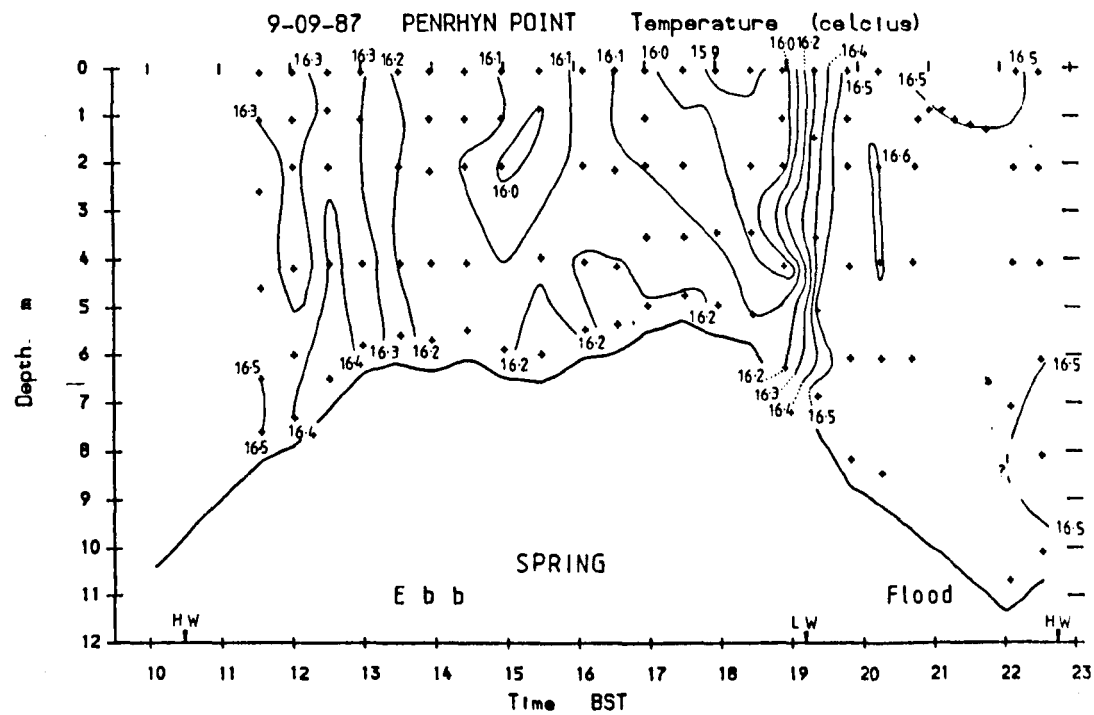
9-09-87 PENRHYN POINT Temperature (celcius)
Depth m
Time BST
HW
LW
HW
Ebb
Flood
SPRING
16.3
16.3
16.2
16.1
16.1
16.1
16.0
15.9
16.0
16.2
16.4
16.5
16.5
16.5
16.3
16.6
16.0
16.2
16.5
16.4
16.3
16.2
16.2
16.2
16.2
16.3
16.4
16.5
16.5
16.4
16.5
16.5

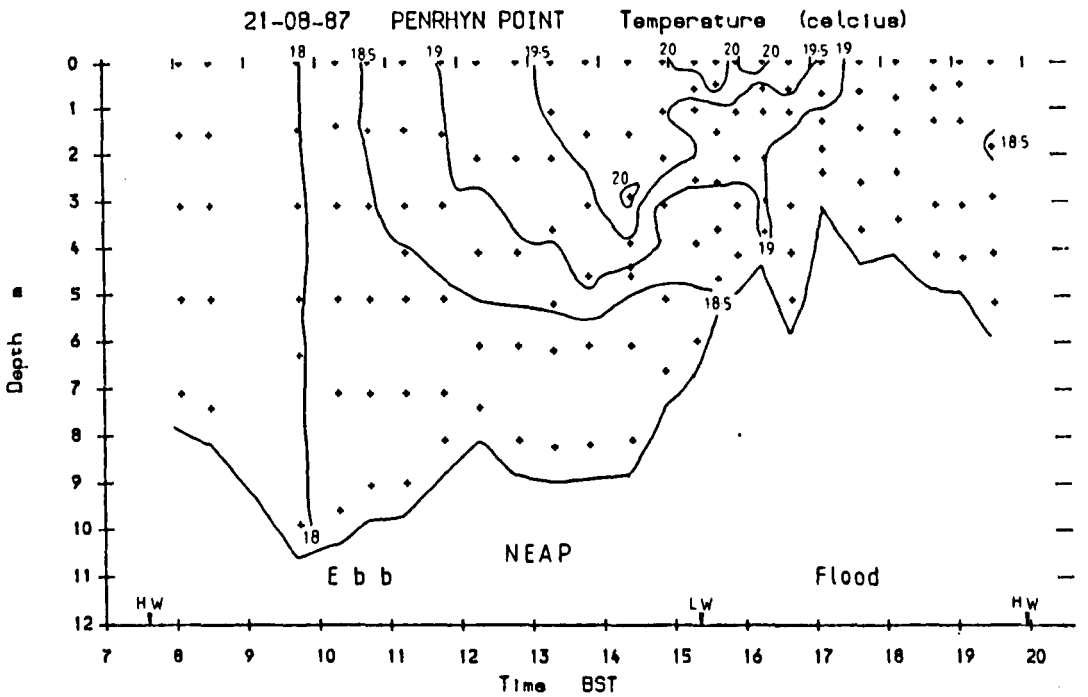
21-08-87 PENRHYN POINT Temperature (celcius)
Depth m
Time BST
NEAP
Ebb
Flood
HW
LW
HW

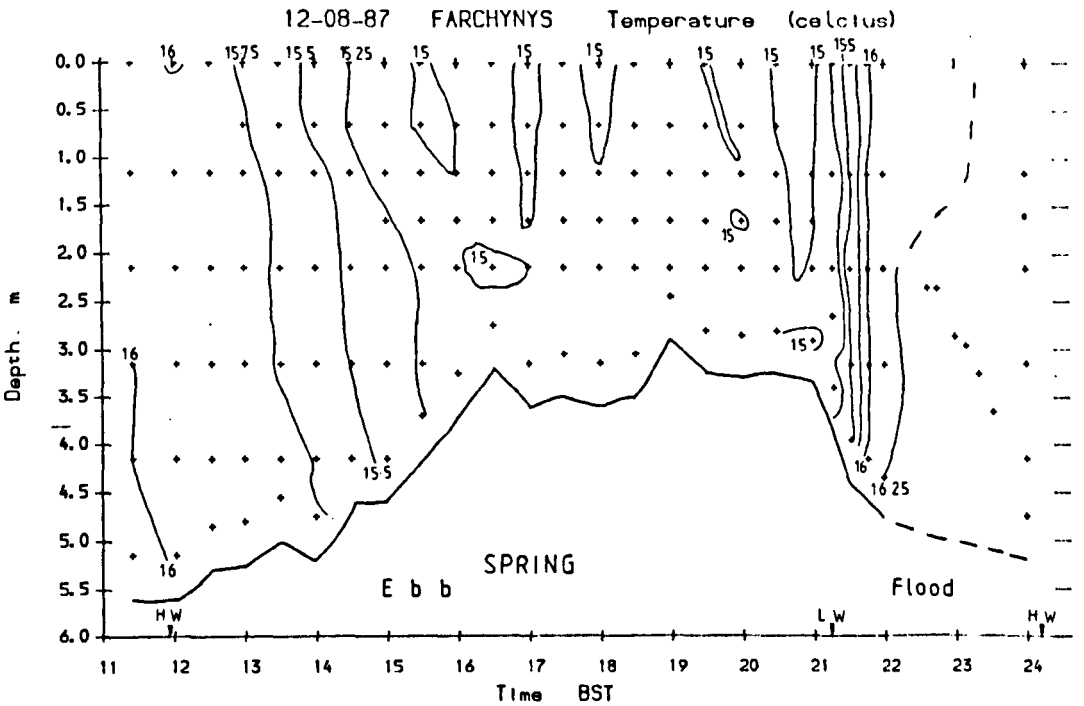
12-08-87 FARCHYNYS Temperature (celcius)
Depth m
Time BST
SPRING
Ebb
Flood
HW
LW
HW

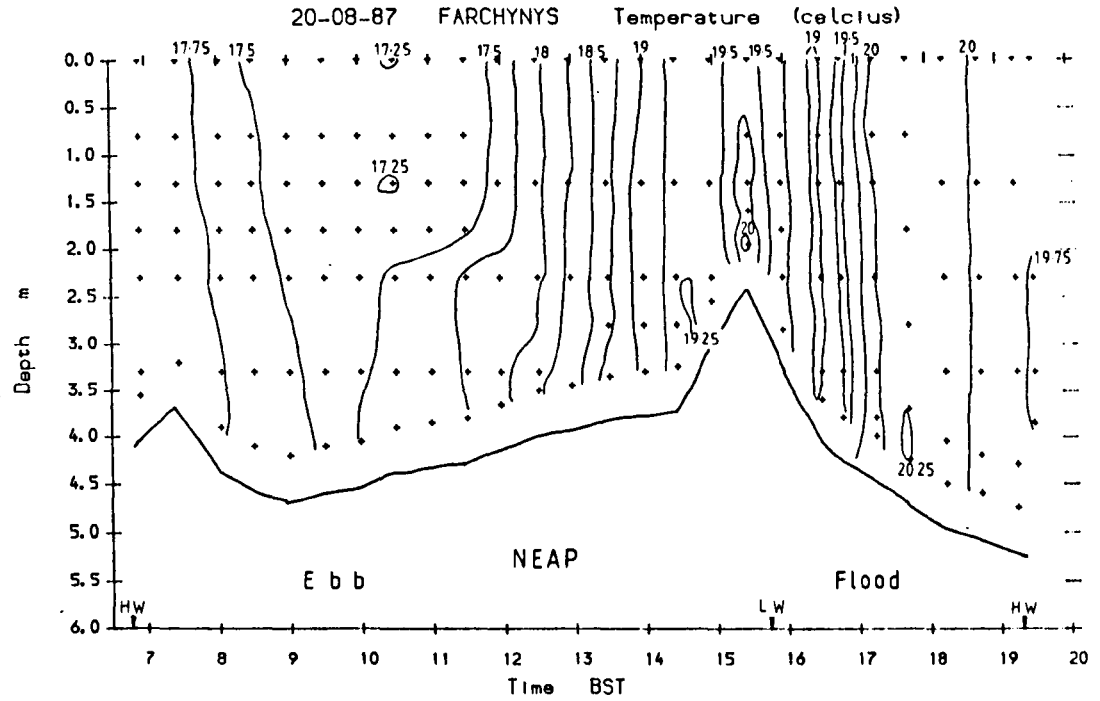
20-08-87 FARCHYNYS Temperature (celcius)
Depth m
0.0
0.5
1.0
1.5
2.0
2.5
3.0
3.5
4.0
4.5
5.0
5.5
6.0
17.75
17.5
17.25
17.5
18
18.5
19
19.5
19.5
19
19.5
20
20
19.75
19.25
20
20.25
NEAP
Ebb
Flood
HW
LW
HW
7
8
9
10
11
12
13
14
15
16
17
18
19
20
Time BST